# Stability Analysis of Non-homogeneous Soil Slopes under Rainfall Conditions

*A Thesis*

*Submitted in Partial Fulfilment of the Requirements*

*for the Degree of*

**DOCTOR OF PHILOSOPHY**

*by*

**DOORADARSHI CHATTERJEE**


Department of Civil Engineering
**Indian Institute of Technology Guwahati**
**Guwahati – 781039**

**May 2019**

TH-2008_136104008

# STATEMENT

I do hereby declare that the matter embodied in this thesis is the result of investigations carried out by me in the Department of Civil Engineering, Indian Institute of Technology Guwahati, Guwahati, Assam, India.

In keeping with the general practice of reporting scientific observations, due acknowledgments have been made wherever the work described is based on findings of other investigators.

Place: IIT Guwahati

Date: 02/05/2019 Dooradarshi Chatterjee

TH-2008_136104008

# CERTIFICATE

This is to certify that the thesis entitled "**Stability Analysis of Non-homogeneous Soil Slopes under Rainfall Conditions**", submitted by Dooradarshi Chatterjee (Roll No. 136104008), to the Indian Institute of Technology Guwahati, for the award of degree of Doctor of Philosophy in Civil Engineering, is a record of bonafide research work carried out by him under my supervision and guidance. The thesis work, in my opinion, has reached the requisite standard fulfilling the requirement for the degree of Doctor of Philosophy.

The results contained in this thesis have not been submitted in part or full to any other University or Institute for the award of any degree or diploma.

**Dr. A. Murali Krishna**
Associate Professor
Department of Civil Engineering
Indian Institute of Technology Guwahati
Guwahati-781039, India

TH-2008_136104008

# ACKNOWLEDGEMENT

*I take the opportunity and immense pleasure to convey my wholehearted gratitude to all the generous people to whom I have been associated at IIT Guwahati. The work reported in this thesis was carried out under the esteemed supervision and guidance of* ***Dr. A. Murali Krishna****. I remain deeply grateful to him not only for his guidance and constant encouragement throughout the course, but also for his invaluable advice and encouragement that enriched my doctoral study.*

*I would like to thank my Doctoral Committee members, Dr. Rajib Kumar Bhattacharjya., Dr. Baleshwar Singh and Dr. Kaustav Dasgupta, for sparing their valuable time in reviewing my work. I extend my sincere thanks to the other faculty members of the Geotechnical Engineering Division of IIT Guwahati for their cooperation, whenever required. I would like to thank Head of the Department, Dr. Chandan Mahanta, and the former Head of the Department Dr. Subhasisha Dutta, for the facilities provided for conducting the research. I also express my heartfelt gratitude and thanks to Dr. Arindam Dey and Dr. T V Bharat, for providing valuable suggestions during the course of my study. I gratefully acknowledge the unstinted help provided by Mr. Hari Ram Upadhyaya, Mr. Madhav and Mr. Upen Gohain, during different phases of my research work. Furthermore, I would like to thank the office staff of Civil Engineering Department, for their support in administrative works.*

*I convey my special thanks to my friends: Dr. Shiv S. Kumar, Mr. Chiranjib P. Sarma, Ms. Chinumani Choudhury, Dr. Arghadeep Biswas, Mr. Pradeep K. Dammala, Dr. Rana Acharyya, Dr. Jagori Dutta, Dr. Jumrik Taipodia, Mrs. Pallavi Mukherjee, Mrs. Papori Buragohain, Ms. Pushpita Das, Dr. Yagom Gapak, Dr. Sandipan Mukherjee, Mr. Dhanesh S. Das, Mr. Michael Koch, Mr. George, Mr. Bereket Mamo, Mr. Phalgun Moturu, Mr. Sanandam Bordoloi, Mr. Ardhendu S. Choudhury, Mr. Krishanu Mukherjee, Mr. Biplab Ghosh, Mr. Nishant Sharma, Mr. Printal Haldar, Mr. Atanu K. Paul, Mr. Chandrabhanu, Dr. Sudheer K. Yamsani, Mr. Janarul Saikh, Mr. Dipjyoti Baglari, Mr. Biplab Ghosh, Dr. Debraj Biswas, Dr. Tanmoy Deb, Mr. Sathwik Kashyap, Mr. Sai Sandeep, Mr. Prasath SB, Mr. K. Naveen Reddy and many others, who made my time enjoyable during my research at IIT Guwahati.*

*Dooradarshi Chatterjee*

TH-2008_136104008

# ABSTRACT

Natural slopes are non-homogeneous in the form of stratifications or variation in different material properties and hydraulic conditions with depth because of various geological formations and climatic conditions. Even in case the of uniform stratification, variations of different hydraulic properties like saturated permeability, and unsaturated permeability function with depth make the slope non-homogeneous in nature. Many slopes have failed due to rainfall infiltration. Presence of a ground water level (GWL) divides the slope into saturated and unsaturated zones. In the unsaturated zone, the matric suction significantly contributes to enhanced shear strength. Under rainfall conditions, rainwater infiltration occurs leading to the rise of ground water levels as well as the pore water pressures. The rise of pore water pressures in the unsaturated zone leads to shallow failure of slopes under infiltration conditions due to the reduction in suction levels and thereby the shear strength. Behaviour of non-homogeneous slopes will be different from that of homogeneous slopes, particularly under rainfall conditions, which may lead to failure under critical situations.

Present research work targets to investigate the slopes of different configurations under different conditions. The objective of the present study is to investigate the stability of non-homogeneous slopes of different forms of non-homogeneity, particularly under rainfall conditions. The effect of coarse-grained soil (high hydraulic conductivity) over fine-grained soil (low hydraulic conductivity) and vice versa under infiltration conditions is studied. Seepage behaviour of such layered configurations and its effect on the stability of the slope will be analyzed. The critical slip surfaces for different types of non-homogeneous slopes has been studied to understand the failure mechanisms.

Three different soils were selected with different mechanical and hydraulic properties to model the homogeneous and non-homogeneous slopes. Two-dimensional (2D) numerical models of



TH-2008_136104008

homogeneous and non-homogeneous slopes are prepared using a numerical package SLIDE2. Transient seepage analysis for the slopes with rainfall infiltration was performed in the finite element framework. The pore pressures obtained from the seepage analysis were used in the slope stability analysis, which was performed using the limit equilibrium framework. Parametric studies have been carried out to investigate the influence of rainfall intensity, duration, slope angle and slope height. The effect of transient seepage under rainfall infiltration is investigated to gain information about the changes in pore water pressures, a factor of safety, and critical slip surface within the slopes.

The study reemphasizes the importance of consideration of ground water level (GWL) and unsaturated soil characteristics in the analysis, as the slope behaviour totally depends on the suction levels and the associated shear strength values. The suction for soils with relatively high permeability reduces quickly which initiates shallow failure within the slope. The effect of rainfall on low permeable soils is rather slow, the suction reduces very slowly and hence the changes in safety factor is minimal. The study highlights the behaviour of different types of soils under rainfall consideration with due importance to unsaturated soil behaviour. As the slope behaviour is totally depends on the type of soil exist at the top layers, due consideration shall be given for the non-homogeneous nature including the variation of the moisture levels and the associated changes in suction and permeability characteristics.



TH-2008_136104008

# TABLE OF CONTENTS





TH-2008_136104008

TH-2008_136104008

TH-2008_136104008

# LIST OF FIGURES





TH-2008_136104008

TH-2008_136104008

TH-2008_136104008

TH-2008_136104008

TH-2008_136104008

TH-2008_136104008

TH-2008_136104008

TH-2008_136104008

TH-2008_136104008

भारतीय प्रौद्योगिकी संस्थान गुवाहाटी • Indian Institute of Technology Guwahati •



TH-2008_136104008

# LIST OF TABLES





TH-2008_136104008

# NOTATIONS AND ABBREVIATIONS

| | |
|---|---|
| $\alpha$ | Inverse of air entry value |
| $\beta$ | Slope angle |
| $\gamma$ | Unit weight of soil |
| $\gamma_w$ | Unit weight of water |
| $\lambda$ | Scaling factor |
| $\rho$ | Density of water |
| $\theta$ | Volumetric water content |
| $\theta_r$ | Residual volumetric water content |
| $\theta_s$ | Saturated volumetric water content |
| $\sigma'$ | Normal effective stress |
| $\tau$ | Shear strength |
| $\phi'$ | Effective angle of internal frictional of soil |
| $\phi^b$ | Unsaturated friction angle |
| $c'$ | Effective cohesion |
| $c_u$ | Undrained shear strength |
| $dW$ | Slice weight |
| $D$ | Total depth |
| $E$ | Horizontal interslice force |
| $f(x)$ | Assumed function |
| $g$ | Acceleration due to gravity |
| $h$ | Hydraulic head |
| $H$ | Height of slope |
| $H_c$ | Critical height of slope |
| $i$ | Hydraulic gradient |
| $k$ | Seismic coefficient |
| $k_h$ | Horizontal seismic coefficient |
| $k_s$ | Saturated hydraulic conductivity |
| $k_x$ | Coefficient of permeability in horizontal direction |
| $k_z$ | Coefficient of permeability in vertical direction |
| $K$ | Coefficient of permeability |
| $m$ | n-(1/n) |



TH-2008_136104008

| | |
|---|---|
| $m^2_w$ | Slope of SWCC |
| $n$ | Curve fitting parameter |
| $N_s$ | Stability number |
| $N$ | Normal force on base of a slice |
| $q$ | Externally applied flux |
| $r_u$ | Pore pressure ratio |
| $s$ | Suction |
| $S_e$ | Effective degree of saturation |
| $S_r$ | Degree of saturation |
| $S_v$ | Interslice shear strength |
| $u$ | Pore pressure |
| $u_a$ | Pore air pressure |
| $u_w$ | Pore water pressure |
| $v$ | Discharge velocity |
| $x_1$ | Front extent of slope |
| $x_2$ | Back extent of slope |
| $X$ | Vertical interslice force |
| $Z$ | Resultant interslice force |
| *FEM* | Finite element method |
| *FOS* | Factor of safety |
| *GWL* | Ground water level |
| *LB* | Lower bound |
| *LEM* | Limit equilibrium method |
| *MP* | Morgenstern and Price |
| *SRF* | Strength Reduction Factor |
| *SRM* | Shear strength reduction method |
| *SWCC* | Soil−water characteristic curve |
| *UB* | Upper bound |



TH-2008_136104008

# Chapter 1 INTRODUCTION

## 1.1 GENERAL

Stability of slopes (natural or man-made) has been a major area of concern for geotechnical engineers and researchers. Evaluation of slope stability is an inter-disciplinary area involving basic principles of geology, soil mechanics and rock mechanics. The vast area of applications of slope stability include excavations, hill slopes, embankments, earthen dams, river banks, coastal slopes, etc. Many slopes have failed due to rainfall infiltration, seismic activity, engineering activities, etc. to consider a few. Presence of a ground water level (GWL) divides the slope into saturated and unsaturated zones. Under rainfall conditions, rainwater infiltration occurs leading to the rise of ground water levels as well as the pore water pressures (Cho and Lee 2001, Cai and Ugai 2004, Gavin and Xue 2008, Cho 2009, Ni et al. 2018). The rise of pore water pressures in the unsaturated zone leads to shallow failure of slopes under infiltration conditions. Figure 1.1 shows typical rainfall induced slope failures.

Slopes are inherently non-homogeneous in nature. Non-homogeneity can be divided into two types. The first one i.e., lithological non-homogeneity is due to stratification of different soil layers having different hydraulic and mechanical properties using stiff layers inside soft material or vice versa. The second one accounts for the inherent spatial variability of soil, which represents the variation of engineering soil properties at different points in space due to previous deposition characteristics and stress history (Elkateb et al., 2003). Behaviour of non-homogeneous slopes will be different from that of homogeneous slopes, particularly under rainfall conditions, which may lead to failure under critical situations.

The study and analysis of non-homogeneous soil slopes are therefore essential for understanding their behaviour and performance, in particular, under rainfall conditions. Present research work targets to investigate the slopes of different configurations under different



TH-2008_136104008

conditions. The different conditions include slope without a GWL, a slope with a GWL, slope with a GWL under rainfall infiltration.

Figure 1.1 Examples of rainfall induced slope failures

## 1.2 IMPORTANCE OF NON-HOMOGENEOUS SLOPES

Soil properties normally vary with depth and direction for non-homogeneous slopes. Practical slopes are generally non-homogeneous with considerable variation in their mechanical properties like unit weight, cohesion and angle of internal friction. Non-homogeneity can be due to the variation of cohesion with depth or angle of internal friction with depth. A void ratio near the slope surface may be high but reduces as the depth increases. Saturated permeability of soils varies considerably within a slope. Soil with loose material representing near the



TH-2008_136104008

surface material is more permeable than soil encountered at higher depths. Another important hydraulic property is the soil–water characteristic curve (SWCC), a variation of suction with a degree of saturation, which is different for different type of soils.

Several researchers considered the soil non-homogeneity in slopes in different ways. Qian et al. (2014) considered simple non-homogeneous two-layered slope commonly encountered in levees with a distinct foundation layer as depicted in Figure 1.2. Rahardjo et al. (2010) conducted rainfall infiltration analysis on a layered slope as shown in Figure 1.4. A three-layered slope with inclined layers illustrated in Figure 1.3 was considered by Arai and Tagyo (1985). Hammouri et al. (2008) considered a multi-layered slope with the GWL and tension crack as represented in Figure 1.5. Koppula (1984), Chen and Liu (1990) and Kim et al. (2002) have considered the variation of cohesion with depth as shown in Figure 1.6. Elkateb et al. (2003) suggested that there is a huge scope of work concerning lithological heterogeneity on the total behaviour of non-homogeneous soil media.

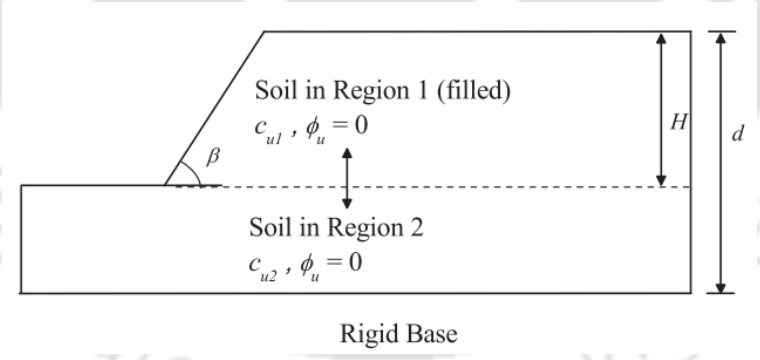


Figure 1.2 A two-layered slope modelled by Qian et al. (2014)

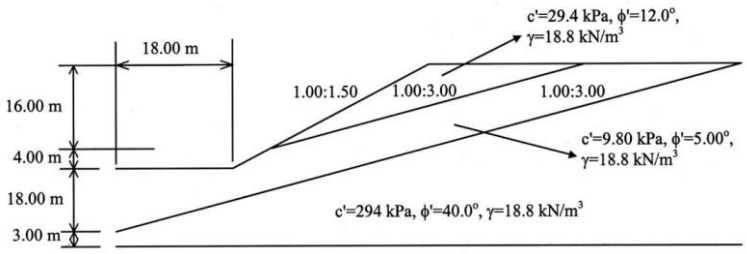


Figure 1.3 Slope geometry and soil profile (Arai and Tagyo, 1985)



TH-2008_136104008

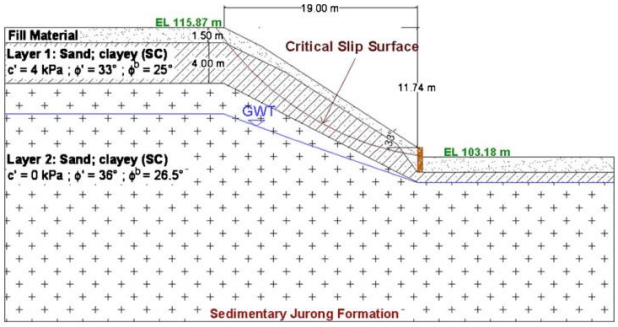


Figure 1.4 Layered slope profile from Jurong formation at Jalan Kukoh (Rahardjo et al., 2010)

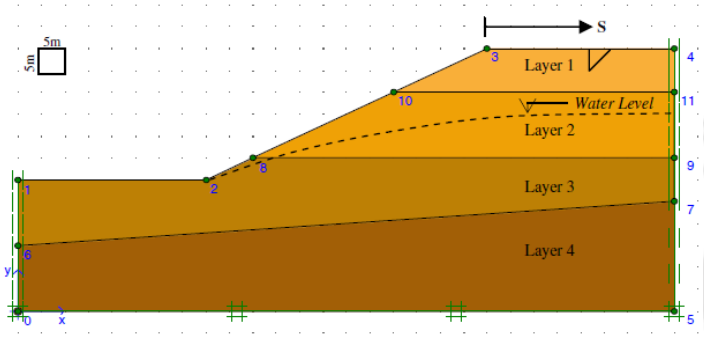


Figure 1.5 A layered slope with the GWL and tension crack (Hammouri et al., 2008)

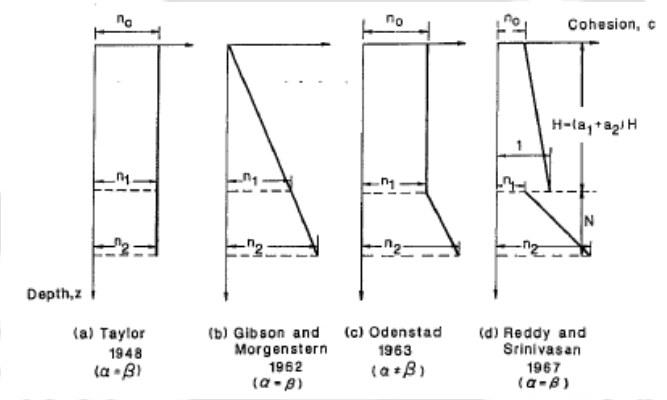


Figure 1.6 Some types of linear variation of cohesion with depth (after Chen and Liu, 1990)

## 1.3 IMPORTANCE OF RAINFALL IN SLOPE STABILITY ISSUES

Gavin and Xue (2008) analyzed rainfall infiltration into unsaturated soil slopes and discussed about its effects on soil stability. Consequences of rainfall infiltration are the rise of groundwater level, increase in pore water pressures or the decrease in matric suction, development of perched GWL and increase in unit weight due to increase in moisture content. With the infiltration of rainwater into the slope, a wet zone or the wetting front



TH-2008_136104008

advances from the slope surface. The suction at the ground surface becomes zero first, then the pore pressures increase at more depths.

The negative pore water pressures in unsaturated soils are significantly influenced by the flux boundary condition changes (i.e., infiltration, evaporation and transpiration) resulting from rainfall conditions. As rainfall infiltration occurs, the water redistributes in the unsaturated zone of the slope. With ongoing infiltration, the infiltration capacity and matric suction reduce (pore water pressure increases) in the slope. Thereby the additional shear strength due to matric suction will decrease which lead to the slope to be more susceptible to failure (Rahardo et al. 2012). Figure 1.7 schematically depicts the mechanism of rainfall induced slope failure (Rahardjo et al., 2007), wherein advancement in the wetting front, raising of ground water level under rainfall conditions (precipitation) can be seen.

Slope flux conditions (infiltration and/or runoff) will depend on the nature of the surficial soil i.e., its soil–water characteristics curve (SWCC) behaviour and saturated permeability. Further, the slope geometry (inclination and height), the soil stratifications and the initial position of the ground water level govern the rate at which infiltration occurs and the associated phenomenal behaviour as explained above.

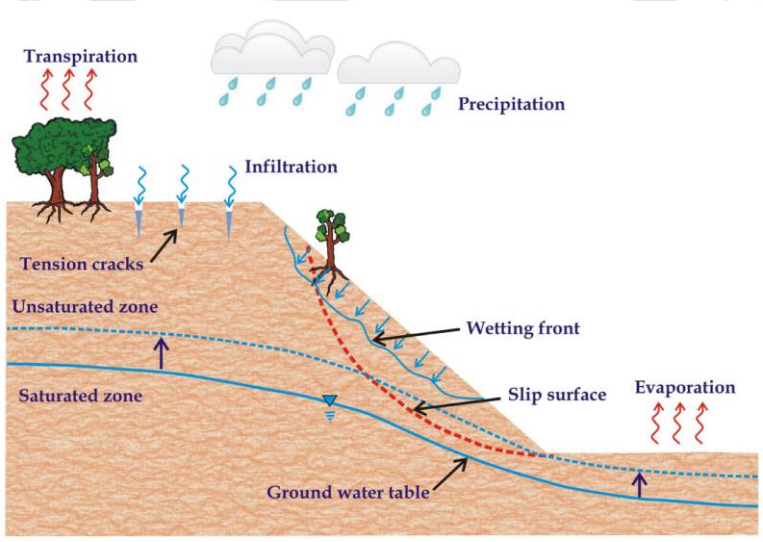


Figure 1.7 Mechanism of rainfall-induced slope failure (after Rahardjo et al., 2007)



TH-2008_136104008

## 1.4 BROAD OBJECTIVE OF THE STUDY

The broad objective of the present study is to investigate the stability of non-homogeneous slopes of different forms of non-homogeneity, particularly under rainfall conditions. Mainly the heterogeneity arising due to distinct layers (lithologic heterogeneity) in a slope will be focussed. The slip surfaces for different types of non-homogeneous slopes will be studied to understand the failure mechanisms.

## 1.5 ORGANIZATION OF THESIS

The present study has been structured sequentially in a systematic way described in chapters, which are briefly summarised as follows:

**Chapter 1** introduces the topic of research briefly, the broad objective of the study and the structure of the thesis.

**Chapter 2** provides a review of literature relevant to the present research work. The literature review is followed by a critical appraisal of the literature and the scope of work.

**Chapter 3** describes the materials selected for study, their basic characterization, mechanical properties and hydraulic properties. The chapter also discusses about the methods followed in analysing the stability of slopes.

**Chapter 4** presents the validation of the methodology adopted for the study and the development of various numerical models of homogeneous and non-homogeneous slopes.

**Chapter 5** presents the analysis of homogeneous slopes without GWL and with GWL under infiltration conditions. Effects of rainfall intensity, duration, slope angle and slope height on the stability of homogeneous slope are discussed.



TH-2008_136104008

**Chapter 6** presents the analysis of non-homogeneous slopes without GWL and with GWL under infiltration conditions. Two-layered slopes and three-layered slopes are selected to show the effect of rainfall intensity, duration, slope angle and slope height on the stability of non-homogeneous slopes.

**Chapter 7** provides a summary of the thesis, conclusions derived from the research were performed, limitations of the study and possible future scope of the work are also presented.

Indian Institute of Technology Guwahati



TH-2008_136104008

# Chapter 2 LITERATURE REVIEW

## 2.1 INTRODUCTION

Broadly, the review of literature is classified into two categories, homogeneous slopes, and non-homogeneous slopes. Various methods of analyzes used for slope stability problems are summarized. Analytical, numerical and experimental studies on the stability of slopes are reviewed, priority being given to slopes with non-homogeneous materials under infiltration conditions. Before reviewing the studies on homogeneous and non-homogeneous slopes, various methods used for slope stability analyzes are reviewed.

## 2.2 SLOPE STABILITY ANALYSIS METHODS

Many researchers have performed a stability analysis of slopes by using different methods with different assumptions satisfying a variety of conditions. These methods are applicable to both homogeneous and non-homogeneous slopes. The simplest and most used method is the limit equilibrium method, which considers force and moment equilibrium of a mass of soil above a potential failure surface. The soil above the potential failure surface is assumed to be rigid (i.e., shearing can occur only on the potential failure surface). Various methods based on limit equilibrium for homogeneous as well as non-homogeneous soil slopes are illustrated in Table 2.1. Their assumptions, equilibrium conditions, and unknowns are also shown in the table. Limit equilibrium method is generally based on satisfying three equilibrium conditions. The summation of forces in the horizontal and vertical direction should be zero and the summation of moments about any point should be zero. Some of the methods in the following table satisfy only force equilibrium and are known as force equilibrium methods while few methods satisfy both force and moment equilibrium which are known as complete equilibrium methods or rigorous methods. The methods are also classified based on the nature of the slip surface



TH-2008_136104008

assumed. The nature of the failure surface can be log-spiral, planar, circular and composite. For non-homogeneous conditions, the nature of failure surface is generally assumed as non-circular.

Limit analysis (Chen et al., 1969) is generally based on the theory of mechanics, more precisely plasticity theory. The assumption used is that soil deformations follow the flow rule associated with the Coulomb yield criterion. Thus, the rigid body type of sliding of a soil mass must occur discontinuously with an angle $\phi$ between the velocity vector and the discontinuous slip surface (Chen and Sawada, 1982). Fredlund and Krahn (1977) selected six different methods of slices to compare the stability of a slope. They proposed a new solution of Morgenstern and Price method known as the best-fit regression solution. Matsui and San (1992) developed the shear strength reduction technique for the stability analysis of slopes using the finite element method.

Duncan (1996) provided a review of the limit equilibrium method and finite element method used in stability analyzes of slopes. The different advantages and disadvantages of the two methods were also discussed in the study. Cheng et al. (2007) compared the limit equilibrium method and finite element method for different soil slopes and concluded that the results from the two methods were comparable for homogeneous slopes. Zhang et al. (2011) presented a review of studies of rainfall induced slope failures.

## 2.3 ANALYSIS OF HOMOGENEOUS SLOPES

Lumb (1962) proposed an equation for advancing wetting front during rainfall infiltration. Eckersley (1990) highlighted flowslides in coking coal slopes which eventually led to static liquefaction. Rapid retrogressive sliding was observed in the slope toe due to high seepage pressures and to prevent it, effective toe drainage was suggested for cohesion less slopes to prevent premature sliding. Ng and Shi (1998) utilized the finite element method to perform a parametric study on a steep unsaturated slope from Hong Kong.



TH-2008_136104008

Table 2.1 Assumptions, Equilibrium Conditions, and Unknowns in Limit Equilibrium Procedures (after Duncan and Wright 2005)

| **Procedure** | **Assumptions** | **Equilibrium equations satisfied** | **Unknowns solved for** | **Applicability** |
|---|---|---|---|---|
| Infinite Slope (Taylor, 1948) | A slope of infinite extent; slip surface parallel to slope face. | 1 Σ Forces perpendicular to the slope<br>1 Σ Forces parallel to slope<br>2 Total equations<br>(Moment equilibrium is implicitly satisfied) | 1 The factor of safety (*FOS*)<br>1 Normal force on the shear surface (*N*)<br>2 Total equations | Homogeneous cohesionless slopes and slopes where the stratigraphy restricts the slip surface to shallow depths and parallel to the slope face. Very accurate where applicable. |
| Logarithmic Spiral (Frohlich, 1953) | The slip surface is a logarithmic spiral | 1 Σ Moments about the center of the spiral<br>1 Total equations<br>(Force equilibrium is implicitly satisfied) | 1 The factor of safety (*FOS*)<br>1 Total equations | Applicable to homogeneous slopes; accurate. Potentially useful for developing slope stability charts and used some in software for design of reinforced slopes. |
| Swedish Circle ($\phi$=0) (Fellenius, 1922; Skempton, 1948) | The slip surface is circular; the friction angle is zero. | 1 Σ Moments about the center of the circle<br>1 Total equations<br>(Force equilibrium is implicitly satisfied) | 1 The factor of safety (*FOS*)<br>1 Total equations | Applicable to slopes where $\phi$=0 (i.e., undrained analyzes of slopes in saturated clays). Relatively thick zones of weaker materials where the slip surface can be approximated by a circle. |
| Ordinary Method of Slices (also known as Fellenius's, 1936 Method; Swedish Method of Slices) | The slip surface is circular; the forces on the sides of the slices are neglected. | 1 Σ Moments about the center of the circle<br>1 Total equations | 1 The factor of safety (*FOS*)<br>1 Total equations | Applicable to non-homogeneous slopes and $c$–$\phi$ soils where slip surface can be approximated by a circle. Very convenient for hand calculations. Inaccurate for effective stress analyzes with high pore water pressures. |



TH-2008_136104008

| Procedure | Assumptions | Equilibrium equations satisfied | Unknowns solved for | Applicability |
|---|---|---|---|---|
| Simplified Bishop's Method (Bishop, 1955) | The slip surface is circular; the forces on the sides of the slices are horizontal (i.e., there is no shear force between slices). | 1 Σ Moments about the center of the circle<br>*n* Σ Forces in the vertical direction.<br>n+1 Total equations | 1 The factor of safety(*FOS*)<br>*n* Normal force on the base of slices (*N*)<br>*n* + 1 total unknowns | Applicable to non-homogeneous slopes and $c$–$\phi$ soils where slip surface can be approximated by a circle. More accurate than Ordinary Method of Slices, especially for analyzes with high pore water pressures. Calculations are feasible by hand or spreadsheet. |
| Force Equilibrium (Lowe and karafiath, Lowe and Karafiath, 1959, Simplified Janbu, Janbu et al., 1956, Corps of Engineer's Modified Swedish, U.S. Army Corps of Engineers, 1970, Janbu's GPS procedure) | The inclinations of the interslice forces are assumed; assumptions vary with the procedure. | *n* Σ Forces in the horizontal direction<br>*n* Σ Forces in the vertical direction<br>2*n* Total equations | 1 The factor of safety (*FOS*)<br>*n* Normal force on the base of slices (*N*)<br>*n* - 1 Resultant interslice forces (*Z*)<br>2*n* Total unknowns | Applicable to virtually all slope geometries and soil profiles. The only procedures are suitable for hand calculations with noncircular slip surfaces. Less accurate than complete equilibrium procedures and results are sensitive to assumed inclinations for interslice forces. |
| Spencer's Method (Spencer, 1967) | Interslice forces are parallel (i.e. all have the same inclination). The normal force (*N*) acts at the center of the base of the slice (typically). | *n* Σ Moments about any selected point<br>*n* Σ Forces in the horizontal direction<br>*n* Σ Forces the vertical direction<br>3*n* Total equations | 1 The factor of safety (*FOS*)<br>1 Interslice force inclination (θ)<br>*n* Normal force on the base of slices (*N*)<br>*n* - 1 Resultant interslice forces (*Z*)<br>*n* - 1 Location of side forces (line of thrust)<br>3*n* Total unknowns | An accurate procedure applicable to virtually all slope geometries and soil profiles. The simplest complete equilibrium procedure for computing the factor of safety. |



TH-2008_136104008

| Procedure | Assumptions | Equilibrium equations satisfied | Unknowns solved for | Applicability |
|---|---|---|---|---|
| Morgenstern and Price's Method (Morgenstern and Price, 1965) | Interslice shear force is related to interslice normal force by $X=\lambda f(x)E$; the normal force ($N$) acts at the center of the base of the slice (typically). | $n\Sigma$ Moments about any selected point<br>$n$ Σ Forces in the horizontal direction<br>$n$ Σ Forces in the vertical direction<br>3$n$ Total equations | 1 The factor of safety ($FOS$)<br>1 Interslice force inclination ''scaling'' factor (λ)<br>$n$ Normal force on the base of slices ($N$)<br>$n$ - 1 Horizontal interslice forces ($E$)<br>$n$ - 1 Location of interslice forces (line of thrust)<br>3$n$ Total unknowns | An accurate procedure applicable to virtually all slope geometries and soil profiles. Rigorous, well-established complete equilibrium procedure. |
| Chen and Morgenstern's Method (Chen and Morgenstern, 1983) | Interslice shear force is related to interslice normal force by $X=[\lambda f(x)+f_o(x)]E$; the normal force ($N$) acts at the center of the base of the slice (typically). | $n\Sigma$ Moments about any selected point<br>$n$ Σ Forces in the horizontal direction<br>$n$ Σ Forces in the vertical direction<br>3$n$ Total equations | 1 The factor of safety ($FOS$)<br>1 Interslice force inclination ''scaling'' factor (λ)<br>$n$ Normal force on the base of slices ($N$)<br>$n$ - 1 Horizontal interslice forces ($E$)<br>$n$ - 1 Location of interslice forces (line of thrust) | Essentially an updated Morgenstern and Price procedure. A rigorous and accurate procedure applicable to any shape of slip surface and slope geometry, loads, etc. |
| Sarma's Method (Sarma, 1973) | Interslice shear force is related to the interslice shear strength, $Sv$, by $X=\lambda f(x)Sv$; interslice shear strength depends on shear strength parameters, pore water pressures, and the horizontal component of interslice force; the normal force ($N$) acts at the center of the base of the slice (typically). | $n\Sigma$ Moments about any selected point<br>$n$ Σ Forces in the horizontal direction<br>$n$ Σ Forces in the vertical direction<br>3$n$ Total equations | 1 Seismic coefficient ($k$) [or a factor of safety ($FOS$) if trial and error is used]<br>1 Interslice force scaling factor (λ)<br>$n$ Normal force on the base of slices ($N$)<br>$n$ - 1 Horizontal interslice forces ($E$)<br>$n$ - 1 Location of side forces (line of thrust)<br>3$n$ Total unknowns | An accurate procedure applicable to virtually all slope geometries and soil profiles. A convenient complete equilibrium procedure for computing the seismic coefficient required to produce a given factor of safety. Side force assumptions are difficult to implement for any but simple slopes. |



TH-2008_136104008

They showed the effects of the initial GWL, rainfall intensity, rainfall duration etc. on the stability of the slope. Figure 2.1b depicts the pore water pressure profiles prior to rainfall infiltration at the three sections in the slope shown in Figure 2.1a. Hydrostatic conditions are observed at the three sections of the slope.

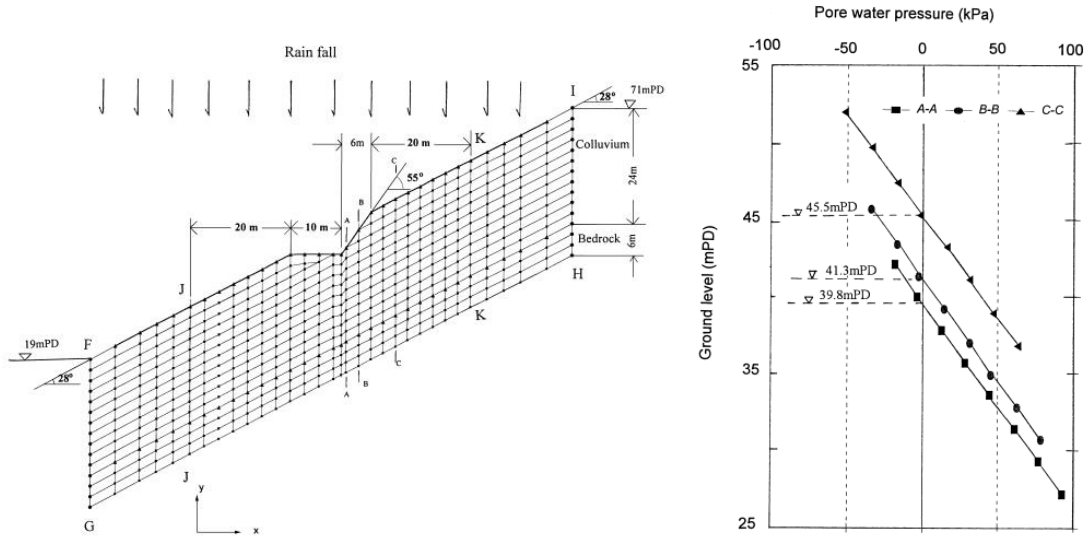


(a) (b)

Figure 2.1 (a) Finite element mesh of a steep cut slope (b) Initial pore pressure distribution within the slope at three sections (Ng and Shi, 1998)

Griffiths and Lane (1999) utilized the finite element method to analyze different homogeneous and non-homogeneous slopes. It was inferred that failure in slopes occurred naturally through the zones where the shear strength was unable to resist the shear stresses. Tsaparas et al. (2002) attempted to bring out a relationship between climatic conditions, soil properties and initial conditions within a slope, which can result in failures. From the parametric study, they concluded that rainfall amount of 240 mm spread over 16 h caused more damage to a slope of 10 m height. Antecedent rainfall evenly spread over a period of 5 days constituted worst-case scenarios. Gallipoli et al. (2003) proposed a new relationship between the degree of saturation, suction and specific volume. Cai and Ugai (2004) performed stability analysis using finite element strength reduction technique on the homogeneous slope to study the effects of initial degree of saturation, rainfall intensity, boundary condition etc. under rainfall conditions.



TH-2008_136104008

Zhang et al. (2004) showed that under certain conditions matric suction in the slope does not dissipate which is a major factor in causing failure in slopes. They performed a numerical study on a 20 m high slope (Figure 2.3) under different rainfall intensities. They concluded that the pore water pressure profiles under transient seepage conditions depend on the rainfall intensity, saturated permeability, soil–water characteristic curve and water storage capacity. Figure 2.2 depicts the pore water pressure profiles under steady state seepage, at flux less than the saturated permeability of the soil and at flux greater than the saturated permeability of the soil.

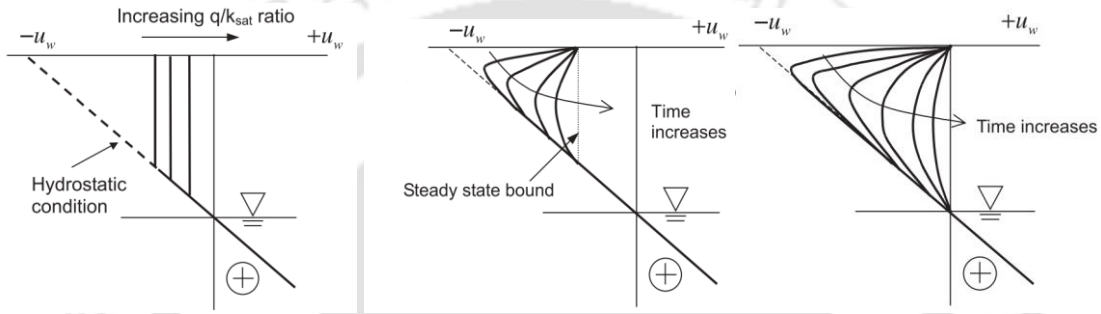


Figure 2.2 Pore pressure profiles at (a) steady state (b) $q < k_{sat}$ (c) $q > k_{sat}$ (Zhang et al., 2004)

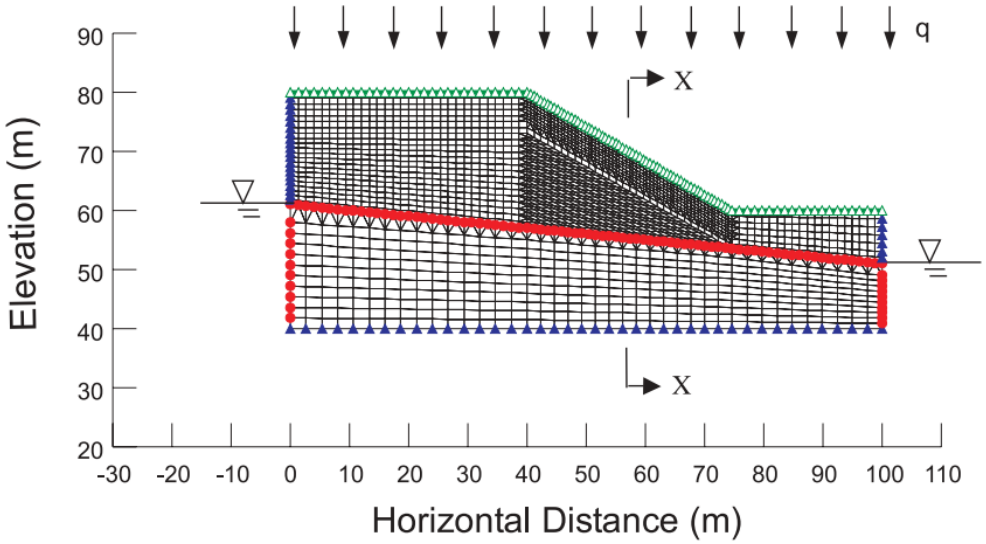


Figure 2.3 Finite element mesh of a 20 m slope inclined at 30° to the horizontal (Zhang et al., 2004)

Jimoh (2006) performed laboratory shear tests on lateritic soil with a variation of moisture content. The relationship between strength properties and moisture content obtained from the



TH-2008_136104008

correlation analysis showed linear and parabolic forms. Rahardjo et al. (2007) conducted parametric studies on a homogeneous slope under various rainfall intensities to investigate the effects of soil parameters, rainfall intensity, initial ground water level location and slope angle and height. They concluded that rainfall intensity and soil properties were the most important factors responsible for slope failures under infiltration conditions. Gavin and Xue (2008) established a method to evaluate the time taken for the wetting front to develop. The Green-Ampt infiltration model was modified to develop this method, which assumes that there is no ponding of water at the slope surface. Ray et al. (2010) derived an improved infinite slope stability model to study the influence of vadose zone soil moisture on the stability of the slope. They concluded that safety factors were sensitive to the unsaturated zone soil moisture for shallow soil layers less than 2 m depth. Rahimi et al. (2010) conducted parametric studies on homogeneous slopes to investigate the effects of soil properties like saturated hydraulic conductivity and unsaturated permeability function. They came to the conclusion that the SWCC fitting parameters affected the stability of low permeable soils more than high permeable soils. Song et al. (2016) evaluated the stability of an unsaturated natural slope under rainfall infiltration utilizing the suction stress concept. The SWCC and the suction stress characteristic curve (SSCC) used in the infinite slope model were obtained from Van Genuchten (1980) and Lu and Likos (2006) model. Rahimi et al. (2011) performed parametric studies on homogeneous slopes (Figure 2.4) to investigate the influence of pattern and distribution of antecedent rainfall on slope failures. It was concluded that the less permeable soils were more affected than high permeable soils. The decrease in the factor of safety with time was controlled by the pattern of antecedent rainfall.



TH-2008_136104008

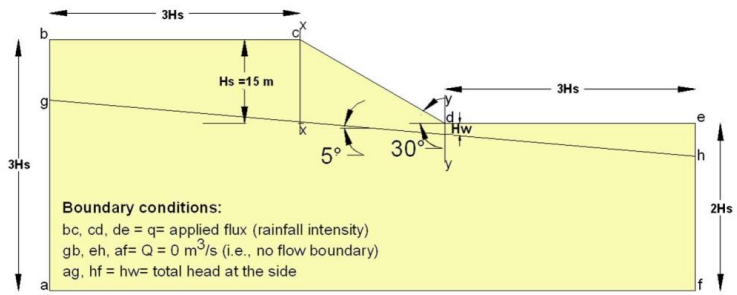


Figure 2.4 Homogeneous slope model with boundary conditions (Rahimi et al., 2011)

Figure 2.5 depicts the rainfall and infiltration rate for antecedent rainfall patterns near the crest of the slope and the pore pressure distribution at the crest and toe of a low permeable soil slope. Zhang et al. (2013) suggested on the correct value of $\phi^b$ parameter of soil that should be used in the unsaturated analysis of soil slopes.

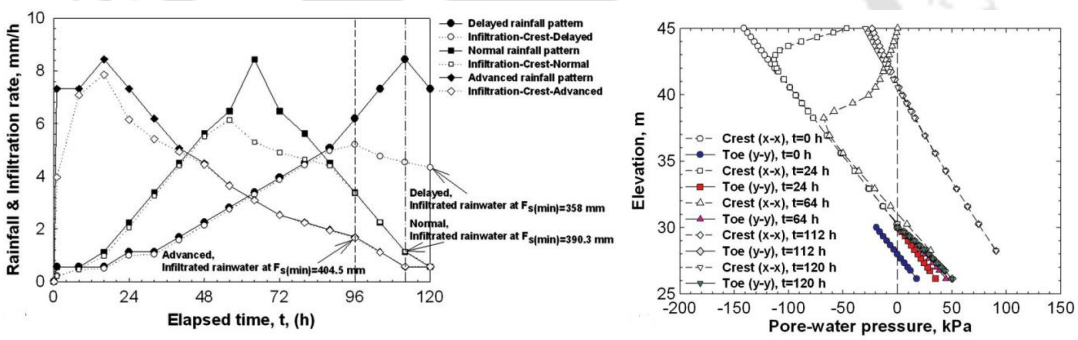


(a) (b)

Figure 2.5 Low conductivity soil slope (a) Rainfall and infiltration rate for antecedent rainfall patterns at the crest (b) Pore water pressure distribution due to antecedent rainfall at crest and toe (Rahimi et al., 2011)

Li et al. (2015) performed unconfined compressive strength and tensile strength tests at different gravimetric moisture contents on two types of soil. A new method was established for the prediction of unconfined compressive strength and tensile strength at specific moisture contents. Figure 2.6 depicts that the unconfined compressive strength increases with decrease in gravimetric moisture content.



TH-2008_136104008

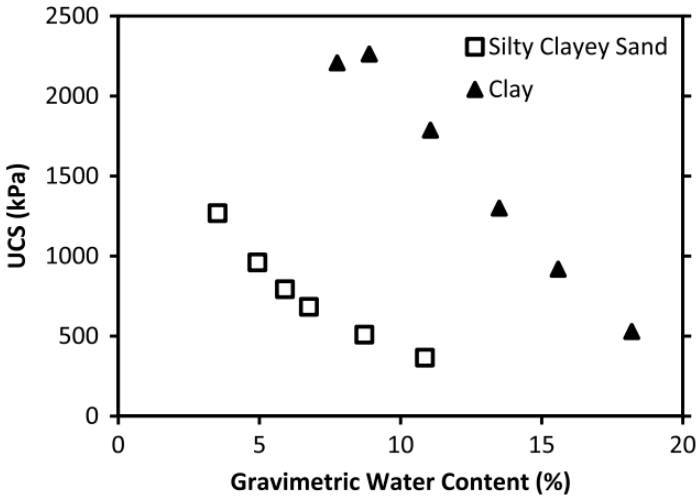


Figure 2.6 Relationship between moisture content and unconfined compressive strength (Li et al., 2015)

Yubonchit et al. (2016) conducted parametric studies utilizing the finite element method to investigate the effects of antecedent rainfall, saturated permeability of the soil and slope angle on a shallow slope. The model of the slope is depicted in Figure 2.7. They concluded that the shallow slope failures occur due to either rise of ground water level or rainfall infiltrating the soil slope. Figure 2.8 illustrates the influence of slope inclination on the intensity of rainfall at the failures state.

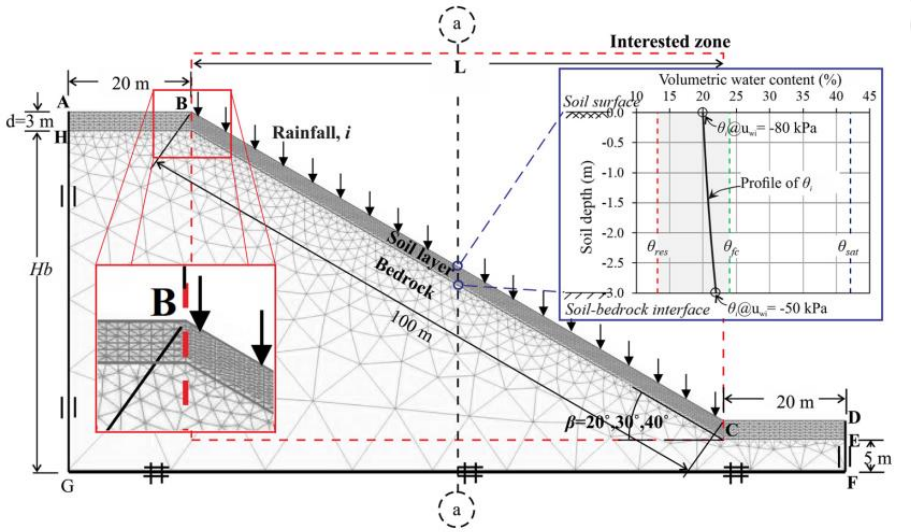


Figure 2.7 Slope model with a shallow soil layer (Yubonchit et al., 2016)



TH-2008_136104008

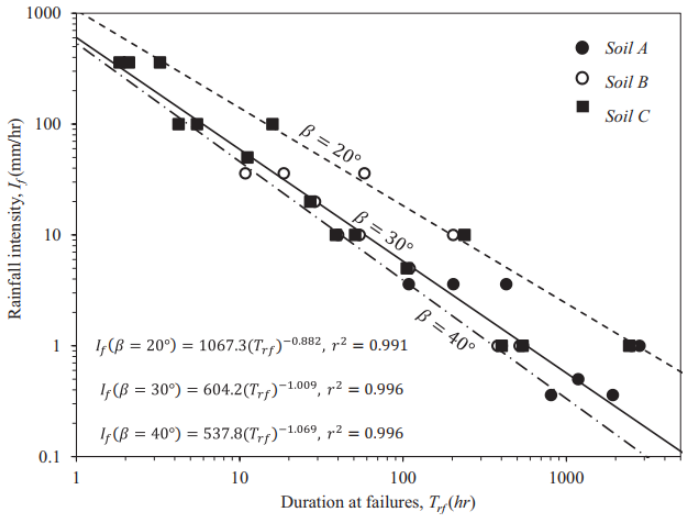


Figure 2.8 ID thresholds based on different slope angles with various rainfall intensities (Yubonchit et al., 2016)

Cai et al. (2016) established a spatial correlation between the saturated permeability distribution and pressure head distribution within a hillslope. A negative correlation was obtained between saturated permeability and pressure head in the partially saturated area with uniform flux boundary condition.

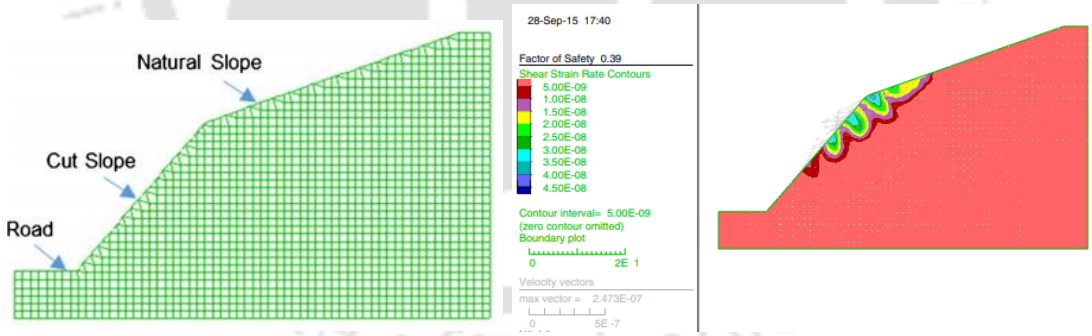


(a) (b)

Figure 2.9 (a) Slope model (b) Shear strain rate contours (Umrao et al., 2017)

Umrao et al. (2017) performed numerical slope stability analysis on both soil and rock slopes using FLAC on hill cut slopes along National Highway-40 in India. The model of the cut slope is shown in Figure 2.9a. They concluded that due to the high moisture content of the plastic rich soils, debris flow and slides occur frequently. The results from the numerical analysis



TH-2008_136104008

showed failures of the steep cut slopes adjoining the road. Figure 2.9b represent the zone of maximum shear strain developed within the slope for the sedimentary soil material. Lin et al. (2017) performed a numerical analysis to investigate the effect of hydraulic parameters on the final saturation line and slope stability. Filho and Fernandes (2018) studied shallow landslides occurring on a highway-cutting slope of aeolian sandstone soil origin. From different field tests, laboratory tests, surface and sub-surface investigation, they concluded that the slope failures were caused by matric suction reduction due to rainfall infiltration. Lin and Zhong (2018) performed numerical analysis on homogeneous slopes (Figure 2.10a) to study the effects of rainfall intensity and its pattern on the stability of a slope. Figure 2.10b depicts the relationship between factor of safety and rainfall duration for a clay slope.

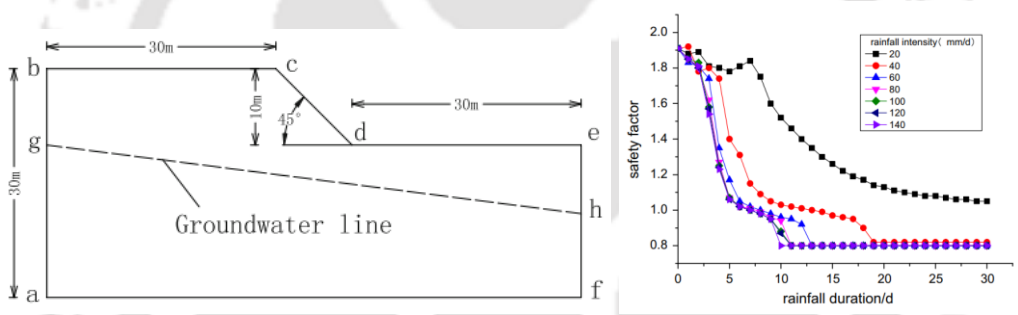


(a) (b)

Figure 2.10 (a) Homogeneous slope model (b) Variation of safety factor with rainfall duration under different rainfall intensities (Lin and Zhong, 2018)

Ni et al. (2018) performed unconsolidated undrained tests on remolded soil specimens at different moisture contents. A correlation between shear strength parameters cohesion and angle of internal friction with moisture content was evaluated as shown in Figure 2.11. It was observed that both the shear strength parameters reduced with an increase in moisture content of the soil. Analysis of slopes with raised ground water level illustrated in Figure 2.12b suggested that soil properties should change with moisture content or else the determined factor of safety of the slope will be unsafe. The three dimensional slope model is shown in Figure 2.12a.



TH-2008_136104008

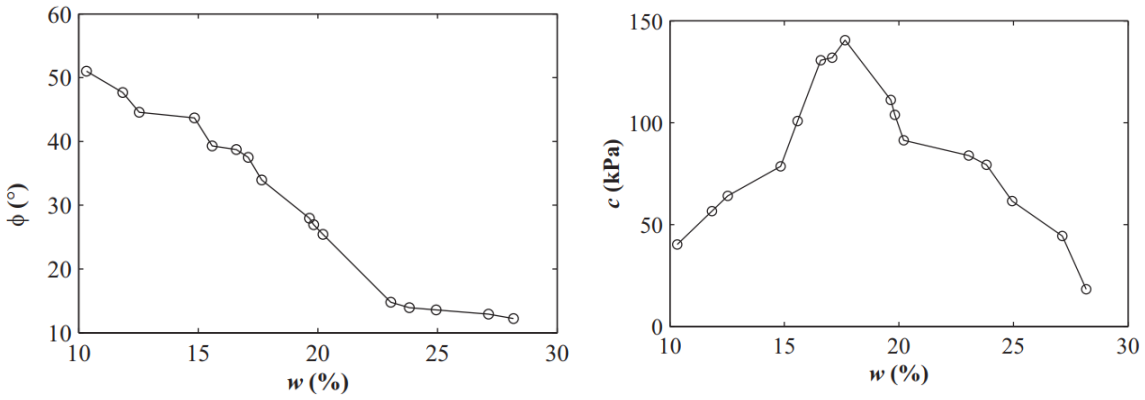


(a) (b)

Figure 2.11 Variation of (a) friction angle and (b) cohesion with moisture content (Ni et al., 2018)

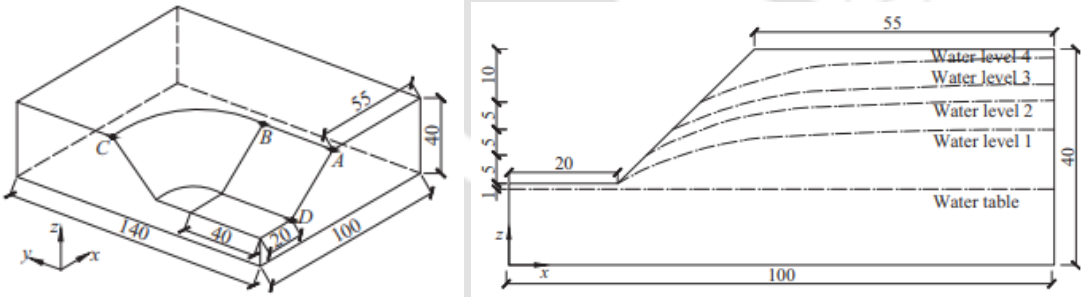


Figure 2.12 Schematic diagram of a (a) 3D slope model (b) 2D model showing variation of water-table (Ni et al., 2018)

## 2.4 ANALYSIS OF NON-HOMOGENEOUS SLOPES

Various methods based on limit equilibrium method for non-homogeneous soil slopes are illustrated in Table 2.1. Most of the methods are applicable to non-homogeneous slopes under static conditions except Sarma's method. Elkateb et al. (2003) reviewed that very less work has been presented concerning the effect of lithologic heterogeneity in various types of soil structures in civil engineering projects. The soil profile was considered non-homogeneous by dividing the soil into several homogeneous layers by Childs and Bybordi (1969) and Bouwer, (1969). Chen et al. (1975) developed expressions for stability number, $N_s$ using the upper bound limit analysis. The non-homogeneous and anisotropic slope selected is shown in Figure 2.13. The cohesion varies only linearly with depth as depicted in the figure. A log-spiral failure was assumed for the analysis.



TH-2008_136104008

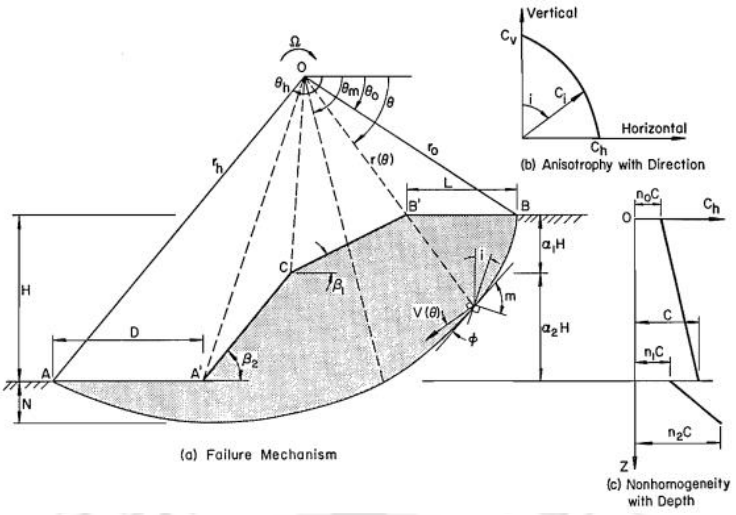


Figure 2.13 Anisotropy and non-homogeneity in soil slopes (after Chen et al., 1975)

Koppula **(**1984**)** presented a solution for the stability of slopes in purely cohesive soils exhibiting a linear variation in shear strength with depth (Figure 2.14 (a) and (b)), assuming the strength at the surface to be greater than zero. The effect of seismicity is included in a quasi-static analysis. The potential failure surface was assumed to be circular. A series of plots have been provided that are of use in the assessment of the stability of slopes in soils whose strength is constant with depth and whose strength varies linearly with depth. The general trend from the results show that the dimensionless parameter, stability number *N* decreased with an increasing seismic coefficient and slope inclination as illustrated in Figure 2.15.

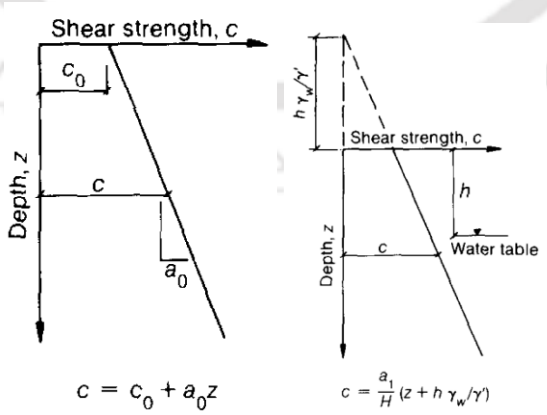


(a) (b)

Figure 2.14 (a) and (b) Variation of shear strength with depth (Koppula, 1984)



TH-2008_136104008

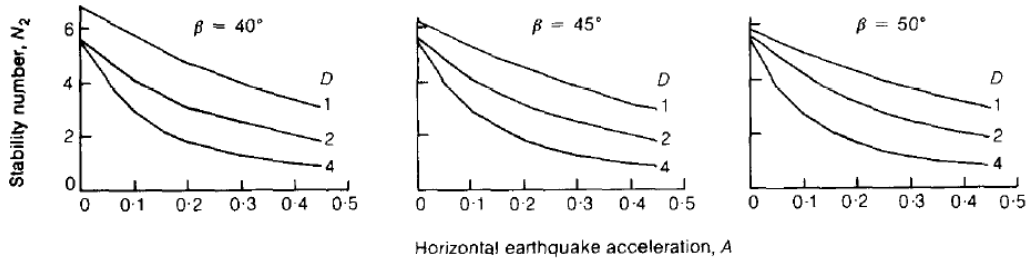


Figure 2.15 Relationship between stability number $N_2$ and seismic coefficient $A$ for various slope inclinations $\beta$ (Koppula, 1984)

Chuang (1992) developed a kinematic formulation that satisfies both the static and kinematic admissibility of a discretised soil mass with varying pore water pressure, for inhomogeneous materials having both cohesion and internal friction. The failure surface can take any arbitrary shape. The soil domain was divided into rigid elements connected by interfacing Mohr-Coulomb layers. The example problem shown in Figure 2.16 was analyzed by the above method which previously has been studied using the limit equilibrium method and the incremental loading method assuming elastoviscoplastic material behaviour.

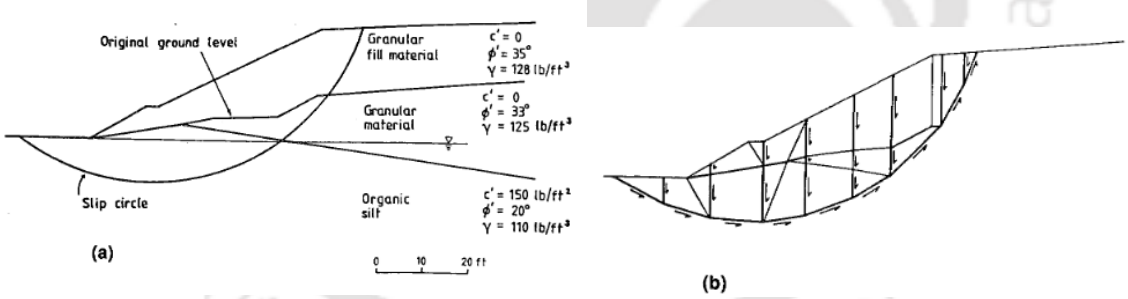


Figure 2.16 Example problem (a) Geometry and material properties [modified from Whitman and Bailey (1967)]; (b) Finite element model and failure mechanism (Chuang, 1992)

Jiang and Magnan (1997) presented a versatile finite element method and demonstrated the validity of the upper bound method and some advantages of limit analysis over methods of slices. They incorporated the general definition of a factor of safety into the limit analysis to compare the results of limit analysis directly with the method of slices. This method of upper bound limit analysis proved viable and gave correct results of limit load or safety factors. The failure mechanisms provided by this method also proved to be rational, which will give the



TH-2008_136104008

least resistance of the structure to the applied loads. The numerical example shown in Figure 2.17a was analyzed using the finite element method incorporated in a finite element software CESAR-LCPC. Figure 2.17b illustrates the failure mechanism by nodal velocity vectors. The factors of safety obtained from the limit analysis method were found to be more accurate than the slice based methods.

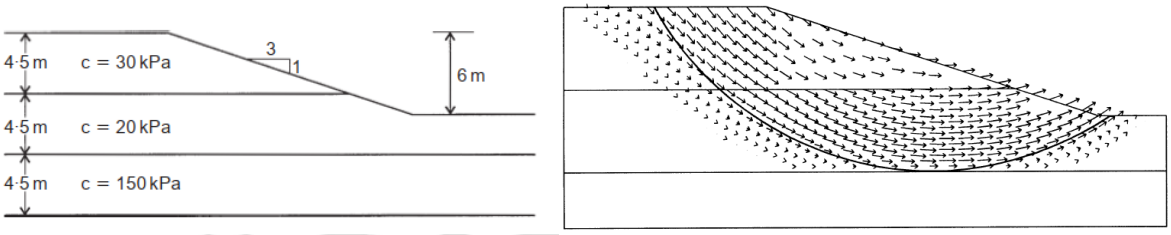


(a) (b)

Figure 2.17 (a) Three-layerd slope (Low 1989) (b) Collapse velocities (Jiang and Magnan, 1997)

Liang et al. (1999) developed reliability and probability theories for assessing the reliability index and the corresponding probability of failure of multi-layered embankment dams and slopes. To calculate the risk of slope failure, they proposed a reliability based algorithm using the First Order Second Moment Method (FOSM). A modified Fellenius method was used with a horizontal seismic force taken to act within the slope. Two definitions were used to calculate the reliability index (i.e. the normal distribution and the log–normal distribution). The computer program RESLOP was developed and validated by the Congress Street open cut failure case (Figure 2.18). The developed approach was used to study the stability of the King Talal embankment dam. From the results it was concluded that the critical surface obtained from the minimum factor of safety value, was not the most critical one but it would be prudent to use the above surface as the initial trial value for the search of the critical surface with minimum reliability index or maximum probability of failure. This approach easily incorporates the inherent variability of soil properties into the analytical procedure.



TH-2008_136104008

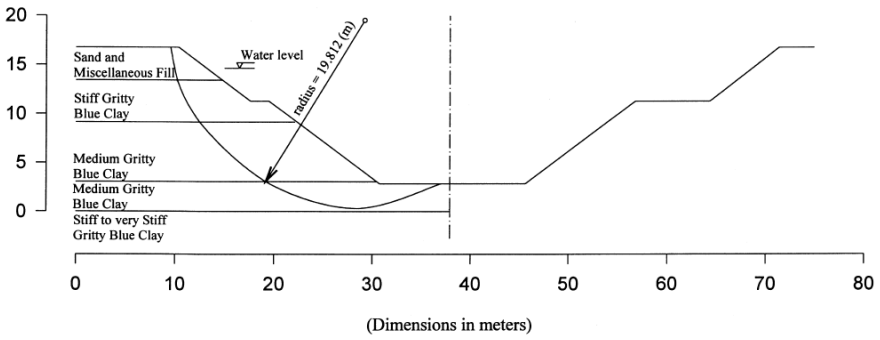


Figure 2.18 Approximate cross-section of the cut and actual slip surface at Congress Street open cut (after Ang and Tang, 1984).

Gasmo et al. (2000) performed numerical analysis on a slope to quantify the amount of infiltration into a slope. A case study of a two-layered slope was also shown where they concluded that numerical models were unable to calculate the exact amount of infiltration occurring within a slope. Figure 2.19a illustrates the two-layered slope used for the case study and the comparison of pore pressure profiles (Figure 2.19b) obtained from field and numerical analysis.

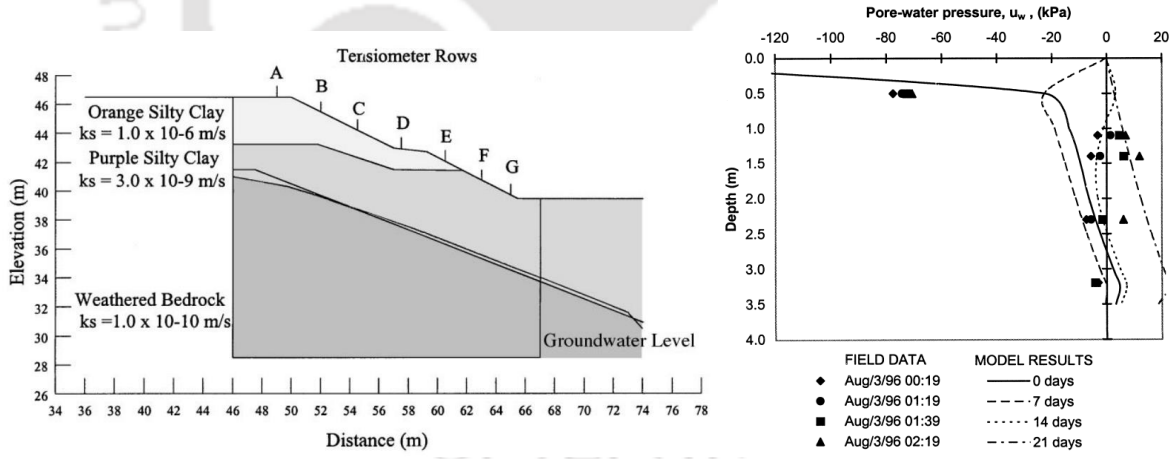


(a) (b)

Figure 2.19 (a) Slope model and (b) comparison of pore pressure profiles (Gasmo et al., 2000)

Rahardjo et al. (2001) performed numerical analysis on a multi-layered slope (Figure 2.21a) to investigate the effects of antecedent rainfall in Singapore. A 5-day antecedent rainfall was recorded which resulted in the shallow failure of more than 20 slopes. Figure 2.20 represents



TH-2008_136104008

the relationship between the occurrence of landslides and antecedent rainfall. The rainfall data for the period 7-12 November, 1994 is shown in Figure 2.21b.

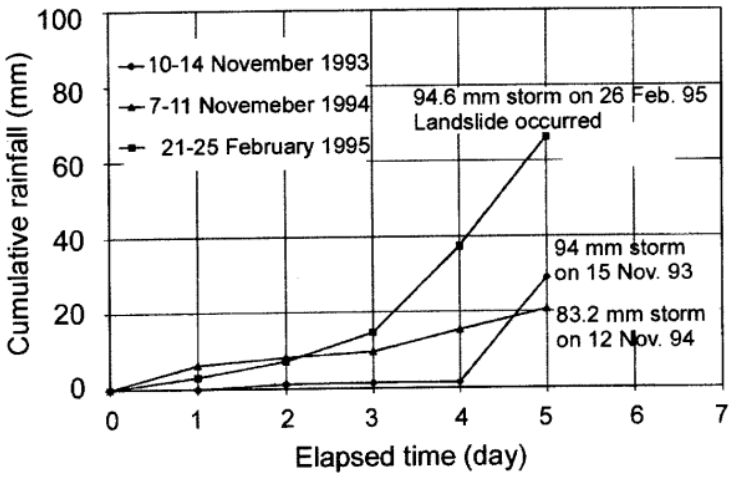


Figure 2.20 Relation between antecedent rainfall and occurrence of landslides (Rahardjo et al., 2001)

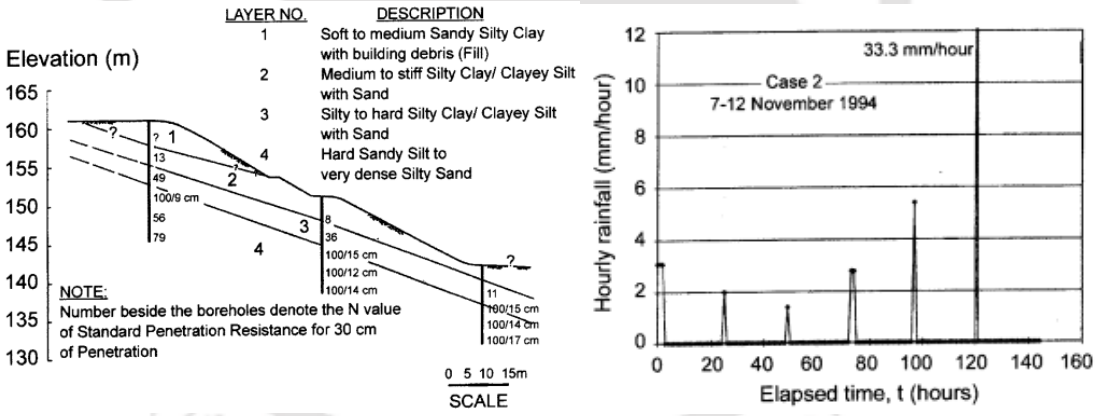


(a) (b)

Figure 2.21 (a) Layered slope profile (b) Rainfall Intensity (case-2) (Rahardjo et al., 2001)

Figure 2.22a illustrates the pore pressure profile under the case-2 rainfall intensity at 0 hours, 120 hours, 122.5 hours and 144 hours. The storm (rainfall) started at 120 hours and stopped at 122.5 hours. The variation of a factor of safety with time is shown in Figure 2.22b. The factor of safety dropped rapidly after the storm started but it increased as the storm stopped.



TH-2008_136104008

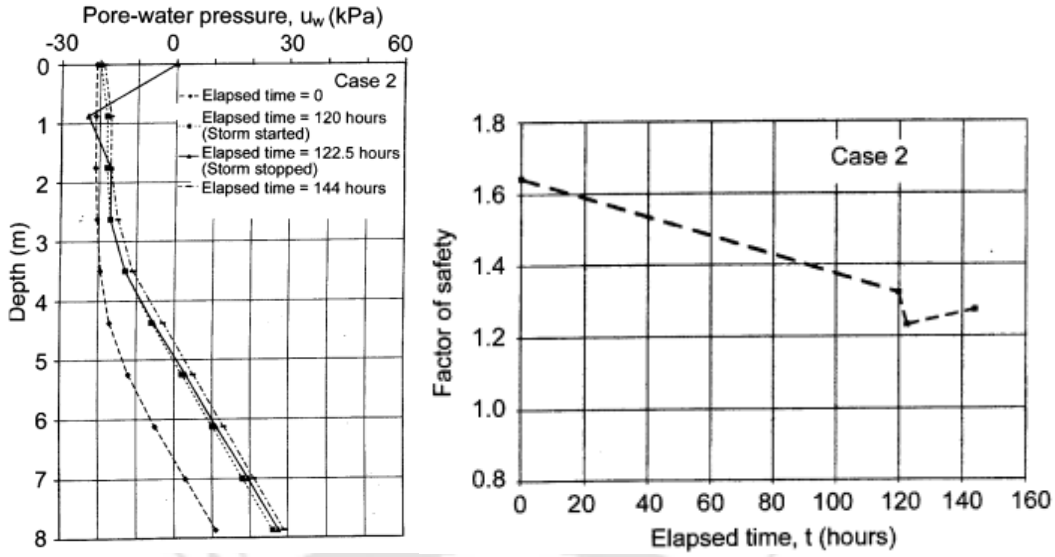


(a) (b)

Figure 2.22 (a) Pore pressure profile (b) Variation of safety factor with time (Rahardjo et al., 2001)

Cho and Lee (2001) performed an unsaturated infiltration analysis on non-homogeneous slopes utilizing the finite element method. The model of the slope with different dimensions is shown in Figure 2.23. The factor of safety was evaluated from the stress field obtained from the finite element analysis. They concluded that with rainfall infiltration the critical slip surface moves towards the slope surface due to a decrease in matric suction.

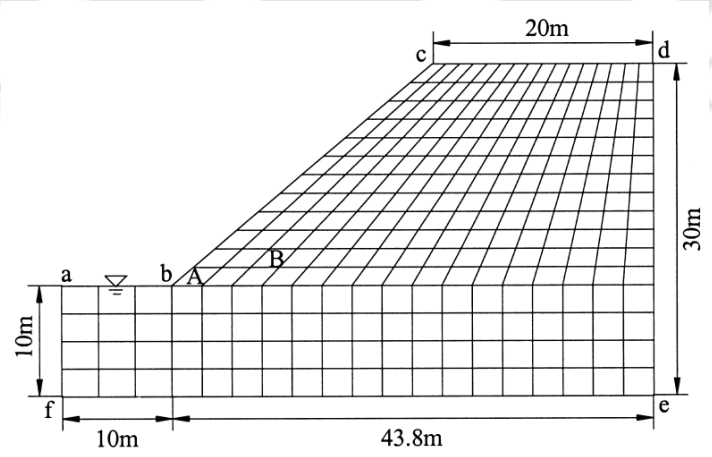


Figure 2.23 Slope model with finite element mesh (Cho and Lee, 2001)

They modelled two types of non-homogeneous slopes based on the direction of hydraulic conductivity. The first is where the slope is modelled horizontally with three layers having



TH-2008_136104008

different hydraulic saturated conductivities. The second model consists of slope parallel layers with high permeable material at the top and low permeable soil at the bottom. The pore pressure contours of the layered slopes are shown in Figure 2.24 (a) and (b). Figure 2.25a illustrates the critical slip surfaces obtained for the horizontally layered slope at different times during rainfall infiltration. Figure 2.25b represent the critical slip surfaces of the slope with layers parallel to the slope surface.

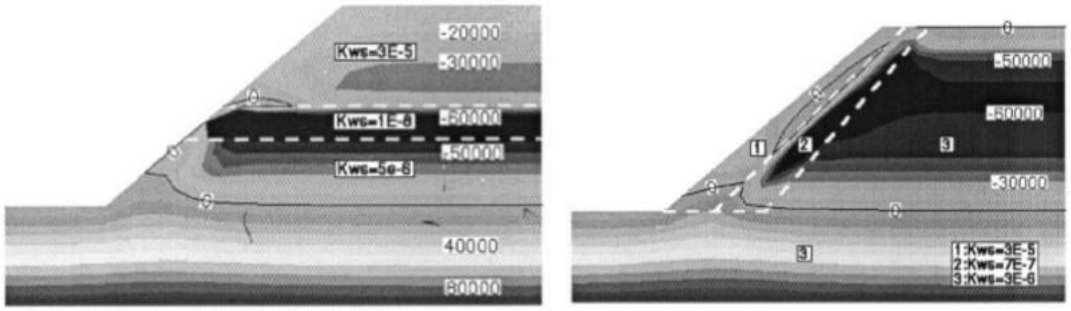


Figure 2.24 Pore pressure (Pa) distribution (a) horizontally layered slope (b) slope parallel layers (Cho and Lee, 2001)

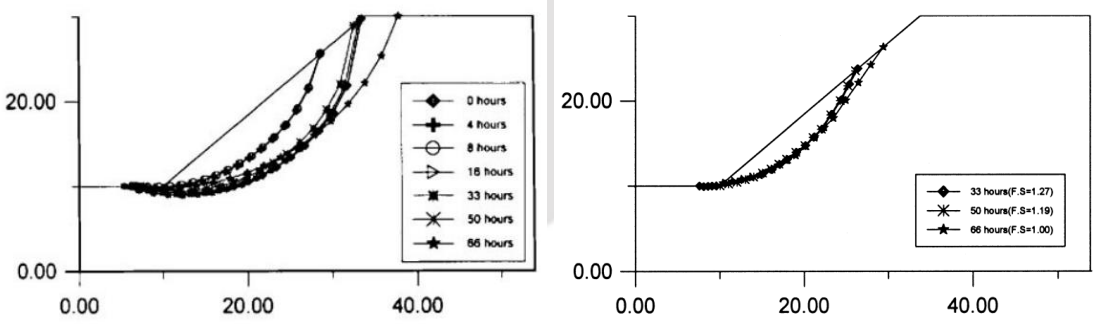


(a) (b)

Figure 2.25 Critical slip surface (a) horizontal layers and (b) slope parallel layers (Cho and Lee, 2001)

Kim et al. (2002) applied finite-element limit analysis to slopes with inhomogeneous soil profiles (in terms of unit weight, cohesion, or friction angle) and irregular slope geometry (Figure 2.26), subjected to the effects of pore water pressures. PCSTABL6 (Bandini and Salgado, 1999) was used for the determination of safety factor by limit equilibrium method, Spencer's method. They made a comparison of the critical slip surface, which produces the



TH-2008_136104008

minimum factor of safety for limit equilibrium, and the velocity field from the lowest upper bound and with the stress field from the highest lower bound.

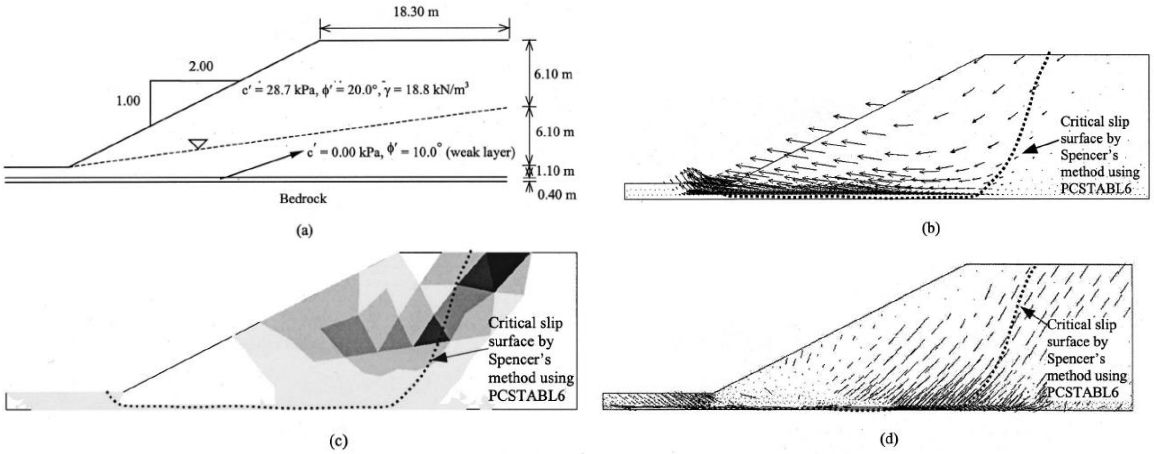


Figure 2.26 Slope analyzed in example [with pore water pressure defined by GWL; dotted line in (a)]: (a) slope geometry and soil profile (after Fredlund and Krahn 1977); (b) velocity field from upper-bound analysis; (c) plastic zone from upper-bound analysis; and (d) principal stress zone from lower-bound analysis. (Kim et al., 2002)

A slope with a weak layer underneath (Figure 2.26) was used and the lower and upper-bound factors of safety were found to be 1.10 and 1.23. Figure 2.26 represents the results obtained by different approaches. Fredlund and Krahn's (1977) solution lies close to the upper-bound result while Leshchinsky and Huang's (1993) result lies in between the upper and lower bound solution obtained from this study.

Kumar and Samui (2006) used the upper bound limit analysis to compute stability numbers for layered soil slopes. The rupture surface was assumed as a combination of different logarithmic spiral arcs with a common focus. The computations, however, were exclusively performed only for a two layered soil slope (Figure 2.27). The cohesion and unit weight of the two layers were assumed to be the same but the angle of internal friction was different. The effect of the pore water pressure and horizontal earthquake body forces was also incorporated in the computations. The critical height ($H_c$) of the slope is determined when the sloping mass is on the verge of collapse (shear failure). The method was successfully applied for a two-layered soil slope and a series of non-dimensional charts providing the values of stability numbers were



TH-2008_136104008

developed by incorporating the effect of pore water pressure as well as horizontal earthquake body forces. For given values of $\gamma$ and $c$, a reduction in $N_S$ (Figure 2.27) with an increase in the relative thickness of the strata having a smaller value of $\phi$, especially for mild slopes, was clearly noted.

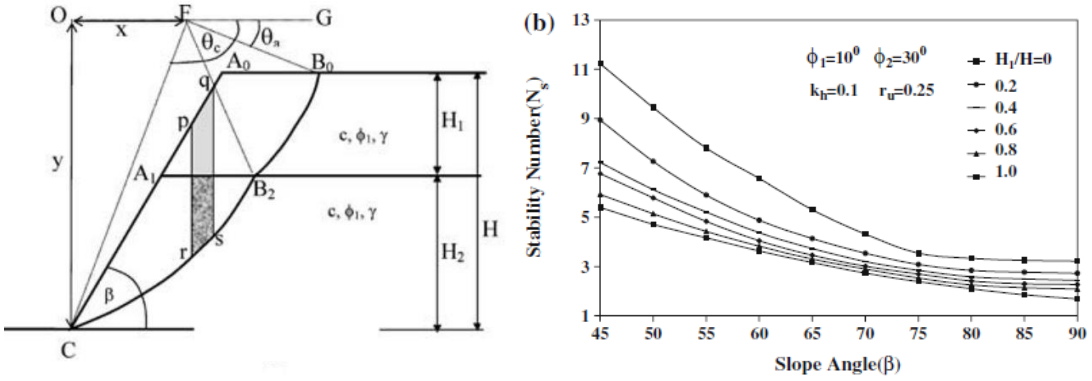


(a) (b)

Figure 2.27 (a) Collapse mechanism for a two-layered slope (b) Variation of $N_s$ with $\beta$ for $k_h$ = 0.1, $r_u$ = 0.25, $\phi_1$ = 10°; $\phi_2$ = 30° (Kumar and Samui, 2006)

Hammouri et al. (2008) compared finite element analysis with limit equilibrium approach for both homogeneous and inhomogeneous soils taking into account the rapid drawdown condition, the undrained clay soils and the presence of tension cracks. The analyzes were carried out using PLAXIS 8.0 (finite element method) and SAS-MCT 4.0 (limit equilibrium approach). The location of the critical failure surface and a factor of safety were compared. Figure 2.28 shows that slip surface obtained using FEM remains constant for different location of cracks. From the results, they suggested that the value of the safety factor was controlled by the weight of the water and observed that by increasing the cohesion for the foundation layer, the stability increased when the critical slip surface passed through that layer. However, if the critical slip surface passed through the toe, the value of the safety factor will not change because of the fixed value of cohesion for the top layer. Therefore, the location of the critical slip surface controls the safety factor. As the FEM presents a deep slip surface (i.e. base failure), the safety factor is higher.



TH-2008_136104008

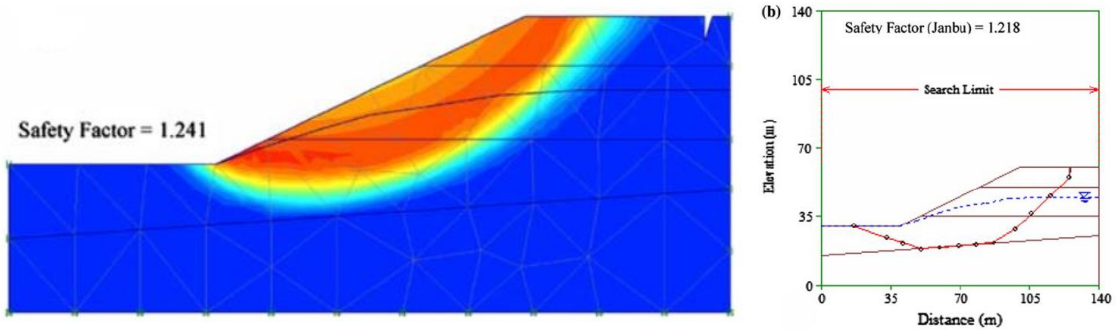


(a) (b)

Figure 2.28 (a) Contour of total displacement using FEM for *S* = 25 m (b) Critical noncircular slip surface using LEM for *S* = 25 m (after Hammouri et al., 2008)

Cho (2009) modified the Moore's infiltration model (Moore 1981) to include situations that are more general where water moves upward from a perched water table in a reducing conductivity profile. A one-dimension infiltration model within the infinite slope framework was used to evaluate the consequences of infiltration on a two-layered slope. Rahardjo et al. (2010) performed parametric studies to investigate the effects of groundwater level position, rainfall intensity and soil properties on slope stability. Figure 2.29 shows the slope geometry of Bukit Timah Granite from Marsiling road location and the variation of safety factor with time for the two slopes from Marsiling Road and Jalan Kukoh.

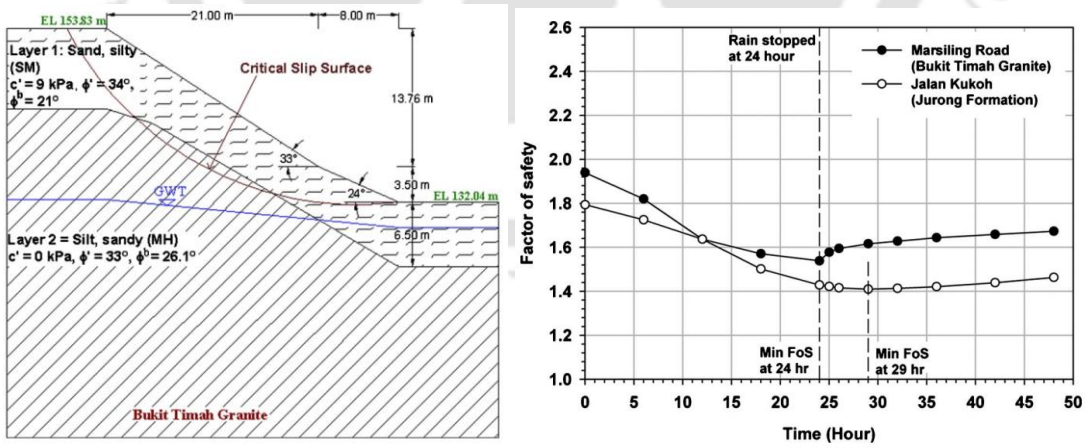


(a) (b)

Figure 2.29 (a) Soil slope from Bukit Timah at Marsiling Road (b) Factor of safety variation (Rahardjo et al., 2010)

Results from the case studies of two-layered slopes from two different places show considerable agreement with the parametric results. Lu and Godt (2013) investigated a steep



TH-2008_136104008

hillslope as shown in Figure 2.30a. A 5 m deep profile B-B′ observed in the figure was used to represent moisture and pressure profiles.

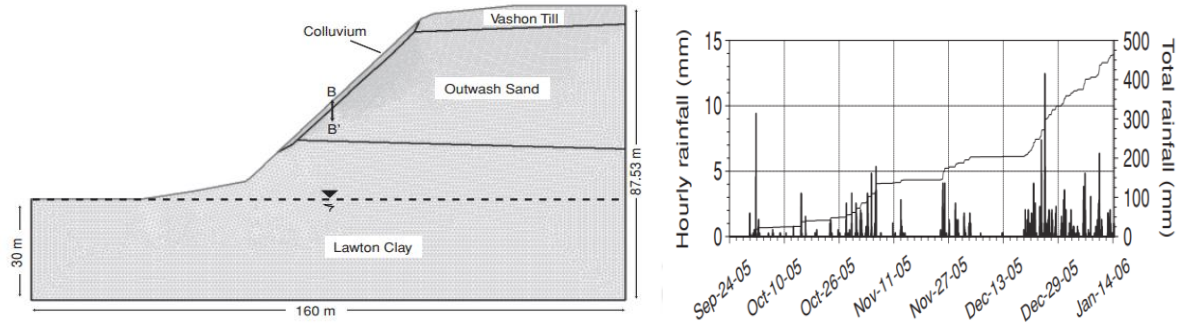


(a) (b)

Figure 2.30 (a) Geometry, finite-element mesh, initial conditions, and simplified geology of the slope (b) Hourly and cumulative rainfall (Lu and Godt, 2013)

The hillslope is a coastal bluff north of Seattle, Washington. The bluff consists of a glacial sedimentary sequence of fine-grained lacustrine silt (Lawton Clay) overlain by an advance outwash sand, which is capped by a till. The bluff face is mantled by a thin (<2 m thick) sandy colluvium. The rainfall data recorded is shown in Figure 2.30b. A shallow landslide occurred on 14 January 2006, which had a depth of 1.5 m below the original ground surface. The progress of wetting front with time is illustrated in Figure 2.31a, which shows the variation of moisture content with depth. The sudden decrease in moisture content occurs at the interface of colluvium and outwash sand that is at a depth of 2 m from the surface. On the day of the slide, (14 January 2006) the moisture content at the surface was 0.4 near to full saturation. Figure 2.31b depict the variation of a factor of safety with depth. It is observed that the safety factor of the colluvium layer increased with depth to almost 1.2 to 2 m from the surface. The safety factor suddenly decreased at the interface very much similar to the moisture profile of the slope. With water infiltrating into the slope, the pore pressures increased ultimately leading to failure in the top few centimetres of the slope surface.



TH-2008_136104008

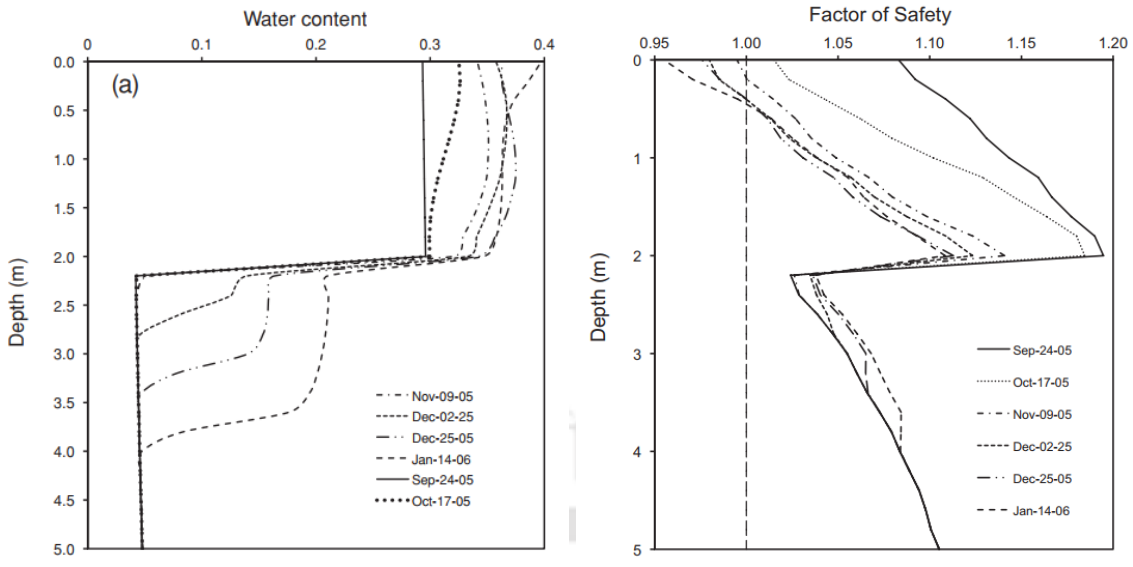


(a) (b)

Figure 2.31Simulated evolution of (a) moisture content (b) factor of safety at the B-B′ profile (Lu and Godt, 2013)

Qian et al. (2014) used finite-element upper and lower bound limit analysis to assess the short-term stability of slopes in which the slope material and subgrade foundation material have two distinctly different undrained strengths (Figure 2.33). Stability charts were proposed, and the exact theoretical solutions were bracketed to within 4.2% or better. In addition, results from the limit-equilibrium method (LEM) has been used for comparison. The numerical upper-bound (UB) and lower-bound (LB) limit analysis methods developed by Lyamin and Sloan (2002) and Krabbenhoft et al. (2005) are used to produce stability charts by considering two-layered purely cohesive soils. Limit-equilibrium analysis [Bishop's (1955) simplified method] was adopted for comparison. In this study, the stability numbers were presented using chart solutions. The true solutions were bracketed within 8% or better. By observing the UB plastic zones, the majority slope failure mode was a base failure. A range of slope inclinations ($\beta$ = 15-75$^o$) and depth factors ($d/H$ = 1.5-5) are taken into account. The variation of stability number with $d/h$ ratio is shown in Figure 2.32a. Figure 2.32b shows the plastic zones for $\beta$ = 30°, $c_{u1}/c_{u2}$ = 0.66 and $d/h$ ratios 3-5. Figure 2.32b shows that the depth of failure surface increases as $d/h$ ratio increases and the failure surface involves soils in both the regions.



TH-2008_136104008

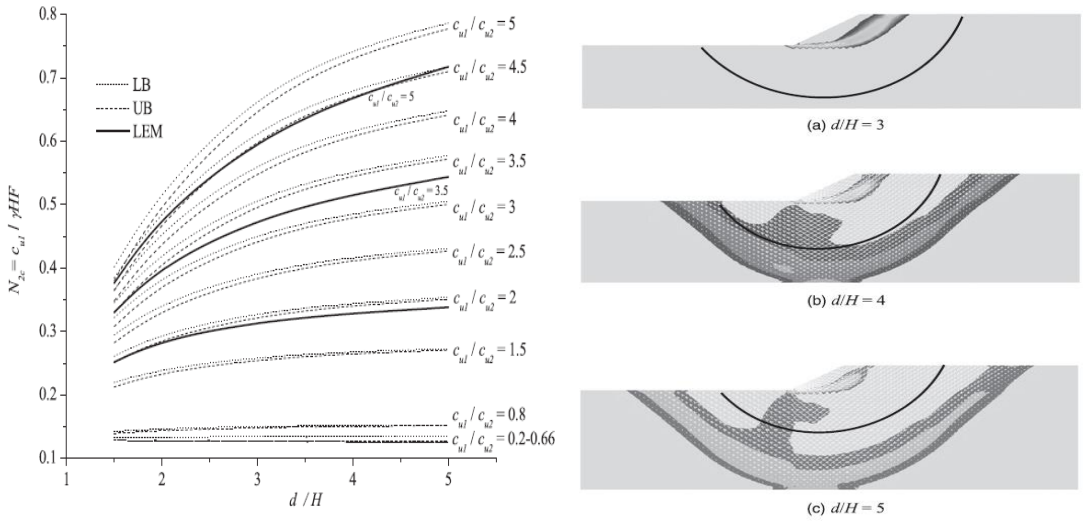


(a) (b)

Figure 2.32 (a) Chart solutions for β=30° (b) Transition of UB plastic zones for $\beta$ = 30° and $c_{u1}/c_{u2}$ = 0.66: (a) $d/H$ = 3; (b) $d/H$ = 4; (c) $d/H$ = 5 (Qian et al., 2014)

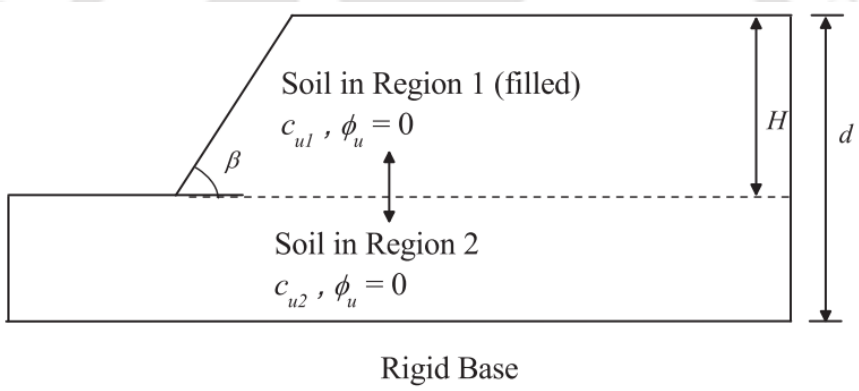


Figure 2.33 Problem configuration for cohesive material filled on purely cohesive soil (Qian et al., 2014)

Ni et al. (2016) created two-layered slope models with a different interface with surcharge loading. A parametric study was also performed to study the influence of interface, slope inclination and strength properties. Figure 2.34 illustrates the failure surfaces for a homogeneous slope and non-homogeneous slope with a weak foundation material. Elkamhawy et al. (2018) performed two-dimensional seepage analysis on a slope with a thin soft layer inclined at 30° to the horizontal, to study the influence of rainfall storm and its duration. Pore water pressures and horizontal earth pressures from the experimental model showed that the stability of the slope decreased during rainfall.



TH-2008_136104008

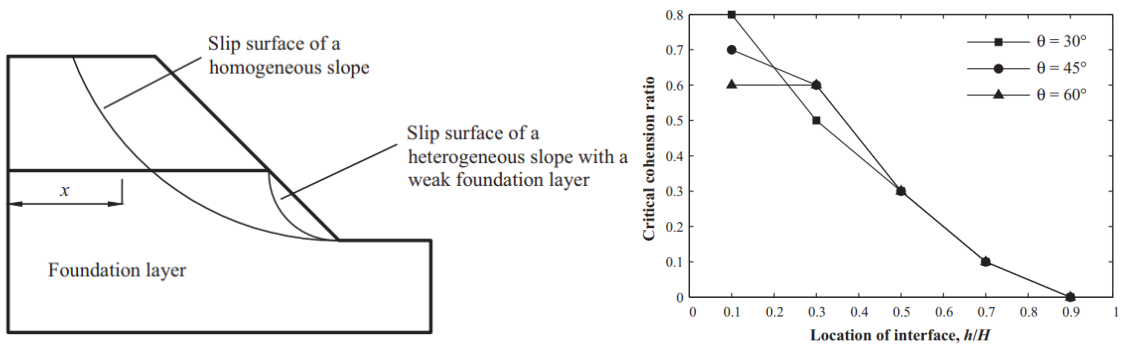


(a) (b)

Figure 2.34 (a) slip surfaces of a homogeneous and heterogeneous slope with a weak foundation layer (b) derivation of critical cohesion ratio as a function of slope geometry and interface formation (Ni et al., 2016)

Dey and Sengupta (2018) presented the details of their study performed on a rainfall induced landslide which caused 160 deaths and destroyed the village at Malin, India. The profile of the slope is shown in Figure 2.35, which consists of two regions. The reported height of the landslide is 190 m and the slide width ranged from 45 to 134 m. They conducted a 2D numerical study of the slope and observed that with continuous rainfall infiltration, a perched water table gets developed near the slope surface which saturates the soil near it. It was concluded that the slope was initially stable but with continued rainfall and increasing rainfall intensity, the slope reached failure state more rapidly. The downward motion of the slope debris under rainwater infiltration destroyed the residential area.

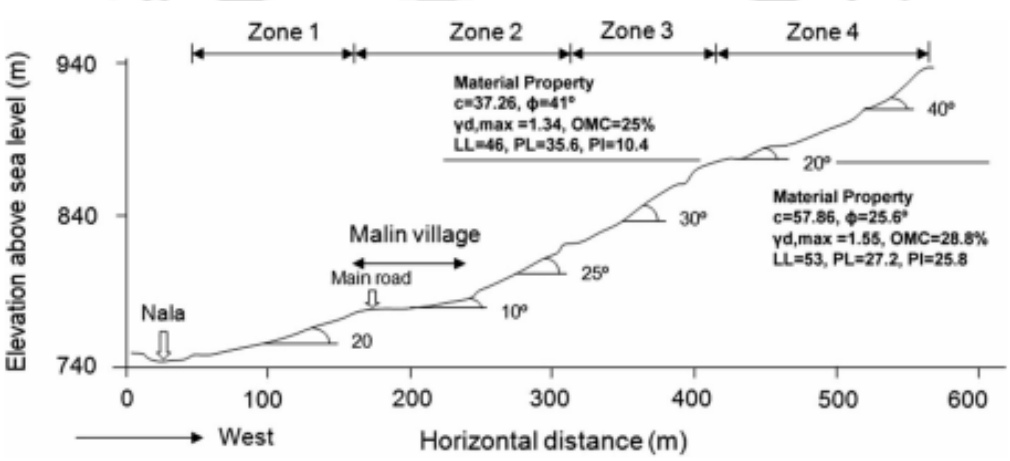


Figure 2.35 Cross sectional profile of the Malin slope (Dey and Sengupta, 2018)



TH-2008_136104008

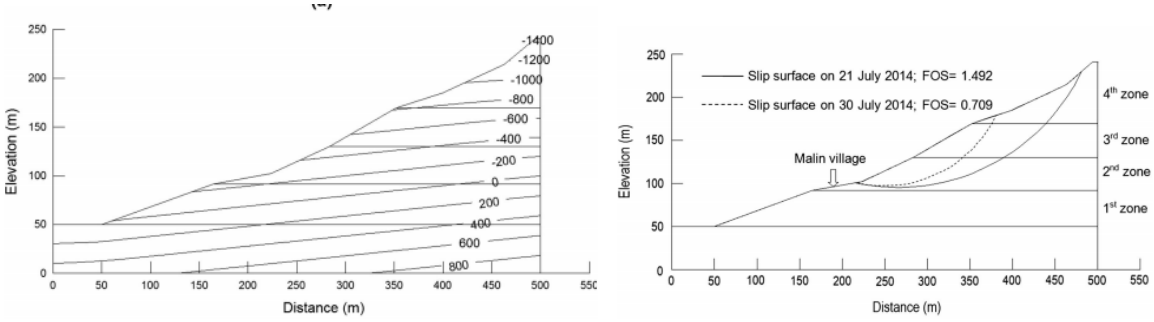


(a) (b)

Figure 2.36 (a) Pore pressure contours at hydrostatic condition (b) Critical slip surface before rainfall and the day when the slide occurred (Dey and Sengupta, 2018)

Figure 2.36a depict the pore pressure contours of the slope prior to rainfall infiltration. Hydrostatic conditions prevail within the slope during the initial stage. Figure 2.36b illustrate the critical slip surface at the initial condition and at a time when the failure occurred after rainfall infiltration. They also conducted a parametric study with variation in rainfall intensity and duration. Figure 2.37a show the critical slip surfaces of the Malin slope at different times under 10 mm/h rainfall intensity. It was observed that the slip surfaces gradually move towards the slope surface with the passage of time. The variation in the factor of safety with time is represented in Figure 2.37b.

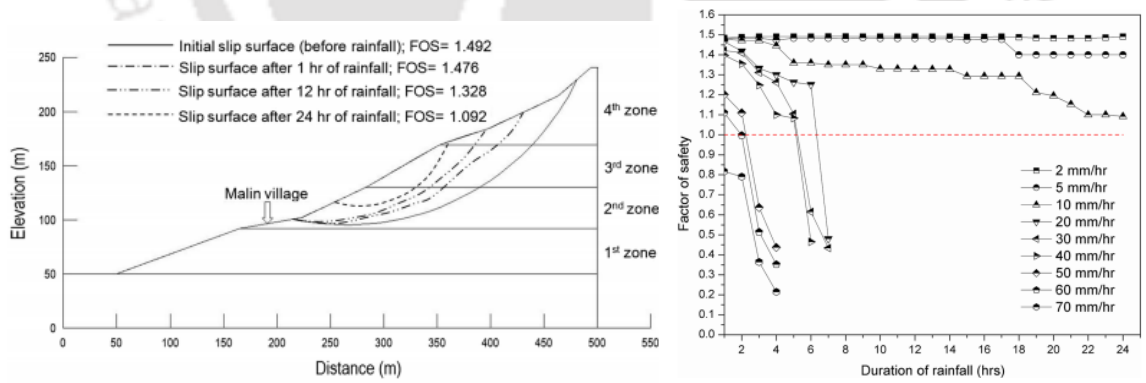


(a) (b)

Figure 2.37 (a) Slip surfaces under 10 mm/h rainfall intensity (b) Change in safety factor with time under different rainfall intensities (Dey and Sengupta, 2018)

It was observed that the slope stays stable until 24 hours under 10 mm/h rainfall intensity. With higher rainfall intensity (> 10 mm/h) the slope reached failure conditions at as low as 7 hours of infiltration and this time reduces with increasing rainfall intensity.



TH-2008_136104008

## 2.5 CRITICAL APPRAISAL OF LITERATURE REVIEW

Stability analysis of slopes is an ancient problem and it is vital for earth structures and hilly regions, which has gathered the attention of many researchers. Rainfall infiltration causes more slope failures than any other natural event. Infiltration leads to variation in hydraulic and mechanical properties in the soil. Different methods are available to analyze slopes ranging from limit equilibrium method to the finite element method. Available literature on homogeneous slopes under rainfall infiltration focusses on the effects of antecedent rainfall, rainfall intensity, duration, slope geometry, ground water level etc. It is evident that soil properties like unit weight, cohesion, friction angle, saturated permeability, soil–water characteristic curve and unsaturated permeability function change as per the stratification or prevailing climate conditions which forms non-homogeneous nature.

Non-homogeneous slopes are normally referred to as slopes consisting of two or more layers or the variation of property with depth. Two-layered slopes commonly encountered in the levee problems consist of different soil material in the foundation and embankment regions. Shear strength property and hydraulic property may vary with depth. The unsaturated permeability function obtained from SWCC is the variation of permeability with suction and suction varies with depth. Most of the literature concerning rainfall infiltration is on homogeneous slopes. The available literature provides information on the advancement of wetting fronts for mainly homogeneous slopes. Considering the importance of non-homogeneous soil slopes behaviour would be different from homogeneous slopes, particularly under rainfall infiltration, a thorough study in this regard is very essential for better understanding the mechanism.

## 2.6 OBJECTIVES AND SCOPE OF THE STUDY

The main objective of the study is to investigate the stability of non-homogeneous layered soil slopes with different types of soil under rainfall conditions. To analyze the non-homogeneous slopes properly under rainfall infiltration, the detailed scope of work is as follows:



TH-2008_136104008

1. Three different soils will be selected with different mechanical and hydraulic properties to model both homogeneous and non-homogeneous slopes.

2. Validation of the methodology will be done with models taken from literature. Homogeneous and non-homogeneous layered slope models will be created with the different soils based on different case studies.

3. To interpret the results of non-homogeneous slopes in a systematic way, first the behaviour of the homogeneous slopes with the different soils will be studied under rainfall infiltration. Parametric studies with varying rainfall intensity, duration, slope angle, and slope height will be performed for non-homogeneous slopes.

4. The effect of transient seepage under rainfall infiltration will be investigated to gain information about pore water pressures. The change in pore pressures, the rise of water level and a factor of safety within the slopes will be studied.

5. Two-layered and three-layered non-homogeneous slopes will be studied under rainfall infiltration. The influence of different parameters like rainfall intensity, duration, slope angle, and slope height will be studied.

6. The different types of failure mechanisms from critical slip surfaces occurring within the slopes will be investigated.

## 2.7 SUMMARY

The present chapter presented literature relevant to the research topic in brief with emphasis on non-homogeneous slopes. The review of the literature illustrates the different approaches adopted to analyze the stability of slopes. Slopes were analyzed using limit equilibrium, limit analysis, strength reduction finite element techniques. Studies on both homogeneous and non-homogeneous slopes were discussed in brief. Examples of non-homogeneous slopes include variation of cohesion with depth and presence of different layers. Stratified layers of soil within



TH-2008_136104008

the slope were mainly used as case studies. Two-layered slopes with different foundation material were modelled as non-homogeneous slopes and the effect of strength ratio was presented. Most of the work on non-homogeneous slopes were based on the limit analysis procedure. The critical appraisal of the literature review was presented along with the objective and scope for further work.

भारतीय प्रौद्योगिकी संस्थान गुवाहाटी • Indian Institute of Technology Guwahati •



TH-2008_136104008

# Chapter 3 MATERIALS AND METHODOLOGY

## 3.1 INTRODUCTION

Different soils were selected to study the stability of both homogeneous and non-homogeneous slopes. Various laboratory tests were conducted to determine the engineering properties of the soils. Basic physical properties, mechanical properties and hydraulic properties of the soils were evaluated. Two different methods are discussed which were used to determine the stability of the slopes. One each from the limit equilibrium method and finite element method. The method, which was used to search for the critical slip surface, is explained. The basic theory pertaining to seepage in unsaturated soils is discussed later. The unsaturated strength model incorporating the suction factor has been also discussed in this chapter.

## 3.2 MATERIAL PROPERTIES

Hill slopes in and around Guwahati consists of residual soils. The slopes are moderately steep in nature and experience heavy rainfall during the rainy seasons. In general ground water level is situated at great depths, which rises during the monsoon season. This region generally consists of two types of soils viz the reddish soil (silty clay) and the yellowish soil (silty sand). Figure 3.1 show how the slopes are formed with two types of soils. The reddish soil (silty clay) covers the major portion of the slopes while the yellowish soil is found at various depths due to weathering of rocks. This yellow soil (silty sand) is primarily the major concern for landslides occurring in this area. There are numerous cases of slope failures (Umrao et al., 2017) occurring in this area mainly due to rainfall effects. A third soil is selected from the literature of similar nature found in hilly areas.

To evaluate the physical and engineering properties of the soils, different laboratory tests were conducted. The details of the material properties obtained from the tests are presented in the following sections.



TH-2008_136104008

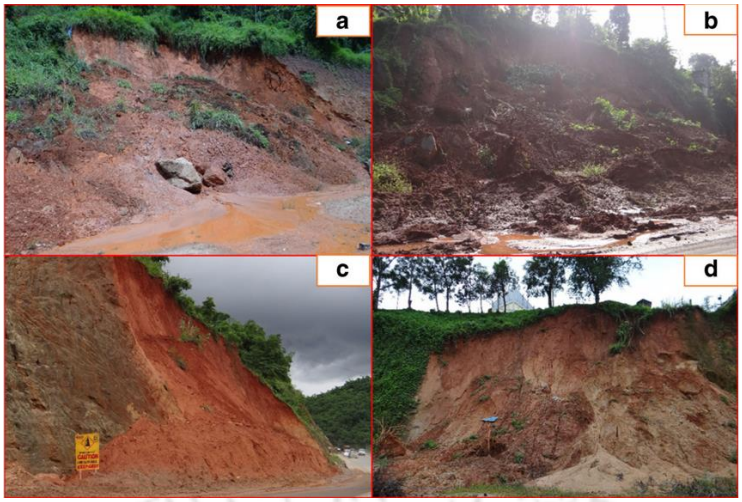


Figure 3.1 Rain induced slope failures along NH-40 due to saturation of soil masses at (a) Sumer village (b) 1 km south of Sumer village (c) Karbalu village and (d) Jyntru village (Umrao et al., 2017)

### 3.1.1 Soil-1

Soil-1 is reddish in colour (Figure 3.2) and is the most common in hills around Guwahati. Its specific gravity was determined as per the ASTM D 0854-06 (IS: 2720 part 3) and was found to be 2.61. The combined particle size analysis of this soil was determined using the wet sieve analysis, as per ASTM D6913-17 (IS: 2720 part 4) and sedimentation analysis as per ASTM D7928-17, particle-size distribution curve is shown in Figure 3.3. The soil has $D_{10}$ = 0.12 mm, $D_{30}$ = 0.18 mm, $D_{60}$ = 0.29 mm, uniformity coefficient ($C_u$) of 2.42 and coefficient of curvature ($C_c$) of 0.93. As per the Unified Soil Classification System (USCS) (ASTM D2487-06) (IS: 1498), the soil is classified as silty clay (CL).

Figure 3.2 Soil-1 (Silty clay)



TH-2008_136104008

The maximum dry density and optimum moisture content, of this soil, as determined according to ASTM D 698 are 1.58 g/cc and 22.4%, respectively. The field density is 1.76 g/cc and its corresponding moisture content is 20.3%. The permeability of the soil specimen was found to be $8.38\times10^{-6}$ m/sec. The friction angle ($\phi'$) and cohesion ($c'$) was approximately 30° and 10 kPa respectively.

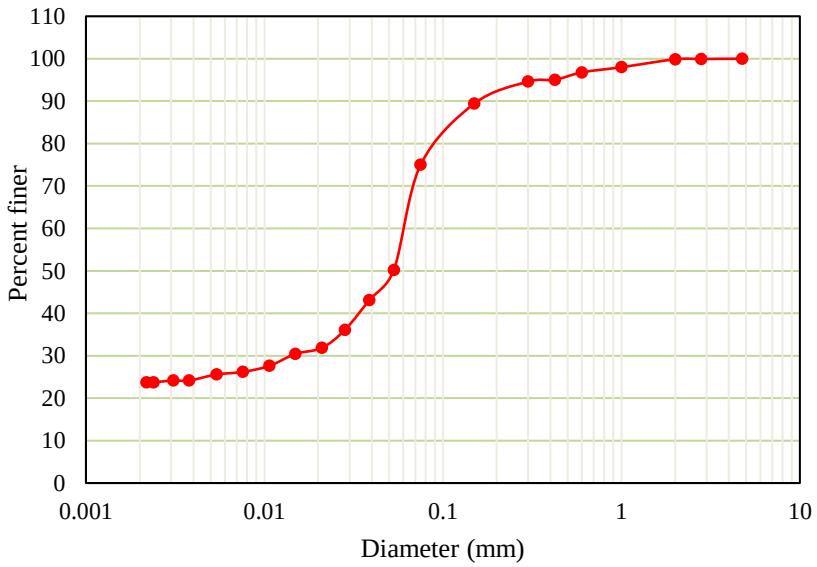


Figure 3.3 Particle size distribution curve for Soil-1

### 3.1.2 Soil-2

Soil-2 is yellowish in colour (Figure 3.4) and is overlain by the red soil in most of the hill slopes in Guwahati. Its specific gravity was determined as per the ASTM D 0854-06 (IS: 2720 part 3) and was found to be 2.44. The particle size analysis of this soil was determined using the wet sieve analysis, as per ASTM D 6913-04 (IS: 2720 part 4) and sedimentation analysis as per ASTM D7928-17, particle-size distribution curve is illustrated in Figure 3.5. The soil has $D_{10}$ = 0.095 mm, $D_{30}$ = 0.16 mm, $D_{60}$ = 0.25 mm, uniformity coefficient ($C_u$) of 2.63 and coefficient of curvature ($C_c$) of 1.08. As per the Unified Soil Classification System (USCS) (ASTM D2487-06) (IS: 1498), it is classified as poorly graded silty sand (SM).



TH-2008_136104008

Figure 3.4 Soil-2 (Silty sand)

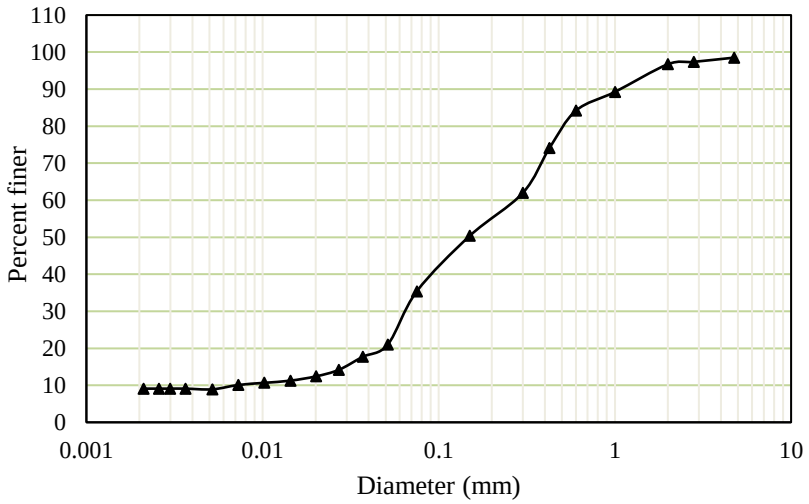


Figure 3.5 Particle size distribution of Soil-2

The permeability of the soil specimen was determined to be $6.6\times10^{-5}$ m/sec. The friction angle ($\phi'$) from the direct shear test and simple triaxial tests at maximum dry density (MDD) and optimum moisture content (OMC) was approximately 36°. Standard Proctor tests were carried out on remoulded samples to determine the MDD and OMC of the soil sample. The maximum dry density and optimum moisture content, of this soil, as determined according to ASTM D 698 are 1.52 g/cc and 14.8%, respectively shown in Figure 3.6. The field density is 1.68 g/cc and its corresponding moisture content is 10.92%. The field density and moisture content of the soil was measured using core-cutter method. The soil samples were collected from three different heights of the slope.



TH-2008_136104008

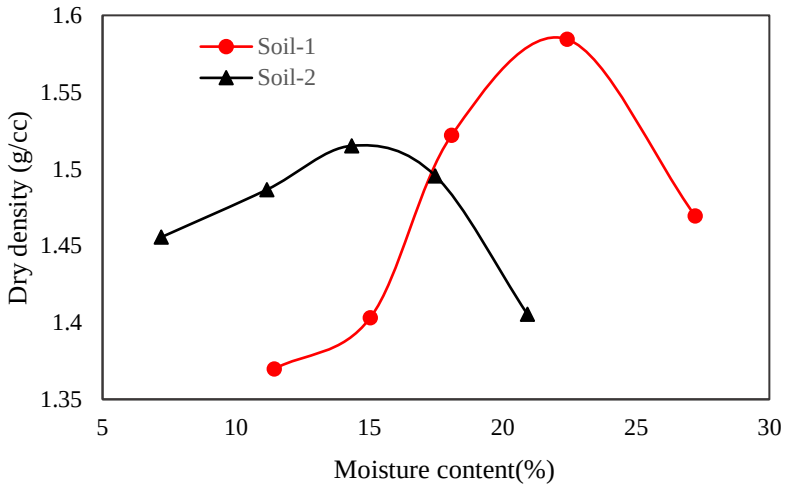


Figure 3.6 Compaction test curves for two soils

### 3.1.3 Soil-3

Properties of the third soil (Soil-3) were obtained from Kellezi et al. (2005) which was also classified as silty clay (CL), similar to Soil-1. The reported properties were: specifc gravity - 2.7; Liquid limit - 41.5% and plastic limit -23.2%; and Void ratio - 0.78. The friction angle ($\phi'$) and cohesion ($c'$) were reported as 18° and 25 kPa, respectively. The saturated permeability of the soil is $8.3\times10^{-7}$ m/sec.

The complete physical and mechanical properties of Soil-1, Soil-2 and Soil-3 are tabulated in Table 3.1. The $\phi^b$ values for the soils were assumed to be equal to $\phi'$ as suggested by Zhang et al. (2013). Zhang et al. (2013) recommended that $\phi^b$ can be taken equal to $\phi'$ for soils with air entry value (AEV) greater than 200 kPa. The three soils selected for study have AEVs greater than 200 kPa and considering the logistical difficulties in determining the $\phi^b$ value, the $\phi^b = \phi'$ assumption was considered. The two different friction angles are angle of internal friction ($\phi'$) and the angle ($\phi^b$) defining the increase in strength due to suction in unsaturated analysis.

### 3.1.4 Soil–water characteristic curves of the soils

Three experimental soil–water characteristic curves (data) were taken from Bordoloi et al. (2018), corresponding to Soil-1, Soil-2 and Soil-3 in the present study as shown in Figure 3.7.



TH-2008_136104008

To derive the soil–water characteristic curves of the soils, the Van Genuchten (1980) model was used as shown in Eq. 4. The SWCC of the three soils is depicted in Figure 3.7.

Table 3.1 Physical properties and shear properties of three soils

| **Property** | **Soil-1** | **Soil-2** | **Soil-3** (Kellezi et al., 2005) |
|---|---|---|---|
| Specific gravity | 2.61 | 2.44 | 2.7 |
| Void ratio | - | - | 0.78 |
| Liquid limit (%) | 46 | 39 | 41.5 |
| Plastic limit (%) | 23 | Non-plastic | 23.2 |
| Moisture content (%) | 20.3 | 10.92 | 24.6 |
| Maximum dry density (g/cc) | 1.58 | 1.52 | - |
| Optimum moisture content (%) | 22.4 | 14.8 | - |
| USCS classification | CL | SM | CL |
| $\gamma$ (kN/m$^3$) | 17.6 | 16.8 | 19 |
| $c'$ (kPa) | 10 | 0 | 25 |
| $\phi'$ ($^o$) | 30 | 36 | 18 |
| $\phi^b$ ($^o$) | 30 | 36 | 18 |
| Saturated hydraulic conductivity, (m/s) | $8.38\times10^{-6}$ | $6.6\times10^{-5}$ | $8.3\times10^{-7}$ |

Based on Van Genuchten (1980) fitting parameters obtained from RETC (Retention Curve) program (Van Genuchten et al. 1991) for the three soils tabulated in Table 3.2, the permeability functions of the three soils were evaluated. Mualem's (1976) model (Eq. 5) was used to determine the permeability functions of the three soils. The Van Genuchten parameters ($\alpha$, $n$, $m$, $\theta s$) and saturated permeability of the three soils were used to determine the permeability function of the three soils. Figure 3.8 illustrates the permeability functions of the three soils. The air entry value obtained from the SWCC of the three soils is all above 200 kPa. The air entry value of Soil-1, Soil-2 and Soil-3 are 400 kPa, 300 kPa and 350 kPa, respectively.

RETC (Van Genuchten et al. 1991) is a computer code used to evaluate the soil–water



TH-2008_136104008

characteristics curve (soil–water retention curve) and unsaturated permeability functions of partially saturated soils. It utilizes different models like Brooks-Corey (1964), van Genuchten (1990), Durner (1994) to define the SWCC of soils. Some of the models incorporated in the program to define the unsaturated permeability functions are Burdine (1953) and Mualem (1976). To evaluate the unknown parameters of the above-mentioned models, it employs a non-linear least squares optimization procedure. This program can be used to get the permeability function from the retention data and the saturated permeability of the soil. It allows the user to fit analytical functions with observed laboratory or field data.

Table 3.2 Parameters used to evaluate SWCC and permeability functions of soils

| Soil type | $\alpha$ | $n$ | $m$ | $\theta_s$ |
|---|---|---|---|---|
| Soil-1 | 0.005 | 1.26 | 0.21 | 0.43 |
| Soil-2 | 0.065 | 1.22 | 0.18 | 0.22 |
| Soil-3 | 0.0013 | 1.92 | 0.48 | 0.33 |

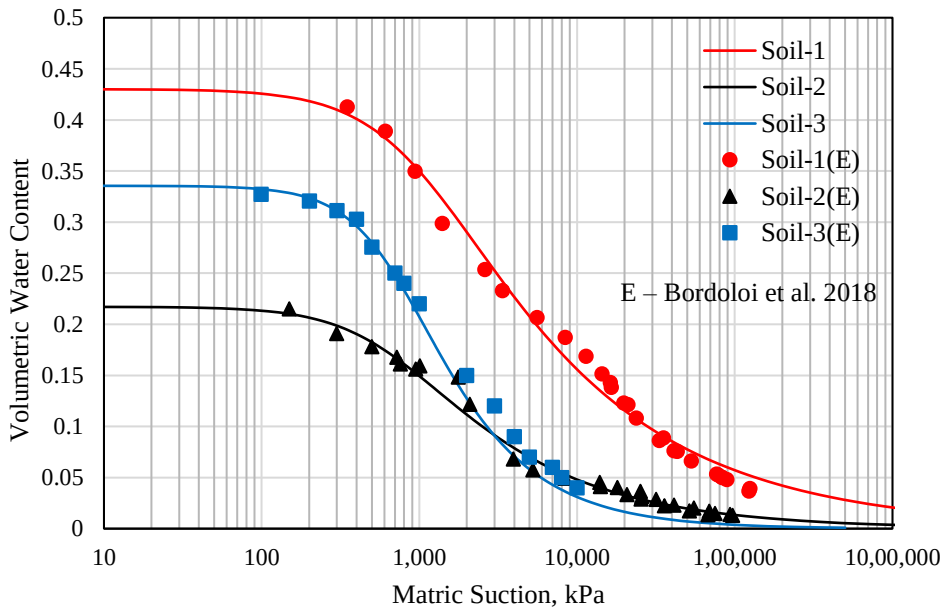


Figure 3.7 Experimental data and fitted curve of SWCC of the three soils used in the study



TH-2008_136104008

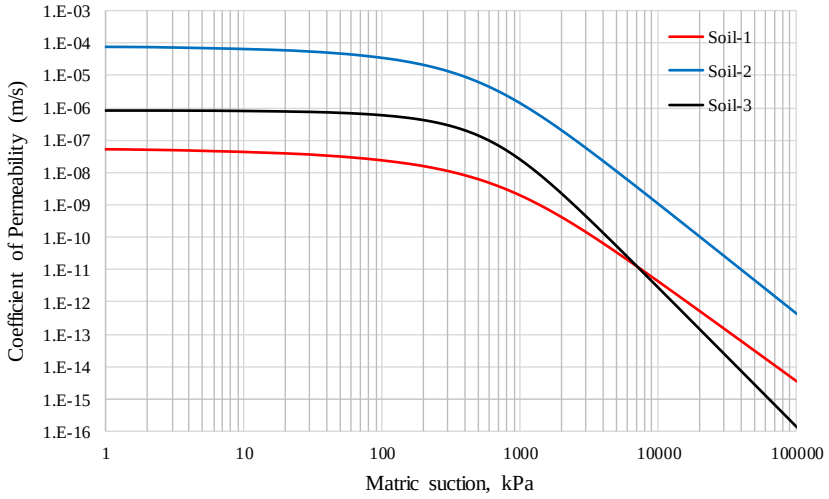


Figure 3.8 Permeability functions of the three soils used

### 3.1.5 Strength variation with moisture content (Soil-1)

The degree of saturation in a natural slope is generally more at a depth near the surface and ranges from 20% to 70% (Song et al. 2016) and may vary with depth. To represent in-situ conditions prevailing in the field, different moisture contents were selected and accordingly Soil-1 samples were prepared to represent the various saturation levels. To attain the different moisture contents, the degree of saturation, $S_r$ was varied as 0%, 20%, 40%, 60% and 80%. Unconfined compression strength (UCS) tests (ASTM D2166-00, 2000) and Unconsolidated Undrained (UU) triaxial tests were performed to evaluate the strength properties at different saturation values. A sample length of 140 mm and a diameter of 70 mm was selected as the sample size for the UCS tests. The density ($\rho$) of the soil sample was kept as 1.57 g /cc and the saturated moisture content for the soil is 25.19%. The dry density and the volume of the mould, the amount of dry soil sample was found out. From the respective degree of saturation, the amount of water required was calculated and mixed with the dry soil sample. From the mould dimensions, the dry weight of the soil sample comes 846 gm, which was mixed with 42.6 ml (5.04%) of water to prepare the sample at 20% degree of saturation for Soil-1. Similarly, the other samples were prepared for other saturation percentages as shown in Table 3.3. After the preparation of the cylindrical sample, the total weight was again calculated before the



TH-2008_136104008

commencement of the test. The tests were performed at a displacement rate of 0.128 mm/min strain rate and sheared till 20% strain or until the failure of the sample.

Figure. 3.9 depicts the axial stress-strain relation for the soil at different degrees of saturation. As the saturation percentage of the soil is increased, the strength of the soil is gradually decreased. The increase in strength of the soil is low when the saturation of the soil reduces from 80% to 40%. Table 3.3 enlists the shear strength values for the soil at different degrees of saturation. The soil has a maximum unconfined compressive strength of 98 kPa at 0% saturation. The strength of the soil reduces to 73 kPa at 20% saturation. The rate of decrease of UCS is maximum till 40% saturation. The UCS of the soil is 36 kPa at 60% saturation. With further increase in saturation, the strength of the soil reduces to 24 kPa at 80% saturation. At the same strain level, the soil depicts reduced strength with increase in degree of saturation. It is observed that with the increase in degree of saturation of the soil, the stiffness of the soil decreases.

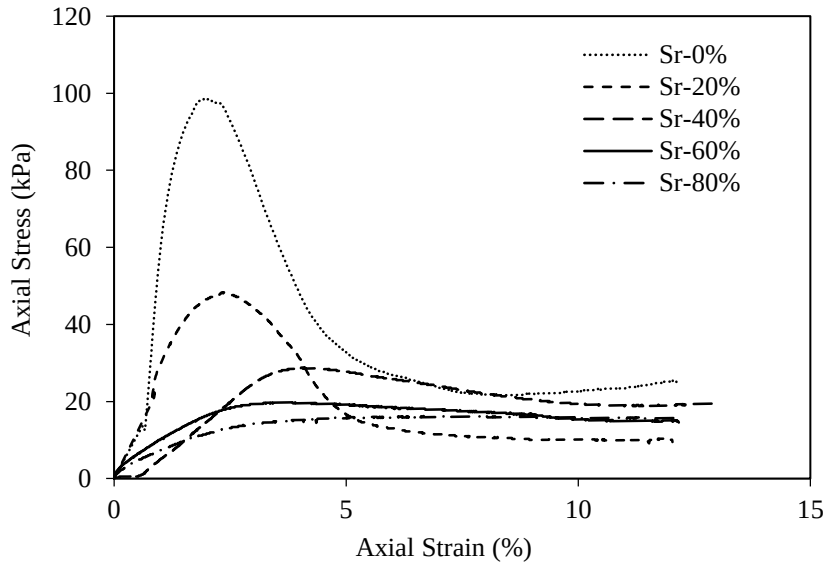


Figure. 3.9 Stress-strain curves for soil at different initial degree of saturation $S_r$

The relationship between UCS and the degree of saturation for the soil is shown in Figure. 3.10. The soil shows a non-linear pattern of decrease of unconfined compressive strength with a degree of saturation.



TH-2008_136104008

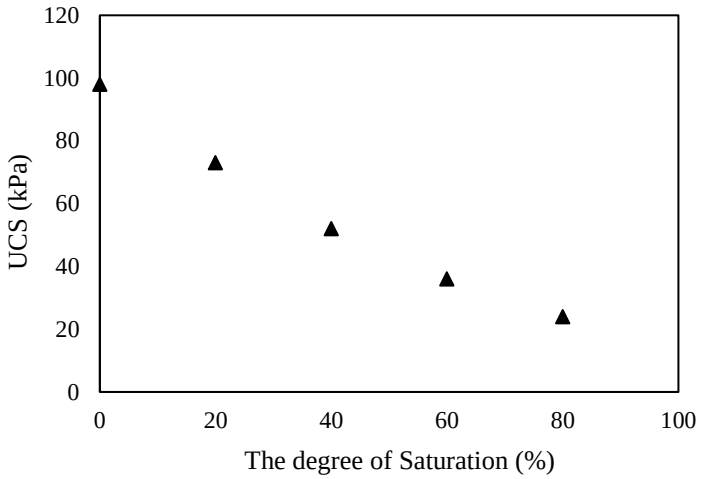


Figure. 3.10 Relationship between degree of saturation and peak UCS values

Figure 3.11 shows the stress-strain curves of the soil specimens obtained from UU tests at 100 kPa confining pressure. The maximum deviator stress of the soil is decreased with increase in moisture content of the soil. It is observed that there is no peak stress but the soil strain hardens with an increase in strain. The failure of the soil sample was marked by a bulging phenomenon at the middle portion of the sheared soil sample.

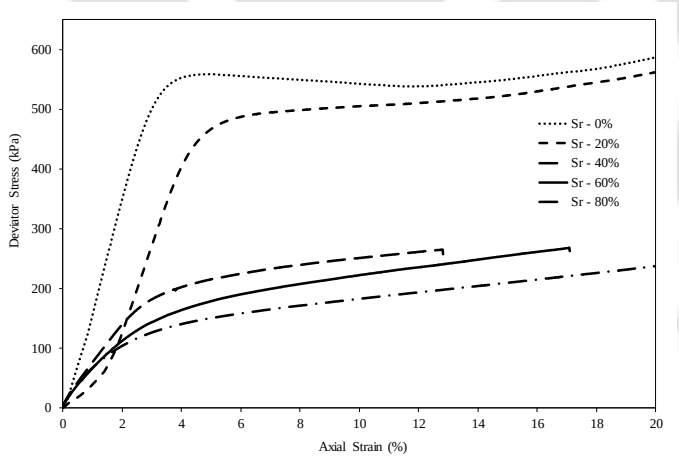


Figure 3.11 UU triaxial test results (100 kPa confining pressure) for soil specimens at different saturation levels

For the evaluation of strength parameters, Mohr's circles were drawn at different confining pressures. The strength of the soil i.e., cohesion and angle of internal friction was determined at each moisture content based on Coulomb failure theory. Table 3.3 shows the strength properties evaluated for the Soil-1 material at different degrees of saturation. It is observed that



TH-2008_136104008

both the friction angle and cohesion are reducing with an increase in moisture content. The friction angle ($\phi$) and cohesion ($c$) at 0% saturation were approximately 44° and 10 kPa, respectively. At 20% saturation, $c$ = 8.5 kPa and $\phi$ = 36°, similarly at 40%, 60% and 80% saturation levels, the shear strength parameters were $c$ = 8, 7, 6 kPa and $\phi$ = 32°, 27°, 24.5°, respectively.

Table 3.3 Variation of strength properties with moisture content

| Degree of Saturation, (%) | Moisture Content, (%) | Unit Weight, (kN/m$^3$) | UCS, $q_u$ (kPa) | Cohesion, (kPa) | Friction Angle, (deg) |
|---|---|---|---|---|---|
| 0 | 0 | 15.4 | 98 | 10 | 44 |
| 20 | 5.04 | 16.22 | 73 | 8.5 | 36 |
| 40 | 10.07 | 17.04 | 52 | 8 | 32 |
| 60 | 15.11 | 17.85 | 36 | 7 | 27 |
| 80 | 20.15 | 18.67 | 24 | 6 | 24.5 |

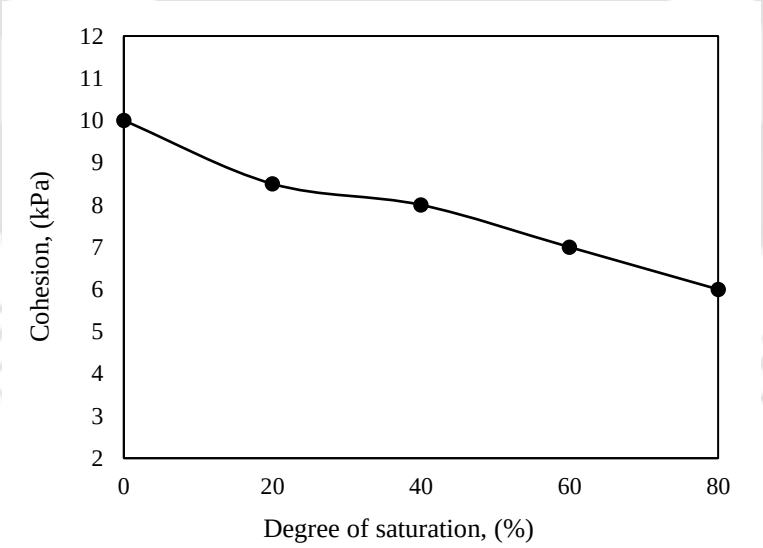


Figure 3.12 Variation of cohesion with moisture content

Figure 3.12 depicts the reduction of cohesive strength with increase in moisture content of the Soil-1. The decrease in the angle of internal friction of the soil is shown in Figure 3.13. The reason for the decrease of friction angle is that when the moisture content increases, the resistance between soil particles decrease due to water acting as a lubricating agent. Studies have shown that for hill slopes containing weathered material at the top 2 m, inter-particle



TH-2008_136104008

frictional resistance mainly provides the shear strength and the cohesive strength typically stays less than 10 kPa (Lu and Godt 2008).

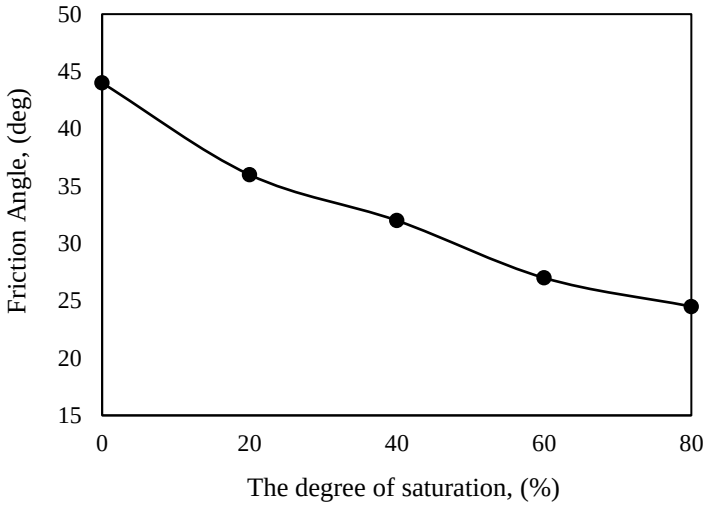


Figure 3.13 Variation of friction angle with moisture content

## 3.3 METHODOLOGY

Different homogeneous and non-homogeneous slope models are considered with three different types of soils, having different mechanical and hydraulic properties, for analysing the slope stability under rainfall conditions. First, seepage analysis will be performed in the finite element framework using the software SLIDE2 v8 (Rocscience 2018a) to obtain pore water pressures in the slopes. The stability analysis for the slopes was performed using the Morgenstern and Price (1965) limit equilibrium framework available in SLIDE2 by selecting random search procedure (Malkawi et al., 2001) to evaluate the lowest factor of safety of the slope and to determine the critical slip surface. While analysing the slopes under rainfall conditions it is essential to consider the seepage in unsaturated soil and shear strength of unsaturated soil, which will be significantly governed by the SWCC of the different soils.

The finite element method (FEM) in RS2 has been used in a limited portion only i.e., for cases where there is no GWL for the stability analysis. For the infiltration analysis, the transient seepage analysis is performed using the FEM in SLIDE2. As the present study requires pore



TH-2008_136104008

water pressures for the analysis under rainfall conditions, finite element method was selected to obtain the pore water pressures at different points from the seepage analysis.

***Seepage in Unsaturated Soil***

The flow of water through the soil (both saturated and unsaturated) is based on Darcy's law (Childs and Collis-George, 1950) (Eq. 1) which states that the hydraulic gradient is proportional to the discharge velocity of water.

$$v = -ki = -\mathrm{k}\frac{\partial h}{\partial z} \tag{1}$$

where, $h$ is the hydraulic head (m), $k$ is the hydraulic conductivity (m/s), $i$ is the hydraulic gradient in $z$-direction, and $v$ is the discharge velocity (m/s) of water. The total head is comprised of elevation head, pressure head and velocity head. Neglecting the velocity head because the velocity is very small inside pore spaces, the total hydraulic head $h$ is represented by Eq. 2.

$$h = z + \frac{u}{\rho g} \tag{2}$$

where, $u$ is the pore water pressure (kPa), $\rho$ is the density of water and $g$ is the acceleration due to gravity. The governing partial differential equation (Eq.3) for the flow of water through a two-dimensional partially saturated soil is represented by the equation proposed by Fredlund and Rahardjo (1993).

$$\frac{\partial}{\partial \mathrm{x}}\left(-k_x \frac{\partial h}{\partial \mathrm{x}}\right) + \frac{\partial}{\partial \mathrm{z}}\left(-k_z \frac{\partial h}{\partial \mathrm{z}}\right) + \mathrm{q} = m_w^2 \gamma_w \frac{\partial h}{\partial \mathrm{t}} \tag{3}$$

where, $k_x$ and $k_z$ are the hydraulic conductivities in the x- and z- directions, respectively, $q$ is the applied flux, $m_w^2$ is the slope of SWCC and $\gamma_w$ is the unit weight of water.

The transient seepage analysis through partially saturated soil use soil–water characteristic curve and permeability function. The soil–water characteristic curve represents the volumetric



TH-2008_136104008

moisture content of soil at different matric suction values (van Genuchten 1980). The difference between pore-air pressure and pore water pressure is termed as matric suction. The volumetric water content of the soil decreases when matric suction increases. This affects the movement of water through the soil because there are less water-filled spaces available for water flow. As matric suction increases, the permeability of the soil decreases. The permeability of soil at various matric suction values is represented by the permeability function. The soil–water characteristic curve or water retention curve formulated by van Genuchten (1980) represents partially saturated soil behaviour in a very simple way as represented by Eq. 4,

$$\theta = \theta_r + \frac{\theta_s - \theta_r}{[1+(\alpha h)^n]^m} \quad (4)$$

where, $\theta$ is the volumetric water content; $\theta_s$ is the saturated water content; $\theta_r$ is the residual water content; $h$, the pressure head (matric suction) is positive; $\alpha$ is the inverse of the air entry value of soil; $n$ and $m$ = 1-1/n are curve fitting parameters. The hydraulic conductivity $k$, is predicted using the statistical pore size distribution model of Mualem (1976) shown by Eq. 5.

$$k = k_s S_e^{1/2} \left[1 - \left(1 - S_e^{1/m}\right)^m\right]^2 \quad (5)$$

$$S_e = \frac{\theta - \theta_r}{\theta_s - \theta_r} \quad (6)$$

$S_e$ is the effective degree of saturation shown in Eq. 6 and $k_s$ is the saturated permeability of the soil.

***Unsaturated Shear Strength Model***

Unsaturated shear strength parameters are required for evaluation of the factor of safety of the slope. As water is removed from the void spaces of saturated soil, negative pore water pressures develop between the particles of soil and the matric suction increases, which lead to some additional value of shear strength due to surface tension (Gasmo 2000). The slope



TH-2008_136104008

stability model makes use of the shear strength equation for unsaturated soils to determine the factor of safety. The shear strength equation for unsaturated soils is an extension of the Mohr-Coulomb failure criterion into the third dimension. The extended Mohr−Coulomb failure criterion (Figure 3.14) uses effective cohesion, $c'$, net normal stress, $(\sigma - u_a)$, and matric suction, $(u_a - u_w)$ to represent shear strength in unsaturated soils. Fredlund et al. (1978) proposed the extended model, which is shown in Eq. 7.

$$\tau = c' + \sigma' \tan\phi' + s \tan\phi^b \quad (7)$$

where, $\sigma' = (\sigma - u_a)$, $s = (u_a - u_w)$ and $\phi^b$ = parameter controlling increase in shear strength with suction.

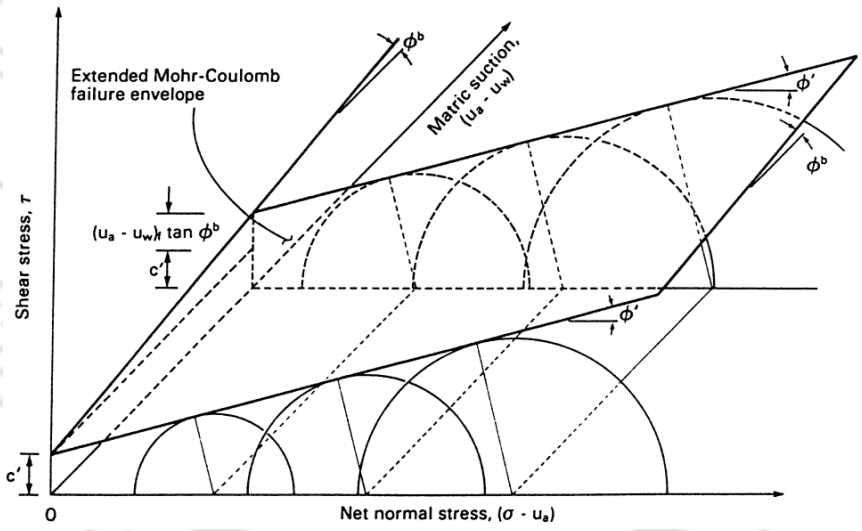


Figure 3.14 Failure envelope for partially saturated soils (Fredlund and Rahardjo, 1993)

***Factor of Safety Equations considering Unsaturated Strength Model***

The effect of matric suction can be incorporated into the method of slices based on limit equilibrium procedures by utilizing the unsaturated strength equation proposed by Fredlund et al. 1978. The general limit equilibrium (GLE) method has been taken and modifications have been made to include the linear increase in shear strength due to the presence of suction in the



TH-2008_136104008

unsaturated zone. GLE method satisfies both the force and moment equilibrium. The mobilized shear force, $S_m$, at the base of each slice is represented as:

$$S_m = \frac{l}{FOS}[c' + (\sigma_n - u_a)\tan\phi' + (u_a - u_w)\tan\phi^b] \quad (8)$$

where $l$ is the length of base of the slice.

The total normal force, $N$, on the slice base is represented as:

$$N = \frac{W-(X_R-X_L)+[-c'+u_a\tan\phi'-(u_a-u_w)\tan\phi^b]\frac{l}{FOS}\sin\alpha}{m_\alpha} \quad (9)$$

where $X$ denotes vertical interslice normal forces and $\alpha$ is the angle between the horizontal and the tangent to the slice base.

$$m_\alpha = \cos\alpha + (\sin\alpha\tan\phi')/FOS \quad (10)$$

Factor of safety, $FOS_m$, obtained from the moment equilibrium of the slice is represented as:

$$FOS_m = \sum\frac{\{c'lR+\left[N-u_al+(u_a-u_w)l\frac{\tan\phi^b}{\tan\phi'}\right]R\tan\phi'\}}{\sum Wx-\sum Nf} \quad (11)$$

where $W$ is the weight of the slice; $R$ is the radius of the circular slip surface; $f$ is the perpendicular offset of the normal force from the center of moments and $x$ is the horizontal distance from the center line of each slice to the center of moments.

Factor of safety, $FOS_f$, obtained from the force equilibrium of the slice is represented as:

$$FOS_f = \sum\frac{\{c'l\cos\alpha+\left[N-u_al+(u_a-u_w)\frac{\tan\phi^b}{\tan\phi'}\right]\tan\phi'\cos\alpha}{\sum N\sin\alpha} \quad (12)$$

### 3.1.6 Morgenstern and Price (1965) limit equilibrium method

Limit equilibrium method is used in this study for stability determination of soil slopes. A failure surface is assumed (circular, non-circular or composite) and the soil mass is divided into a number of slices and each slice is checked for the equilibrium of forces and moments. This method considers force and moment equilibrium of a mass of soil above a potential failure surface. The soil above the potential failure surface is assumed to be rigid (i.e., shearing can occur only on the potential failure surface). The available shear strength is assumed to be mobilized at the same rate at all points on the potential failure surface. Hence, the factor of



TH-2008_136104008

safety is constant over the entire failure surface. A search procedure is used to find the critical slip surface giving the minimum factor of safety of the slope.

Slope stability is usually expressed as an index, commonly known as the factor of safety (*FOS*).

$$FOS = \frac{available\ shear\ strength}{shear\ stress\ required\ to\ maintain\ equilibrium} \tag{13}$$

Morgenstern and Price (1965) method satisfy complete equilibrium and the numerical difficulties involved are minimum. It assumes that shear forces between slices and normal forces are related in the form given by

$$X = \lambda f(x)E \tag{14}$$

where *X* is the vertical interslice force, *E* is the horizontal interslice force, *f(x)* is an assumed function and $\lambda$ is an unknown scaling factor. Two equilibrium equations are satisfied. Moment equilibrium of the slices leads to the following equation

$$X = \frac{d}{dx}\left(E'y_t'\right) - y\frac{d}{dx}E' + \frac{d}{dx}(P_w h) - y\frac{d}{dx}P_w \tag{15}$$

where *X* represents the vertical shear force on the side of the slice, *E'* denotes the lateral thrust in terms of effective stress, $P_w$ is the water pressure. Referring to Figure 3.15, the assumed slip surface is represented by

$$y = y(x) \tag{16}$$

and line of thrust of internal water pressure is taken as

$$y = h(x) \tag{17}$$

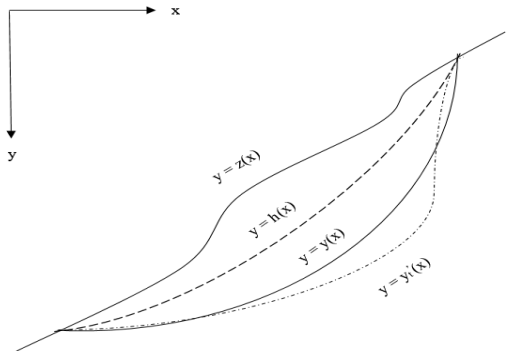


Figure 3.15 Potential sliding mass (after Morgenstern and Price, 1965)



TH-2008_136104008

Different forces acting on a slice of width dx are shown in Figure 3.16. Force equilibrium is considered perpendicular to the base of the slice and parallel to the base. Simplification of the equations, without the consideration of matric suction in force equilibrium, results in Eq. 18.

$$\frac{d}{dx}E'\left[1-\frac{\tan\phi'}{FOS}\frac{dy}{dx}\right]+\frac{dX}{dx}\left[\frac{\tan\phi'}{FOS}+\frac{dy}{dx}\right]=\frac{c'}{FOS}\left[1+\left(\frac{dy}{dx}\right)^2\right]+\frac{dP_w}{dx}\left[\frac{\tan\phi'}{FOS}\frac{dy}{dx}-1\right]+\frac{dW}{dx}\left\{\frac{\tan\phi'}{FOS}+\frac{dy}{dx}-r_u\left[1+\left(\frac{dy}{dx}\right)^2\right]\frac{\tan\phi'}{FOS}\right\} \quad (18)$$

where $c'$ is the cohesion, $\phi'$ is the friction angle, $FOS$ is the safety factor, $dW$ is the slice weight, $r_u$ is the pore-pressure ratio. Therefore, it is a statically indeterminate problem with $E'$, $X$ and $y_t'$ being the unknowns. Hence, the assumption relating $X$ and $E$ was considered as represented in Eq. 9. Different types of functions can be assumed to represent the way in which the relationship between $X$ and $E$ forces varies from one end of a sliding mass to the other. Some of the functions are a constant value, half sine, clipped half sine, trapezoidal, full sine wave, arbitrary, etc. The half sine function is used so that the curve will have zero amplitude at the slope toe, which is important for slopes receiving high water pressures at the toe region Choudhury et al. (2010). Zhu et al. (2005), Bai et al. (2014), Fredlund and Krahn (1977) used the half sine function in their analysis while using the MP method.

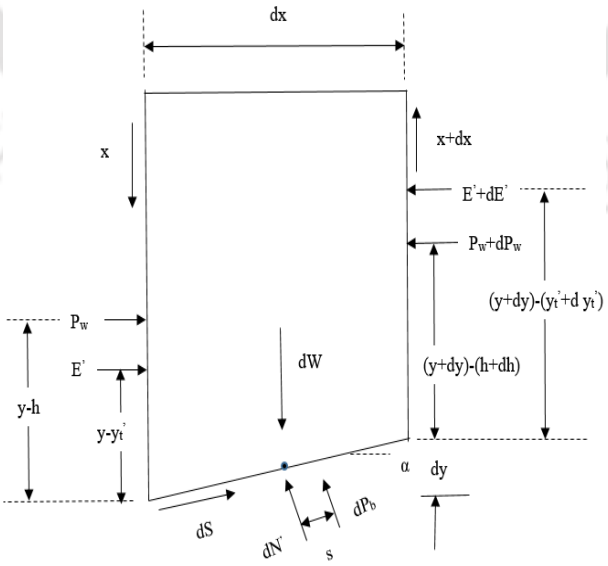


Figure 3.16 Forces acting on a slice (redrawn from Morgenstern and Price, 1965)



TH-2008_136104008

***Optimization Procedure***

A method is utilized for evaluating the minimum factor of safety of a slope. A starting slip surface is selected and then it is optimized to get the critical slip surface with a minimum factor of safety. Some of the commonly applied procedures are random search methods, genetic algorithm, cuckoo search, simulated annealing, particle swarm search, etc.

The basic algorithm followed is a random search method (Malkawi et al., 2001) based on a Monte-Carlo procedure. The procedure is also known as random walking. The factor of safety is calculated for the initial slip surface. The location of one vertex on the surface is randomly modified. The factor of safety is calculated for the new surface. If the factor of safety for the modified surface is lower than the factor of safety for the initial surface, the new surface replaces the original surface, and the location of another vertex is modified. The process is then repeated. If the factor of safety for the modified surface is higher than the factor of safety for the initial surface (or the change in the factor of safety is lower than some tolerance) the process ends.

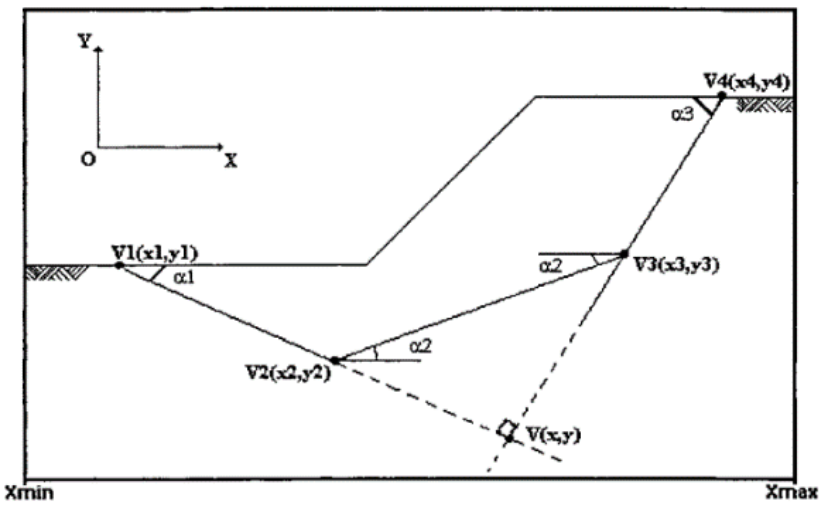


Figure 3.17 Generation of first slip surface (Malkawi et al., 2001)

To start the search for the potential critical slip surface, the domain on the x, y-plane where the search is to be made must be specified. Then the end vertices V1 and V4 are randomly chosen



TH-2008_136104008

as shown in Figure 3.17. Figure 3.18 represents the complete rotation of three parts around four points.

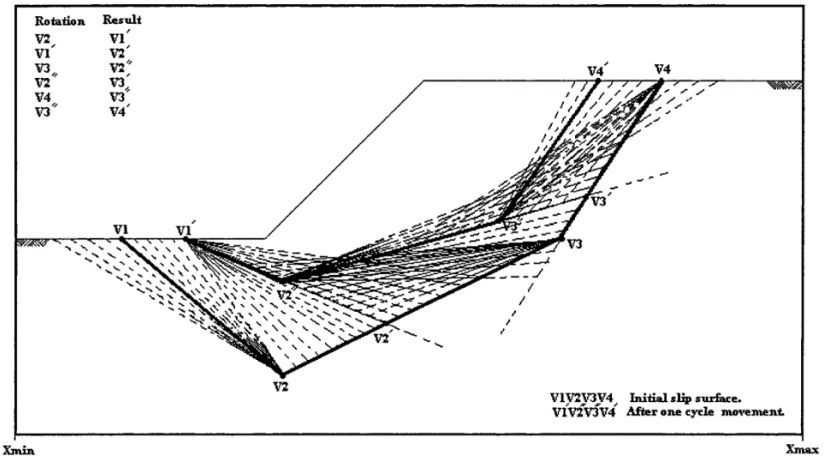


Figure 3.18 Depicts complete rotation of three-segment example around their four vertices (Malkawi et al., 2001)

### 3.1.7 Strength reduction technique in the finite element method

Finite element method has been used for analysis of stability problems. With complex geometries and material heterogeneity, it gives a better understanding of failure mechanisms, displacements and deformations. To obtain the factor of safety in finite element method, strength reduction technique (Smith and Hobbs 1974) has been adopted by several researchers.

Smith and Hobbs (1974) reported results for undrained clayey slopes considering the strength reduction method. In this method, the strength parameters $c'$ and $\phi'$ are gradually reduced by some factor until the failure condition of the slope is observed. The safety factor, *FOS* is defined as the factor by which the original shear strength parameters need to be reduced to bring the slope to a failure point. Hence, the reduced strength parameters $c_f'$ and $tan\phi_f'$ at failure are defined as follows

$$c_f' = \frac{c'}{FOS} \tag{14}$$

$$\tan \phi_f' = \frac{\tan \phi'}{FOS} \tag{15}$$



TH-2008_136104008

This method is known as the shear strength reduction technique. Here failure is taken at that point where the solutions fail to converge within a specified number of iterations. The stress distribution fails which implies that the Mohr-Coulomb failure criterion and the global equilibrium is not satisfied (Griffiths and Lane1999). Failure of slopes is accompanied by a sudden rise of displacements. Zienkiewicz et al., (1975) studied $c$ - $\phi$ slopes showing good comparison with slip circle results. With more use and confidence gained, researchers like Naylor, (1981); Griffiths, (1989); Potts et al., (1990); Matsui and San, (1992); Ugai and Leshchinsky, (1995); Griffiths and Lane, (1999); Cheng et al., (2007); Zheng et al., (2009) used the strength reduction method for stability analysis of slopes.

## 3.4 SUMMARY

The present chapter discussed the different soil materials used for the study. The mechanical and hydraulic properties of the soils obtained from laboratory tests were discussed. Soil-1 and Soil-2 were classified as silty clay (CL) and silty sand (SM), respectively. Properties of the third soil (Soil-3) were obtained from Kellezi et al. (2005) were summarized. The saturated permeability of the three soils differs considerably with Soil-3 having the least value ($8.3\times10^{-7}$ m/s) and Soil-2 being the most permeable ($6.6\times10^{-5}$ m/s). The methodology adopted in this study to achieve the objective to analyze slopes using the limit equilibrium method and finite element method is explained.



TH-2008_136104008

# Chapter 4 DEVELOPMENT OF NUMERICAL MODELS

## 4.1 INTRODUCTION

Different numerical models were prepared for stability analysis of both homogeneous and non-homogeneous slopes. Prior to the preparation of models, two model slopes were selected from literature to validate the adopted methodologies. The first slope is a non-homogeneous slope without any GWL or seepage analysis. The second one is a homogeneous slope with the GWL and infiltration analysis. With comparable outcomes from the validation, various homogeneous and non-homogeneous models were prepared.

## 4.2 SOFTWARE - ROCSCIENCE

The limit equilibrium and finite element methods adopted for the study are implemented using commercially available software, Rocscience (Rocscience 2018). Rocscience is an analysis and design software applicable to civil, mining and geotechnical engineering. Currently there are sixteen products available in the suite. The products include SLIDE2, SLIDE3, RS2, RS3, Settle, RocFall, Dips, RSPile, RocTopple, RocPlane, RocSupport, Examine3D, Unwedge, Swedge, CPillar, RocData. All these products cover a vast area of civil and mining engineering applications which includes slope stability analysis, pile analysis, seepage analysis, soil settlement analysis, rockfalls, support requirement for tunnels, consolidation, underground rock structure analysis and many more (Rocscience 2018). Mostly the limit equilibrium method and finite element method are used for modelling purposes. The software supports the use of both soil and rock materials. Out of all the products, two of them have been used consistently in this study, SLIDE2 and RS2.

SLIDE2 is a 2D limit equilibrium software for analysis of slope stability for both the soil and rock slopes. It can be used in embankments, dams and retaining wall problems also. The analysis procedures include various methods of slices based on the limit equilibrium method.



TH-2008_136104008

Options for slip surface shapes include circular and non-circular surfaces. There are a number of search methods for determining the factor of safety of the slope like grid search, slope search, block search, path search, and auto-refine search. The optimization techniques utilized for the critical slip surface are random search method, cuckoo search, simulated annealing, particle swarm search, etc. Both steady-state and transient seepage analysis can be performed using the finite element method. The soil above the GWL is considered unsaturated in any model (mentioned in Slide2 v8 Rocscience 2018a manual). Wherever suction is found, the unsaturated shear strength model (Fredlund et al. 1978) is utilized otherwise the general Mohr–Coulomb equation is used.

RS2 is a 2D finite element program for analysis of slopes, excavation design, groundwater seepage, consolidation, seismic analysis, and probabilistic analysis. Progression of failure can be simulated here. Different types of failure criterion are available like Mohr-Coulomb, Hoek-Brown, Cam-Clay, Softening Hardening model, etc. The shear strength reduction method is available for the analysis of slopes. Modelling of reinforced earth structures is also possible here.

## 4.3 SLIDE2 AND RS2 NUMERICAL MODEL SENSITIVITY

There are many parameters in the software, which control the output of the analysis. The basis of using specific values of these parameters are represented in the following section in the form of plots. The main parameters controlling the value of safety factor in the limit equilibrium method are a number of slices, tolerance value, and a number of iterations. The factors having an influence on the strength reduction method (FEM) are a type of elements and the number of elements used to discretise the slope.

A sensitivity study of the different parameters was performed on the slope model depicted in Figure 4.1. The slope is inclined at 35° to the horizontal. The slope height is kept as 10 m. The



TH-2008_136104008

following plots show their effect on the factor of safety of the slope. This convergence study is performed with Soil-1 only. The properties of Soil-1 listed in Table 3.1 were used in this SLIDE2 and RS2 model.

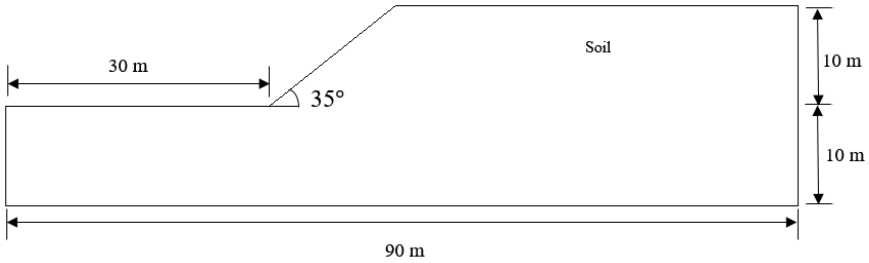


Figure 4.1 Geometry of slope model

For SLIDE2 model, the effect of variation of slice number on *FOS* is shown in Figure 4.2. Morgenstern and Price (1965) method was selected for this analysis. This method was used for the analysis because it satisfies complete equilibrium by considereding both force and moment equilibriums of a mass of soil above a potential failure surface. It is applicable to general (non-circular) slip surfaces as well. A number of slices were varied from 5 to 40. The tolerance value and a number of iterations were kept constant at 0.005 and 50 for this analysis. It is observed that there is no effect of slice number after ten slices on the factor of safety of the slope.

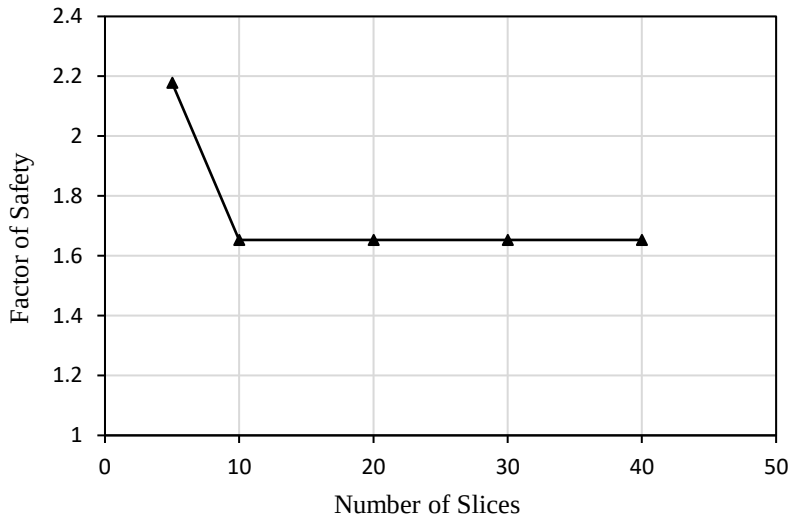


Figure 4.2 Relationship between slice number and safety factor



TH-2008_136104008

The effect of tolerance on the safety factor is represented in Figure 4.3. For this analysis, the number of slices was fixed at 20 and the iterations at 50. Different tolerance values of 0.0005, 0.001, 0.005, 0.01 were considered. It is observed that there is negligible change in the factor of safety of the slope with a change in tolerance value.

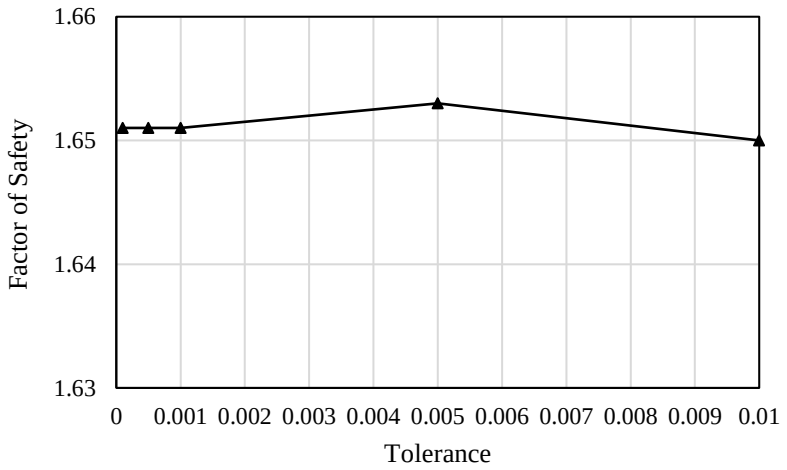


Figure 4.3 Relationship between tolerance value and a factor of safety

Table 4.1 Effect of element type on SRF

| Type | | Strength Reduction Factor |
|---|---|---|
| 3-Node Triangular | Graded | 2.0 |
| | Uniform | 2.01 |
| 6-Node Triangular | Graded | 1.64 |
| | **Uniform** | 1.63 |
| 4-Node Quadrilateral | Graded | 2.01 |
| | Uniform | 1.96 |
| 8-Node Quadrilateral | Graded | 1.62 |
| | Uniform | 1.62 |

Table 4.1 enumerates the different type of elements available and their influence on the strength reduction factor using the finite element method. The model shown in Figure 4.1 is used for this analysis. Triangular and quadrilateral type of elements is available in RS2 for modelling purposes. 2500 elements were used to discretize the slope. The SRF closest to the factor of safety from the LEM is given by uniform 6-noded triangular and uniform 8-noded quadrilateral



TH-2008_136104008

elements. In RS2 model, the uniform six-noded triangular and four-noded quadrilateral elements were selected to discretize the slopes.

Figure 4.4 shows the effect of a number of elements used to create the finite element mesh. Six noded uniform triangular elements were selected to discretize the slope. The number of elements was varied from 500 to 3500. Number of elements does not have any effect on strength reduction factor after 2000 elements. Therefore, approximately 2500 elements were utilized to discretize different slopes in the present study.

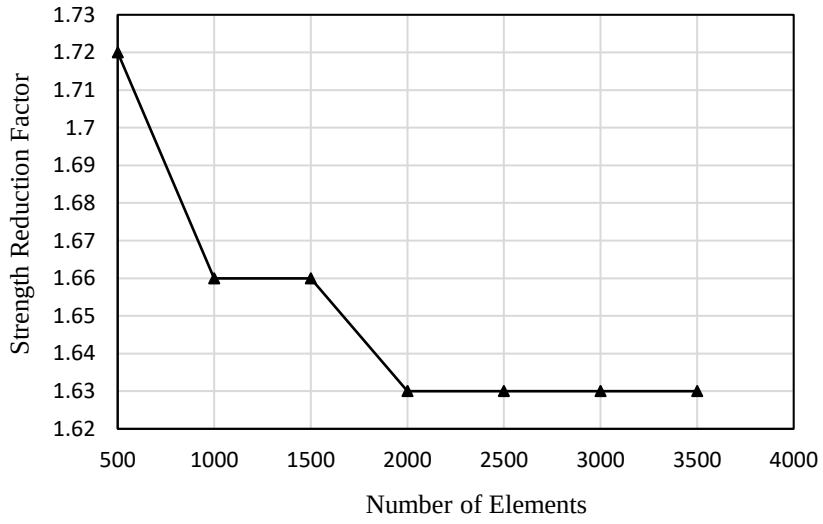


Figure 4.4 Relationship between the number of elements and SRF

## 4.4 MODEL VALIDATION

To validate the methods used for the analysis of slopes in this study, two models were validated from literature. The first one is a three-layered non-homogeneous slope used by Low (1989). The second model is a homogeneous model with seepage analysis performed by Gasmo et al., (2000).

A three-layered cohesive slope (Figure 4.5a) has been taken from literature (example 1 of Low 1989) and analyzed to validate the methodology adopted in using the SLIDE2 and RS2 programs. Figure 4.5b illustrate the numerical model prepared in Slide for the validation. Table 4.2 shows the strength properties of the three soils used in the problem.



TH-2008_136104008

Table 4.2 Soil properties used in validation model (Low, 1989)

| Properties | Soil-1 | Soil-2 | Soil-3 |
|---|---|---|---|
| Unit weight (kN/m$^3$) | 18 | 18 | 18 |
| Cohesion (kPa) | 30 | 20 | 150 |
| Friction angle (deg) | 0 | 0 | 0 |

The ordinary method of Slices (Fellenius, 1936) and Bishop's Simplified method (Bishop, 1955) have been chosen in SLIDE2 for the limit equilibrium analyzes. The factor of safety (*FOS*) values obtained were 1.446 from SLIDE2 and 1.46 from RS2 model, which are very close to the reported *FOS* values of 1.44 (Low 1989), which validates the methodology of analyzes.

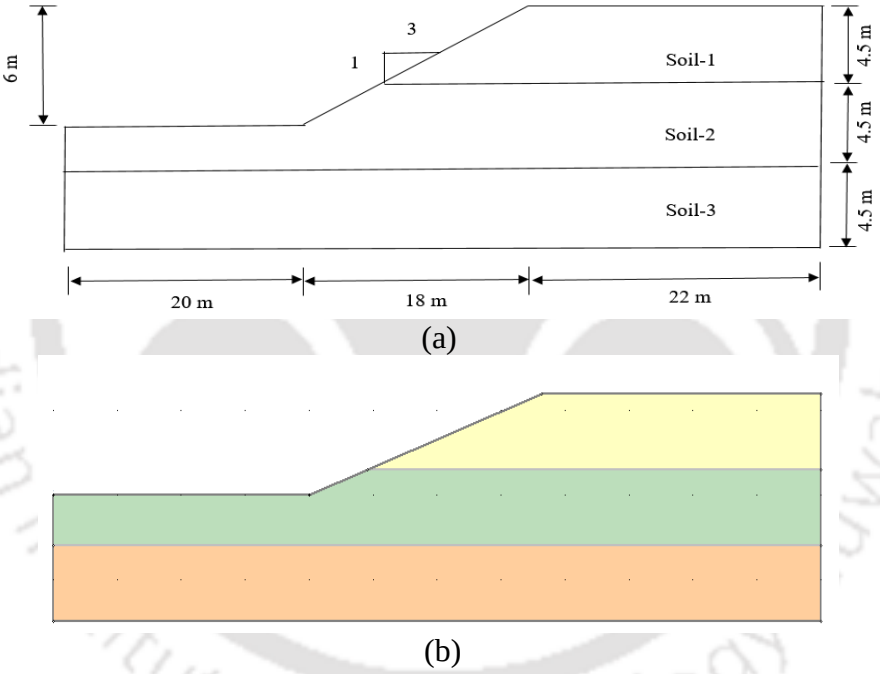


(a)

(b)

Figure 4.5 (a) Slope model for validation problem (after Low 1989) (b) Similar model prepared in Slide

To validate the methodology adopted in using the SLIDE2 (Rocscience 2018a) program for performing seepage and stability analyzes for this study, a homogeneous slope model (Figure. 4.7a) used by Gasmo et al. (2000) was considered. Gasmo et al., (2000) performed numerical analysis on a homogeneous slope to study how much of the applied rainfall intensity became infiltration. Silty clay soil with a saturated hydraulic conductivity of $8.3\times10^{-7}$ m/s was used



TH-2008_136104008

with rainfall intensities varying from $1\times10^{-8}$ m/s and $1\times10^{-3}$ m/s. Three flux sections (crest, face and toe) were used to calculate the infiltration. A similar model was developed in SLIDE2 (Figure. 4.7b) with identical soil characteristics to perform seepage analysis under different rainfall (surface flux) conditions. Figure 4.6 represents the soil–water characteristic curve for the soil (silty clay) having a saturated permeability of $8x10^{-7}$ m/s.

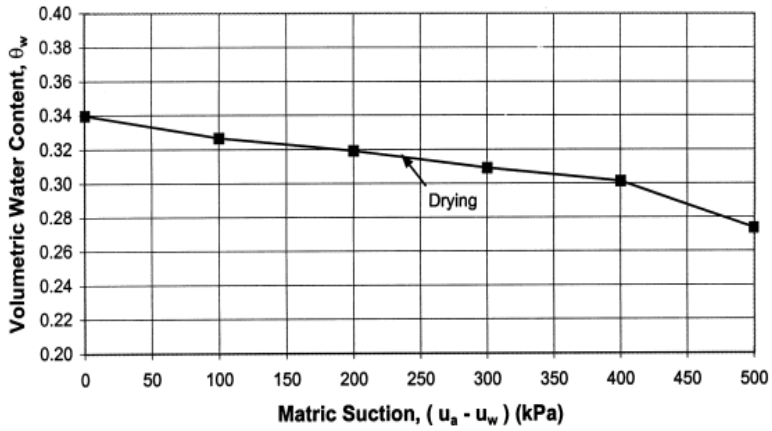


Figure 4.6 SWCC of the soil used by Gasmo et al. (2000)

To calculate the flux, three different sections (crest, face, and toe) were created at the surface prior to the analysis. After the infiltration analysis, the amount of water that infiltrated each section was noted and plotted in graphs. Figure. 4.8 shows the calculated flux plotted with respect to the applied flux (rainfall) scenarios. The diagonal reference line illustrates the situation where all the applied flux infiltrates completely into the slope. The horizontal reference line denotes the saturated permeability of the soil, which would be the maximum rate at which water can enter the soil when the soil is fully saturated (with a hydraulic gradient equal to one). The three curves with circular markers represent the flux across the crest, face, and toe of the slope as reported by Gasmo et al. (2000). The curves (R) with triangular markers depict results obtained from the validation model using SLIDE2 model. It was observed that at low infiltration intensity from $1\times10^{-8}$ m/s to $1\times10^{-7}$ m/s, the applied and calculated flux is similar in nature. With higher rainfall intensity, the calculated flux becomes less than the



TH-2008_136104008

applied flux. The flux calculated at the crest is nearest to the $k_s$ ($8.3\times10^{-7}$ m/s) line. Maximum infiltration occurs at the crest followed by the face and toe of the slope. The slope crest received the maximum infiltration because the water here flowed vertically downwards. As the water moved downwards, it increased the moisture content of the slope thereby reducing the void spaces in the soil. Hence, the amount of water infiltrating into the slope gradually reduced. The figure shows the reasonable match between both the results, which indicate the validation of the methodology.

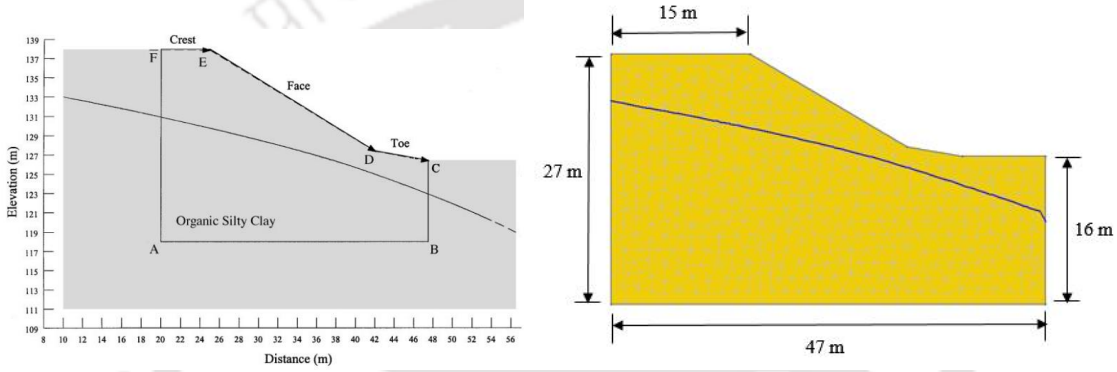


(a) (b)

Figure. 4.7. (a) Slope model used in Gasmo et al., 2000 (b) Model prepared in Slide

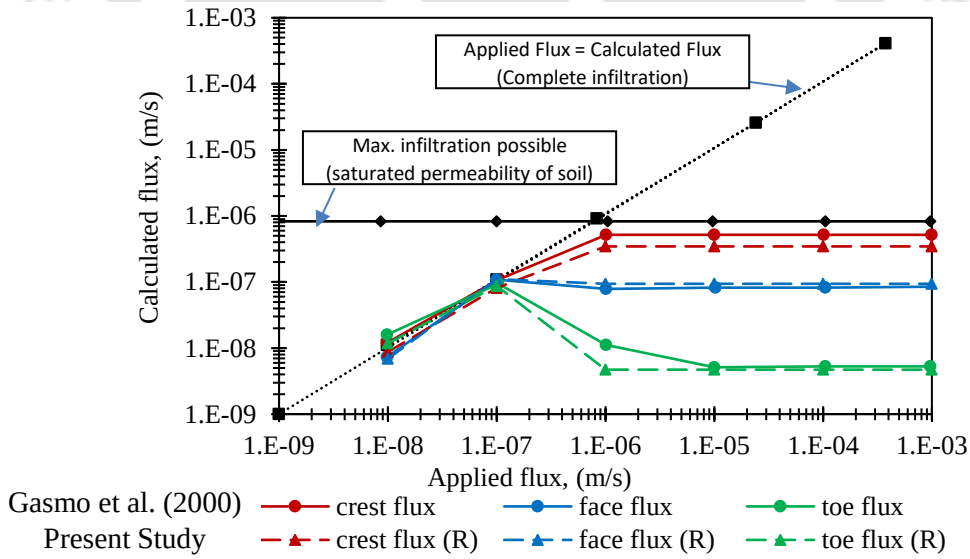


Figure. 4.8. Seepage analysis results obtained from validation model



TH-2008_136104008

## 4.5 VARIOUS SLOPE MODELS

The stability analysis of slopes has been divided into two parts, homogeneous slopes, and non-homogeneous slopes. The slope angle represented by $\beta$, was selected as 35°. The height of the slope ($H$) is 10 m. The inclination and height of the slope are kept constant throughout the study except for the models to study on the effect of slope geometries under infiltration situations. For the parametric study of the effect of slope angle on the stability of the slope, five different slope angles were selected. The five slope angles are 26.57°, 35°, 45°, 55°, and 65°. To study the effect of slope height on stability under infiltration conditions, four slope heights selected are 5 m, 10 m, 15 m and 20 m respectively. The other dimensions like the front extent ($x_1$), back extent ($x_2$) and depth ($D$) of the slope have been kept constant throughout the study as shown in Figure 4.9. The front portion of the slope beyond the toe ($x_1$) is 30 m which is thrice the slope height while the back, beyond the crest ($x_2$) is 45 m taken as five times the slope height so that the effect of model boundaries get nullified. The total depth $D$ was kept equal to 2$H$. For the parametric study on slope heights, the total depth was varied as 3$H$, 2$H$, 1.67$H$ and 1.5$H$.

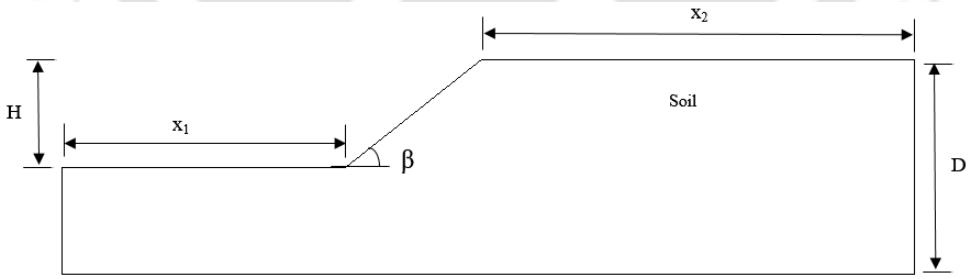


Figure 4.9 Dimensions of slope model

***Homogeneous Slopes***

Different homogeneous slopes were modelled representing different in-situ conditions in the field. First of all a homogeneous slope (Figure 4.9) with different soils were prepared without any loading or seepage occurring within the slope. Another slope model consists of the Soil-1



TH-2008_136104008

at various constant saturation levels as depicted in Figure 4.10. The third model (Figure 4.11) of the homogeneous slope consists of a GWL prevalent in the slope used for the infiltration analysis. Numerical models of slopes consisting of single uniform soil material were prepared to study the stability of slopes under rainfall infiltration.

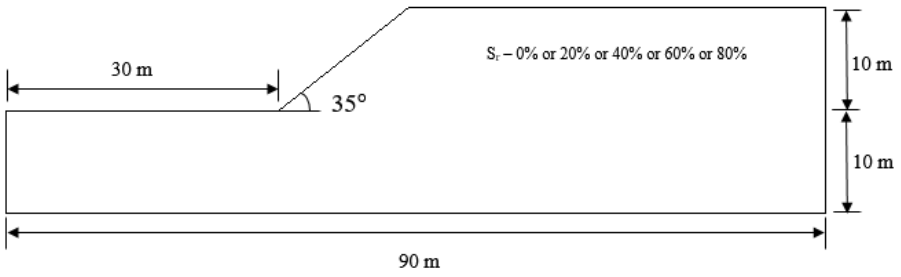


Figure 4.10 Homogeneous slope with different constant moisture contents

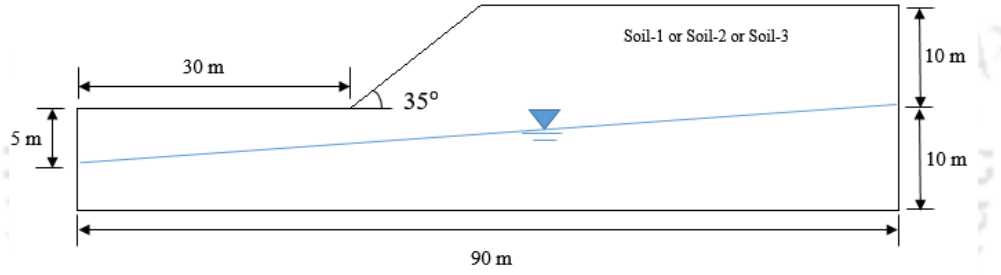


Figure 4.11 Homogeneous slope model with the GWL

A typical finite element model prepared in software SLIDE2 v8 (Rocscience 2018a) is shown in Figure. 4.12 used to perform the steady-state and transient seepage analysis. The two-dimensional finite element model slope was discretised with 4-noded quadrilateral type elements consisting of 2500 elements. For the steady-state seepage analysis, a constant total head boundary condition was applied beneath the GWL on both the sides of the slope. The portion above the GWL was specified as zero nodal flux boundary. To simulate transient conditions, the slope surface was specified as flux equal to rainfall intensity of 30 mm/h for 24 hours. The side boundaries are kept free so that the GWL may rise and fall with rainwater infiltration. Rainfall flux applied is 30 mm/h equivalent to $8.3\times10^{-6}$ m/s, which is less than the



TH-2008_136104008

saturated permeability of Soil-2, equal to Soil-1 and more than Soil-3. A no flow boundary was applied to the bottom of the slope in the transient seepage analysis as well.

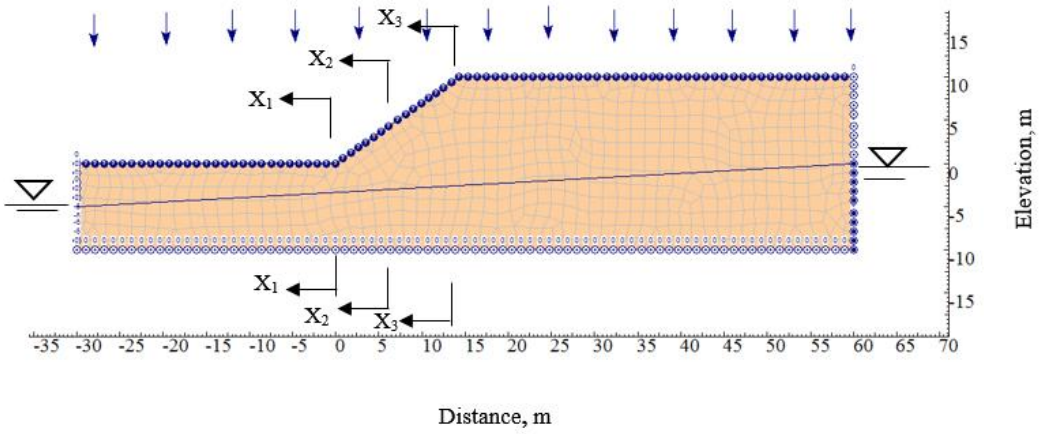


Figure. 4.12. Model of the homogeneous slope used in the study

The rainfall flux was applied for a duration of 24 hours but the slope was monitored until 48 hours. Three different sections were selected to represent the pore water pressure profiles as depicted in Figure. 4.12. Section $X_1-X_1$ is at the toe, $X_2-X_2$ is at the middle of slope and $X_3-X_3$ is at the crest of the slope surface.

The influence of different parameters on the stability of the slope was studied under rainfall infiltration. The most important parameter in a rainfall analysis is the rainfall intensity, which controls the change in suction and rise and fall of a ground water level. The effect of rainfall intensity, slope angle, slope height and duration of rainfall were investigated. To study the effect of slope angle on stability, five different slope angles were selected. The slope angles selected were 26.56°, 35°, 45°, 55°, and 65°. Similarly, for the study of the influence of slope height on stability four slope heights were selected at intervals of 5 m starting with 5 m slope height.

***Non-homogeneous Slopes***

To study the effect of layer height, two-layered slope models with different top soil and bottom soil were modelled keeping the other dimensions same. A two-layered slope (Figure 4.13),



TH-2008_136104008

which is frequently encountered in the levee and earthen dam problems, was modelled using both the limit equilibrium and finite element methods. Three different soils were considered to model different cases of two layered slopes. To represent the two-layered slope configuration, two regions were considered which comprises of different types of soils. The height of the top layer (region 1), is selected as 0.5*D*. The two-dimensional finite element soil model shown in consists of 2500 elements and 3800 nodes. For finite element framework using RS2, strength reduction technique (Griffiths and Lane 1999) is adopted to study the deformations/strains within the slope. Uniform triangular 6-noded elements were used to discretise the slope. Interface elements were not considered in between two different layers.

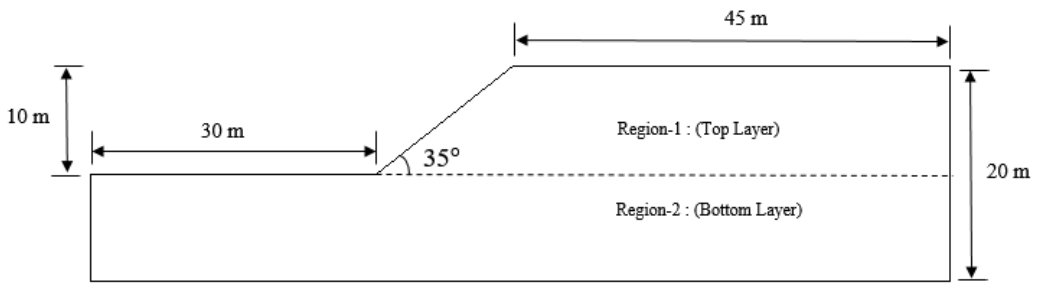


Figure 4.13 Horizontal two-layered slope model

Further multi-layered slopes have been modelled to represent different moisture levels is depicted in Figure 4.14. Model-1 indicates groundwater level rise shown in Figure 4.14a. The increase in the GWL is a transient phenomenon and hence the slope was modelled with unconsolidated undrained properties to convey short-term conditions. The degree of saturation is generally more at depth than near the surface and ranges from 0.2 to 0.7 (Song et al. 2016). Figure 4.14b illustrate the model where the saturation levels decrease with depth representing infiltration in the slope. The slope parallel layers (Cho and Lee 2001) in the model convey soil material with different moisture contents in terms of undrained shear strength to represent the variation of the degree of saturation in the natural slope. The slope was numerically modelled as non-homogeneous (w.r.t moisture contents) slope. The limit equilibrium model was



TH-2008_136104008

prepared in SLIDE2 v8 (Rocscience 2018a). Three different layer heights of 0.5 m, 1 m and 2 m were selected for the analysis.

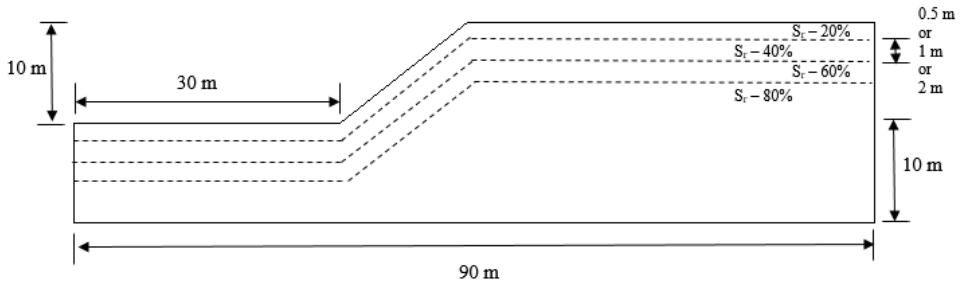


(a)

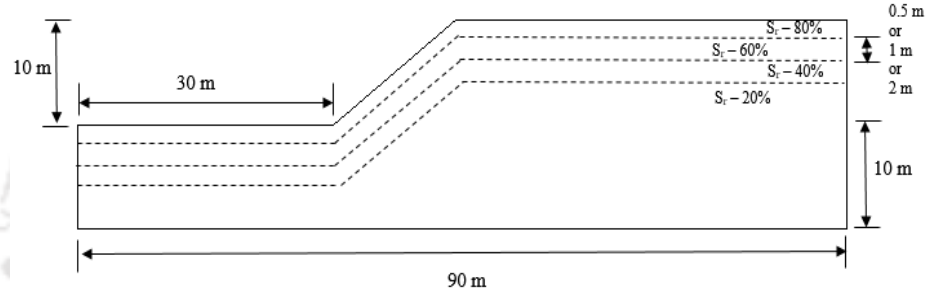


(b)

Figure 4.14 Multi-layered slope (a) model-1 and (b) model-2

The finite element model of the layered slope with layers of different moisture contents is shown in Figure 4.15. The height of the layers was fixed at 2 m each. Four different layers were defined in the slope denoting degree of saturation from 20% to 80%. Two models were created to represent the variation of degree of saturation with depth. One model is prepared to exhibit increase of saturation with depth while the other represents decrease of saturation with depth. Physically one model resembles rainwater infiltration while the other shows influence of GWL rise. The slope was discretised with six-noded triangular elements. The 2D finite element model of the slope was prepared in RS2 v9 (Rocscience 2018b) which consists of 2500 elements and 3688 nodes. Gravity type of loading was applied to the elements. Poisson's ratio of 0.45 was used for the analysis. Modulus of elasticity of 5 MPa was used in the stability analysis.



TH-2008_136104008

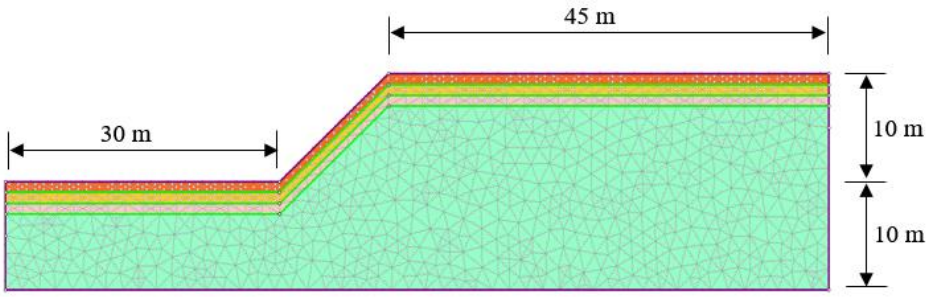


Figure 4.15 Model of layered slope used in the study with 1 m layer thickness

A non-homogeneous two-layered slope with Soil-1 as the main slope material is represented in Figure 4.16. The layer thickness is selected as 2 m. The layer is created parallel to the slope to represent a surficial top layer of loose nature often encountered in slopes. The top layer is alternated between Soil-2 and Soil-3. The water is assumed to flow from the right to the left. A total head of 10 m is taken on the right boundary and 5 m on the left boundary.

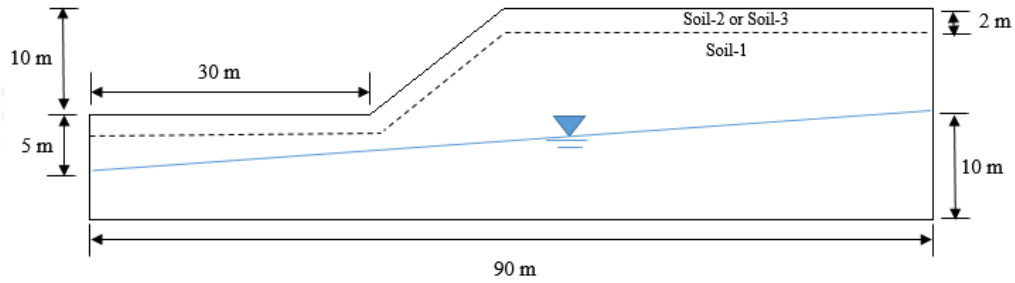


Figure 4.16 Slope parallel two-layered slope model with the GWL

Figure 4.17 illustrates a three-layered slope with either Soil-2 or Soil-3 as the top material. The bottom layer filling the major portion of the slope is Soil-1. Soil-3 is selected as the middle material if the top layer is taken as Soil-2 in one of the cases. In the other model, the top layer is selected as Soil-3 while the middle layer is taken as Soil-2. The location of the GWL is kept unchanged. The layer thickness is also kept as 2 m.



TH-2008_136104008

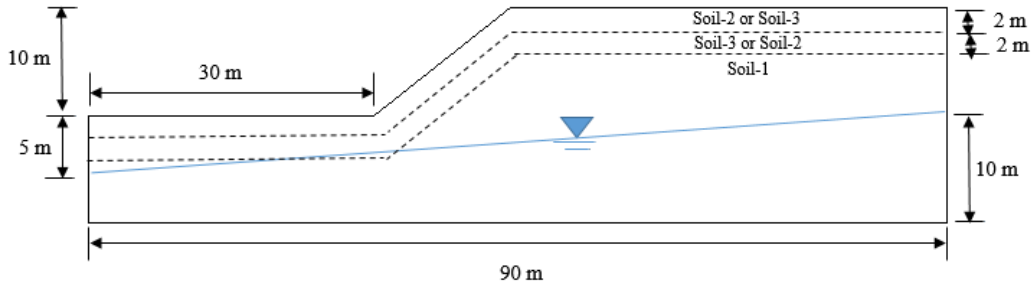


Figure 4.17 Slope parallel three-layered slope model with the GWL

A 2D finite element model of the three-layered slope is depicted in Figure 4.18. The slope is discretised with 4-noded quadrilateral elements. The model consists of 2500 elements. The transient boundary conditions are depicted in the figure as well.

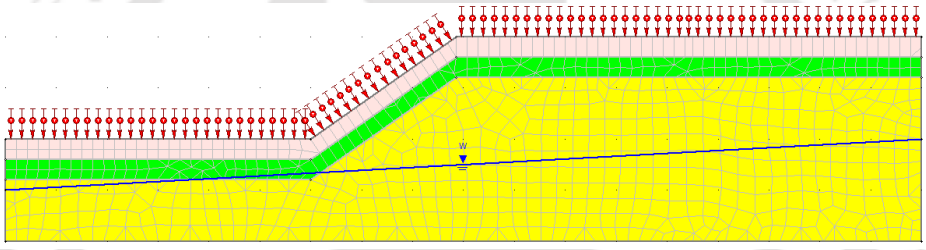

Figure 4.18 Finite element model of a three-layered slope with the GWL

## 4.6 SUMMARY

The present chapter discussed about the development of different types of homogeneous and non-homogeneous slope models. The influence of different model parameters like a number of slices, tolerance value, number of elements, etc. on the stability of a slope is discussed. Validation of the methodologies has been presented by comparing the results of two models from literature. Various models developed for further analyses as per the objective of the thesis are introduced. Primarily the slopes were modelled as slopes without GWL and with a GWL for the infiltration analysis. Multi-layered slopes were modelled to represent the variation in moisture within the slope.



TH-2008_136104008

# Chapter 5 ANALYSIS OF HOMOGENEOUS SLOPES

## 5.1 INTRODUCTION

The analysis of homogeneous slopes was primarily divided into two sections, without rainfall infiltration and with rainfall infiltration. Homogeneous slopes with different soils have been analyzed using both the limit equilibrium method and finite element method. Different cases were created and the study was accordingly presented into different sections. Influence of rainfall intensity and duration, slope angle, slope height on the stability of the slope is presented under infiltration conditions.

## 5.2 ANALYSIS WITHOUT RAINFALL INFILTRATION

The homogeneous slopes with three different soils were first analyzed without rainfall infiltration or any kind of seepage within the slope. Under this condition, three cases are taken for the analysis without infiltration. The first case is a slope without the consideration of ground water level (GWL). The second case represents homogeneous slopes at different moisture contents without the consideration of ground water level. The third case considered the existence of ground water level along with unsaturated behaviour of soils.

### 5.1.1 Case 1: Analysis without GWL

The homogeneous slope model of 10 m height and at 35° inclination with horizontal was considered for this case as shown in Figure 5.1. Three different models with three soils were adopted with no ground water level and water seepage. Properties of the three soils used for the numerical models are enlisted in Table 3.1. The slopes have been analyzed using both the limit equilibrium method and finite element method. Details of the typical results obtained using both the methods are discussed for Soil-1 model. All the other cases for the three soils are compared together to illustrate the difference in behaviour of the three soils considered.



TH-2008_136104008

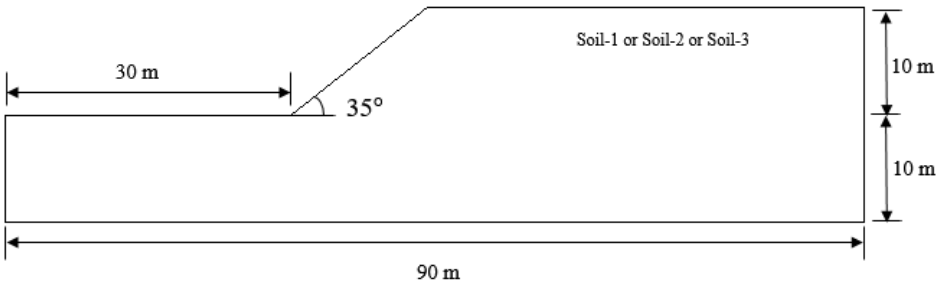


Figure 5.1 Homogeneous slope model

Table 5.1 Physical properties and shear properties of three soils

| **Property** | **Soil-1** | **Soil-2** | **Soil-3** |
|---|---|---|---|
| USCS classification | CL | SM | CL |
| $\gamma$ (kN/m$^3$) | 17.6 | 16.8 | 19 |
| $c'$ (kPa) | 10 | 0 | 25 |
| $\phi'$ ($^o$) | 30 | 36 | 18 |

In the limit equilibrium method, the slope was analyzed for its stability in SLIDE2 using Morgenstern and Price's procedure. The model was analyzed with 20 vertical slices considering 5000 non-circular failure surfaces. Random path search method (as discussed in Chapter 3) was chosen for determining the critical failure surface with the minimum factor of safety (*FOS*). Figure 5.2 depicts all the slip surfaces searched to find the critical slip surface for Soil-1 model. The slices are also shown for the critical slip surface, which were used to determine the *FOS* by the method of slices. The lowest *FOS* for the model is 1.541. The critical slip surface depicts toe type of failure mechanism within the soil. For further analyzes and comparisons, the lowest *FOS* values and the position of the critical slip surface are compared among different models. The co-ordinates of the critical slip surface were obtained separately and plotted in graphs to show the critical slip surface comparisons.

The stresses and strains within the slope were obtained utilizing the finite element method. The total displacement contours resembled the critical slip surfaces obtained from LEM.



TH-2008_136104008

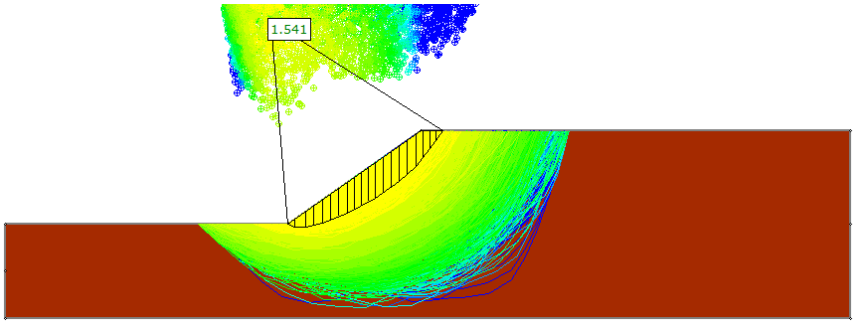


Figure 5.2 Multiple slip surfaces considered in limit equilibrium method of homogeneous slope with Soil-1

In finite element analyzes, the slope was analyzed using a strength reduction technique in RS2 to determine the stability of the slope. The model was discretised using uniform meshing scheme with six-noded triangular elements. Vertical and horizontal displacements are restricted at the bottom of the model and horizontal displacements are restricted at left and right extremes of the model for its fixed boundary conditions. Figure 5.3 displays the total displacement contours of the slope. Strength reduction factor (SRF) of the model was obtained as 1.58, which is close to the *FOS*, value (1.541) obtained from the limit equilibrium method. Figure 5.4 shows maximum shear strains developed in the slope, which gives an idea of the portion where a slip can be developed. This slip zone is also identical to the critical slip surface obtained from the limit equilibrium method analysis. Figure 5.5 represents the deformed mesh indicating a composite type (combination of translational and rotational) of failure. Further, it can also be observed that the figures show a toe failure mechanism.

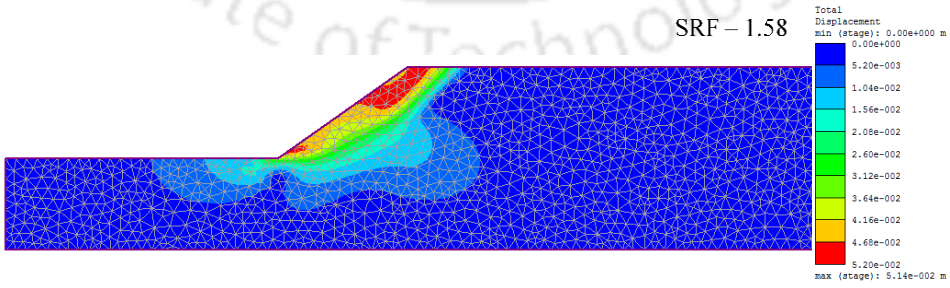


Figure 5.3 Total displacement contours of the homogeneous slope with Soil-1



TH-2008_136104008

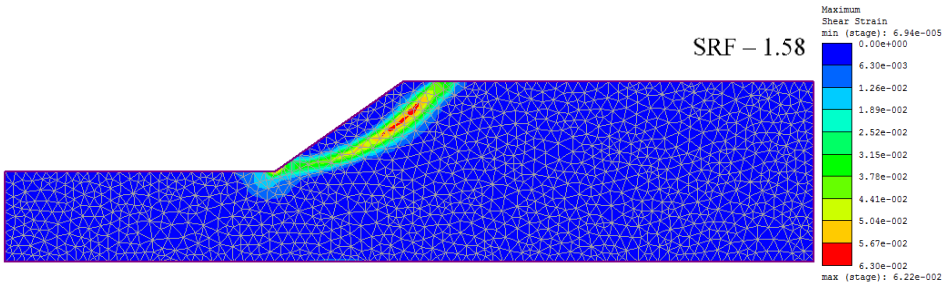


Figure 5.4 Maximum shear strain contours of the homogeneous slope with Soil-1

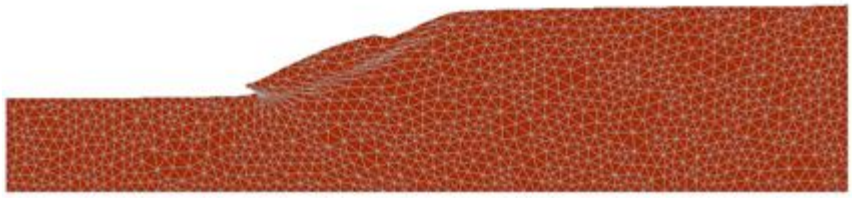

Figure 5.5 Deformed mesh of homogeneous slope with Soil-1

Table 5.2 summarizes the results of analyzes for the slopes with homogeneous soil configurations. Stability factors obtained from both the methods (LEM and FEM) are tabulated. MP represents Morgenstern and Price method in the limit equilibrium method (LEM) and SRM indicates strength reduction method in the finite element method (FEM). It is seen that Soil-3 model has the highest safety factor, *FOS* of about 1.774, than the other two models. The homogeneous slope with Soil-2 can be considered the least stable with FOS of 1.038. The strength reduction factors for Soil-1 is 1.58 while for Soil-2, it is 1.06 and for Soil-3 the SRF is 1.73, which are reasonably close to the *FOS* values obtained from LEM.

Table 5.2 Factor of safety for the homogeneous slopes

| Soil Type | LEM-MP | FEM-SRM |
|---|---|---|
| Soil-1 | 1.541 | 1.58 |
| Soil-2 | 1.038 | 1.06 |
| Soil-3 | 1.774 | 1.73 |

The critical slip surfaces (failure surfaces) of the homogeneous slopes with each of the three soils obtained from LEM analyzes are shown in Figure 5.6. The slip surfaces are evidently different, which can be attributed to the different type of soil in each case. Slopes with Soil-1



TH-2008_136104008

and Soil-3 (fine-grained, CL materials) depict rotational failure mechanism (generally observed for finite slopes) while slope with Soil-2 (coarse-grained, SM material) shows translational failure mode (generally observed for infinite slopes). Among the CL material slopes, the slope with Soil-1 has a relatively shallow slope failure mechanism while Soil-3 has deep-seated toe failure mechanism because they possess different cohesion values. It is to be noted here that high cohesion soils show deeper critical slip surfaces in comparison to the soils with smaller cohesion values. Soil-2 being silty sand (relatively coarse-grained) is having a failure surface parallel to the slope near the surface.

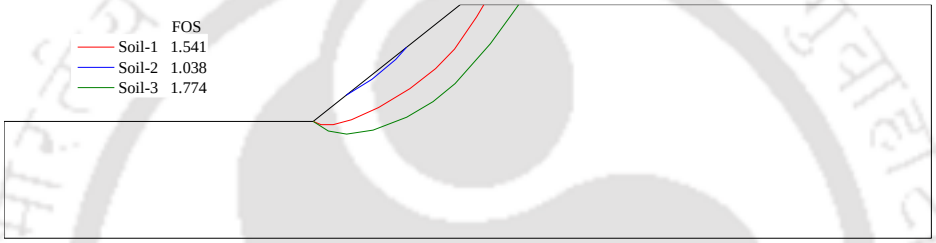


Figure 5.6 Critical slip surfaces for the homogeneous slopes

The results obtained from FEM analyzes for the three different soil models are shown in Figure 5.7, in terms of maximum shear strain contours and strength reduction factors (SRF). Maximum shear strain contours, depicting the zones of possible failure, are similar in nature as obtained from LEM analyzes. Maximum shear strains were developed near the surface of the slope with silty sand soil material (Soil-2). However, critical slip surface for Soil-2 represent different region, which is because they were obtained from different methods of analyses. However, it is to be noted that in both cases the FOS values are nearly similar and showed shallow critical slip surfaces, which are confined to near surface region. Slopes with Soil-1 and Soil-3 show similar kind of strains i.e., the zone of failure is starting near the toe and extending towards the crest region of the ground surface.



TH-2008_136104008


Figure 5.7 Maximum shear strain contours for the homogeneous slopes

Figure 5.8 represents the total displacements and Figure 5.9 show displacement vectors of the three model slopes with three different soils. The dotted lines represent the critical surfaces from the LEM analyzes. The displacements are concentrated to the slope surface for the slope with Soil-2 with a maximum displacement of 0.021 m. The slope with Soil-3 depicts maximum zone of total displacements. The maximum displacement is 0.128 m for Soil-3 slope and 0.051 m for the Soil-1 slope.

The three soils selected for the study depicted different failure modes and the corresponding safety factor values for homogenous slope cases. Soil-1 and Soil-3 are the fine-grained soils (CL) but having different strength parameters showed significantly different slip surfaces and *FOS* (SRF) values. Rotational failure is observed for fine-grained soils, Soil-1 and Soil-3. In contrast, the Soil-2 being a coarse-grained (SM) soil showed very differently, translational type of slip surface (very shallow and close to the surface). Skempton and Hutchinson (1969), Choudhury et al. (2010), and Huang (2014) have reported slope failures at different sites, which showed rotational failures and translational failures.



TH-2008_136104008

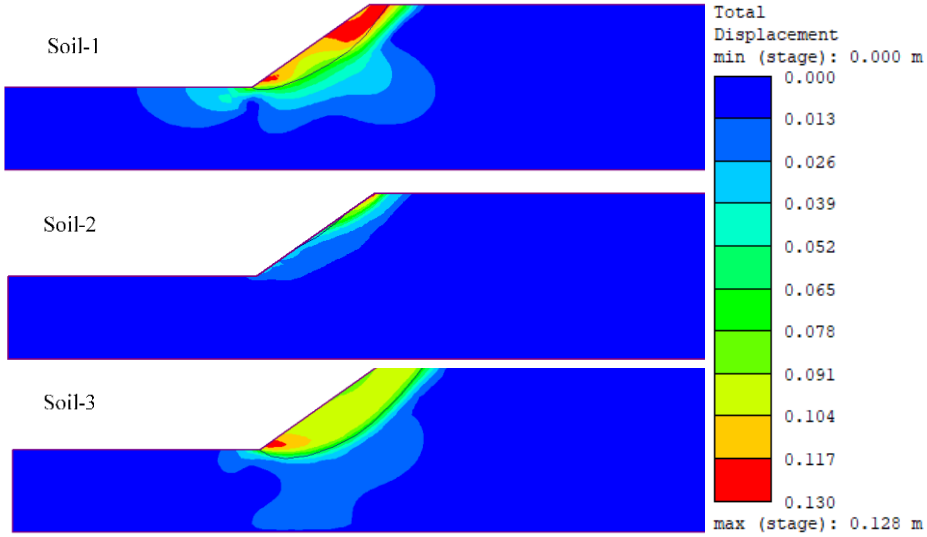


Figure 5.8 Total displacement contours for the homogeneous slopes

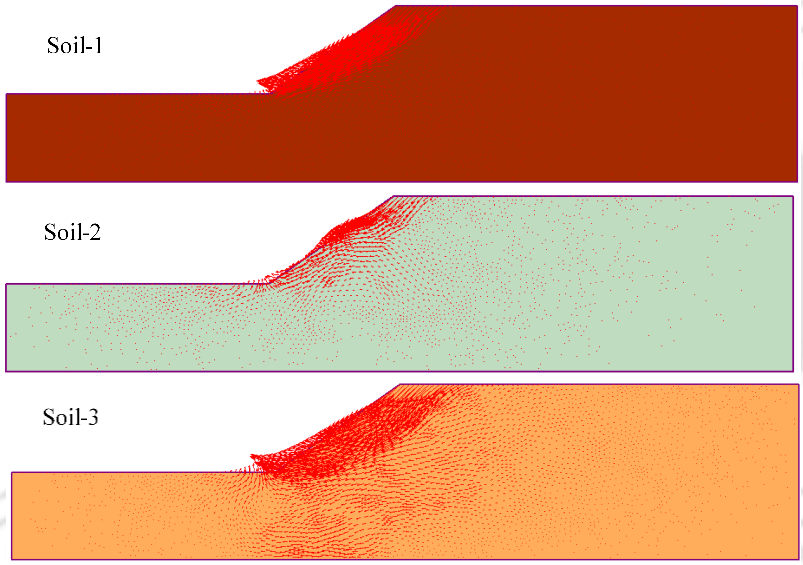


Figure 5.9 Displacement vectors for the homogeneous slopes

***Effect of Moisture Content Variation***

To study the effect of moisture content on the stability of the slope, the slope with Soil-1 was modelled (as shown in Figure 5.10) by considering five different moisture contents (degree of saturation, $S_r$). The dimensions of the slope remain the same. The homogeneous slope models were considered in such a way that each slope model consisted of Soil-1 at a single moisture content. Material properties of Soil-1 at different moisture content as reported in Table 3.3 have



TH-2008_136104008

been used for different models with corresponding moisture content. The soil was tested at different moisture contents (degree of saturation) in the laboratory. From the UU tests, different shear strength parameters were obtained at different initial saturation percentages of the soil. To study the effect of saturation of soil on the stability of a slope, the slopes were modelled with the soil at different saturation percentages. *FOS* values and critical slip surfaces from the LEM analyzes; and SRF and information on stress, strains, and displacements from FEM analyzes were obtained.

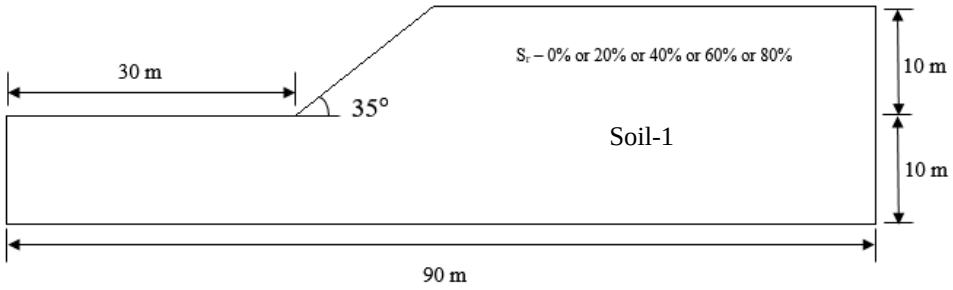


Figure 5.10 Homogeneous slope with Soil-1 at different moisture contents

The results of the homogeneous slopes with different moisture content prevalent in the slope are presented in Table 5.3. The slope is having a high safety factor at 0% degree of saturation. With an increase in the degree of saturation (from 0% to 80%), the safety factor decreases from 2.294 to 1.1. As the moisture content increases in the soil, the material unit weight increases and simultaneously the strength properties decrease which is a reason for the stability of the slope to decrease. Figure 5.11 illustrates the non-linear change in the factor of safety of the slope with an increase in the degree of saturation of the soil.

Table 5.3 Safety factors for the homogeneous slope with different moisture content

| The degree of Saturation, $S_r$ (%) | Factor of Safety | |
|---|---|---|
| | LEM-MP | FEM-SRM |
| 0 | 2.294 | 2.12 |
| 20 | 1.76 | 1.63 |
| 40 | 1.533 | 1.42 |
| 60 | 1.26 | 1.16 |
| 80 | 1.1 | 1.01 |



TH-2008_136104008

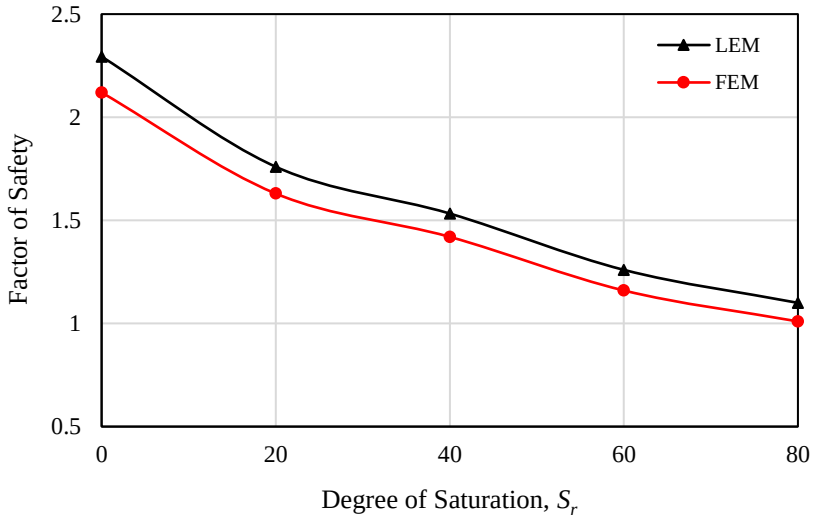


Figure 5.11 Variation of safety factor with saturation

The zones of maximum shear strains developed for the homogeneous soil slopes are shown in Figure 5.12. The first slope is at 0% saturation; the corresponding slopes are at 20%, 40%, 60% and 80% saturation levels. From the contours, it is observed that the slope with 0% saturation has the maximum shear strain of 0.035 with its SRF as 2.12. At 20% saturation, the maximum shear strain is 0.037 and SRF is 1.63 while at 80% saturation; the maximum shear strain is 0.042 and corresponding SRF is 1.01. At 40% and 60% saturation, the slopes are having maximum shear strains of 0.039 and 0.041 respectively. The dotted lines represent the critical slip surfaces obtained using the limit equilibrium method. From the figure, it can be observed that models at all the moisture content levels show toe failure mechanism with almost identical critical slip surfaces. The slip surfaces for all the other moisture contents follow the same path while having their factors of safety so different from each other. The strength properties of the soil change with variation in the degree of saturation, which accounts for the difference in safety factor values but having the path of the critical slip surface same.



TH-2008_136104008

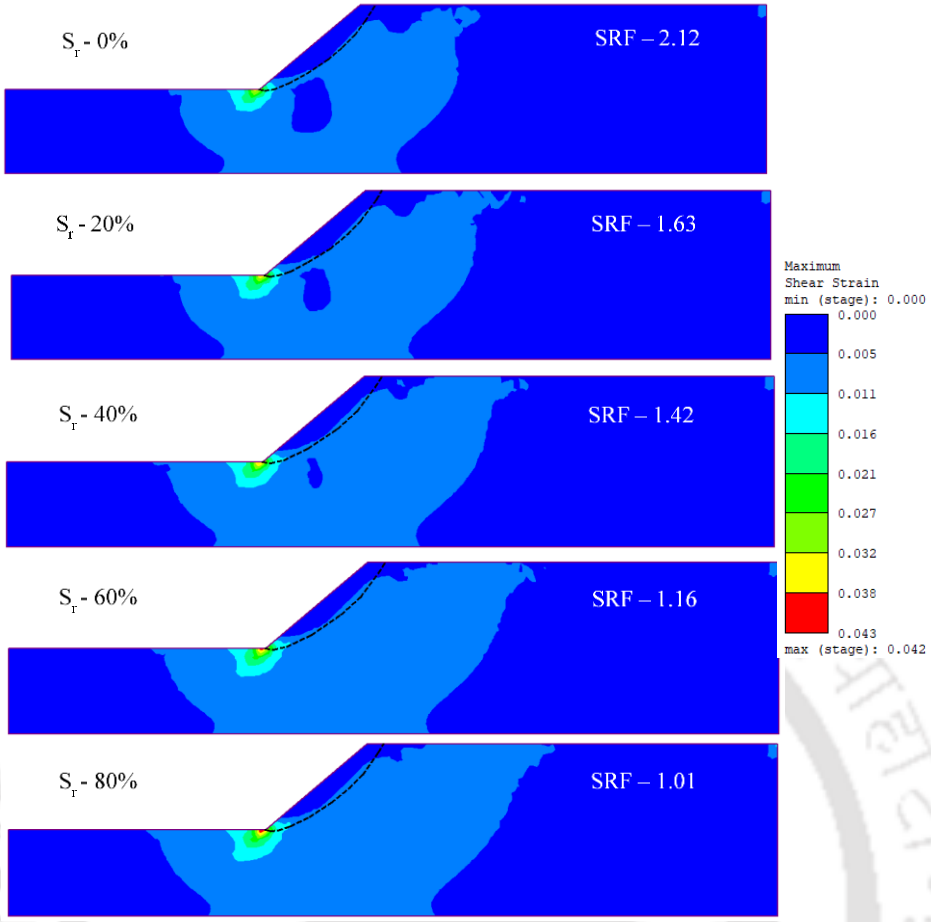


Figure 5.12 Maximum shear strain contours at different moisture contents

The SRF values at 40% and 60% saturation are 1.42 and 1.16 respectively. The maximum shear strains increased and the SRF within the slope gradually reduced with an increase in the degree of saturation of the soil. With an increase in the degree of saturation, the moisture within the slope is increased and as a result, the total unit weight is being enhanced.

### 5.1.2 Case 2: Analysis with GWL

The model of the homogeneous slope prepared with a GWL is illustrated in Figure 5.13. The slope height and inclination have been kept unchanged. The ground water level (GWL) considered to be at a height of 10 m at the right boundary and at 5 m height at the left boundary. The seepage analysis was performed using the finite element method. The pore pressures obtained from the seepage analysis were used in the limit equilibrium method for the stability analysis. In addition to the properties mentioned in Table 3.1, SWCC properties of soils



TH-2008_136104008

discussed in Chapter 3 have been used in the numerical model. In this case, unsaturated behaviour of soils due to the presence of ground water level has been included in the analyzes.

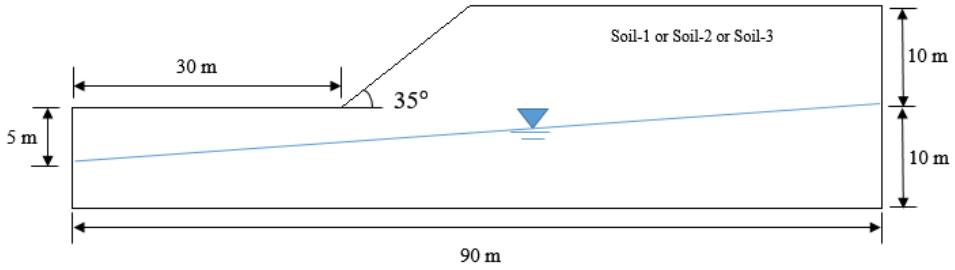


Figure 5.13 Homogeneous slope model with the GWL

Figure 5.14 depicts the pore water pressure profiles at different sections (Figure 4.11) of the slope. Figure 5.14a represent the pressure profiles at the toe section. At the surface, the suction is near to 30 kPa, which decreases as it reaches the GWL. All the three soils represent hydrostatic nature in the slope. Figure 5.14b depict the pore pressure profile at the mid-slope section of the slope. The suction at the surface is near to 75 kPa, which reduces to zero at the water surface. Figure 5.14c represent the pore pressure profile at the crest region of the slope. Here suction recorded at the surface is 120 kPa for all the three soils at a height of 12 m from the ground water level.

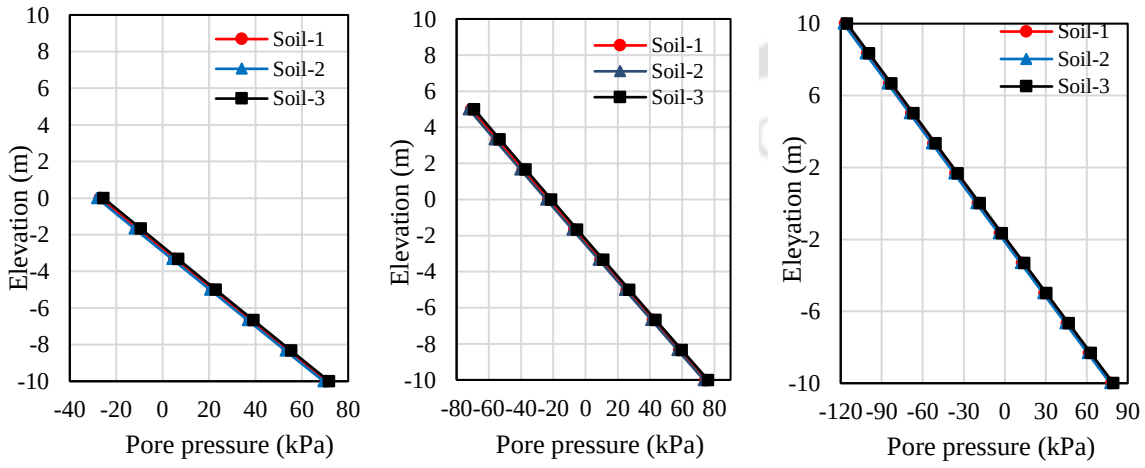


Figure 5.14 Pore water pressure profiles for homogeneous slopes with different soils along different sections at: (a) Toe, (b) Mid-slope, and (c) Crest



TH-2008_136104008

The suction at the surface, at all the three sections, account for the relatively high stability of the slopes. The critical slip surfaces of the homogeneous slopes with a ground water level are shown in Figure 5.15. The critical slip surface for Soil-1 just touches the ground water level depicting a base failure mechanism. The factor of safety for Soil-1 is 2.376. For Soil-2, the critical slip surface just cuts the GWL having a similar path as that of Soil-1. The slope with Soil-2 has a factor of safety of 2.538. The critical slip surface for Soil-3 passes at a considerable distance below the GWL having the deepest failure mode with the lowest safety factor of 1.923. The factor of safety corresponding to the slip surface is denoted in the figure as *FOS*.

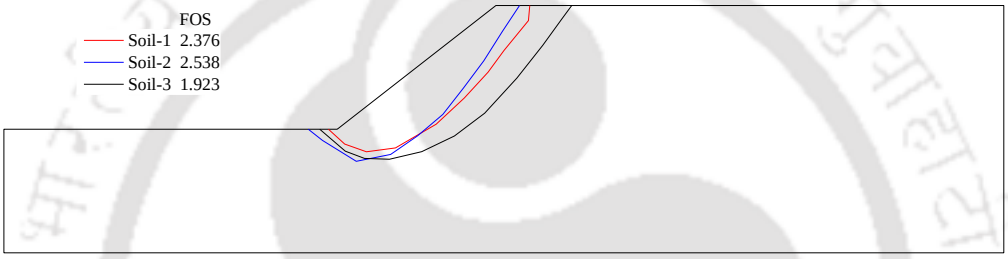


Figure 5.15 Critical slip surfaces of the homogeneous slopes

Referring to the results presented for a case with no GWL and no SWCC characteristics, the present case shows significantly different *FOS* values and critical slip surfaces. Hence it shall be noted that due attention to the GWL and unsaturated behaviour of soils shall be given for slope stability analysis.

## 5.3 ANALYSIS WITH RAINFALL INFILTRATION

The infiltration analysis of homogeneous slopes with the three soils has been performed utilizing the slope model as shown in Figure 5.16. Presence of ground water level (GWL) and SWCC properties along with permeability functions of the soils (as discussed in Chapter 3) were considered in the numerical analyzes. Rainfall intensity (external flux) of 30 mm/h was applied for 24 hours (short duration) on to the surface of the numerical model. The effects of rainfall intensity, slope height, slope angle and duration of rainfall have been studied using this model. For all of the models, the seepage analysis was performed using the finite element



TH-2008_136104008

method. The stability factors of the slopes were then evaluated using the limit equilibrium method.

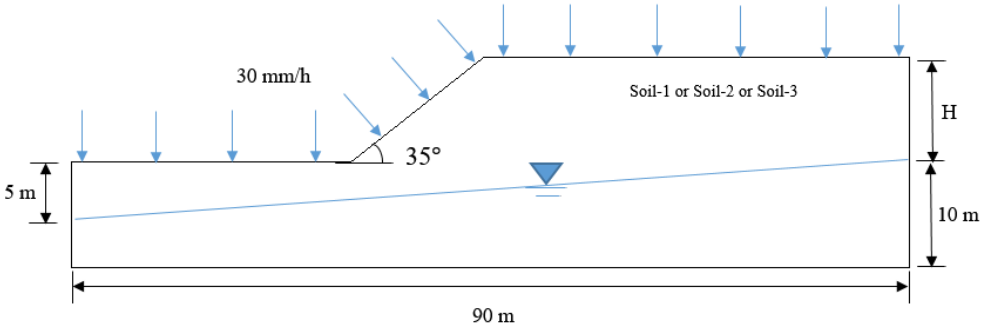


Figure 5.16 Homogeneous slope model with GWL under rainfall conditions

Figure 5.17 represent pore water pressure profiles along vertical sections, under rainfall conditions resulting from transient seepage analysis after 24 hours, for homogeneous models with three different soils. At 24 hours, it was observed that all the three soils have positive pressures at the toe region (Figure 5.17a), which implies that the water level is touching the toe at this moment. At the mid-slope portion shown in Figure 5.17b, Soil-1 has its surface saturated, Soil-2 has negative pore pressure in the region of 17 kPa because the high permeability of the soil allows the water to infiltrate down without saturating the surface. For Soil-3, the pore pressure changes from zero to -19 kPa until 3.3 m from the surface and again starts to increase towards the positive values. At the crest portion (Figure 5.17c); both Soil-1 and Soil-3 exhibit zero suction at the surface where the water saturates the soil due to their low permeability. Soil-2 on the other hand, depict suction value of 25 kPa due to its high permeability. The pore pressures become positive at a depth of 12 m from surface representing ground water level. Surface saturation occurs for Soil-1 and Soil-3 as their permeability is less than the rainfall intensity applied after 24 hours. Runoff starts just after saturation of the surface and the infiltration capacity of the soil is gradually reduced. For Soil-2, the water easily infiltrates the soil due to its higher saturated permeability and the suction gets dissipated at lower depths.



TH-2008_136104008

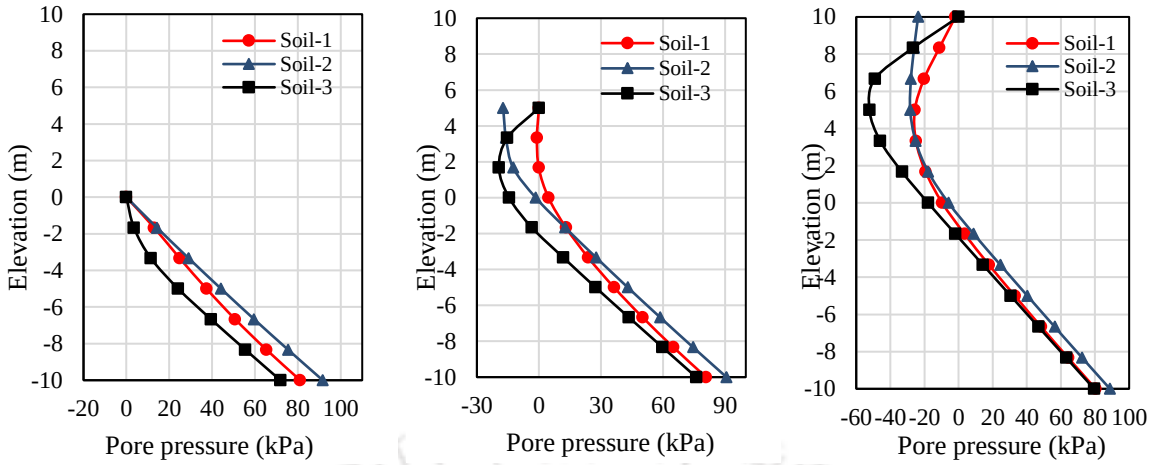


Figure 5.17 Pore water pressure profiles for homogeneous slopes with different soils after 24 hours along different sections at: (a) Toe, (b) Mid-slope, and (c) Crest

Figure 5.18 illustrates the pore pressure profiles of the homogeneous slopes after 48 h. At the toe (Figure 5.18a), the suction at the surface is near to 10 kPa for all three soils, the pressure profile followed by Soil-3 is different from Soil-1 and Soil-2. At the mid-slope region (Figure 5.18b), the soils represent different suction values at the surface. A similar type of pressure profile is observed in the crest region (Figure 5.18c) also. For the pressure profile at the crest region of Soil-3 slope, the pressure profile consists of a portion of constant pore pressure from a height of 8 m to 4 m near the surface.

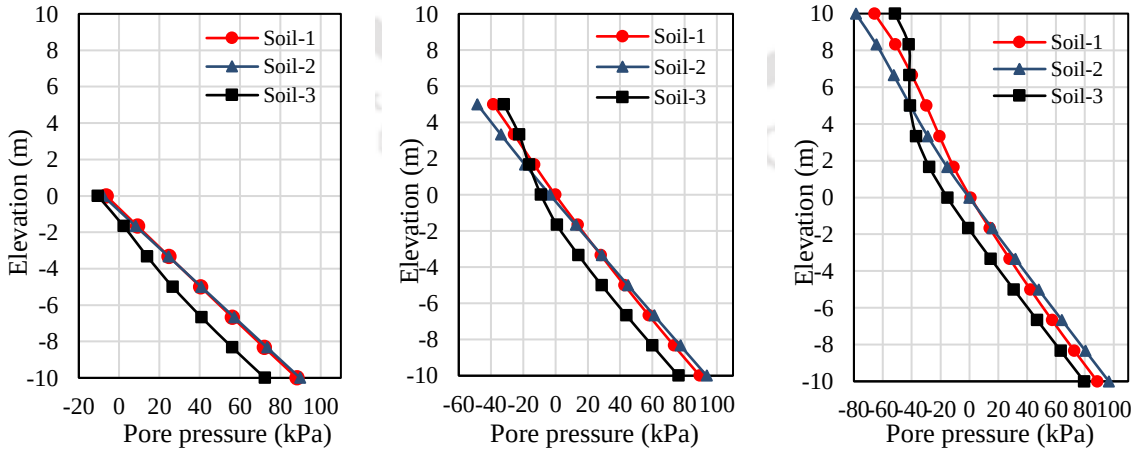


Figure 5.18 Pore water pressure profiles for homogeneous slopes with different soils after 48 hours along different sections at: (a) Toe, (b) Mid-slope, and (c) Crest



TH-2008_136104008

Figure 5.19 illustrates the pore water pressure contours of the slopes with three different soils after 24 hours of rainfall. WT represents the GWL level represented by a line in the figure. It is observed that the maximum negative pore pressures in the region of 63-40 kPa are seen for the slope with Soil-3 due to the low permeability of the soil. The maximum suction values for Soil-1 and Soil-2 stay in the range of 40-17 kPa. The water levels in the slope vary with rainfall infiltration illustrating different behaviour of the three soils. The water level in Soil-1 touches the slope surface near the mid-slope region and then follows the surface. For Soil-2, the water level touches the toe portion and then falls off gradually in a parabolic pattern. The GWL rises and joins the slope surface at the toe for Soil-3, continues for some distance along the surface. The factor of safety of the slopes is also depicted in the figure.

Figure 5.20 depicts the variation of pore pressure with time at a point P within the slope (at a depth of 2 m from the surface). It can be clearly seen from the figure that for all the three slopes the suction reduces during rainfall (until 24 hours) and then it increases after rainfall was stopped. The change in suction is rapid for Soil-1.

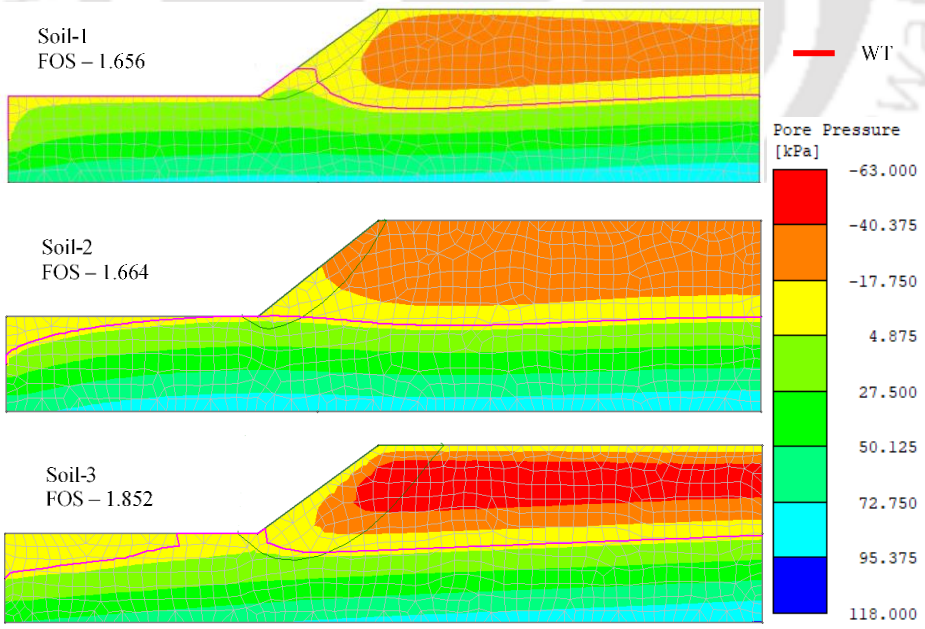


Figure 5.19 Pore water pressure contours of homogeneous slope after 24 hours with different soils



TH-2008_136104008

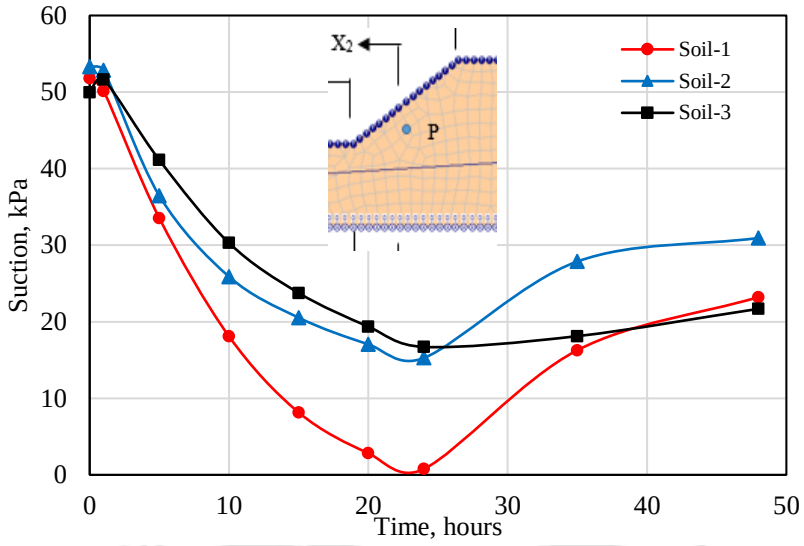


Figure 5.20 Pore water pressure variation of point P with time for the three soils

The variation in the factor of safety of the slope with time is shown in Figure 5.21. It is observed that during rainfall infiltration the safety factor of the slope decreases due to a decrease in matric suction, thereby reducing the effective cohesion in the soil. Slope with Soil-2 has the maximum initial factor of safety near to 2.6 which reduced to 1.683 at 24 hours and recovered to 1.923 at 48 hours. Out of the three soils, the lowest initial safety factor is denoted by the slope with Soil-3. From 1.996 initially, the safety factor reduces to 1.928 at 24 hours and recovered to 1.904 at 48 hrs. The change in safety factor is very small is due to the fact that water is unable to infiltrate due to the low saturated permeability (less than the rainfall intensity) and the water flowed as runoff. The slope with Soil-1 exhibits behaviour very much like Soil-2 with the safety factor decreasing from 2.376 initially to 1.656 at 24 hours. Under rainfall infiltration, the decrease in the factor of safety of Soil-1 is mainly due to the rise of the GWL. For Soil-2, the reduction of stability of the slope was due to a decrease of suction mainly. The recovery rate of the factor of safety after the end of rainfall was high for Soil-1 and Soil-2. The homogeneous slope with Soil-3 was barely affected by the applied rainfall intensity.



TH-2008_136104008

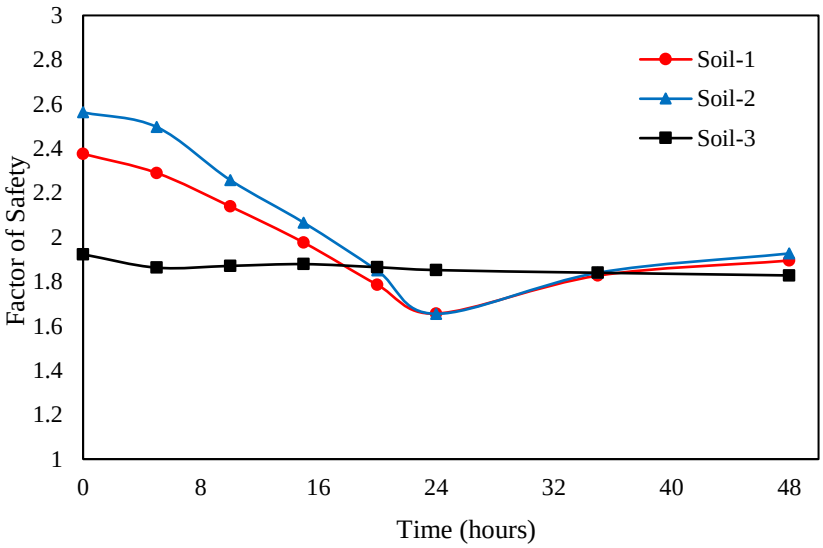


Figure 5.21 Variation of safety factor with time for homogeneous slopes

Figure 5.22 shows the slip surfaces of the three soils after 24 h of rainfall infiltration where it is observed that for Soil-3 the slip surface position is deepest with the highest factor of safety of 1.852. This behaviour of different failure surfaces for different soils could be linked to the GWL levels (Figure 5.19) in different soils due to rainfall infiltration. For Soil-3, the GWL touches the surface near the toe and continues for some distance along the surface. Hence, a small portion of the slip surface is saturated for Soil-3. For Soil-2, the rise in GWL, touches the slope surface at the toe, and continues for some distance along the slope surface. The bottom portion of the slip surface is fully saturated as it cuts through the water level. The GWL rises higher for Soil-1 after rainfall infiltration and touches the slope surface near the mid-slope portion. Hence, a relatively large amount of the failure mass is saturated in the case of Soil-1. Soil-1 represent toe failure while Soil-2 and Soil-3 exhibit base failure mode.

Figure 5.23 depicts the critical slip surfaces of the three soils after 48 h. After 48h, the slip surfaces appear to be similar to the slip surfaces depicted before the onset of rainfall infiltration as shown in Figure 5.15. However, in this case, the *FOS* values for all the three soils are reduced which could be attributed to the change in suction values as depicted in Figure 5.18. All the three soils exhibit base failure mechanism and have safety factor values near to 1.9.



TH-2008_136104008

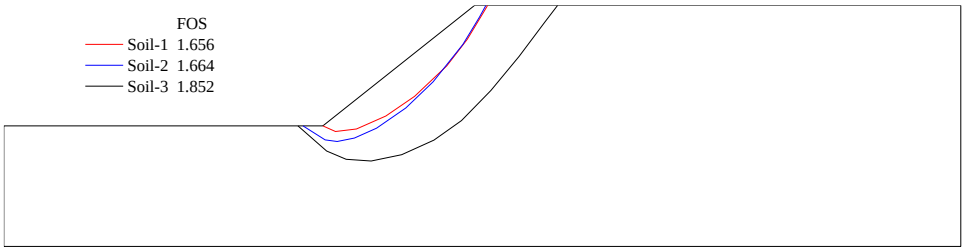


Figure 5.22 Critical slip surfaces of the homogeneous slopes after 24 h

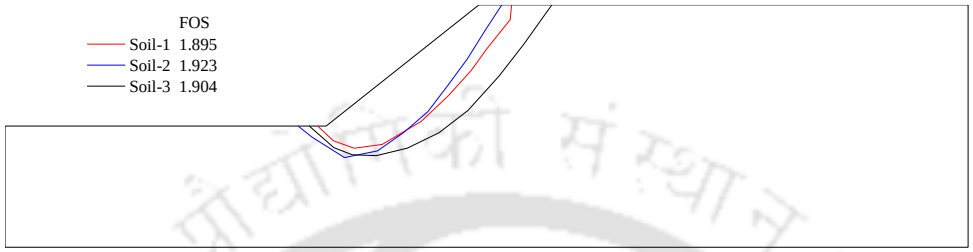


Figure 5.23 Critical slip surfaces of the homogeneous slopes after 48 h

### 5.1.3 Effect of rainfall intensity

To study the effect of rainfall intensity on the stability of slopes with different soils, five different rainfall intensities of 10 mm/h, 30 mm/h, 50 mm/h, 100 mm/h and 200 mm/h were used. A short duration (24 h) rainfall was applied to the slope surface in all scenarios. The results obtained for each type of soil are presented below.

***Soil-1***

The pore–water pressure profiles for Soil-1 at the mid-slope section under different rainfall intensities are depicted in Figure 5.24 after 24 h of rainfall infiltration. Maximum suction of 37 kPa is observed at the surface under 10 mm/h rainfall intensity. At all the other rainfall intensities the surface gets saturated and positive pore pressures to exist throughout the soil depth. Figure 5.24b represent the pore pressure profiles after 48h. Hydrostatic conditions are observed at this stage with the 50 mm/h, 100 mm/h and 200 mm/h intensity having similar profiles. The suction of 57 kPa exists at the surface under 10 mm/h rainfall intensity. 35 kPa suction at the surface is observed under all the other intensities.



TH-2008_136104008

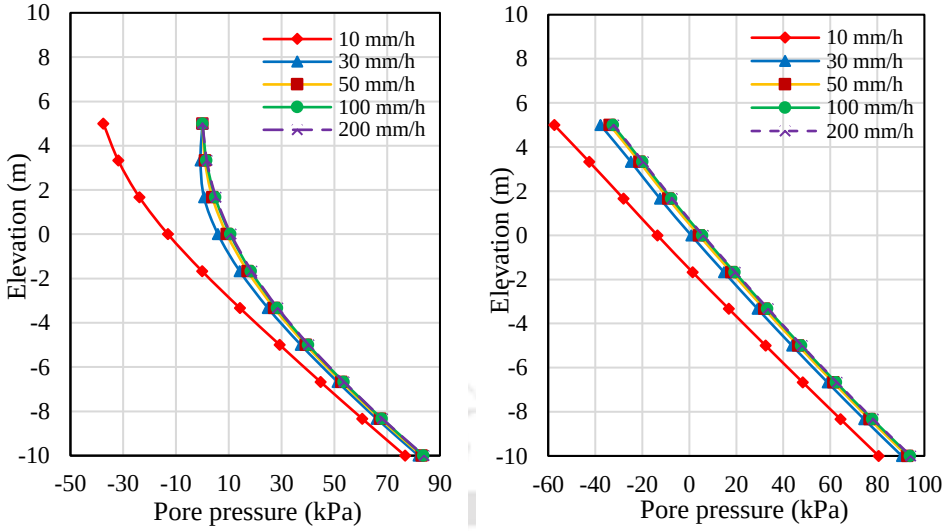


Figure 5.24 Pore pressure profiles at the mid-slope section for Soil-1 under different rainfall intensities after (a) 24 h and (b) 48 h

Figure 5.25 depict the GWL rise after 24 h of rainfall infiltration under different rainfall intensities. It is observed that the water level gradually rises with an increase in rainfall intensity. The dotted line represents the initial water level existing in the slope prior to rainfall infiltration. For rainfall intensities higher than 10 mm/h, the GWL rises and touch the slope surface at the mid point of the sloping region. The mounding of GWL leads to the decrease of the stability of the slope under infiltration conditions.

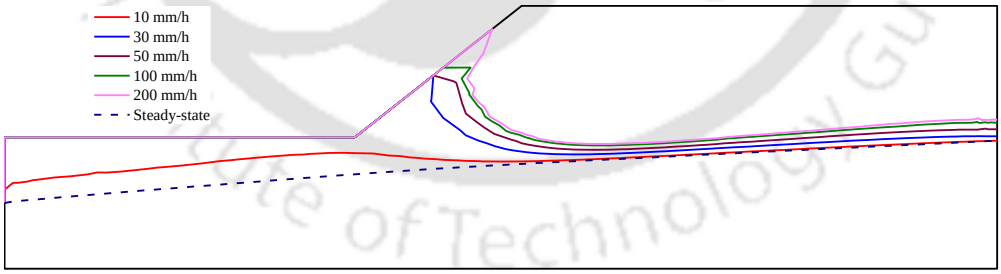


Figure 5.25 GWL location for Soil-1 under different rainfall intensity after 24 h

The variation of a factor of safety with time for different rainfall intensity values is illustrated in Figure 5.26. It is observed that the minimum factor of safety decreases with time. The rate of decrease depends on the magnitude of the rainfall intensity. The curve for 10 mm/h intensity illustrates that the stability of the slope is not much affected because now the intensity is low



TH-2008_136104008

as compared to the permeability of the soil. Hence, there is not much infiltration occurring to reduce the suction within the slope. With an increase in rainfall intensity, at $8.3\times10^{-6}$ m/s (nearly equal to the permeability of Soil-1, $8.38\times10^{-6}$ m/s) the safety factor reduces to 1.638 after 24 h and then increases (*FOS* -1.869) after 48 h. The factor of safety reduces to 1.487 from 2.39 after 24 h of infiltration under 50 mm/h intensity.

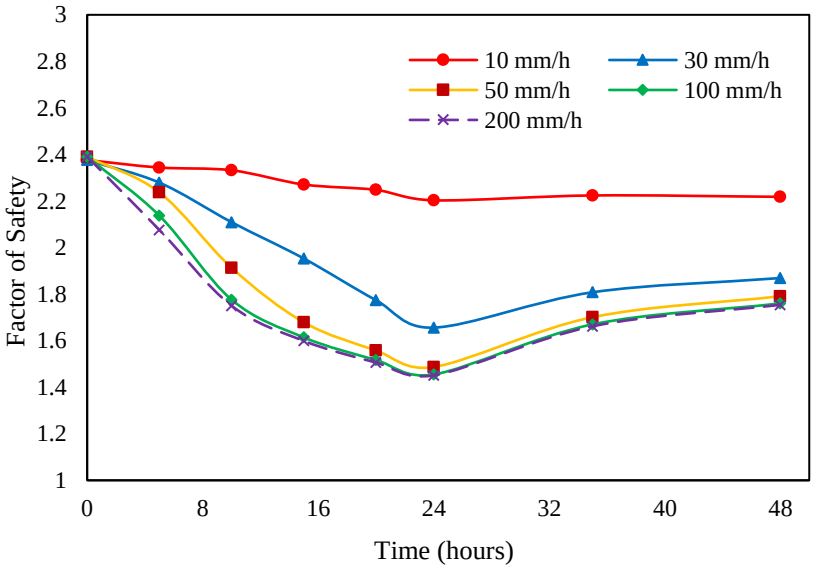


Figure 5.26 Variation of a factor of safety with rainfall intensity for Soil-1

Under 100 mm/h rainfall intensity, the slope has a minimum factor of safety of 1.455 after 24 h of rainfall while the minimum safety factor is 1.451 after 24 h under 200 mm/h rainfall intensity. As rainfall stops, the slope rapidly recovered the safety factor due to the increase of suction. The minimum factors of safety of the slope under rainfall intensities 50, 100 and 200 mm/h are similar which points toward a threshold rainfall intensity. Therefore, 50 mm/h seems to be the threshold intensity beyond which there is no effect on the minimum factor of safety of the slope because now the slope has reached its infiltration capacity. Here, the decrease in the stability of the slope can be attributed to the rise of water level due to an increase in the rainfall intensity.



TH-2008_136104008

Figure 5.27 illustrates the critical slip surfaces for different rainfall intensities after 24h of rainfall infiltration. The slope under 10 mm/h rainfall intensity represents the deepest slip surface with the maximum factor of safety. The slope under the other intensities represent toe failure mechanism and all of them have similar critical slip surface paths. As the intensity increase, the water level in the slope also increase (Figure 5.25) and therefore more portion of the slip zone gets saturated thereby decreasing its factor of safety. It is observed that the influence of rainfall intensities 50 mm/h, 100 mm/h and 200 mm/h are very similar i.e., the rainfall intensity more than 50 mm/h does not have any significant effect on the stability of the homogeneous slope.

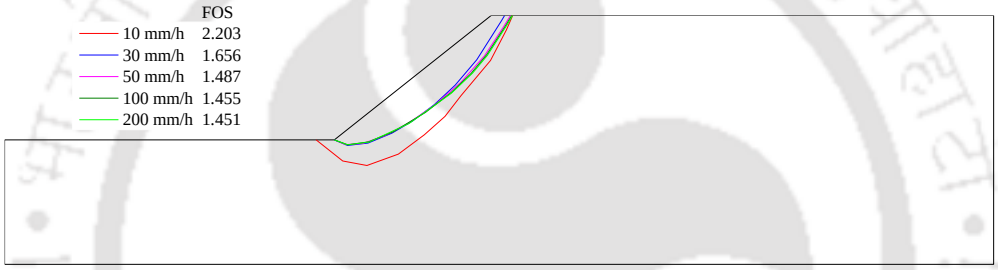


Figure 5.27 Critical slip surfaces at different rainfall intensities after 24 h for Soil-1

The critical slip surfaces under different rainfall intensities after 48h are depicted in Figure 5.28. Rainfall stops after 24h and so the infiltration, resulting in the fall of water level and the increase of suction. Here all the slip surfaces have a base failure mechanism with the surface under 10 mm/h intensity being the most deep-seated. There is very little influence of rainfall intensity after 50 mm/h.

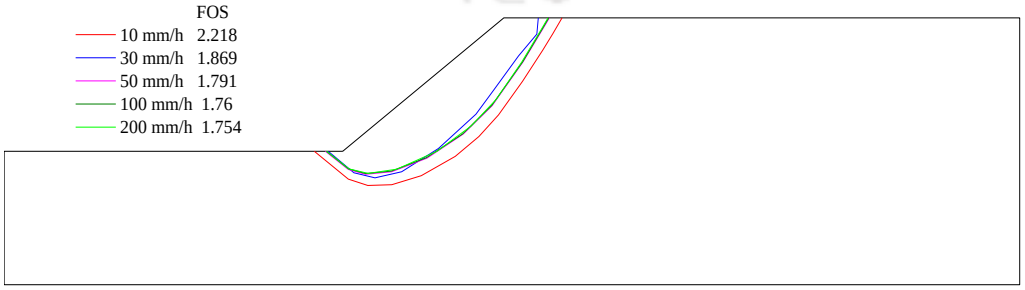


Figure 5.28 Critical slip surfaces at different rainfall intensities after 48 h for Soil-1



TH-2008_136104008

***Soil-2***

The pore pressure profiles of Soil-2 at various rainfall intensities are shown in Figure 5.29. Under, 10 mm/h intensity, the suction at the surface is 45 kPa, which reduced to 17 kPa under 30 mm/h intensity. The surface of the slope is saturated after 24 h under 100 mm/h and 200 mm/h rainfall intensities as the water level rises to the surface. With an increase in rainfall intensity, the pressure profiles gradually shift towards the positive portion of the pressure range.

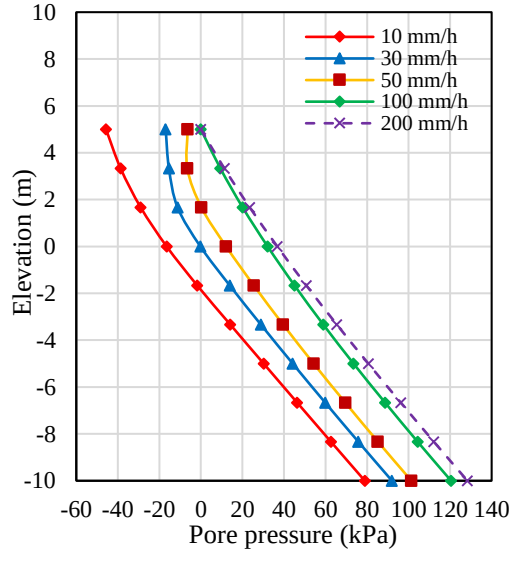


Figure 5.29 Pore pressure profiles at the mid-slope section for Soil-2 under different rainfall intensities after 24 h

Figure 5.30 depict the rise in water level due to rainfall infiltration under different rainfall intensities. The dotted line in the figure shows the initial level of GWL prior to rainfall infiltration. The GWL rises higher under increasing rainfall intensity due to more water infiltration within the slope. It is observed that the GWL gradually rises and touches the slope toe under 30 mm/h intensity and continues to follow the slope surface until a small distance (7 m) and then falls off gradually. Under 100 mm/h intensity, the water flows just below the surface of the slope while under 200 mm/h intensity the water flows along the surface of the slope throughout. The mounding of the water level is higher under higher rainfall intensities.



TH-2008_136104008

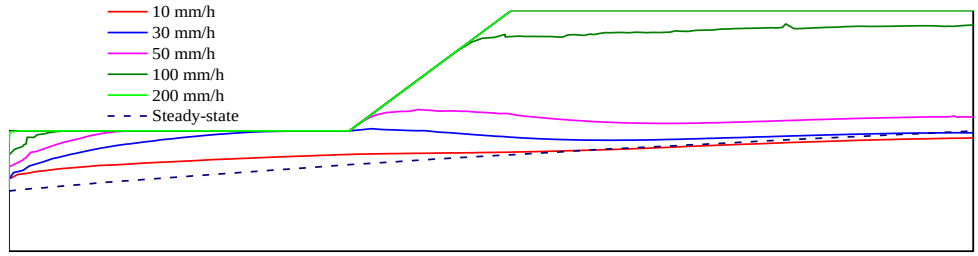


Figure 5.30 GWL location for Soil-2 under different rainfall intensity after 24 h

The variation in the factor of safety of the slope with time is illustrated in Figure 5.31. It is observed that the minimum factor of safety decreases with time. The rate of decrease of the minimum factor of safety depends on the magnitude of the rainfall intensity. After 24 h of rainfall infiltration, the factor of safety reduces from 2.53 to 2.32 under the intensity of 10 mm/h. The 10 mm/h rainfall intensity was not that high to reduce the suction within the slope. Under 30 mm/h intensity, the factor of safety decreases from 2.53 to 1.65. The safety factor reduces to 1.16 after 24 hours under 50 mm/h intensity. The slope reaches failure conditions under the 100 mm/h intensity for just 10 hours of the infiltration process. Under 200 mm/h intensity, the slope fails just 5 hours after the start of the rainfall infiltration. As rainfall stops after 24 hours, the slope recovers some of its stability due to the fall of the GWL. The decrease in the stability of the slope is primarily due to the rise of the GWL. The minimum factors of safety of the slope under rainfall intensities 100 and 200 mm/h are nearly similar which points toward a threshold rainfall intensity. Therefore, 200 mm/h is the threshold intensity beyond which there is no effect on the minimum factor of safety of the slope because now the slope has reached its infiltration capacity.

Soil-2 is highly permeable and under the applied rainfall intensity, all of the rainwater infiltrates which results in the rise of the GWL and decrease of matric suction. The rate of decrease of factor of safety increases with increase in the rainfall intensity. Therefore, this type of soil is highly susceptible to slope failures under the applied rainfall conditions.



TH-2008_136104008

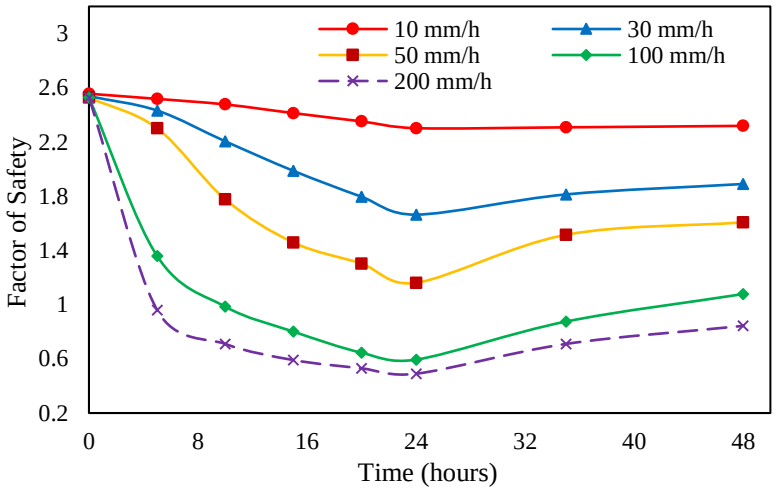


Figure 5.31 Variation of a factor of safety with rainfall intensity for Soil-2

Figure 5.32 represent the critical slip surfaces under different rainfall intensities after 24 hours of rainfall. The base failure mechanism is observed for 10 mm/h and 30 mm/h rainfall intensity. Shallow slope failures were observed for 50mm/h, 100 mm/h and 200 mm/h rainfall intensities. It is also noted that with an increase in rainfall intensity, the slip surfaces move towards the surface of the slope with reducing safety factors. The effective strength of the soil is reduced due to an increase in pore pressure resulting from the higher intensity, which pushes the critical surface towards the surface.

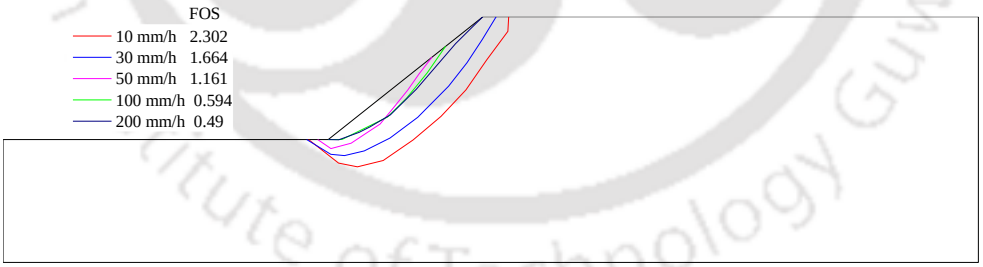


Figure 5.32 Critical slip surfaces at different rainfall intensities after 24 h for Soil-2

***Soil-3***

The effect of rainfall intensity on the pore pressure profiles of Soil-3 is illustrated in Figure 5.33. The surface gets saturated after 24 h under all the five different rainfall intensities selected. The pore pressure decreases with a depth reaching a minimum of -25 kPa under 10 mm/h rainfall intensity. The suction under all the other rainfall intensities reach 20 kPa at a



TH-2008_136104008

depth of 3 m from the surface of the slope. Soil-3 possess a very low saturated permeability, which hinders the infiltration of water into the soil. As the rainfall intensity increases, more water flows as run-off and hence the suction does not decrease more.

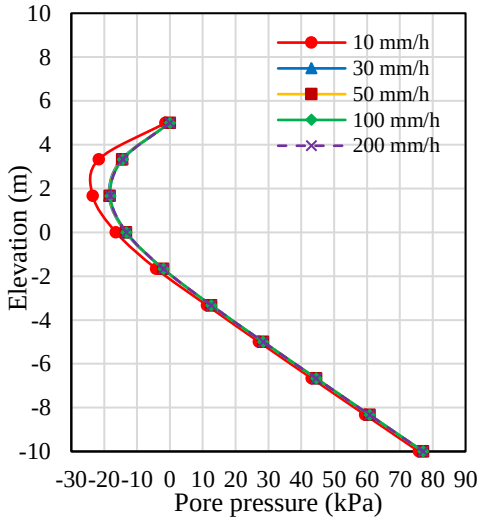


Figure 5.33 Pore pressure profile at the mid-slope section for Soil-3 under different rainfall intensities after 24h

The rise in GWL due to rainfall infiltration under different rainfall intensities is illustrated in Figure 5.34. A dotted line in the figure shows the initial level of GWL. With water infiltrating into the slope, the GWL rises to a constant height under different rainfall intensities. It is observed that the GWL rises and touches the slope toe and continues to follow the slope surface until a small distance (7 m) and then falls off gradually. The mounding of the water level is very less or negligible for soils of very low saturated permeability.

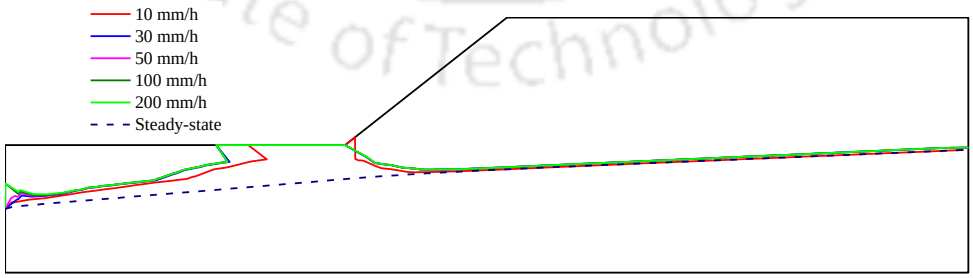


Figure 5.34 GWL location for Soil-3 under different rainfall intensity after 24 h

The variation in the factor of safety of the slope with time is depicted in Figure 5.35. Under 10 mm/h intensity, the factor of safety decreases from 1.925 to 1.865 while under 200 mm/h the



TH-2008_136104008

factor of safety decreased to 1.814. Thus, it is observed that there is very less effect on the slope due to different rainfall intensities. This phenomenon can be attributed to the low permeability of the soil, which prevents water from infiltrating into the slope. After surface saturation occurs, most of the water flows over the surface as run-off and very less water infiltrate the slope.

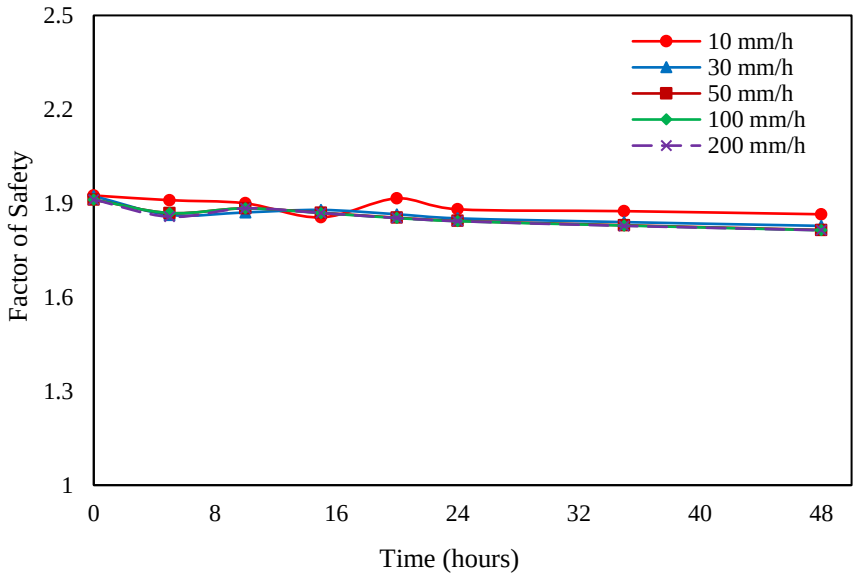


Figure 5.35 Variation of a factor of safety with rainfall intensity for Soil-3

Rather the factor of safety decreased very gradually and reached the minimum value after 48 hours. Due to the low permeability of the soil, the water could not reach the critical slip surface rapidly. For this type of soil, the water takes a longer time to reach the critical zone, which again depends on the infiltration rate. Critical slip surfaces for different rainfall intensities after 24 h is shown in Figure 5.36. All the surfaces represent a base failure mechanism and follow a similar path. Only the critical slip surface under 10 mm/h is slightly deep-seated than the other rainfall intensities. The factors of safety for the surfaces are very close to each other. Hence, for homogeneous slopes with the soil of low permeability the critical slip surfaces are not affected by higher rainfall intensities under the short duration rainfall. The rainwater is only able to infiltrate the surficial layers and therefore the stability of the slope is rarely affected.



TH-2008_136104008

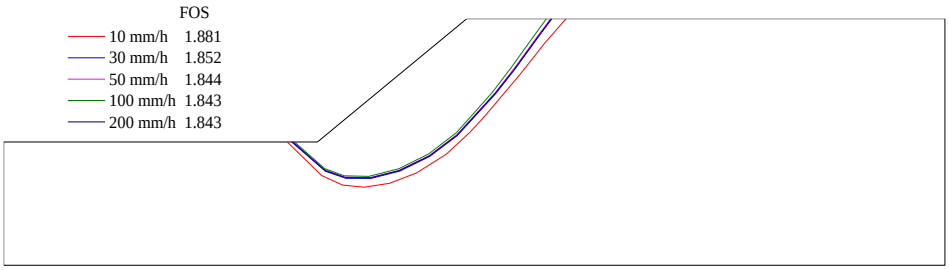


Figure 5.36 Critical slip surfaces at different rainfall intensities after 24 h for Soil-3

Figure 5.37 represents the relationship between the minimum factor of safety and the rainfall intensity for the three homogeneous slopes. It is observed that the minimum factor of safety rapidly decreases from 30 mm/h intensity for Soil-1 and Soil-2. Beyond 100 mm/h rainfall intensity, there is very little effect on the stability. For Soil-3, the curve is nearly horizontal indicating that the rainfall intensity has a negligible effect on the stability of the slope.

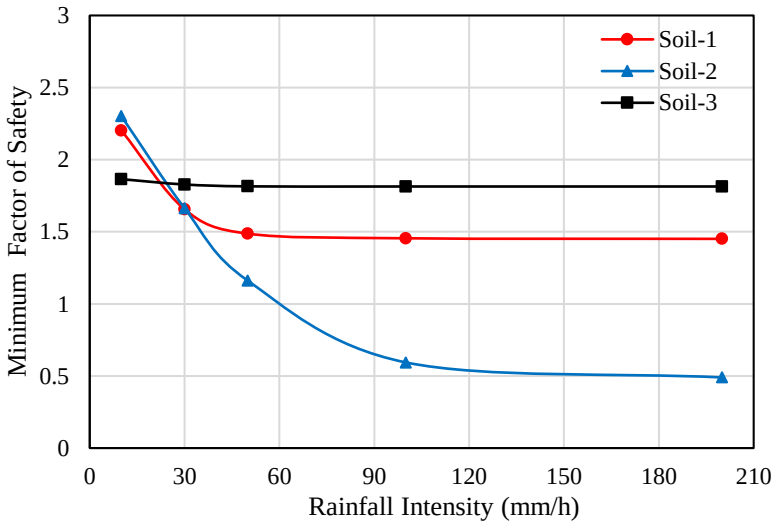


Figure 5.37 Variation of a minimum factor of safety with rainfall intensity for the homogeneous slopes

### 5.1.4 Effect of duration of rainfall

To investigate the effect of duration of rainfall on stability, two different rainfall durations (24 and 48h) were selected with constant rainfall intensity of 30 mm/h. The slope height is 10 m and slope inclination is 35°.



TH-2008_136104008

***Soil-1***

Figure 5.38 illustrates the pore pressure profiles of the homogeneous slope with Soil-1 at different times at the mid-slope section. The pressure profiles at the initial stage depict hydrostatic conditions within the slope. At the surface, the suction is 71 kPa at the initial stage. With rainfall infiltration, the surface suction starts to dissipate. After 24 hours, it is 0 kPa, 25 kPa; after 72 hours and 30 kPa; after 96 hours. With rainfall infiltration, the profile shifts towards the right (positive pore pressures), i.e., suction decreases which results in a decrease in strength of the soil. As rainfall infiltration stops, the profile shifts left towards the initial position regaining some of the lost suction.

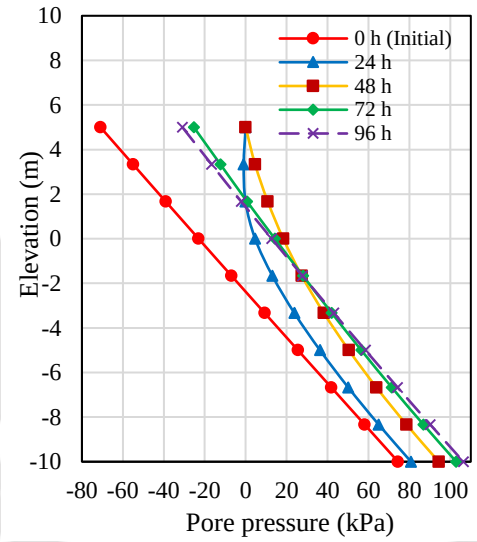


Figure 5.38 Pore pressure profile of the homogeneous slope with Soil-1at the mid-slope section under long duration rainfall

The variation in the factor of safety of the homogeneous slope composed of Soil-1 with time is shown in Figure 5.39. It is observed that during rainfall infiltration the safety factor of the slope decreases due to a decrease in matric suction, which reduces the effective cohesion in the soil. The slope has the maximum initial factor of safety near to 2.37 which reduced to 1.338 at 48 hours and increased to 1.583 after 72 hours for the long duration rainfall infiltration. For the short duration, the factor of safety of the slope decreased to 1.656 after 24 hours and then



TH-2008_136104008

recovered to 1.89 at 48 hours. There was a 19% decrease in stability of the slope under the long duration rainfall.

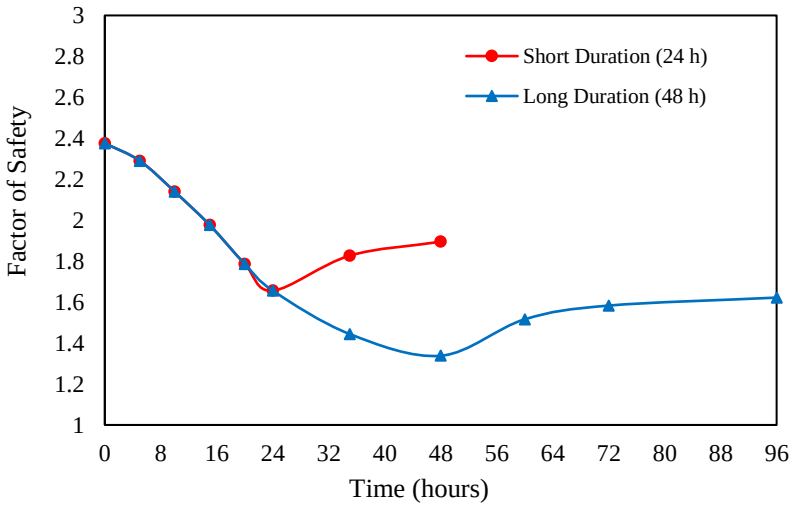


Figure 5.39 Variation of a factor of safety with time for the homogeneous slope with Soil-1 under long duration rainfall

Figure 5.40 illustrates the critical slip surfaces at various times of the homogeneous slope under long duration (48 h) rainfall. The slip surface prior to infiltration is very deep and represents a base failure mechanism with the highest factor of safety (2.376). As water infiltrates the soil, the slip surface moves toward the surface due to a decrease in suction, which reduces the effective strength of the soil. At 24 hours, the factor of safety is 1.656, which decreases to 1.338 at 48 hours where the critical slip surface resembles toe failure mechanism. When infiltration stops, the suction starts to increase and the slip surface now moves right towards the initial position. The factor of safety increases to 1.583 after 72 hours and 1.622 after 96 hours representing base failure due to an increase in suction.

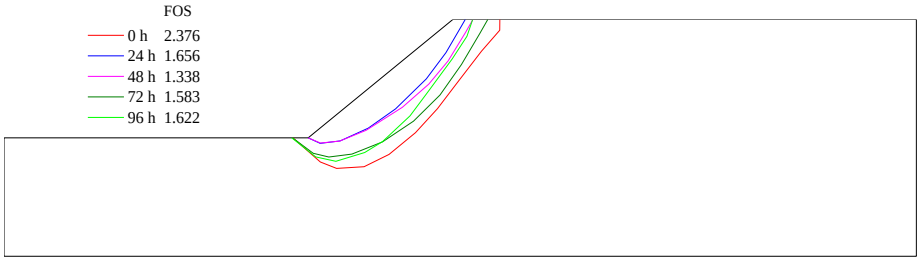


Figure 5.40 Critical slip surfaces of the homogeneous slope with Soil-1 under long duration rainfall



TH-2008_136104008

***Soil-2***

Similar results for Soil-1 and Soil-2 are recorded for pore water pressure profiles.

The variation in the factor of safety of the homogeneous slope composed of Soil-2 with time is shown in Figure 5.41. It is observed that under rainfall infiltration the factor of safety of the slope decreases due to the decrease of matric suction in the soil. The slope has the maximum initial factor of safety near to 2.6 which reduced to 1.227 at 48 hours and 1.543 after 72 hours for the long duration rainfall infiltration. For the short duration, the factor of safety of the slope decreased to 2.6 after 24 hours and then recovered to 1.92 at 48 hours. Under the long duration rainfall, the stability of the homogeneous slope decreased by 27% compared to short duration rainfall.

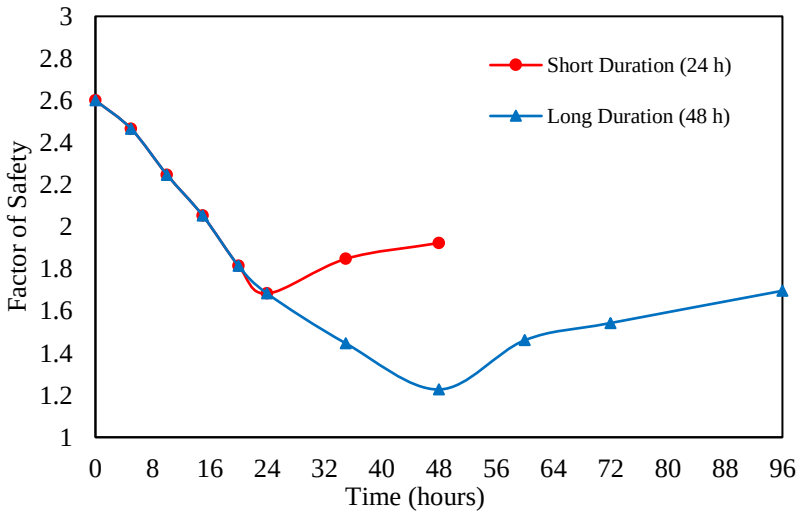


Figure 5.41 Variation of a factor of safety with time for the homogeneous slope with Soil-2 under long duration rainfall

Figure 5.42 illustrates the critical slip surfaces at various times of the homogeneous slope under long duration (48 h) rainfall. The slip surface prior to infiltration is the deepest and represents a base failure with the highest factor of safety (2.601). At 24 hours, the slip surface shifts towards the surface with a reduced failure zone representing base failure mode. With more infiltration, the slip surface further shifts towards the slope surface representing slope failure mode. At 48 hours, now the factor of safety is 1.227. As rainfall stops, the infiltration stops



TH-2008_136104008

and hence the suction increases which results in a much deeper slip surface which falls between the 0 hour and 24 hours slip surface. After 96 hours, the critical slip surface now represents a base failure with a safety factor of 1.656.

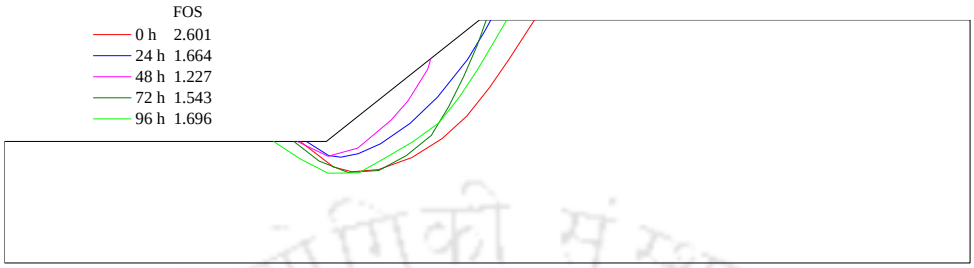


Figure 5.42 Critical slip surfaces of the homogeneous slope with Soil-2 under long duration rainfall

***Soil-3***

The variation in the factor of safety of the homogeneous slope composed of Soil-3 with time is shown in Figure 5.43. The factor of safety of the slope decreases under rainfall conditions due to the decrease of the effective strength of the soil. The slope has the maximum initial factor of safety near to 1.923 which reduced to 1.766 after 48 hours and 1.744 after 72 hours for the long duration rainfall infiltration. For the short duration, the factor of safety of the slope decreased to 1.84 after 24 hours and then continued to decrease to 1.82 at 48 hours. The stability of the homogeneous slope decreased by 4.5% more under the long duration rainfall. Here the water was unable to infiltrate the critical zone at the end of rainfall due to the low permeability of the soil. Hence, the factor of safety gradually reduced to the minimum value when the water reached the critical depth. However, the overall stability of the slope is safe under both short duration and long duration rainfalls.



TH-2008_136104008

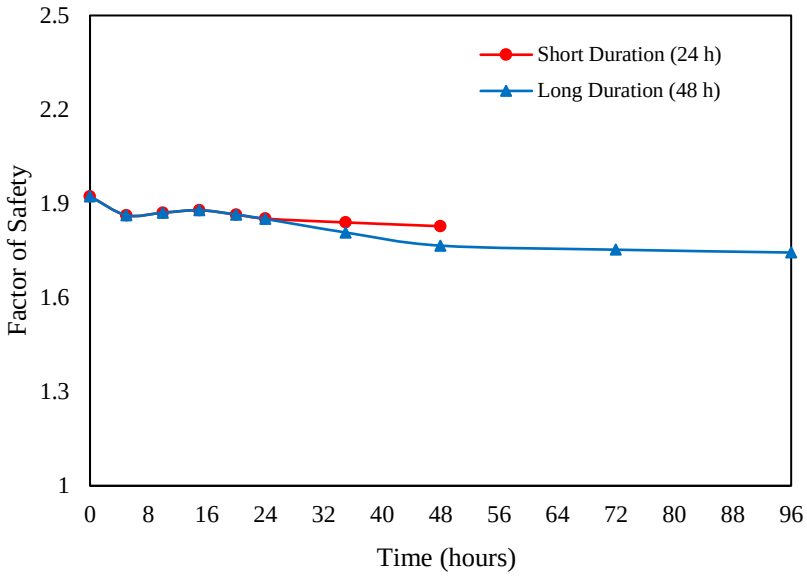


Figure 5.43 Variation of a factor of safety with time for the homogeneous slope with Soil-3 under long duration rainfall

Figure 5.44 illustrates the critical slip surfaces at various times of the homogeneous slope under long duration (48 h) rainfall. The slip surface prior to infiltration is the deepest and represents a base failure with the highest factor of safety (1.923). The slip surfaces for the other durations also indicate base failure mode approximately similar to each other.

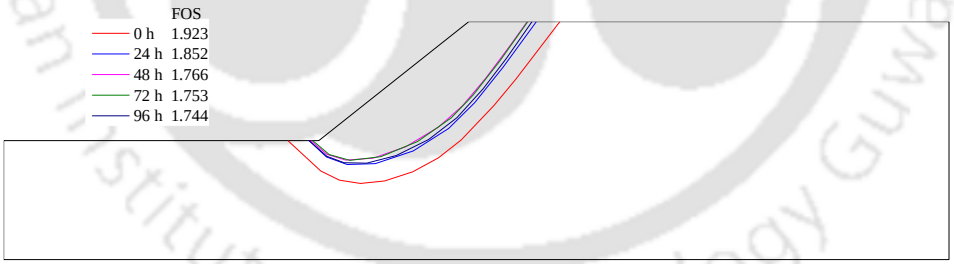


Figure 5.44 Critical slip surfaces of the homogeneous slope with Soil-3 under long duration rainfall

### 5.1.5 Effect of slope angle

A parametric study with five different slope angles was performed under infiltration situations to study the influence of slope inclination on stability of a slope. The slope angles in Figure 5.45 were selected as 26.56°, 35°, 45°, 55°, and 65°. All the other dimensions were kept constant. Rainfall infiltration of 30 mm/h has been considered for all these models.



TH-2008_136104008

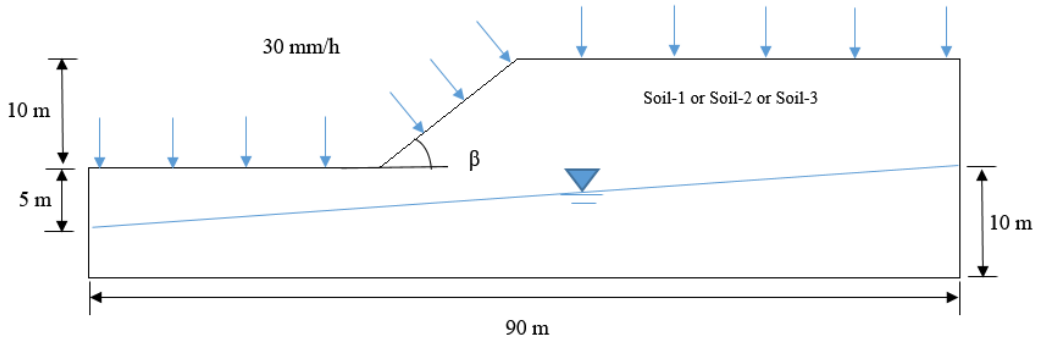


Figure 5.45 Model used for slope angle variation

The pore water pressure variation after 24 hours of rainfall at point P with slope inclination for three different soils is illustrated in Figure 5.46. At slope angle 26.56°, the pore pressure is negative (-0.5 kPa) for Soil-1 which decreases to (-1.7 kPa) pressure at 65°. The water level after 24 hours passes very close to point P, hence the suction is less. For the slope with Soil-1, the pressure remains constant with an increase in slope angle. For Soil-3, the pore water pressure for 26.56° slope angle is -18 kPa and -11 kPa for 65° slope. For Soil-2, the pore water pressure is -15 kPa for slope angle 26.56° and -10 kPa for slope inclination 65°.

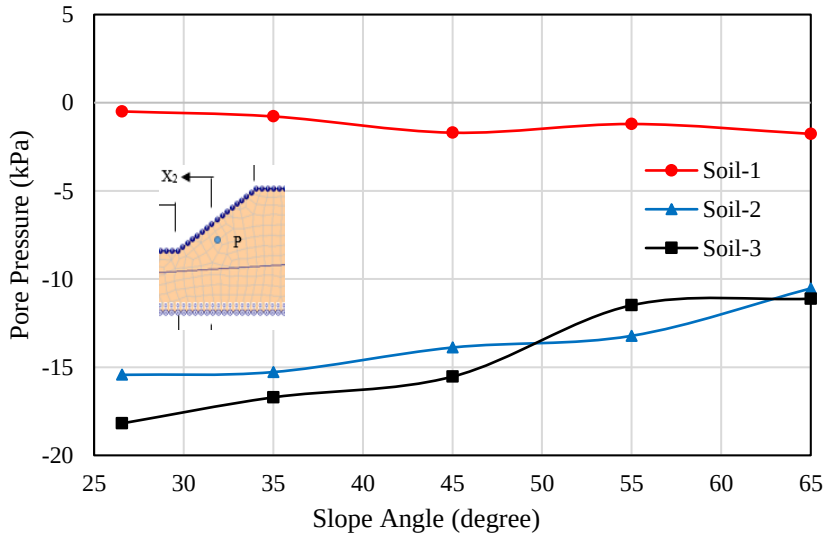


Figure 5.46 Variation of pore water pressure with slope angle at point P for the three soils after 24 hours

The pore water pressures increase gradually with an increase in slope angle for Soil-2 and Soil-3. Point P slightly moves close to the surface with an increase in slope angle. With rainwater,



TH-2008_136104008

infiltration and increase in slope angle the pore water pressures increase at P. However, the rise in water level is not much affected due to infiltration for Soil-2 and Soil-3 after 24 hours. The pressures are shown for point P, which is 2 m below the slope surface. Water freely infiltrates Soil-2, which saturates the deeper layers first. Soil-1 being less permeable, water infiltrates at a much slower rate while saturating the top layers first.

Figure 5.47 illustrate the pore pressure profiles at various inclinations for the homogeneous slope with Soil-1 at two sections of the slope. At the toe section (Figure 5.47a), the suction is zero at the surface after 24 hours of infiltration. The pressure profiles for different slope inclinations follow a similar path. The crest section (Figure 5.47b) of the slopes represent a different scenario with the 45° slope receiving the highest infiltration resulting in more reduction in suction. The slope inclined at 65° shows the least reduction in suction indicating the least amount of infiltration due to its steeper inclination. The suction at the surface ranges from 21 kPa to 28 kPa for the slope inclinations varying from 26.57° to 65°.

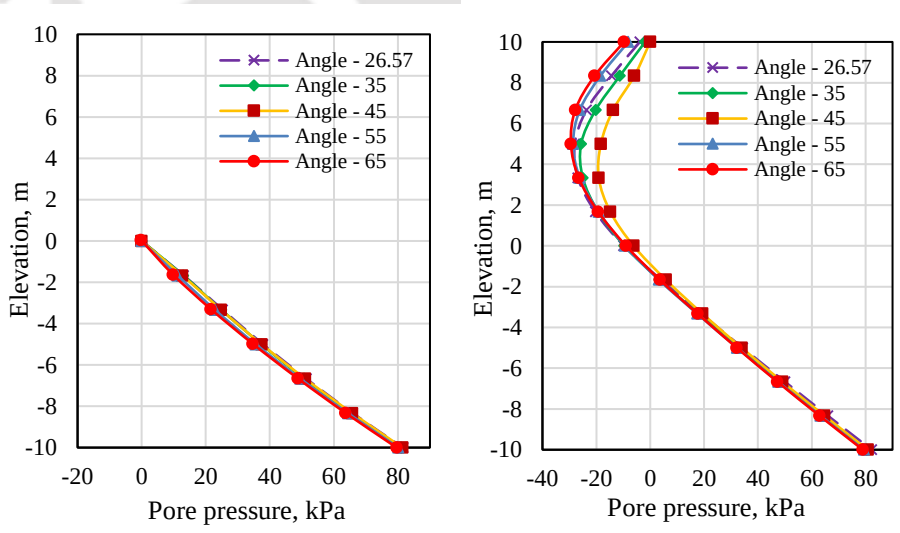


(a) (b)

Figure 5.47 Pore water pressure profiles for different slope angles with Soil-1 at (a) toe section (b) crest section after 24 hours

Figure 5.48 shows the pore water pressure profiles at the two sections for the homogeneous slope with Soil-2 for various slope inclinations. The pressure profiles for the five slope



TH-2008_136104008

inclinations are very similar in nature. Figure 5.48b depict the pressure profiles at the crest section of the slope. The slope inclined at 45° possesses the least suction (20 kPa) at the surface while the maximum suction (28 kPa) at the surface is observed for the 65° slope.

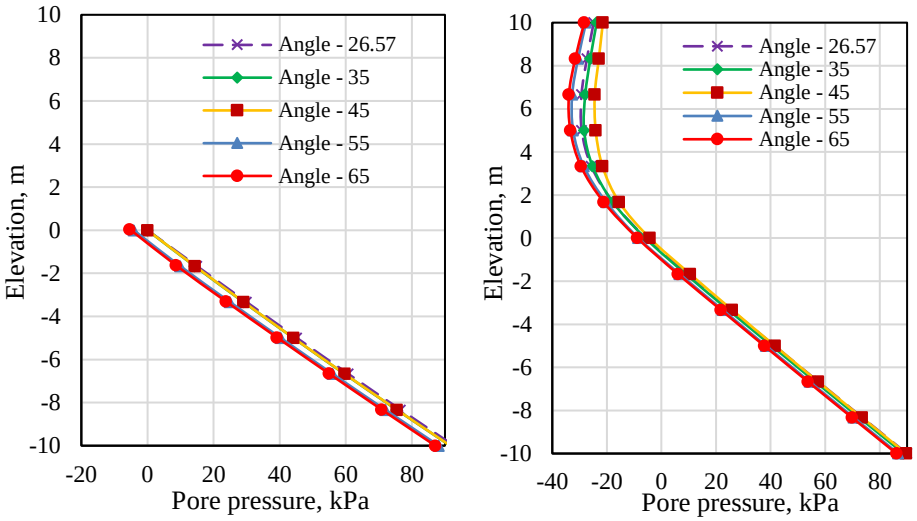


(a) (b)

Figure 5.48 Pore water pressure profiles for different slope angles with Soil-2 at (a) toe section (b) crest section after 24 hours

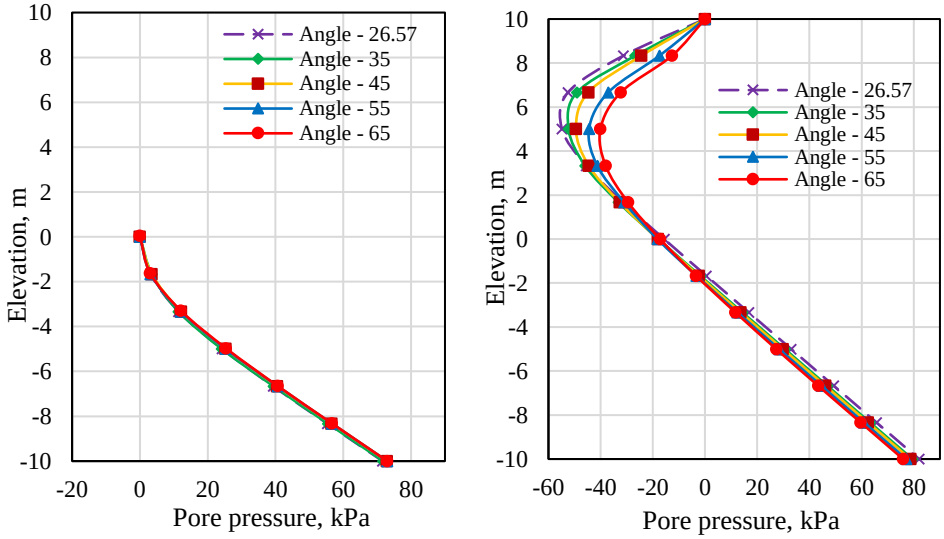


(a) (b)

Figure 5.49 Pore water pressure profiles for different slope angles with Soil-3 at (a) toe section (b) crest section after 24 hours

The rise in water level after 24 h of rainfall infiltration for different slope angles is illustrated in Figure 5.50. The three soils used have different permeability values, which accounts for the



TH-2008_136104008

different water levels in the slope. Figure 5.50a represents the GWL for slope angle 26.56°, where the water level mid-point of the slope surface for Soil-1. The GWL followed by Soil-2 slope is in between the other two, joining the slope near the toe region of the slope. For Soil-3 slope, the GWL passes just below that of Soil-2 and joins the slope surface at the toe. Figure 5.50b shows the water levels for the 35° slope inclination. The GWL for Soil-1 slope touches the slope surface just above the toe region. The GWL for Soil-2 slope touches the toe, follows the surface for some distance, and then dips off. The GWL for Soil-3 also touches the toe and follows the surface for a small distance and then it dips off gradually.

Figure 5.50c depicts the GWL paths for the 45° slope angle. GWL followed by the three soils are similar but they touch the slope surface at marginally different heights. For Soil-1 slope, the water touches the surface just above the toe of the slope and then follows the surface. For Soil-2 slope, the water touches the toe exactly and then dips off after following the surface for some distance. For Soil-3 slope, the water touches the toe, then follows the surface for a very small distance, and then dips off. Figure 5.50d illustrates the water levels for the slope inclination 55°. The GWL paths for all the three soils coincide until the toe region of the slope where they follow different paths. The GWL path followed by Soil-1 slope follows the surface for the most distance, then Soil-2 and the least distance is followed by Soil-3 slope. The water touches the surface near the toe by all the three soil slopes. Figure 5.50e depicts the water levels for 65° slope inclination. Here the three soils follow the same path until they touch the slope surface at the toe and after that, the three soils follow different paths. It is observed that with an increase in slope angle, the water levels for different soils coincide with each other. For flat slopes, different paths could be observed for the three soils but for steep slopes, the GWLs converge and follow similar paths. The GWL for Soil-1 rises more than the other two soils.



TH-2008_136104008

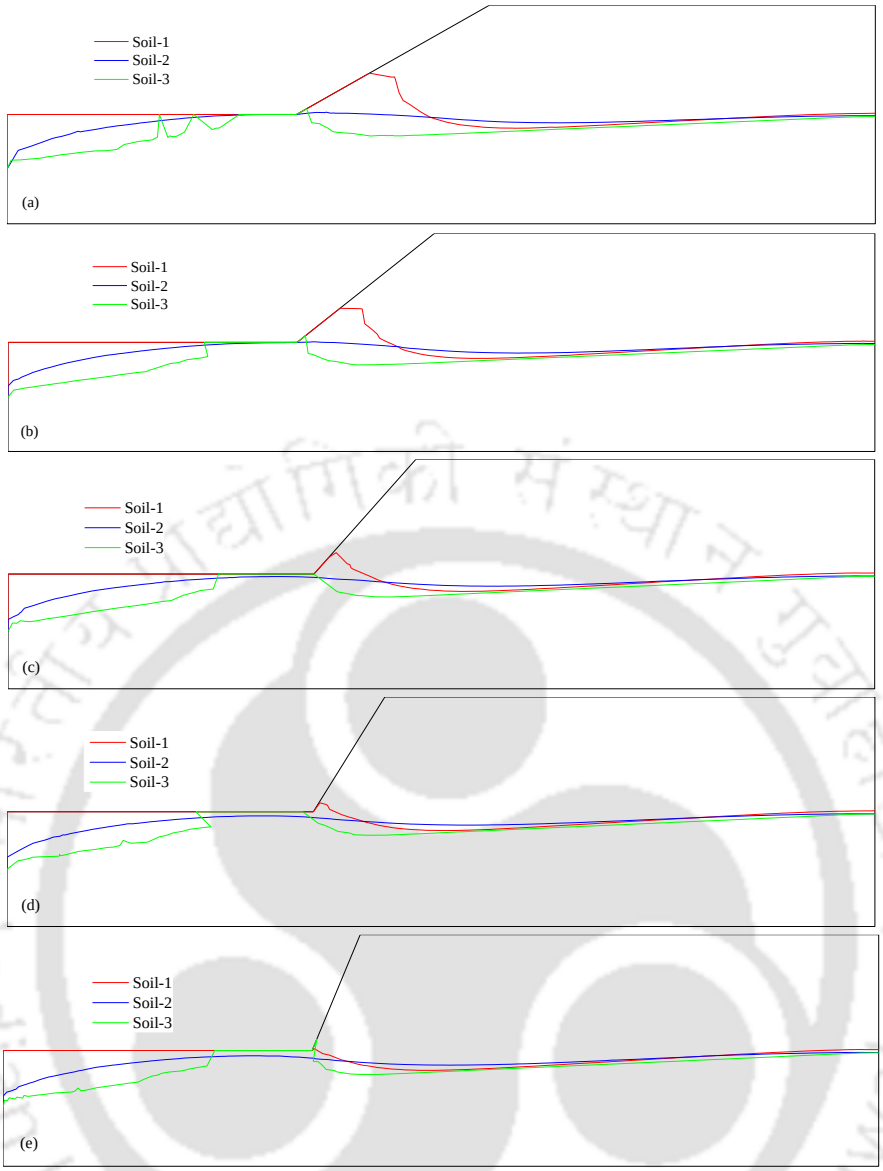


Figure 5.50 GWL location of the three soils at different slope inclinations after 24 hours (a) 26.56°, (b) 35°, (c) 45°, (d) 55° and (e) 65°

Figure 5.51 illustrates the change in the factor of safety of the slope with slope inclination for the three soils after 24 h of rainfall infiltration. The figure also depicts the initial factor of safety of the three soils before infiltration starts with dotted lines. The rate of decrease in the factor of safety of the slope is maximum from 26.57° to 45°. With the increase of slope angle from 26.57° to 45°, for Soil-1, the safety factor decreases from 2.01 to 1.535. Similarly, for Soil-2, the safety factor decreases from 2.04 to 1.365 and for Soil-3 the factor of safety decreases from 2.068 to 1.597. With further increase of slope angle from 45° to 65°, the rate of decrease of a factor of safety reduces significantly. The factor of safety decreases from 1.535 to 1.4 for a



TH-2008_136104008

decrease in slope angle of 45° to 65° with Soil-1 material. The safety factor reduces from 1.365 to 1.323 with Soil-2 material in the slope. With Soil-3 material inside the slope, the safety factor reduces from 1.597 to 1.379. The change in the factor of safety of all the three soils is not much evident after 55° slope angle. From the results, it is observed that slopes with high slope inclination and high saturated permeability of soil represent critical condition. Slopes with the soil of low saturated permeability may not fail at steep slope inclinations.

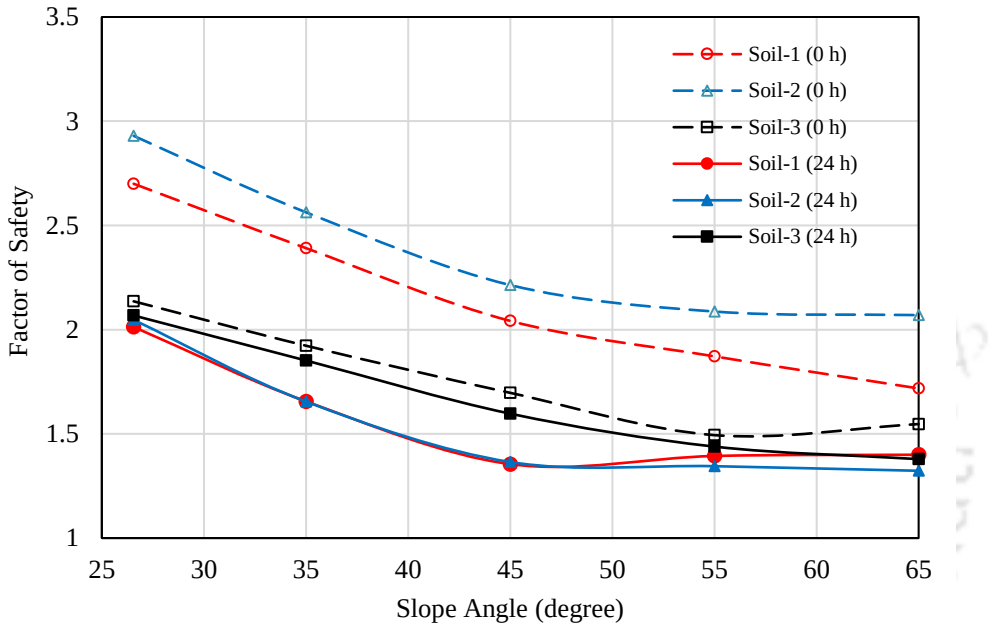


Figure 5.51 Variation of safety factor with slope angle for the three soils at the initial stage and after 24 h

The critical slip surfaces for different soils at different slope inclinations are represented in Figure 5.52. For slope angle 26.56° (Figure 5.52a), Soil-1 depicts a toe failure mechanism, Soil-2 depicts a base failure mode with a shallow slope failure and Soil-3 depicts a base failure with a deep surface due to the higher cohesion of the soil material. Figure 5.52b illustrates the slip surfaces for inclination 35°. In this case, Soil-1 and Soil-2 follow similar paths. Figure 5.52c, Figure 5.52d and Figure 5.52e represent slip surfaces for slope angles 45°, 55°, and 65° respectively.



TH-2008_136104008

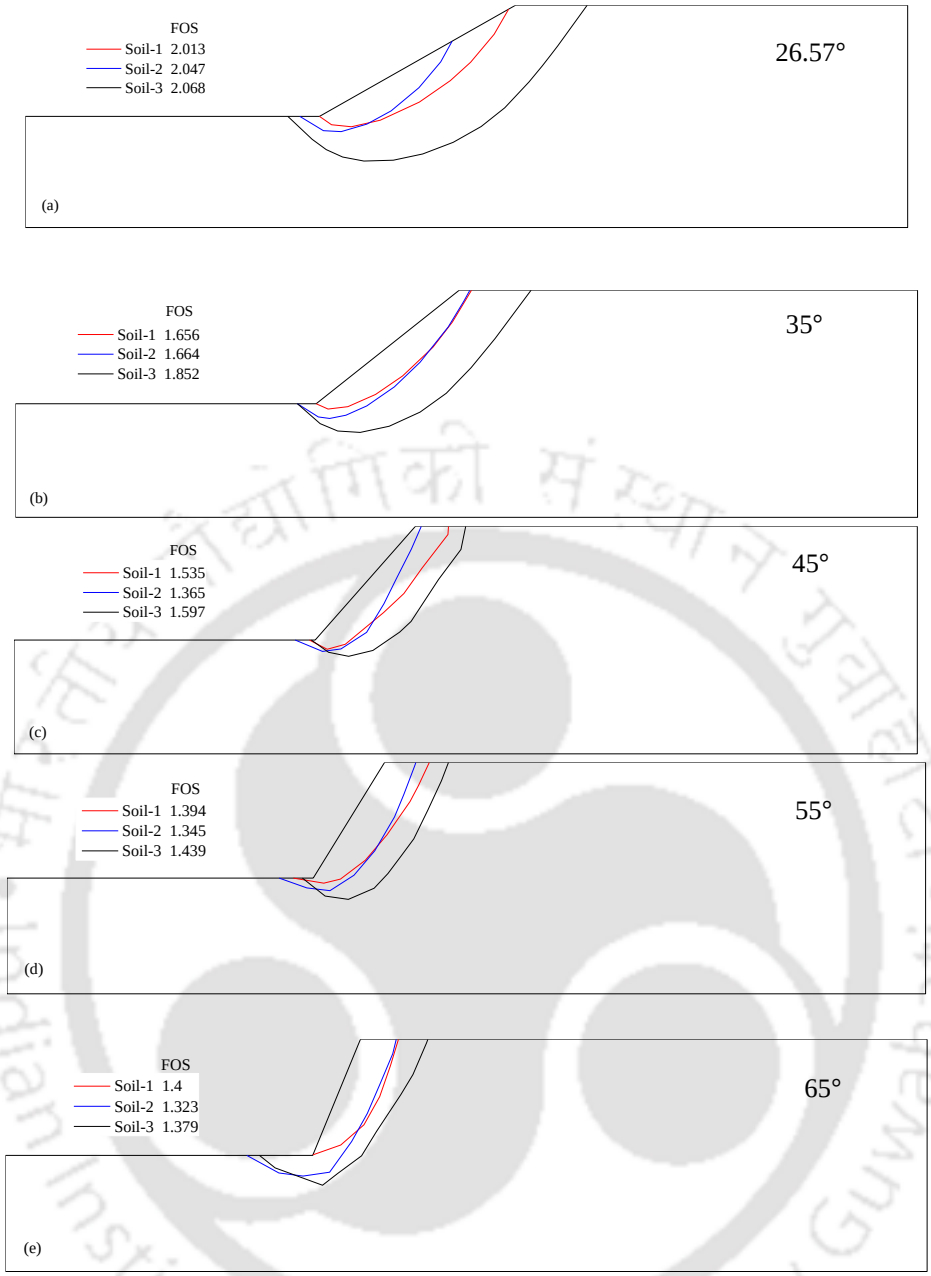


Figure 5.52 Critical slip surfaces for the three soils after 24 h at different slope inclinations: (a) 26.56°, (b) 35°, (c) 45°, (d) 55° and (e) 65°

It was observed that with an increase in slope inclination, the area of the failure mass reduces gradually shifting more towards (becomes shallow) the slope surface. Soil-3 illustrates a deep surface in all the slope inclinations because its cohesive strength is more than the other two soils. At higher slope inclinations, less water infiltrates the surface and more run-off occurs leading to a shallow failure surface.



TH-2008_136104008

### 5.1.6 Effect of slope height

To investigate the effect of slope height on stability, four different slope heights (5 m, 10 m, 15 m and 20 m) were selected in the parametric study. Figure 5.53 represents the models prepared to study the variation of slope height under rainfall infiltration conditions.

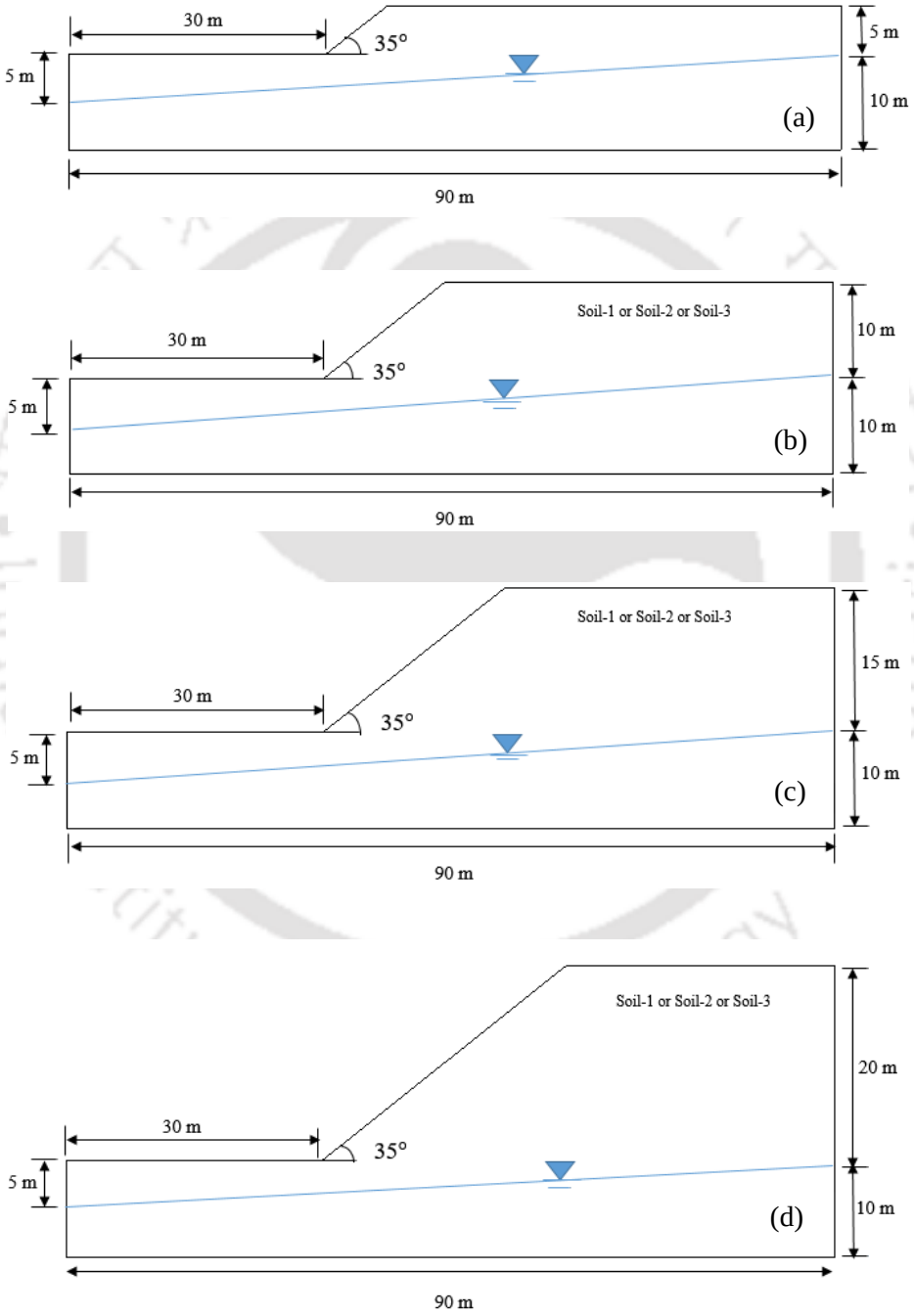


Figure 5.53 Models used to study the effect of slope heights (a) 5 m (b) 10 m (c) 15 m and (d) 20 m on stability under infiltration conditions



TH-2008_136104008

Pore water pressures at point P (2 m below at the midpoint of the inclined slope surface) for different slope heights at the initial stage and after 24h of rainfall are shown in Figure 5.54. In general, the pore water pressures decreases with increase with slope height. The pore pressure is near to -15 kPa for all the soils with 5 m slope height at the initial condition. The negative pore pressure (suction) linearly increases with an increase in slope height because of the distance of point P from GWL increase with slope height. Negative pore pressures of around 100 kPa are observed for slope height 20 m for all the three soils. With rainfall infiltration, the negative pore pressures reduce and therefore positive pressures in the range of 0-10 kPa are observed at point P for slope height 5 m after 24h of infiltration. At 10 m slope height, the point P has negative pressure in the range of 1-15 kPa for the three soils. At even higher slopes (20 m), the negative pore pressures further reduce to 50 kPa.

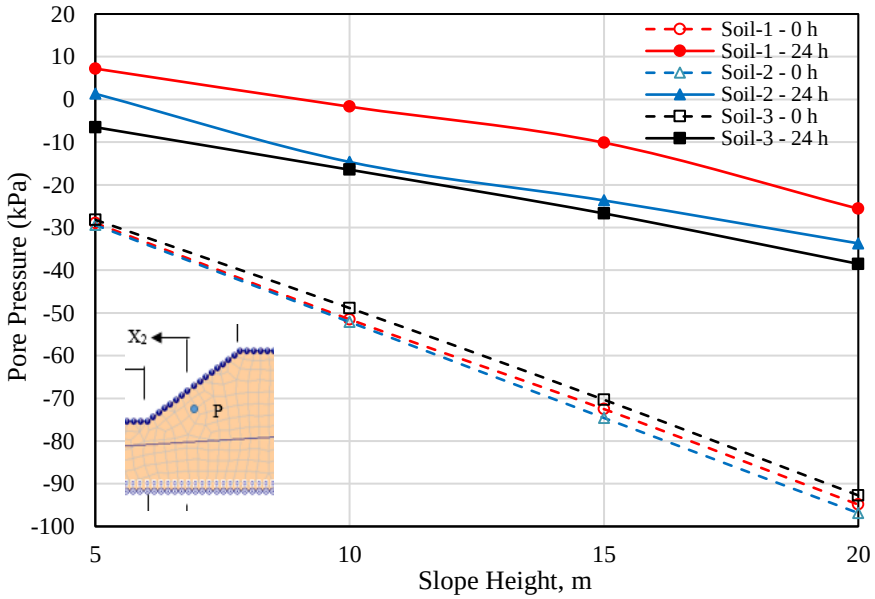


Figure 5.54 Variation of pore pressure at point P with slope height

Figure 5.55 illustrate the variation of a factor of safety with slope height under rainfall infiltration conditions. The factors of safety prior to rainfall (at 0 h) i.e., the initial factor of safety are shown in the figure with solid lines which is controlled by the height of the slope. Before water infiltrates the slope, the factor of safety for all the three soils decreases nonlinearly



TH-2008_136104008

with an increase in slope height. After 24 hours of infiltration, it is observed that the safety factor values reduced from initial values for Soil-3 slope.

For the Soil-2 slope, the *FOS* values after rainfall infiltration (24 h) are increased with slope height, which is because there is relatively less or no mounding of GWL for larger height slopes and the matric suction is very high for higher slopes. However, for Soil-1, the *FOS* values are not significantly affected by rainfall after 24 h and stay approximately constant, which happens due to less amount of water infiltrating the slope and relatively less change in suction.

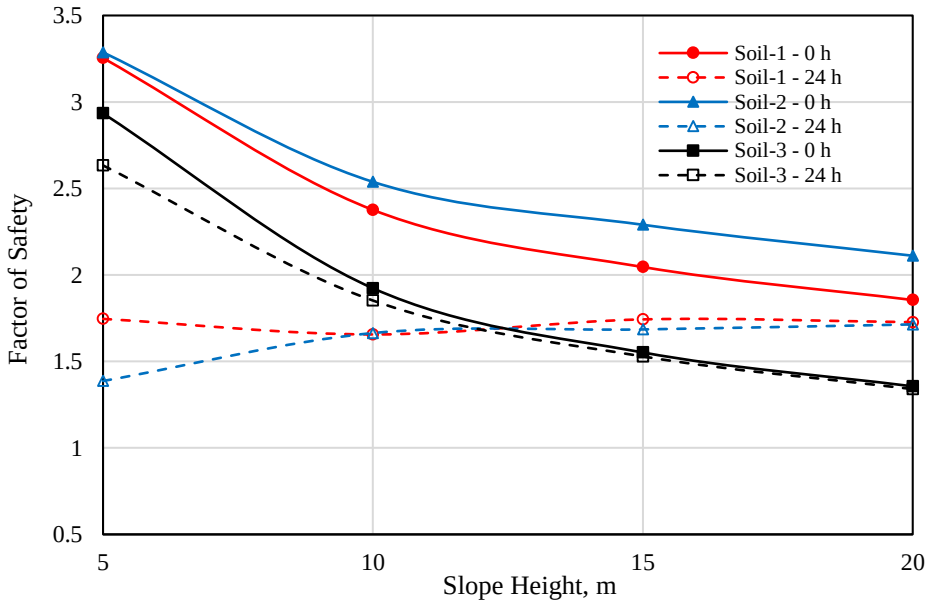


Figure 5.55 Variation of a factor of safety with slope height

For low height (5 m) slopes, the GWL rises more for Soil-1 and Soil-2 and hence the stability of the slope decreases significantly. The mounding of the water level due to infiltration is thus a major concern for low height slopes. Whereas for high slopes, the decrease in stability of the slope is primarily due to the decrease in matric suction of the soil caused by rainfall infiltration above the water level. The slip surfaces for the three soils after 24 hours of rainfall infiltration for different slope heights are depicted in Figure 5.56. In general, all the three soils show toe/base failure modes for different heights of the slopes but having different depths of slip zones. Soil-2 (SM) has a slope failure mode except for slope height 10 m. The depth of the



TH-2008_136104008

critical slip surface has increased with increase in height of the slope after rainfall infiltration.

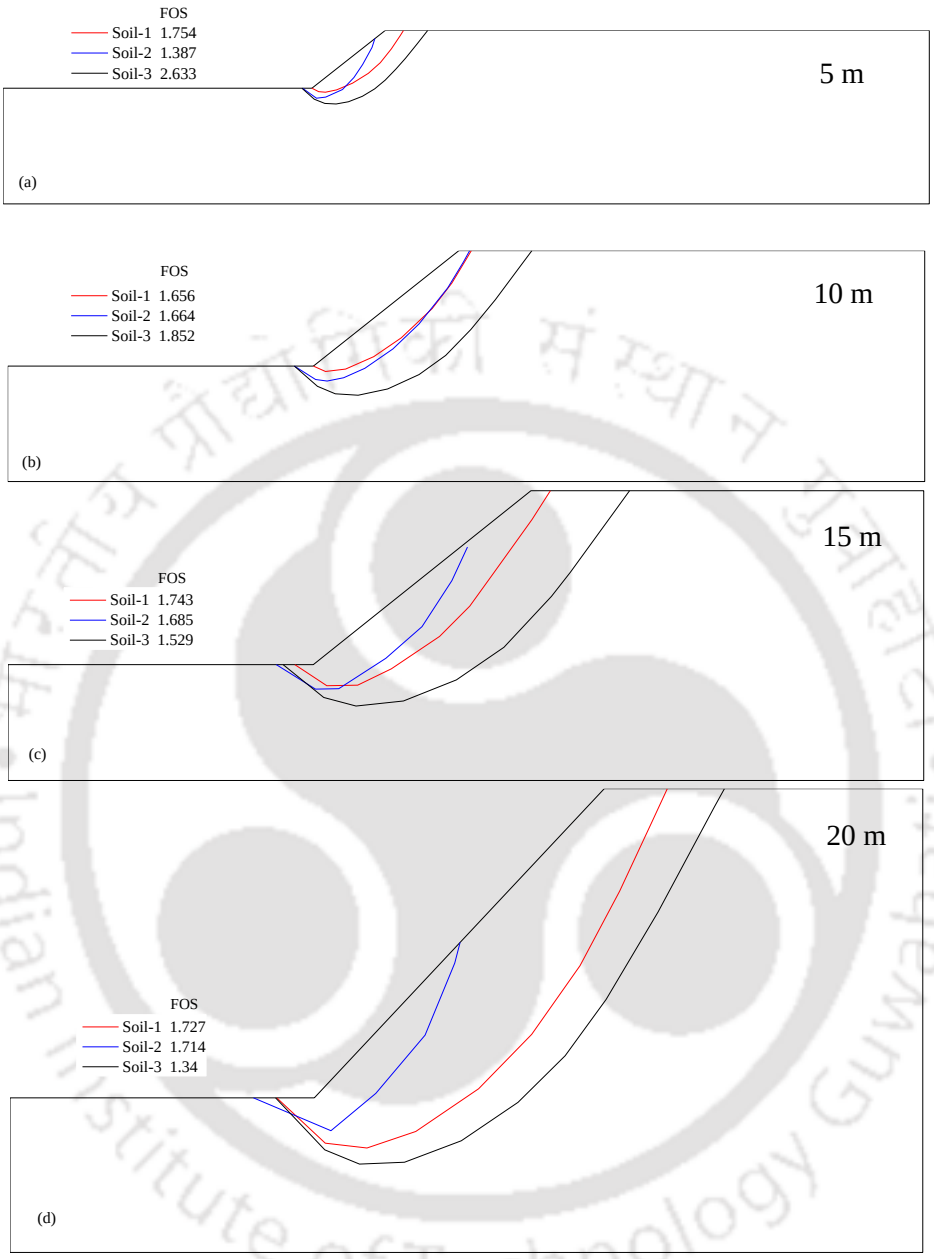


Figure 5.56 Critical slip surfaces for different slope heights (a) 5 m, (b) 10 m, (c) 15 m, and (d) 20 m after 24 hours of infiltration

## 5.4 SUMMARY & DISCUSSION

Analyzes of homogeneous slopes were performed under various conditions with three different types of soils. Stability of the slopes was studied with and without rainfall infiltration. The effect of moisture variation on homogeneous slopes was studied with the degree of saturation of the soil varying from 0% to 80%. Under infiltration conditions, the effects of rainfall



TH-2008_136104008

intensity, slope angle and slope height were observed for homogeneous slopes. The influence of duration of rainfall on homogeneous slopes was also studied.

The stability of the slope gradually decreased with the increase in moisture content of the soil. The slopes were stable with a GWL prior to the start of the infiltration process. The behaviour of the slopes under rainfall infiltration was different for the three soils. The slope with Soil-1 and Soil-2 was more affected under infiltration than the other two soils. Five different rainfall intensities were selected to study the influence of rainfall intensity. The slope with Soil-2 reached failure conditions under 100 mm/h intensity. The effect of rainfall intensity on the stability of the slope with Soil-3 was negligible. The parametric study with five different slope angles revealed that the stability of the slope naturally decreases with increase in slope angle. Under rainfall infiltration, also the same behaviour is observed. The stability of the slope decreased nonlinearly with slope angle under infiltration conditions. Infiltration into the slope decreased with an increase in slope angle. Similarly, a parametric study was conducted with four slope heights to study the effect of slope height on the stability of a homogeneous slope. The study showed that the stability of the slope decreased with an increase in slope height. However, under infiltration conditions, it was observed that the stability of the slope marginally increased with slope height for Soil-1 and Soil-2. For low slopes, the decrease in stability was primarily due to mounding of the GWL. A long duration rainfall (48 hours) was applied to the slope and its behaviour was compared with short duration rainfall. The behaviour of the slopes was similar up to 24 hours of infiltration for both the cases. As the infiltration stopped, the stability of the slopes increased due to an increase of suction but under long duration rainfall (48 hours) the stability of the slope decreased (19%, 27%, and 4.5%) more than the short duration rainfall (24 hours).



TH-2008_136104008

# Chapter 6 ANALYSIS OF NON-HOMOGENEOUS SLOPES

## 6.1 INTRODUCTION

Analysis of non-homogeneous slopes is primarily divided into two sections, without rainfall infiltration, and with rainfall infiltration. Non-homogeneous slopes have been analyzed utilising different soil models with various horizontal and slope-parallel layer configurations. The seepage analysis is performed using the finite element method and stability analysis has been conducted using the limit equilibrium method. Different cases were created and the study was accordingly presented into different sections. Under infiltration conditions, the slopes have been analyzed to study the influence of rainfall intensity and duration, slope angle, slope height on the stability of the slope.

## 6.2 ANALYSIS WITHOUT RAINFALL INFILTRATION

The non-homogeneous slopes with three different soils were first analyzed without rainfall infiltration or any kind of seepage within the slope. Under this condition, three cases are taken for the analysis without infiltration. The first case is a two-layered slope without the consideration of ground water level (GWL). The second case represents non-homogeneous slopes with different moisture contents ranging from 80% saturation to 20% saturation without the consideration of ground water level. The third case considered the existence of ground water level along with unsaturated behaviour of soils within two-layered and three-layered slopes.

### 6.2.1 Case 1: Analysis Without GWL

The non-homogeneous slope model of 10 m height slope inclined at 35° to the horizontal is considered for this case as shown in Figure 4.1. Four different models with three soils were



TH-2008_136104008

prepared with no ground water level and hence water seepage. Properties of the three soils used for the numerical models are enlisted in Table 5.1. The slopes have been analyzed using both the limit equilibrium method and finite element method.

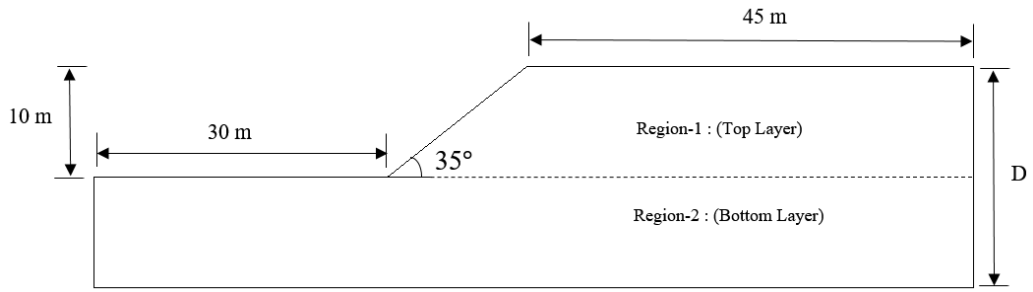


Figure 6.1 Non-homogeneous slope model

The study of two layer non-homogeneous slopes is divided into two different soil combinations. In the first combination, the top soil layer is fixed and the bottom soil is changed. The bottom soil layer is fixed and the top soil is changed in the second combination. The soil material, which was fixed, is Soil-1 for both the cases. Details of different configurations are given in Table 6.1.

In the limit equilibrium method, the slope was analyzed for its stability in SLIDE2 using Morgenstern and Price (1965) method. The model was analyzed with 20 vertical slices considering 5000 non-circular failure surfaces. Random path search method (as discussed in Chapter 3) was chosen for determining the critical failure surface with the minimum factor of safety (*FOS*). In finite element analyzes, the slope was analyzed using a strength reduction technique in RS2 to determine the stability of the slope. The model was discretised using uniform meshing scheme with six-noded triangular elements.

The results of the stability analysis of non-homogeneous slope with Soil-1 as the top layer are shown in Table 6.1. For Soil-1 and Soil-3 combination, i.e., when the bottom layer is Soil-3, the safety factor is 1.552. The *FOS* value is very close to the *FOS* value obtained for homogeneous slope case with Soil-1 (1.541). This implies that Soil-1 and Soil-3 combination



TH-2008_136104008

did not affect the stability of the slope for the slope configuration considered. The stability of slope was not affected by the existence of Soil-3 in comparison to the homogeneous profile with Soil-1. The factor of safety with Soil-2 as the bottom layer is 1.464.

Table 6.1 Details of different non-homogeneous configurations and results for height $H$ = 0.5$D$

| Notation | Top Layer | Top Layer Height, $H$ | Bottom Layer | FOS (LEM-MP) | SRF (FEM-SRM) |
|---|---|---|---|---|---|
| 0.5s1s2 | Soil-1 | 0.5$D$ | Soil-2 | 1.464 | 1.5 |
| 0.5s1s3 | | | Soil-3 | 1.552 | 1.58 |
| 0.5s2s1 | Soil-2 | 0.5$D$ | Soil-1 | 1.073 | 1.05 |
| 0.5s3s1 | Soil-3 | | | 1.583 | 1.63 |

For the second combination analyzes, with the bottom layer fixed as Soil-1, the results are presented in Table 6.1. The safety factor with Soil-2 as the top layer is 1.073. Soil-2 is a shallow failure soil having its critical failure surface within the slope face itself. The stability of the slope with Soil-3 as the top layer is 1.583 much higher than the other combination. Soil-3 being a deep-seated failure soil, for 0.5$D$ thickness case, the critical slip surface was intersected by Soil-1 beyond 0.5$D$ depth and thus *FOS* value is higher. Figure 6.2 illustrates the critical slip surfaces for the non-homogeneous slopes with layer height $h$ = 0.5$D$. The slope with Soil-1 as the top layer and Soil-2 as the bottom layer (0.5s1s2) is having a toe failure mechanism. Slope failure is observed for the slope with Soil-3 as the bottom layer.

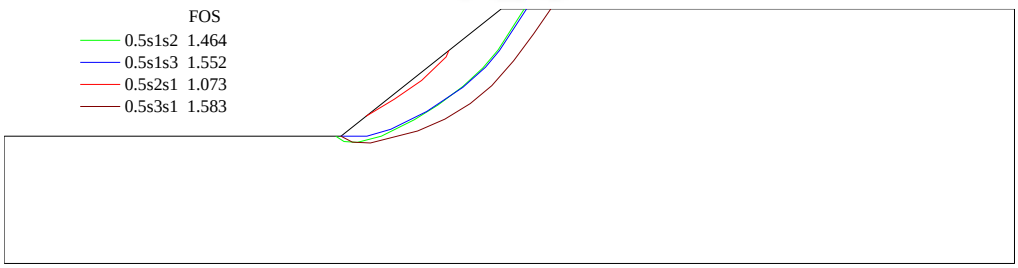


Figure 6.2 Critical slip surface for different combinations



TH-2008_136104008

A very shallow slope failure is observed for the slope with Soil-2 as the top layer due to the coarse nature of the Soil-2. The base failure mode is observed for the slope with Soil-3 as the top layer having the maximum factor of safety of all the models considered. The zone of maximum shear strain for the two-layered slopes with different soil combinations is depicted in Figure 6.3 with Soil-1 as the top layer. Maximum shear strains developed to represent the zone of impending failure within the slope. Both models represent similar kind of failure zones with similar SRF values. The soil in the bottom layer is having very little effect on the stability of the slope.


Figure 6.3 Maximum shear strain contours for the non-homogeneous slopes with Soil-1 as the top layer


Figure 6.4 Maximum shear strain contours for the non-homogeneous slopes with Soil-1 as the bottom layer

Figure 6.4 illustrates the shear strain contours for the slopes with Soil-1 as the bottom layer. It is observed that the slope with Soil-2 as the top material develops maximum shear strains near the slope surface indicating the possibility of the translational type of failure. The zone of



TH-2008_136104008

maximum shear strain developed for the slope with Soil-3 as the top layer resembles more of a rotational type of failure. The stability of the slope with Soil-3 as the top layer is much more (1.63) due to more strength provided by Soil-3.

***Effect of Moisture Content Variation***

To study the effect of moisture content on the stability of the slope, the slope with Soil-1 was modelled as shown in Figure 6.5 by considering four different moisture contents (degree of saturation, $S_r$). The dimensions of the slope remain the same. The non-homogeneous slope model-1(Figure 6.7a) has an increasing moisture profile with depth whereas model-2 (Figure 6.7b) consist of a decreasing moisture profile with depth. Ground water level drawdown can be idealized as where the moisture content increases with depth.

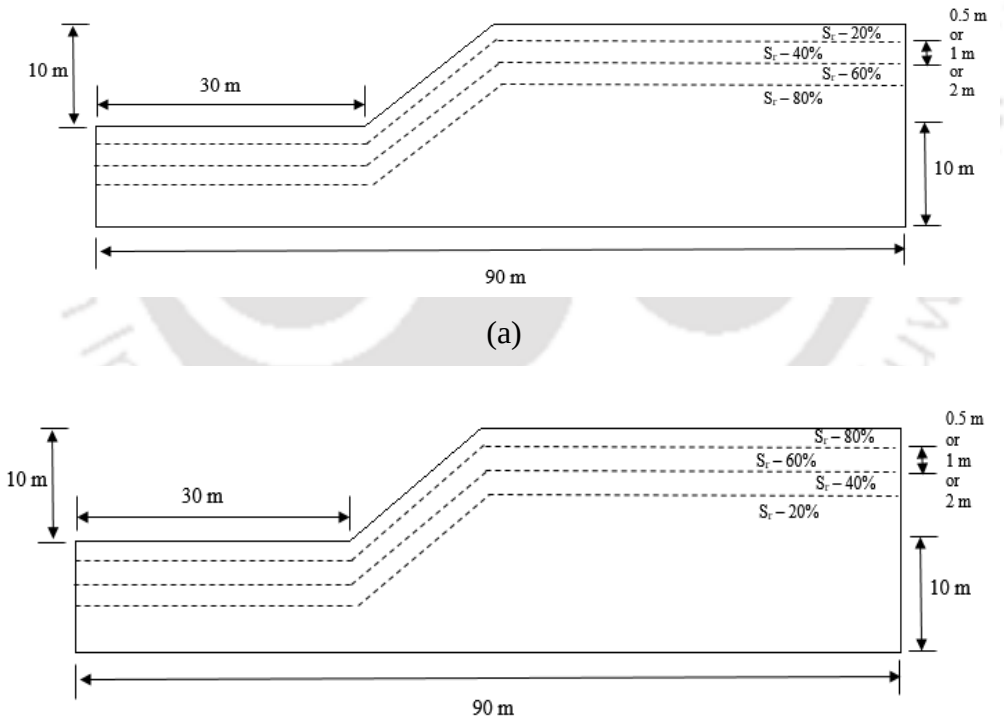


Figure 6.5 Non-homogeneous slope with Soil-1 with different moisture contents (a) Model-1 and (b) Model-2



TH-2008_136104008

Under rainfall infiltration conditions, the moisture content of the soil decreases with depth as the wetting front advances downward. The depths of the different layers were varied from 0.5 m to 1 m to 2 m. Material properties of Soil-1 at different moisture content as reported in Table 3.3 have been used for the two models with corresponding moisture content. *FOS* values and critical slip surfaces from the LEM analyzes; and SRF and information on strains and displacements from FEM analyzes were obtained.

*Model – 1: Saturation of layers increase with depth from the surface*

The results obtained for the non-homogeneous slope model – 1, using the limit equilibrium method and the finite element method are shown in Table 6.2. The slope with a layer thickness of 2 m has the lowest factor of safety of 1.144 while the slope with 0.5 m layer depth has a safety factor of 1.467. The slope with 1 m layer thickness has a safety factor of 1.226 obtained from the limit equilibrium method and 1.27 from the finite element method. The decrease in the factor of safety of the slopes with more layer thickness is due to the presence of high saturation soil material at the bottom. As the amount of drier soil reduces in the slope, the stability of the slope decreases due to a decrease in strength of the soil in the bottom layers.

Table 6.2 Safety factors for the non-homogeneous Model - 1

| Layer Depth, m | LEM-MP | FEM-SRM |
|---|---|---|
| 0.5 | 1.467 | 1.5 |
| 1 | 1.226 | 1.27 |
| 2 | 1.144 | 1.18 |

Figure 6.6 depicts the slip surfaces of the non-homogeneous slope with different layer thicknesses. The layer thickness is the height of the layers selected to represent different moisture contents within the slope as shown in Figure 6.5. A toe failure mechanism is observed for all the cases. With an increase in layer thickness, the critical slip surface mildly shifts towards the right due to a little increase in strength of the soil properties. The slip surface with 0.5 m thickness is closest to the surface with a safety factor of 1.467. At 1 m layer thickness,



TH-2008_136104008

the safety factor increases slightly due to the increase in strength of the soil material. Continuing with the trend, the safety factor at 2 m layer thickness is 1.144, which is a considerable increase from the 1 m layer. As the strength of the soil is increased at the top, the slip surface becomes deep.


Figure 6.6 Critical slip surfaces for the non-homogeneous slope Model - 1

The total displacement contours for the non-homogeneous slopes are represented in Figure 6.7. The layer thickness in the slopes is represented by *d*. It is observed that the maximum displacement (0.034 m) is observed for the slope with 2 m layer thickness with SRF of 1.18. The other two slopes have maximum displacements of 0.008 m and 0.014 m for the slopes with 0.5 m layer thickness and 1 m layer thickness respectively. The results can be related to that of the homogeneous cases.

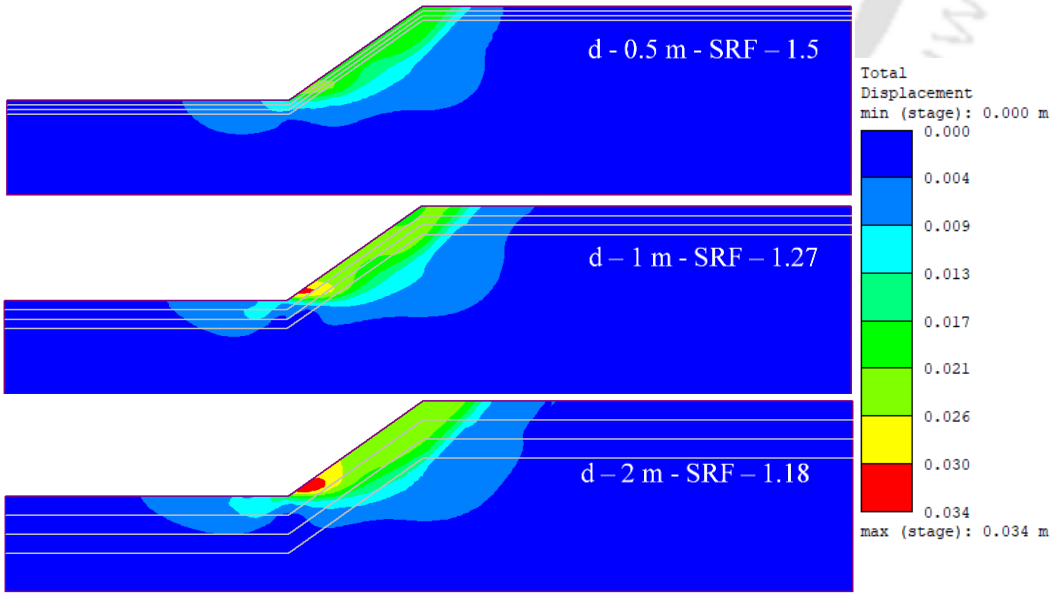


Figure 6.7 Total displacement contours for the non-homogeneous slope Model – 1



TH-2008_136104008

The displacements increased and SRF decreased with a decrease in moisture content in the slope. Here also the SRF reduced and deformations were increased with increase in moisture content (increase in layer thickness at the top which consists of layers at 20%, 40% saturation).

*Model – 2: Saturation of layers decreasing with depth from the surface*

Table 6.3 represents the results of the stability analysis of non-homogeneous slope model – 2 using both the finite element method and limit equilibrium method. The stability of the slope for 0.5 m layer thickness is 1.164, which increases to 1.313 for 1 m layer thickness ultimately reaching 1.693 for 2 m thickness. The strength reduction factors from finite element method increase from 1.23 to 1.71. The increase in stability of the slopes is due to the increase in moisture content in the top layers of the slope only. With soil material of higher strength in the bottom layers increasing, the stability of the slope increases accordingly.

Table 6.3 Safety factors for the non-homogeneous Model - 2

| Layer Depth, m | LEM-MP | FEM-SRM |
|---|---|---|
| 0.5 | 1.164 | 1.23 |
| 1 | 1.313 | 1.38 |
| 2 | 1.693 | 1.71 |

The critical slip surfaces of the three slope models are depicted in Figure 6.8. The surfaces indicate toe failure mode for all the layer thickness. Only the slope with 1 m thickness is slightly shallow than the other two surfaces.

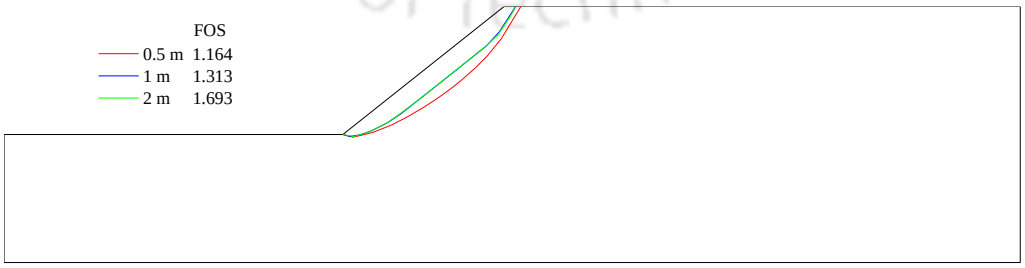


Figure 6.8 Critical slip surfaces for the non-homogeneous slope Model – 2



TH-2008_136104008

The total displacement contours are shown in Figure 6.9 for the layered slope model-2. The maximum displacement (0.036 m) occurs for the slope with layer height 0.5 m. The maximum displacement for layer height 1 m is 0.02 m with an SRF of 1.38. The slope with 2 m thickness illustrate maximum deformation of 0.024 m. In these models, the saturation levels decrease with depth resulting in a relatively dense top layer and the loose bottom portion within the slope. The strength of the material is more at the bottom than near the surface. Therefore, with an increase in height in this type of situation (Model-2) the stability of the slope increases with a decrease in the total displacements.

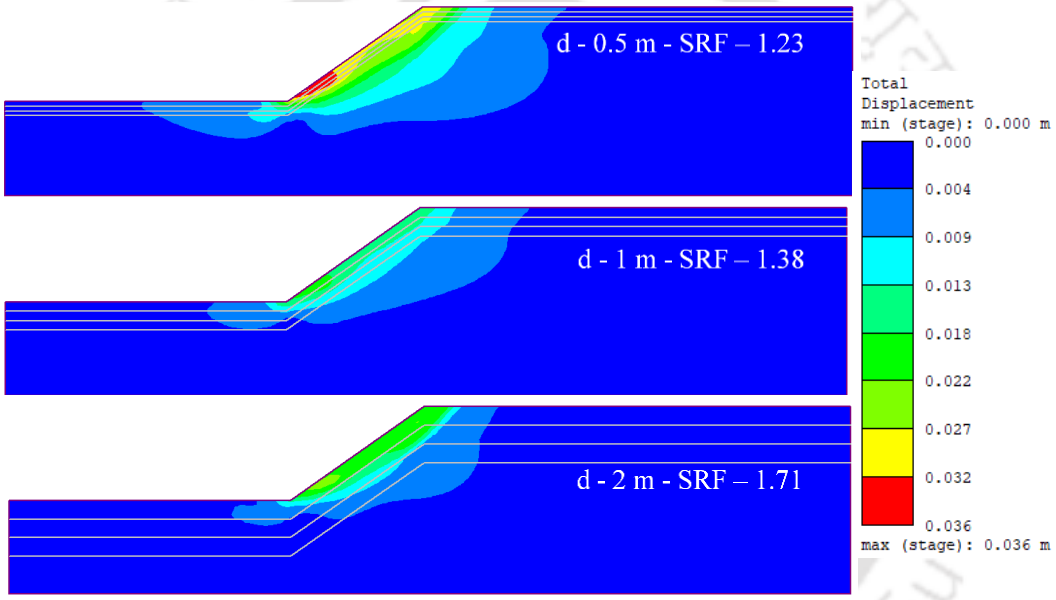


Figure 6.9 Total displacement contours for the non-homogeneous slope Model – 2

### 6.2.2 Case 2: Analysis With GWL

The model of the non-homogeneous slope prepared with a GWL is illustrated in Figure 6.10. Such non-homogeneous layered slopes were selected based on various layered slopes available in case studies of slopes. The layered slopes were prepared with Soil-1 as the fixed base layer and interchanging Soil-2 and Soil-3 as the surficial layers. The slope height and inclination have been kept unchanged. The ground water level (GWL) is considered to be at a height of 10 m at the right boundary and at 5 m height at the left boundary. The seepage analysis was



TH-2008_136104008

performed using the finite element method. The pore pressures obtained from the seepage analysis were used in the limit equilibrium method for the stability analysis. In addition to the properties mentioned in Table 5.1, SWCC properties of soils discussed in Chapter 3 have been used in the numerical model. In this case, unsaturated behaviour of soils due to the presence of ground water level will be included in the analyzes.

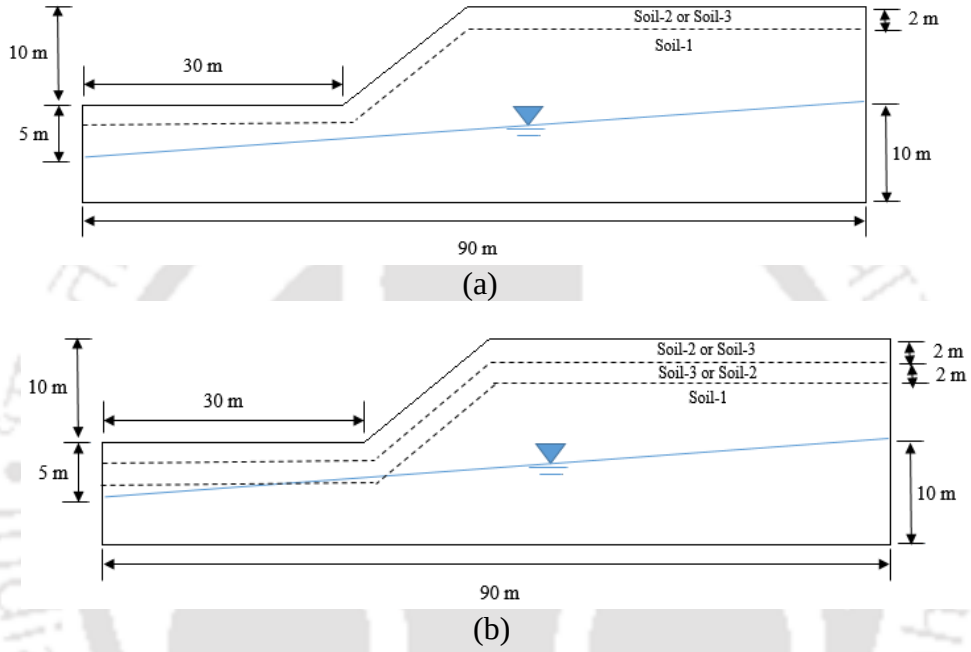


Figure 6.10 Non-homogeneous slope model with GWL (a) Two-layered slope and (b) Three-layered slope

***Two-layered non-homogeneous slope models***

Figure 6.11 depicts the pore water pressure profiles at different sections of the two-layered slopes. Figure 6.11a represent the pressure profiles at the toe section. At the surface, the suction is near to 26 kPa, which decreases as it reaches the GWL. Both the slopes represent hydrostatic conditions prior to rainfall infiltration within the slope. Figure 6.11b depict the pore pressure profile at the mid-slope section of the slope. The suction at the surface is near to 70 kPa, which reduces to zero at the GWL. Figure 6.11c represents the pore pressure profile at the crest region of the slope. Here suction recorded at the surface is 116 kPa for all for both the slopes at an elevation of 12 m from the ground water table.



TH-2008_136104008

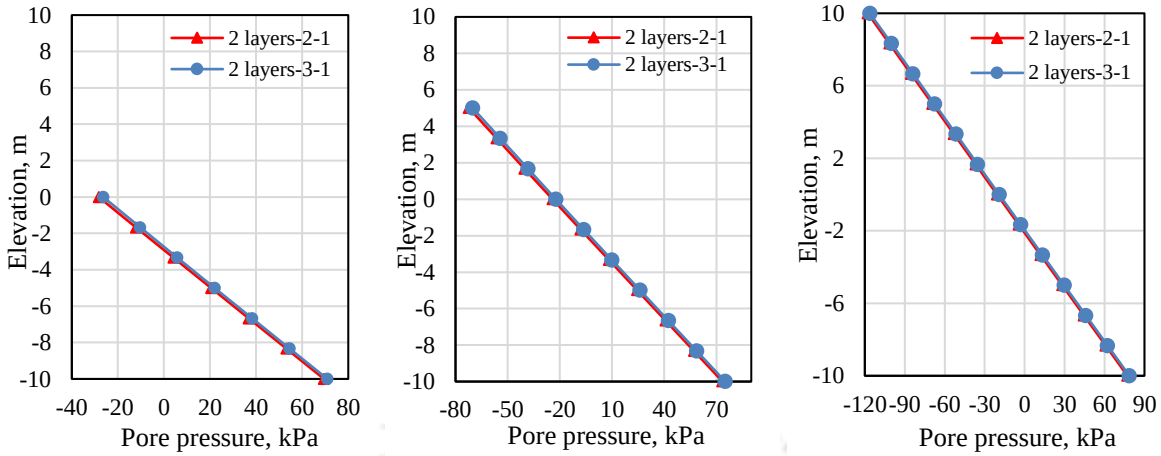


Figure 6.11 Pore water pressure profiles for the two-layered non-homogeneous slopes along different sections at: (a) Toe, (b) Mid-slope, and (c) Crest

The critical slip surfaces of the non-homogeneous slopes consisting of a ground water level are shown in Figure 6.12. The critical slip surfaces for both the slopes exhibit base failure mechanism. The stability of the two-layered slopes cannot be differentiated at this initial condition. Both the slopes have similar pressure profiles and critical slip surfaces. This type of behaviour is observed because most of the layered slope is consists of Soil-1 in both the models. Therefore, mainly the response of Soil-1 is observed in the results.

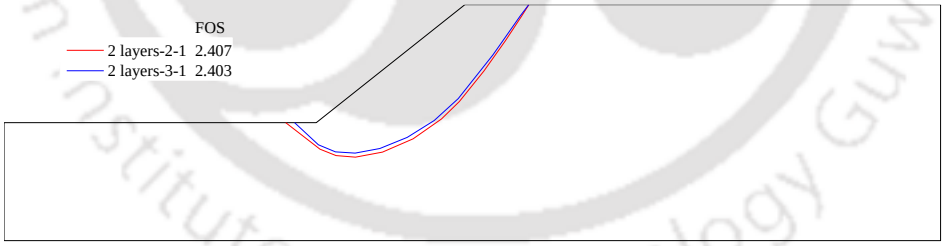


Figure 6.12 Critical slip surfaces of the two-layered non-homogeneous slopes

***Three-layered non-homogeneous slope models***

Figure 6.13 represents the pore water pressure profiles at different sections of the three-layered slopes. Figure 6.13a depict the pressure profiles at the toe section of the slope. At the surface, the suction is near to 30 kPa, which decreases as it approaches the GWL. Figure 6.13b show the pore pressure profile at the mid-slope section of the slope. The suction at the surface is near to 74 kPa, which reduces to zero at the GWL.



TH-2008_136104008

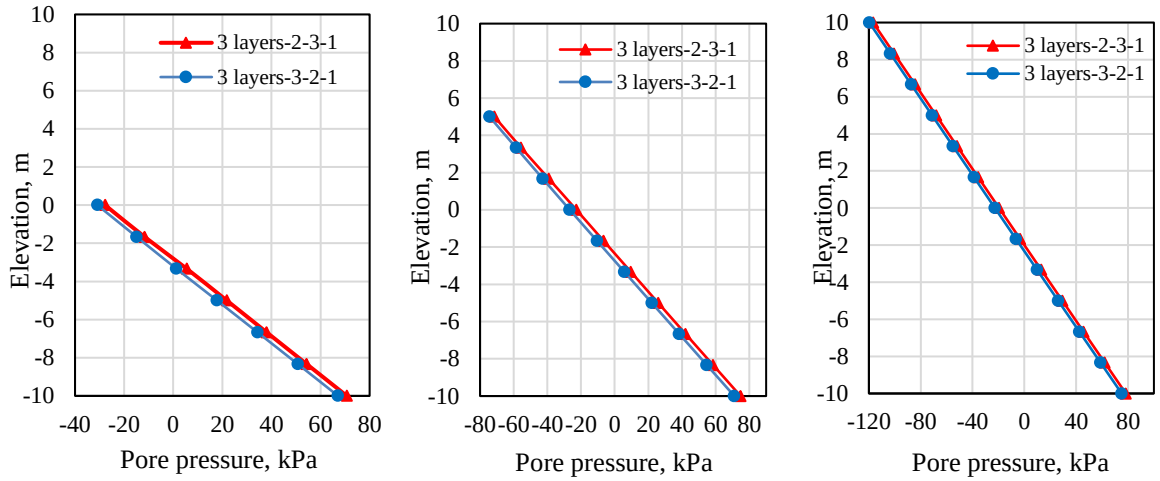


Figure 6.13 Pore water pressure profiles for the three-layered non-homogeneous slopes along different sections at: (a) Toe, (b) Mid-slope, and (c) Crest

Figure 6.13c represent the pore pressure profile at the crest region of the slope. Here suction recorded at the surface is 120 kPa for all for both the slopes at an elevation of 12 m from the ground water table.

The critical slip surface of the three-layered non-homogeneous slopes is shown in Figure 6.14. The critical slip surface of the slope with Soil-2 as the top material exhibit base failure mechanism. The base failure mode is also observed for the slope with Soil-3 at the top with a factor of safety of 2.456. There is an indication of the development of tension crack at the top for the slope with Soil-3 at the surface.

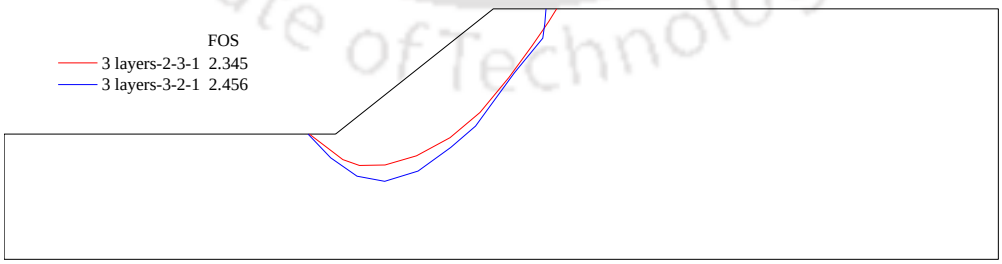


Figure 6.14 Critical slip surfaces of the three-layered non-homogeneous slopes



TH-2008_136104008

## 6.3 ANALYSIS WITH RAINFALL INFILTRATION

The infiltration analysis of non-homogeneous layered slopes with the three soils has been performed utilising the slope models as shown in Figure 6.15. The layered slopes were prepared with Soil-1 as the fixed base layer and interchanging Soil-2 and Soil-3 as the surficial layers. The thickness of the layers has been kept constant at 2 m. Presence of ground water level (GWL) and SWCC properties along with permeability functions of the soils (as discussed in Chapter 3) are considered in the numerical analyzes. Rainfall infiltration (external flux) of 30 mm/h was applied for 24 hours (short duration) on to the surface of the numerical model.

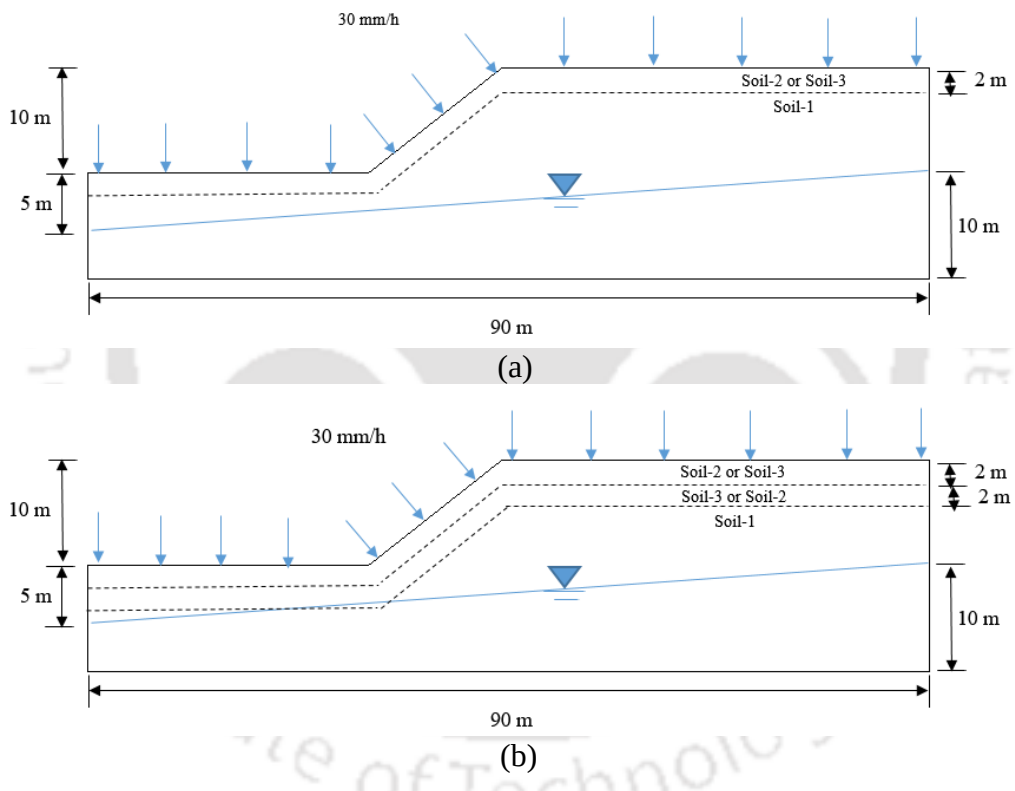


Figure 6.15 Non-homogeneous slope model with GWL under rainfall conditions (a) Two-layered slope and (b) Three-layered slope

The numerical models were analyzed up to 48 hours duration to study on pore pressure dissipation pattern as well, after the rainfall event. The effects of rainfall intensity, slope height, slope angle and duration rainfall have been studied using this model. For all of the models, the seepage analysis was performed using the finite element method. The stability factors of the slopes were then evaluated using the limit equilibrium method.



TH-2008_136104008

***Two-layered non-homogeneous slope models***

Figure 6.16 represents pore water pressure profiles along vertical sections under rainfall conditions resulting from transient seepage analysis after 24 hours. At 24 hours, it is observed that both the models have zero pressure at the toe region (Figure 6.16a), which implies that the surface is saturated at this moment. With depth increasing, the models take different paths. The pressure decreases for the model with Soil-3 at the top because less water infiltrates and does not saturate the sublayer while the pressure continues to increase from zero pressure for the model with Soil-2 at the top. At the mid-slope portion shown in Figure 6.16b, the model with Soil-3 at the top reaches a maximum suction of 20 kPa at 3 m, while the model with Soil-2 at the top loses its suction at an elevation of 2 m where the soil is saturated due to water infiltration.

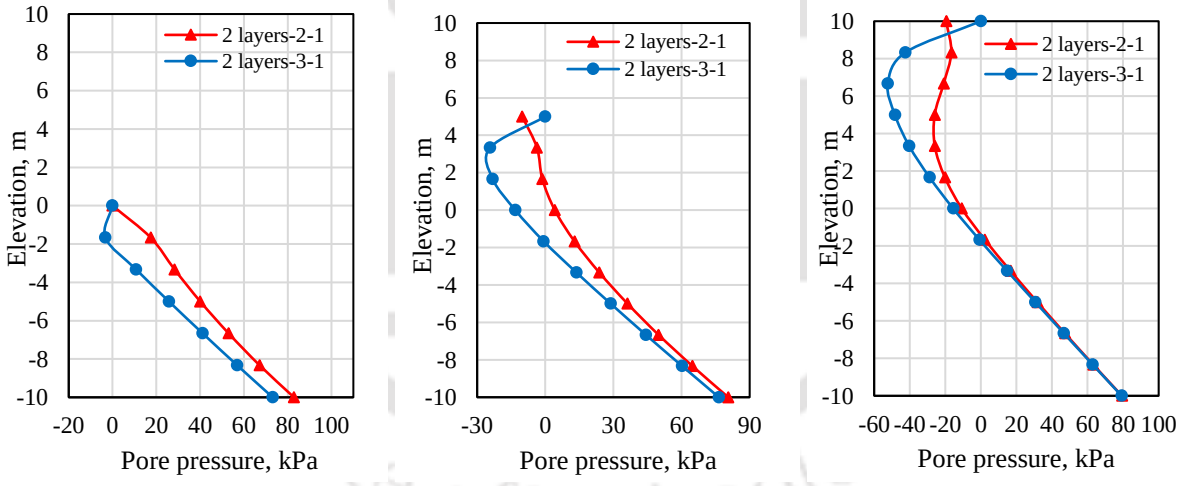


Figure 6.16 Pore water pressure profiles for two-layered non-homogeneous slopes after 24 hours along different sections at: (a) Toe, (b) Mid-slope, and (c) Crest

Figure 6.16c illustrate the pressure profile at the crest section of the slope. The suction is observed to increase with depth from the surface to 52 kPa at an elevation of 6.7 m for the model with Soil-3 at the top due to the low permeability of the soil. For the model with Soil-2 at the top (rainfall intensity is higher than the permeability of Soil-2), therefore all the rainwater will infiltrate until surface saturation occurs for the two-layered model. Runoff starts after



TH-2008_136104008

saturation of the surface and the infiltration capacity of the soil decreases with time. Very less infiltration occurs for the two-layered model with Soil-3 at top because the permeability of Soil-3 is less than the rainfall intensity applied and the sublayer does not saturate. As a result, the matric suction is maintained in the lower layer.

Figure 6.17 illustrates the pore pressure profiles of the two-layered non-homogeneous slopes after 48 hours (end of rainfall). At the toe, the suction at the surface is 17 kPa and 5 kPa for the models with Soil-3 and Soil-2 at the top. The path of the pressure profile of the model with Soil-2 falls slightly to the right of the model with Soil-3 i.e., the pore pressures at each depth for the model with Soil-2 at the top are more than that of the other model. After the stoppage of rainfall, both the slope models observe an increase in suction value trying to reach steady state condition.

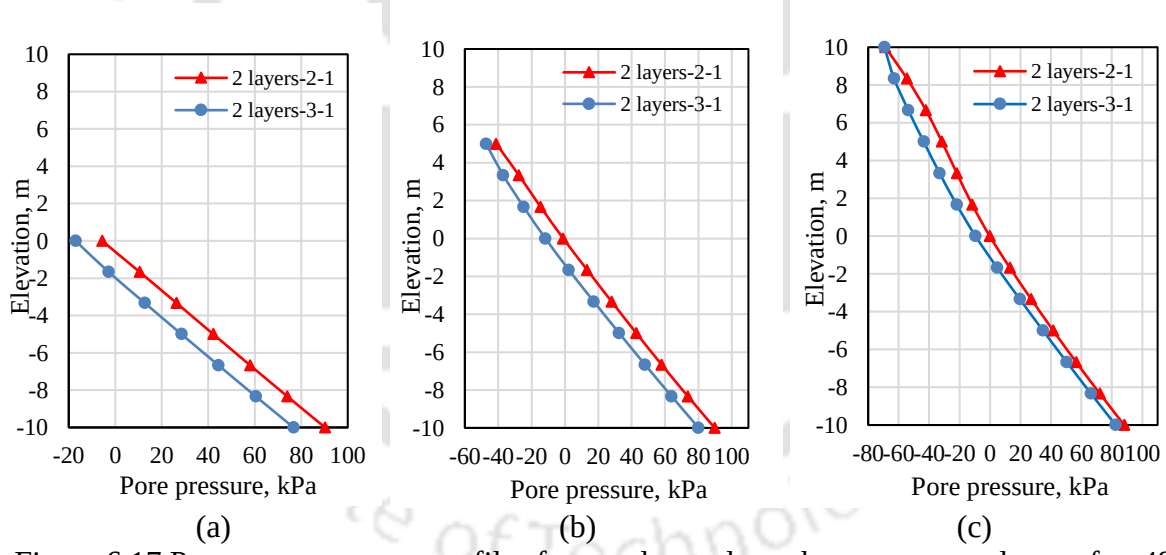


Figure 6.17 Pore water pressure profiles for two-layered non-homogeneous slopes after 48 hours along different sections at: (a) Toe, (b) Mid-slope, and (c) Crest

Figure 6.18 illustrates the pore water pressure contours of the slopes after 24 hours of rainfall. WT represents the GWL level represented by a red line in the slope. It is observed that the maximum negative pore pressures fall in the region of 65-41 kPa are seen for the two-layered slope with Soil-3 at the top due to the low permeability of the soil. The water levels in the slope varies with rainfall infiltration illustrating different behaviour of the two-layered slopes. The



TH-2008_136104008

water level in the model with Soil-2 at the top touches the slope surface near the toe region and then follows the surface very similar to that of homogeneous Soil-1. For the other model with Soil-3, the water level passes approximately 2 m below the toe of the slope. Here it is observed that due to the presence of different soil material at the top both the GWL and pore pressure contours are different. When soil of low permeability is present at the top, less infiltration occurs and hence the rise in water level is less and the suction is maintained enough. With high permeable soil at the top, there is more infiltration occurring and as a result, the GWL and pore pressures increase reducing the effective strength of the soil.

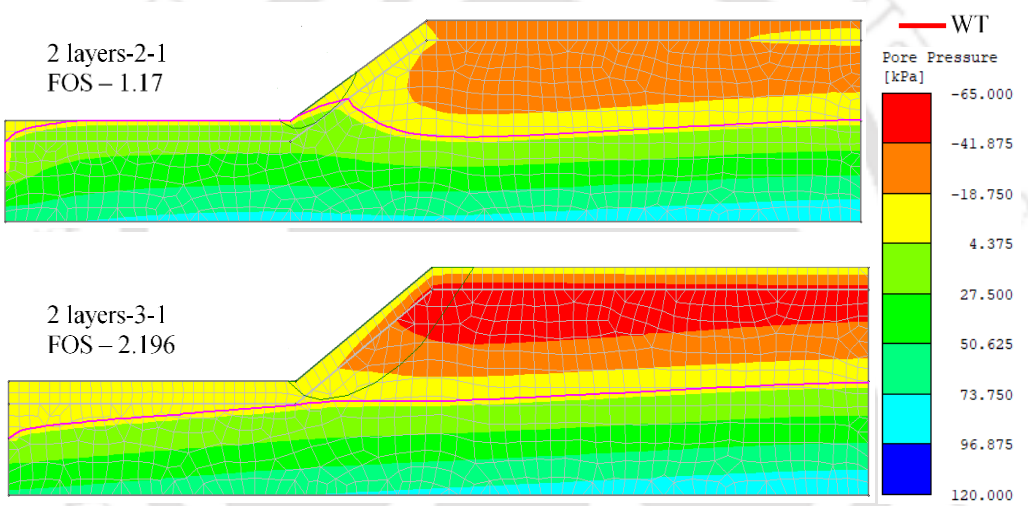


Figure 6.18 Pore water pressure contours of two-layered slopes after 24 hours

The variation in the factor of safety of the slope with time is shown in Figure 6.19. It is observed that during rainfall infiltration the safety factor of the slope decreases due to an increase in pore water pressures, thereby reducing the effective strength of the soil. Slope with Soil-2 at the top has the initial factor of safety near to 2.4 which reduced to 1.17 at 24 hours and then increased to 1.796 at 48 hours. The factor of safety of the slope with Soil-3 at the top reduces to 2.196 from 2.4 after 24 hours. The matric suction is maintained in the model with Soil-3 at the top which accounts for the less variation in the factor of safety. The recovery rate of the stability of the slope is more for the model with Soil-2 at the top as the suction rapidly increases after the rainfall stops. The change in safety factor is very small is due to the fact that water is unable



TH-2008_136104008

to infiltrate due to the low permeability (less than the rainfall intensity) and hence suction doesn't reduce significantly. The homogeneous slope with Soil-1 exhibits behaviour that falls between the two non-homogeneous slope models with the safety factor decreasing from 2.376 initially to 1.656 after 24 hours.

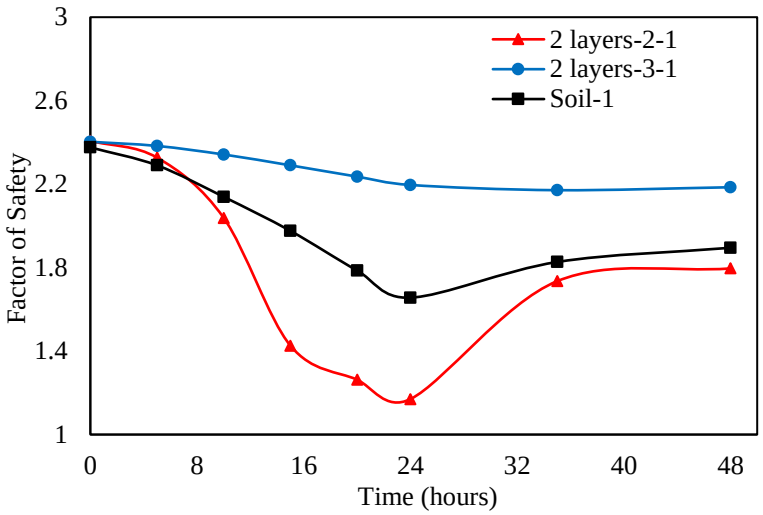


Figure 6.19 Variation of safety factor with time for two-layered non-homogeneous slopes

Figure 6.20 shows the slip surfaces of the two-layered slopes after 24 h of rainfall infiltration where it is observed that the model with Soil-3 at the top has the deepest slip surface position with the highest factor of safety of 2.196 very much similar to the homogeneous slope with Soil-3. For the model with Soil-2 at the top, the rise in GWL, touches the slope surface at the toe, and continues for some distance along the slope surface. The slip surface is confined to the top layer only and half of the slip zone is saturated as it cuts through the water level. Soil-1 exhibits a toe failure mechanism, as it is a homogeneous slope. The GWL rises higher for the homogeneous slope with Soil-1 after rainfall infiltration and touches the slope surface near the mid-slope portion. Hence, a relatively large amount of the failure mass is saturated in the case of Soil-1. Hence, the factor of safety is naturally low at 1.656. Figure 6.21 depicts the critical slip surfaces of the two-layered non-homogeneous slopes after 48 hours. All the slip surfaces represent base failure pattern with the slope model but with different *FOS* values, Soil-3 at the top having the maximum factor of safety (2.185).



TH-2008_136104008

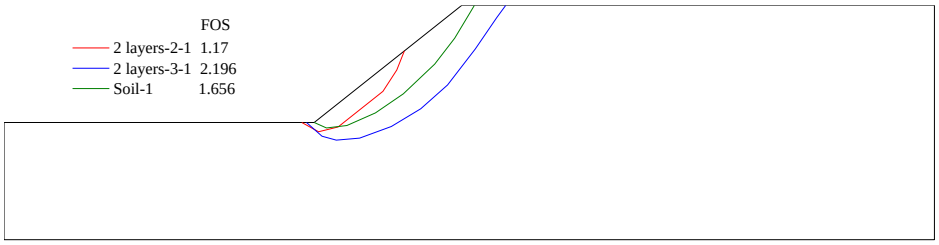


Figure 6.20 Critical slip surfaces of the two-layered non-homogeneous slopes after 24 h

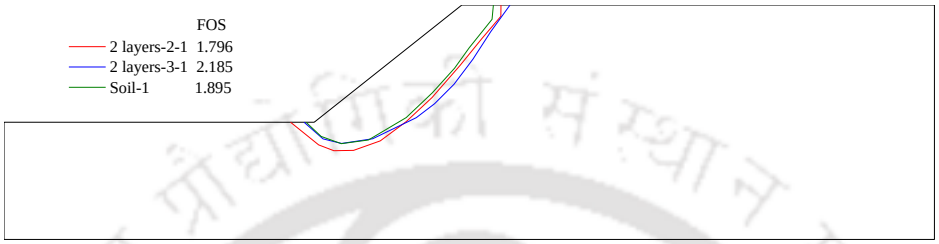


Figure 6.21 Critical slip surfaces of the two-layered non-homogeneous slopes after 48 h

***Three-layered non-homogeneous slope models***

Figure 6.22 represent pore water pressure profiles of two three-layered slope models along three different sections under rainfall infiltration after 24 hours. At 24 hours, it is observed that both the models have zero pressure at the toe region (Figure 6.22a), which indicates saturation of the surface. Runoff starts as the surface is saturated and the infiltration capacity gradually reduces. With depth increasing, the pressure profiles take different paths. Similar kind of pressure profile is observed at the mid-slope portion shown in Figure 6.22b. Maximum suction of 30 kPa is displayed at the interface by the model with Soil-3 at the top due to less water infiltration. Subsurface ponding is observed for the model with Soil-2 at the top with the soil above being saturated slowly. Figure 6.22c depict the pressure profile at the crest of the slope. The subsurface is saturated for the model with Soil-2 as the top layer and then very less water infiltrates as the water encounters Soil-3, which leads to an increase of the suction. The surface is saturated and water infiltration is very less resulting in retaining the suction. The permeability of the subsoil is high enough to drain the rainwater that has percolated through the top layer.



TH-2008_136104008

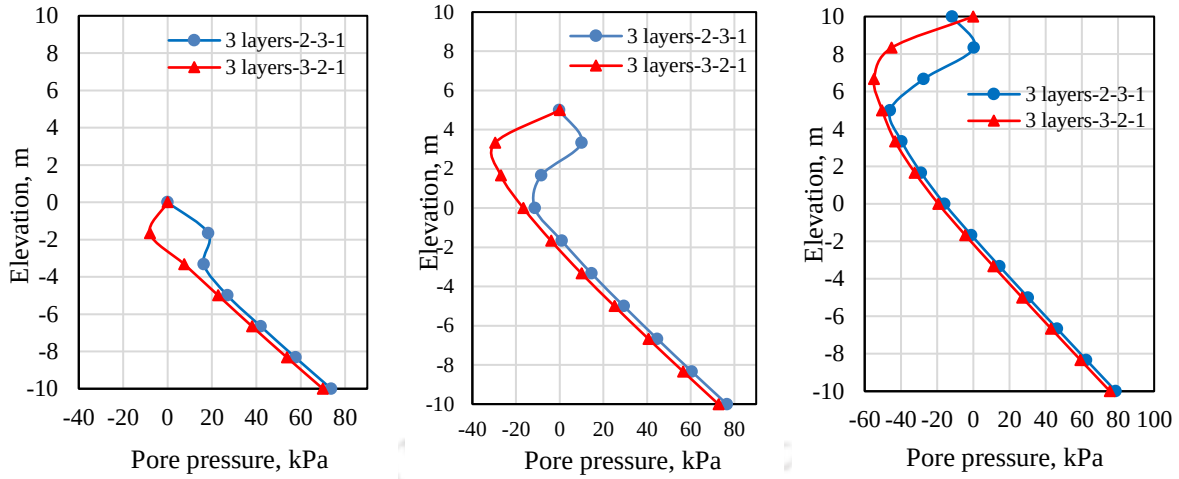


Figure 6.22 Pore water pressure profiles for three-layered non-homogeneous slopes after 24 hours along different sections at: (a) Toe, (b) Mid-slope, and (c) Crest

The pressure decreases for the model with low permeable Soil-3 at the top allowing very less water infiltration and then it increases because of the presence of relatively high permeable Soil-2 as the second layer. The pressure increases from zero pressure at the surface for the model with Soil-2 at the top and then it decreases due to the presence of low permeable Soil-3 as the second layer allowing little infiltration into the sublayer. Beyond this depth, the suction increases as very less water infiltrates the soil.

Figure 6.23 depicts the pore pressure profiles of the three-layered non-homogeneous slopes after 48 hours. At the toe, the suction at the surface is 20 kPa and 6 kPa for the models with Soil-3 and Soil-2 at the top. The path of the pressure profile of the model with Soil-2 falls slightly to the right (i.e., the pore pressures are more at this time) of the model with Soil-3 for the first 4 m where the layers exist. At the mid-slope region, the soils represent different suction values at the surface similar to that of the toe region. The suction of 50 kPa and 34 kPa exists at the surface for the slope models. At the crest region at the surface, 70 kPa of suction is observed for the model with Soil-3 at the top and 53 kPa for the model with Soil-2 at the top. As infiltration stops with the stoppage of rainfall, the matric suction increase gradually and tries to reach the initial condition.



TH-2008_136104008

Figure 6.24 illustrates the pore water pressure contours of the three-layered slopes after 24 hours of rainfall. It is observed that the maximum negative pore pressures fall in the region of 63-42 kPa are seen for the three-layered slope with Soil-3 at the top due to the low permeability of the soil. It is observed that due to the presence of different soil material at the top the pore pressure contours are different.

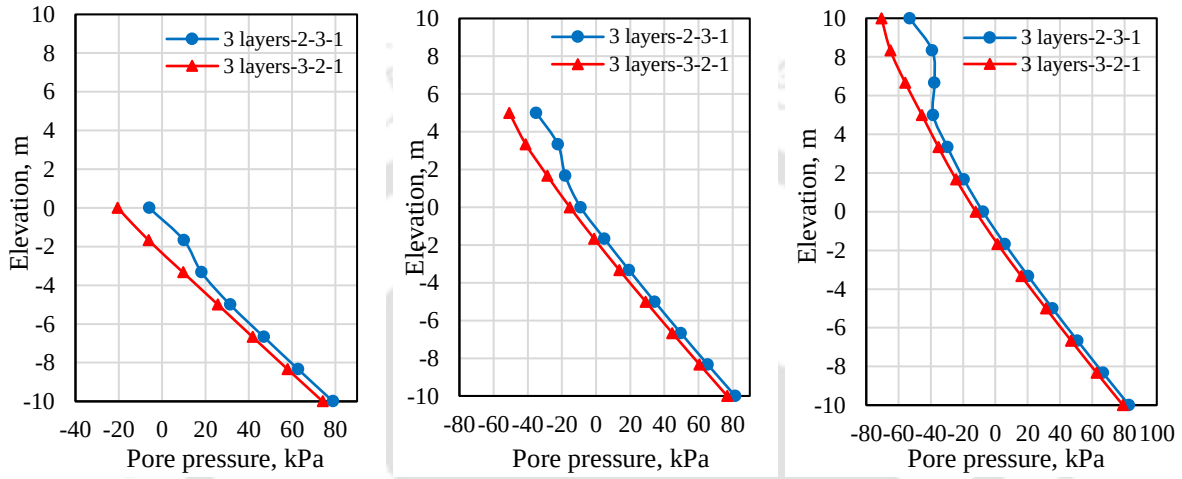


Figure 6.23 Pore water pressure profiles for three-layered non-homogeneous slopes after 48 hours along different sections at: (a) Toe, (b) Mid-slope, and (c) Crest

When soil material of low permeability (Soil-3) is present at the top, less water infiltrates and hence the suction is not reduced considerably. With relatively high permeable soil (Soil-2) at the top, water infiltrates more and as a result, pore pressures increased reducing the effective strength of the soil. The relationship between the factor of safety and time under infiltration conditions is depicted in Figure 6.25. It is observed that during rainfall infiltration the safety factor of the slope decreases due to the reduction of suction, thereby reducing the effective strength of the soil. Slope with Soil-2 at the top has the initial factor of safety near to 2.345 which reduced to 0.616 at 24 hours and then recovered rapidly to 1.918 at 48 hours.



TH-2008_136104008

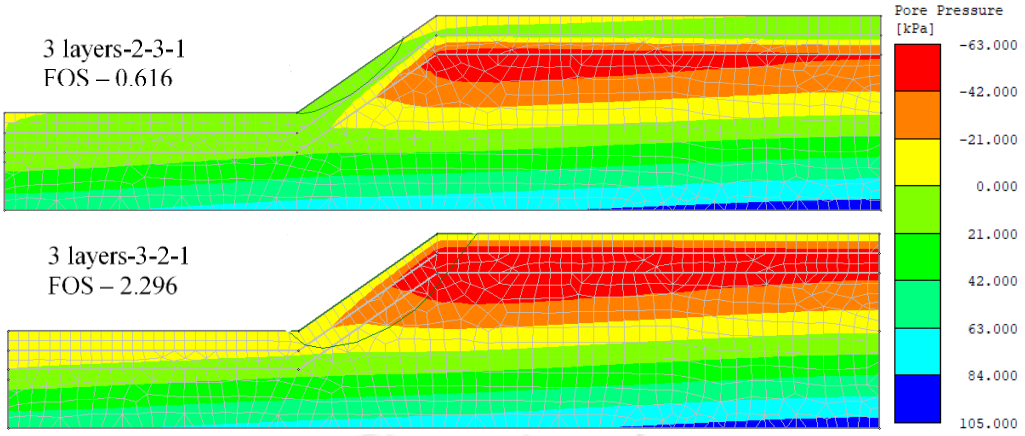


Figure 6.24 Pore water pressure contours of three-layered slopes after 24 hours

As rainfall stops, the infiltration stops and therefore the suction starts to increase which results in an increase in the stability of the slope. The factor of safety of the slope with Soil-3 at the top reduces to 2.296 from 2.456 after 24 hours. The change in the factor of safety is very small which is because the water can not infiltrate more due to the low permeability (less than the rainfall intensity) of the soil (Soil-3) and hence suction doesn't reduce significantly. The homogeneous slope with Soil-1 has its factor of safety decreased from 2.376 initially to 1.656 after 24 hours.

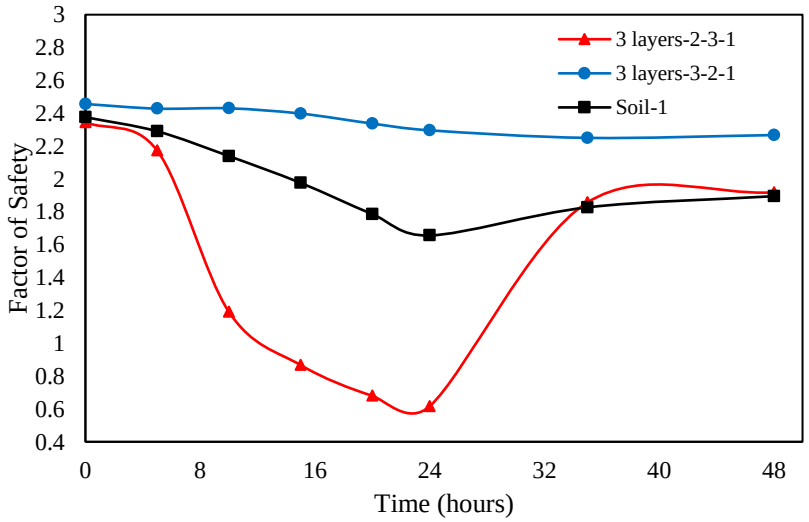


Figure 6.25 Variation of safety factor with time for two-layered non-homogeneous slopes

Figure 6.26 shows the slip surfaces of the three-layered slopes after 24 h of rainfall infiltration. It is observed that the model with Soil-3 at the top has the deepest slip surface position with the highest factor of safety of 2.296 similar to the homogeneous slope with Soil-3. The slip



TH-2008_136104008

surface is confined to the top layer only for the model with Soil-2 at the top representing a shallow slope failure. The critical slip surface for Soil-1 exhibits a toe failure mechanism. The GWL rises higher for the homogeneous slope with Soil-1 after rainfall infiltration and touches the slope surface near the mid-slope portion. Hence, a relatively large amount of the failure mass is saturated in the case of Soil-1. Hence, the factor of safety is naturally low at 1.656. Figure 6.27 illustrates the critical slip surfaces of the three-layered non-homogeneous slopes after 48 hours. All the slip surfaces represent base failure pattern with the slope model with Soil-3 at the top having the maximum factor of safety (2.267) due to the strength provided by the suction. The slip surfaces of the three-layered model with Soil-2 at the top and homogeneous model with Soil-1 follow similar paths having factors of safety very close to each other also.

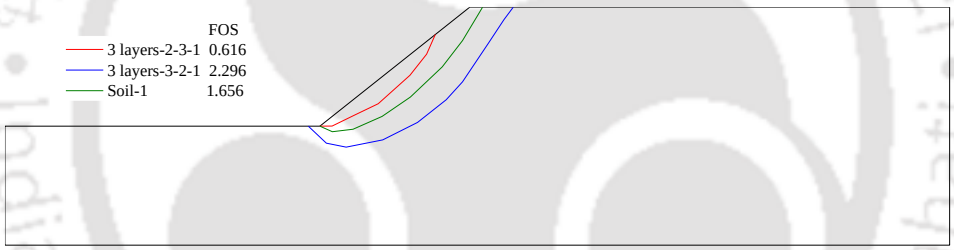


Figure 6.26 Critical slip surfaces of the three-layered non-homogeneous slopes after 24 h

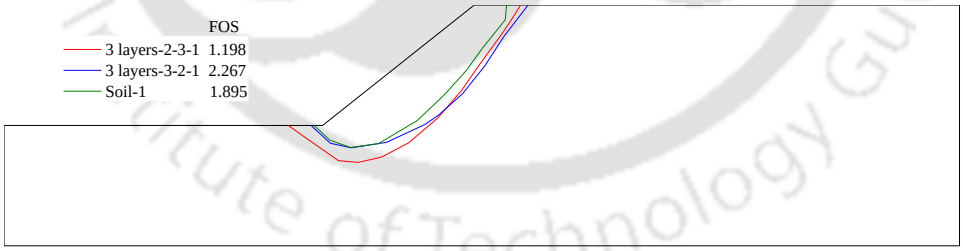


Figure 6.27 Critical slip surfaces of the three-layered non-homogeneous slopes after 48 h

### 6.3.1 Effect of rainfall intensity

To study the effect of rainfall intensity on the stability of slopes with two-layered non-homogeneous slopes, five different rainfall intensities of 10 mm/h, 30 mm/h, 50 mm/h, 100 mm/h and 200 mm/h were used. A short duration (24 h) rainfall was applied to the slope surface in all scenarios. The results obtained for each type of non-homogeneous model are presented



TH-2008_136104008

below.

***Two-layered non-homogeneous slope model (Soil-2 as top layer)***

Figure. 6.28 illustrates the pore pressure profiles of the two-layered slope at the mid-slope section under different rainfall intensities. The pressure profiles at the initial stage (0 h) indicate hydrostatic conditions within the slope mass. Figure. 6.28a shows the pore pressure profile under 10 mm/h rainfall intensity. At the surface, the suction changes from 72 kPa at the initial stage to 42 kPa after 24 h and 59 kPa after 48 h. With rainfall infiltration, the profile shifts towards the right (positive pore pressures), i.e., suction decreases which results in a decrease in strength of the soil. As rainfall infiltration stops, the profile shifts left towards the initial position. Under 50 mm/h intensity (Figure. 6.28c), the 24$^{th}$ hour profile exhibit positive pore pressures throughout indicating saturation of the entire soil profile. There is no suction at all at this stage but with cessation of infiltration, the suction regains its value. Similarly, for 100 mm/h intensity (Figure. 6.29a) and 200 mm/h intensity (Figure. 6.29b) the surface is saturated after 24 hours of infiltration.

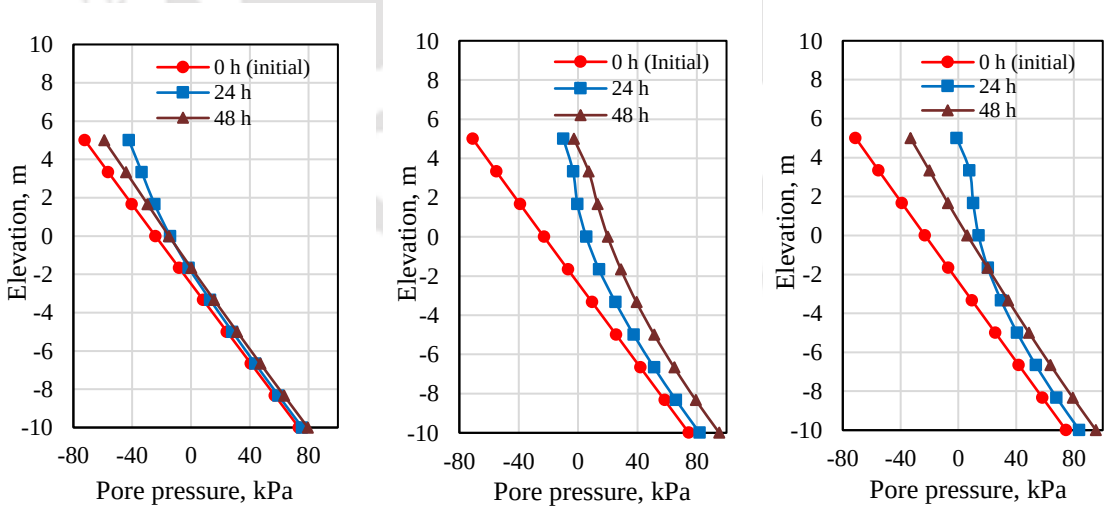


Figure. 6.28 Pore water pressure profiles for the slope at different times under different intensity: (a) 10 mm/h, (b) 30 mm/h, and (c) 50 mm/h



TH-2008_136104008

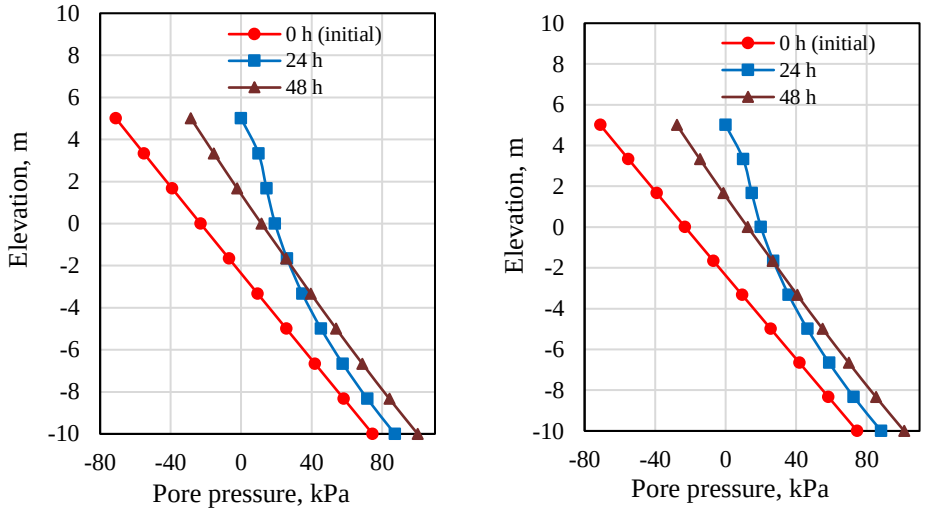


Figure. 6.29 Pore water pressure profiles for the slope at different times under different intensity: (a) 100 mm/h, and (b) 200 mm/h

Figure 6.30a represents the pore pressure profiles of the mid-slope section after 24 h for different rainfall intensities. It is observed that under the lowest rainfall intensity (10 mm/h), the slope possess the maximum suction at the surface. As the rainfall intensity increases, the surface suction begins to reduce rapidly. The top 2 m of the pressure profiles indicate a gradual reduction of suction but at more depth, the drop is almost vertical until the water level. Under 50 mm/h rainfall intensity, the pressures are positive throughout the depth. The pressure profiles for 100 mm/h and 200 mm/h follow the same path depicting that the soil has reached saturation. Figure 6.30b depict the pore pressure profiles after 48 hours at the mid-slope section. Under 10 mm/h rainfall intensity, the suction at the surface is 60 kPa. The suction at the surface for the other rainfall intensities stay near to 27 kPa. The pressure profiles under all intensities follow a parallel and hydrostatic path except the 30 mm/h pressure profile. At the top 4 m, the pressure profile deviates from the hydrostatic behaviour.



TH-2008_136104008

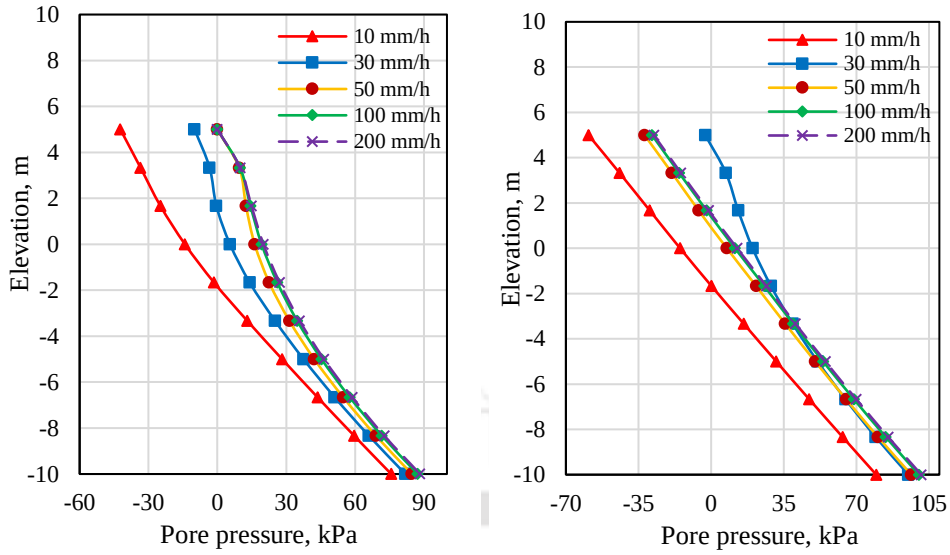


Figure 6.30 Pore water pressure profiles under different rainfall intensity for the two-layered slope (2 layers-2-1) at (a) 24 h and (b) 48 h

Figure 6.31 depicts the pore water pressure contours of the two-layered slope under various rainfall intensities. The negative pore pressure is maximum for rainfall intensity 10 mm/h whose factor of safety is also the maximum at 2.183. The water just passes under the toe of the slope. The water level touches the slope surface under 30 mm/h rainfall intensity bringing the safety factor down to 1.364. With an increase in rainfall intensity, the suction in the slope decreases and with it the safety factor as well. The suction is in the range of 29 kPa to 6 kPa for 50 mm/h rainfall intensity when the safety factor recorded is 0.721. At 100 mm/h, the maximum suction is in the range of 6 kPa to 0 kPa with a safety factor of 0.59. The water now passes through the slope surface as run-off indicating that the soil has reached its infiltration capacity. After this stage, with more rainfall intensity, there is no effect on the pore pressures and the safety factor is similar at 0.587. GWL represents the GWL within the slope. The mounding of GWL is very high under higher rainfall intensities for the two-layered slope with Soil-2 as the top layer.



TH-2008_136104008

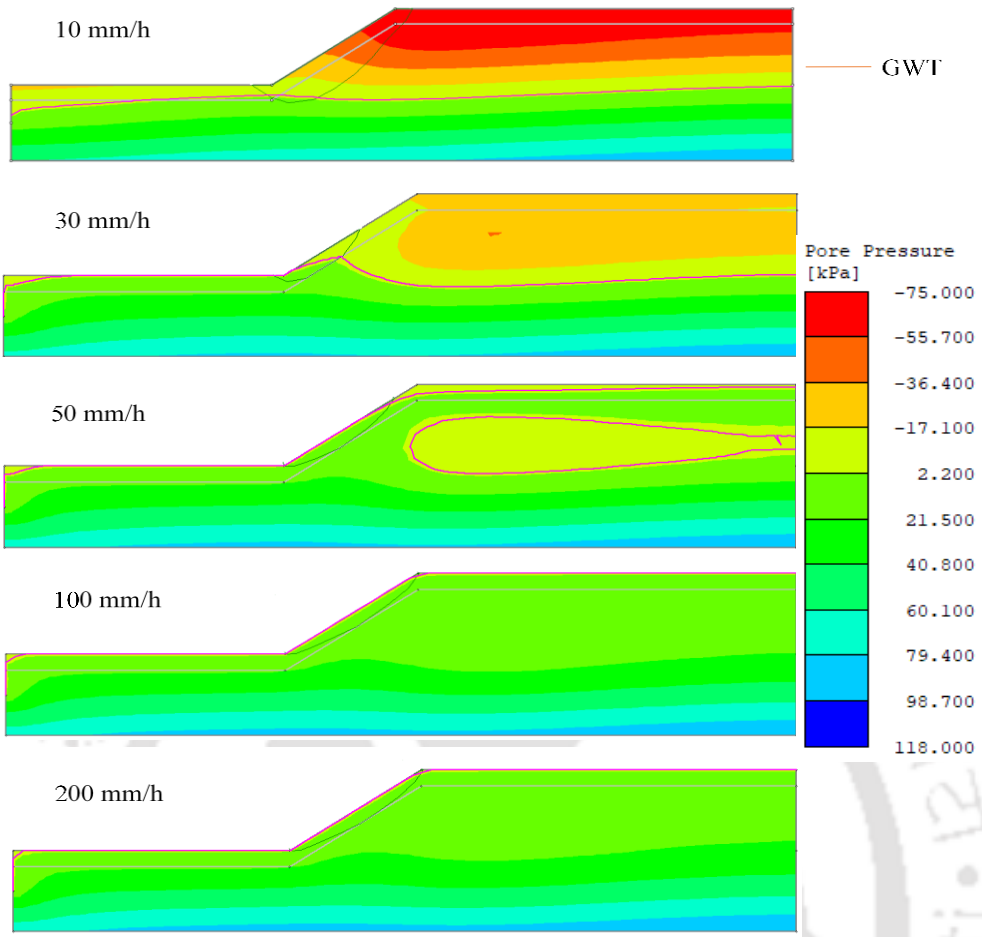


Figure 6.31 Pore water pressure contours under different rainfall intensity after 24 h

The variation factor of safety with time for different values of rainfall intensity for the two-layered slope is illustrated in Figure. 6.32. The minimum factor of safety decreases with time and the rate of decrease depends on the magnitude of the rainfall intensity. The curve for 10 mm/h represents that the stability of the slope is not much affected because now the intensity is very low as compared to the permeability of both the top soil and the subsoil. Hence, there is not much infiltration occurring to reduce the suction within the slope. With the increase in rainfall intensity, at 30 mm/h (nearly equal to the permeability of Soil-1) the safety factor reduces to 1.17 after 24 h and reaching failure conditions (*FOS* - 0.914) after 35 h. The slope reaches failure conditions (*FOS* - 0.801) under 50 mm/h rainfall intensity just after 12 h of rainfall. A perched GWL is formed in the slope under 50 mm/h rainfall intensity due to the presence of a low permeable soil (Soil-1) under a high permeable soil (Soil-2) (Cho and Lee,



TH-2008_136104008

2001). The hydrological behaviour generates shear stress and shear strain above the interface, which ultimately leads to failure. The slope fails (*FOS* - 0.821) just after 5 h of rainfall while the safety factor is 0.658 after 5 h under 200 mm/h rainfall.

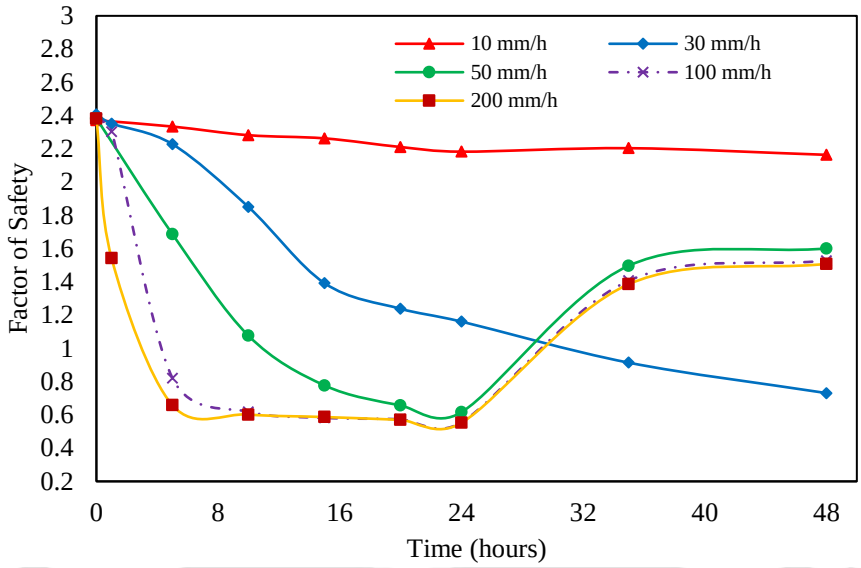


Figure. 6.32 Variation of safety factor with time under various rainfall intensities for the two-layered slope (2 layers-2-1)

As rainfall stops, the slope recovers its factor of safety with an increase in suction. The minimum factors of safety of the slope under rainfall intensities 50, 100 and 200 mm/h are similar which points toward a threshold rainfall intensity. Therefore, 50 mm/h seems to be the threshold intensity beyond which there is no effect on the minimum factor of safety of the slope because now the slope has reached its infiltration capacity. Comparison of the critical slip surfaces under different rainfall intensities after 24 h is shown in Figure. 6.33. The slip surfaces for all the intensities represent shallow slope failure except the 10 mm/h intensity. The 10 mm/h rainfall intensity exhibits the deepest slip surface. The slip surfaces gradually extend towards the crest region with an increase in rainfall intensity from 30 mm/h to 200 mm/h.

Figure 6.34 depicts the slip surfaces under different rainfall intensities for the two-layered slope after 48 hours. The slip surfaces under different rainfall intensities indicate base failure mechanism except the slip surface under 30 mm/h intensity. The slip surface for 30 mm/h



TH-2008_136104008

rainfall intensity is shallow and close to the surface of the slope. Slip surfaces for the 100 mm/h and 200 mm/h rainfall intensity coincide with each other. The deepest slip surface is observed for the rainfall intensity of 10 mm/h.

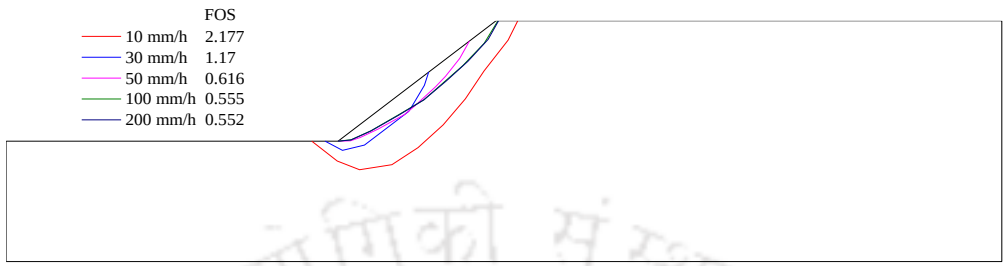


Figure. 6.33 Critical slip surfaces for the two-layered slope (2 layers-2-1) after 24 h for different rainfall intensities

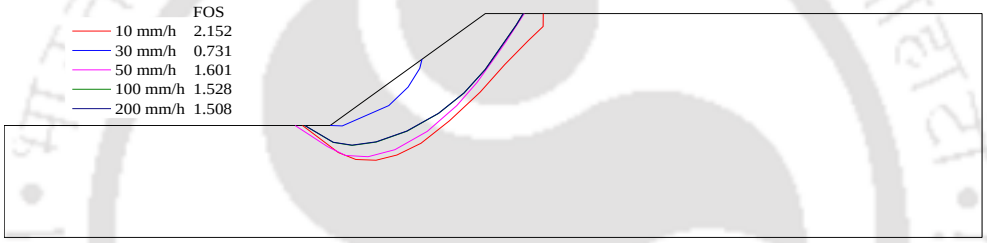


Figure 6.34 Critical slip surfaces for the two-layered slope (2 layers-2-1) after 48 h for different rainfall intensities

***Two-layered non-homogeneous slope model (Soil-3 as top layer)***

Figure 6.35a depicts the pore pressure profiles of the mid-slope section after 24 h under different rainfall intensities. The surface suction reduces to zero after 24 hours of rainfall infiltration. As the top 2 m consists of Soil-3, the suction increases until 30 kPa and thereafter starts to decrease to zero at the water level. The pressure profiles follow similar path under all the rainfall intensities. Only the pressure profile under 10 mm/h rainfall intensity slightly deviates from the other pressure profiles. Figure 6.35b illustrate the pore pressure profiles after 48 hours at the mid-slope section for the two-layered non-homogeneous slope. The pressure profiles under all intensities follow a parallel and hydrostatic path except the 30 mm/h pressure profile. At the top 2 m, the pressure profile deviates from the hydrostatic behaviour. The suction at the surface is observed to be 45 kPa under all the rainfall intensities.



TH-2008_136104008

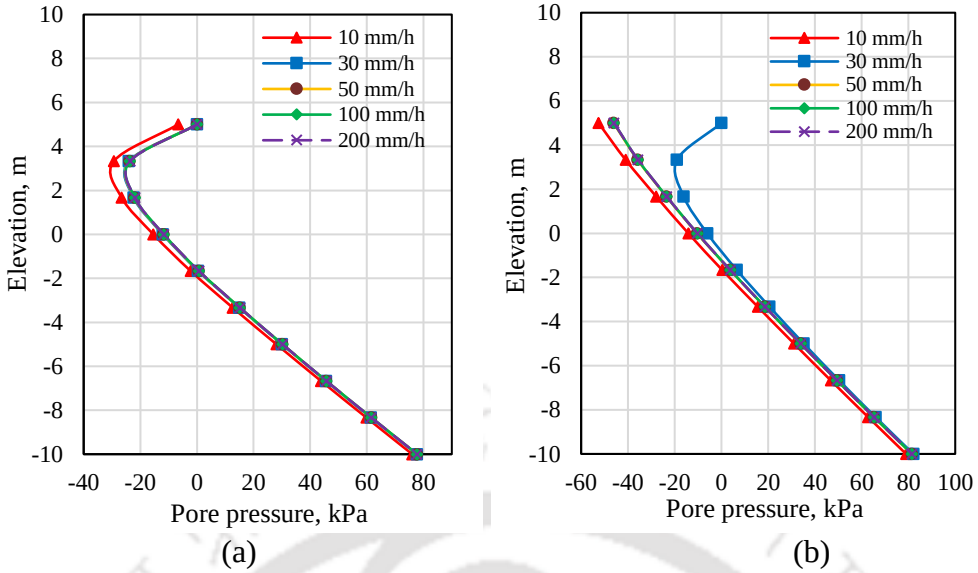


Figure 6.35 Pore water pressure profiles under different rainfall intensity for the two-layered slope (2 layers-3-1) at (a) 24 h and (b) 48 h

Figure 6.36 represents the GWL rise after 24 h of rainfall infiltration under different rainfall intensities. It is observed that the water level rise with an increase in rainfall intensity is very minimal. The dotted line denote the natural water level existing in the slope prior to rainfall infiltration. The two-layered model consists of low permeable Soil-3 at the top which resists the infiltration of water at the top resulting in a very little rise in the GWL. There is relatively no mounding of the GWL under higher rainfall intensities.

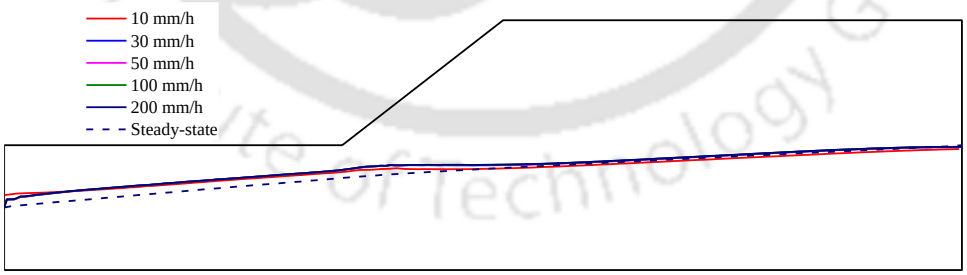


Figure 6.36 GWL location for the two-layered slope (2 layers-3-1) under different rainfall intensities after 24 h

The variation of factor of safety with time under various rainfall intensities for the two-layered slope is illustrated in Figure 6.37. The curve for 10 mm/h represents that the stability of the slope is not much affected because now the intensity is low as compared to the permeability of



TH-2008_136104008

the soils. Hence, there is not much infiltration occurring to reduce the suction within the slope. With an increase in rainfall intensity, at 30 mm/h (nearly equal to the permeability of Soil-1) the safety factor reduces to 2.196 after 24 h ultimately reaching 2.185 after 48 h. The behaviour of the slope under 50 mm/h, 100 mm/h and 200 mm/h rainfall intensity is similar in nature. The factor of safety reduces to 2.173 after 24 hours and then stays almost constant until 48 hours. The stability of the two-layered slope is not affected because of the presence of Soil-3 (less permeable) at the top, which does not allow the water to infiltrate the slope. The effect of rainfall intensity on the stability of the slope is negligible 30 mm/h intensity onwards. Thus, it is observed that there is very less effect on the slope due to different rainfall intensities. This phenomenon can be attributed to the low permeability of Soil-3 at the top, which prevents water from infiltrating into the slope.

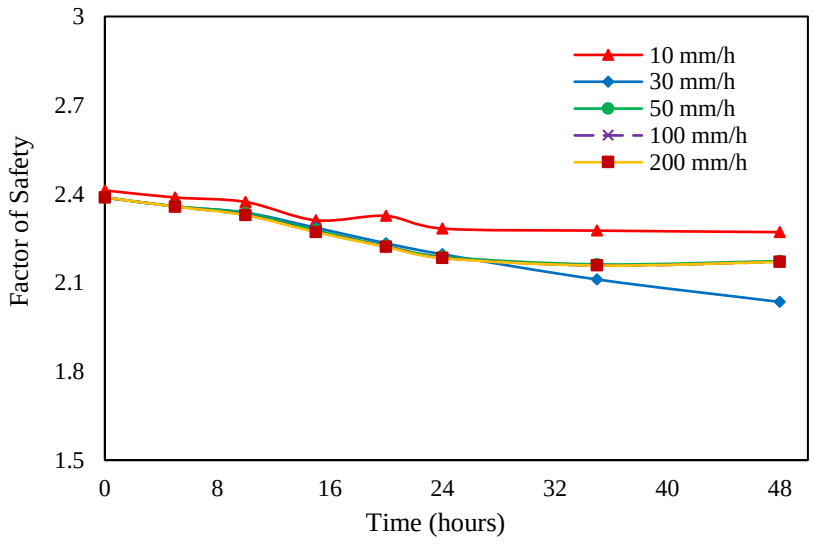


Figure 6.37 Variation of safety factor with time under various rainfall intensities for the two-layered slope (2 layers-3-1)

After surface saturation occurs, most of the water flows over the surface as run-off and very less water infiltrate the slope. Rather the factor of safety decreased very gradually and reached the minimum value after 48 hours. Due to the low permeability of the soil, the water could not reach the critical slip surface rapidly. For this type of soil, the water takes a longer time to reach the critical zone, which again depends on the infiltration rate. Figure 6.38 illustrates the critical



TH-2008_136104008

slip surfaces of the two-layered slope after 24 hours under various rainfall intensities. The mainly base failure mechanism is observed for all the rainfall intensities. The safety factors gradually reduce with an increase in rainfall intensity while having the same slip surfaces.


Figure 6.38 Critical slip surfaces for the two-layered slope (2 layers-3-1) after 24 h for different rainfall intensities

Figure 6.39 represents the slip surfaces of the two-layered slope after 48 hours; 24 hours after rainfall infiltration have stopped. All five slip surfaces represent base failure mode with the slip surface for the 10 mm/h being deeper than the other intensities.

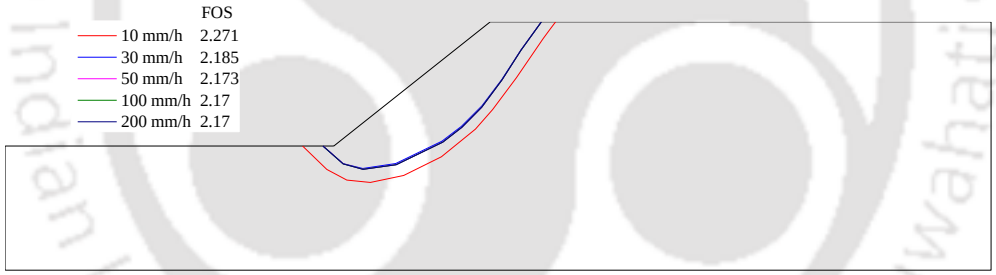


Figure 6.39 Critical slip surfaces for the two-layered slope (2 layers-3-1) after 48 h for different rainfall intensities

### 6.3.2 Effect of duration of rainfall

To investigate the effect of duration of rainfall on stability, two different rainfall durations (24 and 48h) were selected with constant rainfall intensity of 30 mm/h. The slope height is 10 m and slope inclination is 35°. The other dimensions of the model were kept constant.



TH-2008_136104008

***Two-layered non-homogeneous slope model (Soil-2 as top layer)***

Figure 6.40 illustrates the pore pressure profiles of the two-layered slope at different times in the mid-slope section. The pressure profiles at the initial stage depict hydrostatic conditions within the slope. At the surface, the suction is 71 kPa at the initial stage. With rainfall infiltration, the surface suction starts to dissipate. After 24 h the suction is 9 kPa, 3 kPa after 48 h and 35 kPa after 72 h. With rainfall infiltration, the profile shifts towards the right (positive pore pressures), i.e., suction decreases which results in a decrease in strength of the soil. As rainfall infiltration stops, the profile shifts left towards the initial position. Water rapidly infiltrates the soil at the surface due to high permeability of Soil-2 at the top and the soil saturates in the lower layers. The suction dissipates and infiltration stops after the infiltration capacity of the soil is reached.

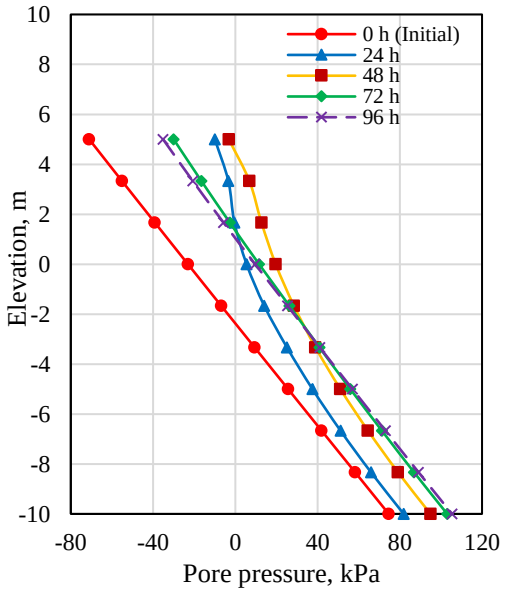


Figure 6.40 Pore pressure profile of the two-layered slope (2 layers-2-1) under long duration rainfall

The variation in the factor of safety of the two-layered slope with time is shown in Figure 6.41. It is observed that during rainfall infiltration the safety factor of the slope decreases due to a decrease in matric suction, thereby reducing the effective cohesion in the soil. The slope has the maximum initial factor of safety near to 2.4 which reduced to 0.735 at 48 hours and then



TH-2008_136104008

increased to 1.571 after 96 hours for the long duration (48 h) rainfall infiltration.

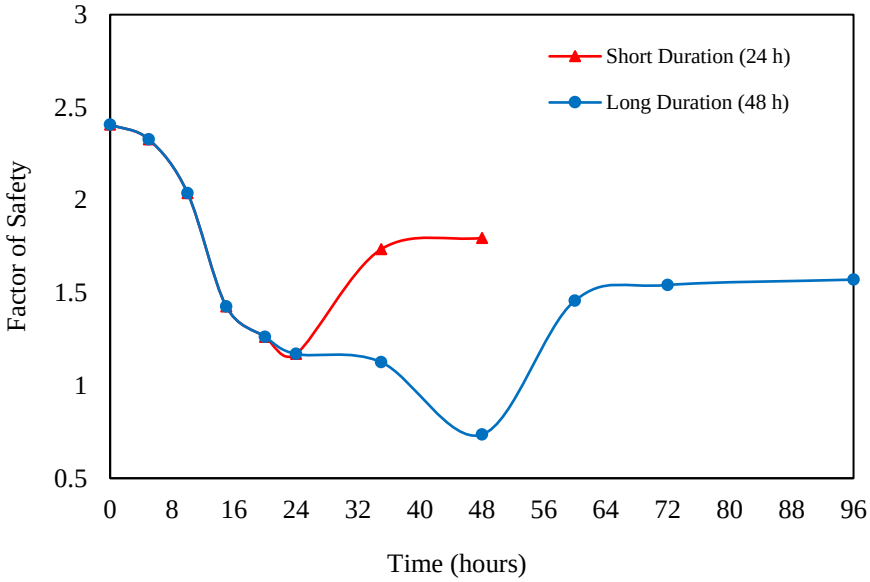


Figure 6.41 Variation of a factor of safety with a time of the two-layered slope (2 layers-2-1) under long duration rainfall

For the short duration (24 h) rainfall, the factor of safety of the slope decreased to 1.17 after 24 hours and then recovered to 1.79 at 48 hours. There was a 37% reduction in the factor of safety of the slope under the long duration rainfall. Figure 6.42 illustrates the critical slip surfaces at various times of the two-layered slope under long duration (48 h) rainfall. The slip surfaces at 0 h, 72 h, and 96 h represent base failures with factors of safety 2.4, 1.54 and 1.57. The other slip surfaces at 24 h and 48 h are shallow and they depict slope failure mode due to water infiltration within the slope.

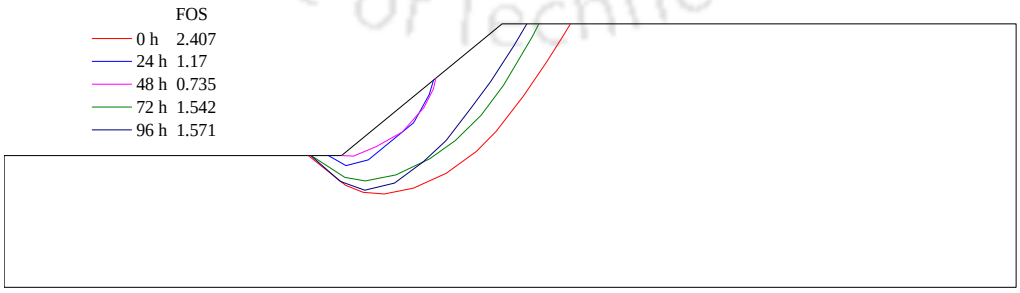


Figure 6.42 Critical slip surfaces of the two-layered slope (2 layers-2-1) under long duration rainfall



TH-2008_136104008

***Two-layered non-homogeneous slope model (Soil-3 as top layer)***

Figure 6.43 illustrates the pore pressure profiles of the two-layered slope at different times in the mid-slope section. The pressure profiles at the initial stage depict hydrostatic conditions within the slope. At the surface, the suction is 68 kPa at the initial stage. With rainfall infiltration, the surface suction starts to dissipate. There is no suction after 24 h, but as rainfall stops the suction increases to 40 kPa after 72 h. With rainfall infiltration, the profile shifts towards the right (positive pore pressures), i.e., suction decreases which results in a decrease in strength of the soil. As rainfall infiltration stops, the profile shifts left towards the initial position. It is observed that the surface is saturated after 24 hours and 48 hours due to very less infiltration taking place at the surface. This happens due to the low permeability of the Soil-3 and as a result, the suction does not dissipate in the lower portion.

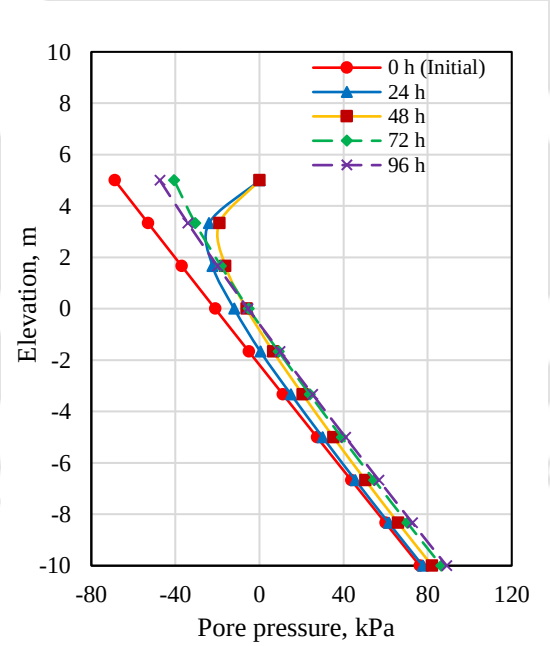


Figure 6.43 Pore pressure profile of the two-layered slope (2 layers-3-1) under long duration rainfall at the mid-slope section

The variation in the factor of safety of the two-layered slope with time is shown in Figure 6.44. It is observed that during rainfall infiltration the safety factor of the slope decreases due to a decrease in matric suction, thereby reducing the effective cohesion in the soil. The slope has



TH-2008_136104008

the maximum initial factor of safety near to 2.4 which reduced to 2.026 after 48 hours and then increased to 2.074 after 96 hours for the long duration (48 h) rainfall infiltration.

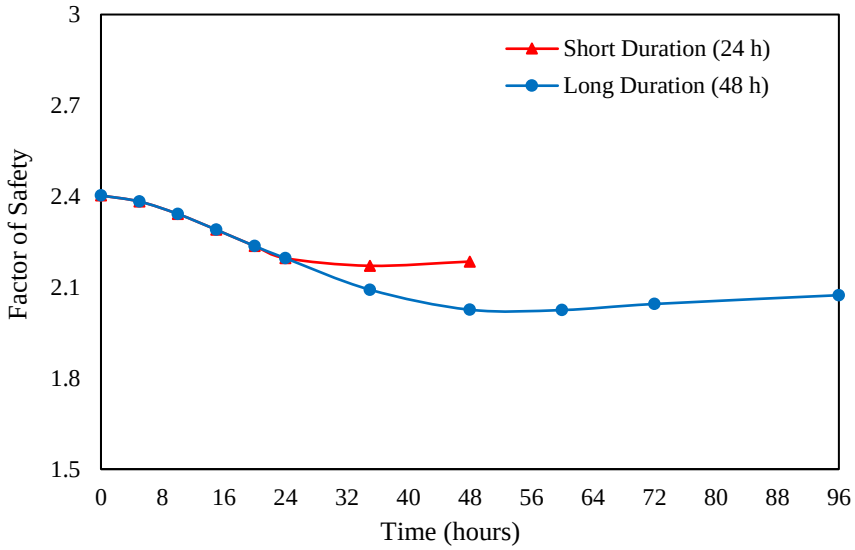


Figure 6.44 Variation of a factor of safety with a time of the two-layered slope (2 layers-3-1) under long duration rainfall

For the short duration (24 h) rainfall, the factor of safety of the slope decreased to 2.17 after 24 hours and then recovered to 2.185 at 48 hours. Under the long duration rainfall, the factor of safety of the slope reduced 6% more than under the short duration rainfall. Figure 6.45 illustrates the critical slip surfaces at various times of the two-layered slope under long duration (48 h) rainfall. All the slip surfaces at various durations represent base failure mechanism.

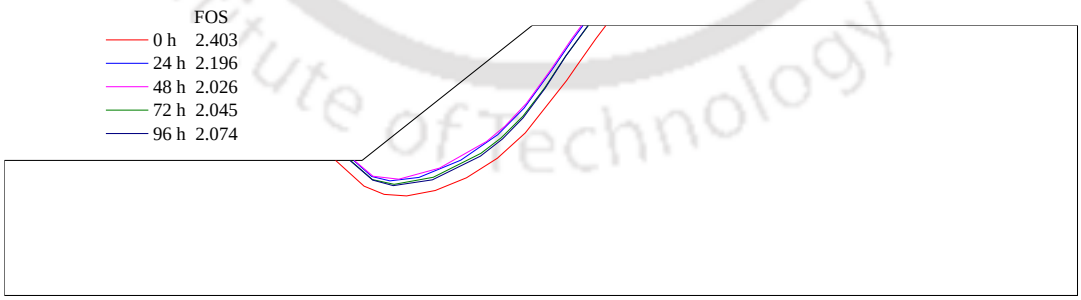


Figure 6.45 Critical slip surfaces of the two-layered slope (2 layers-3-1) under long duration rainfall



TH-2008_136104008

### 6.3.3 Effect of slope angle

A parametric study with five different slope angles as shown in Figure 6.52 was performed under infiltration situations to study the influence of slope inclination ($\beta$) on the stability of a two-layered non-homogeneous slope. The slope angles selected were 26.56°, 35°, 45°, 55°, and 65°. All the other dimensions were kept constant. Rainfall infiltration of 30 mm/h has been considered for all these models.

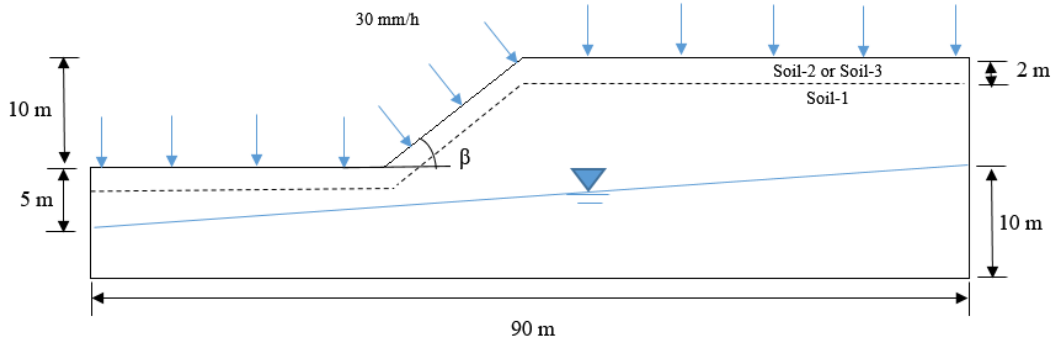


Figure 6.46 Model used for slope angle variation

The pore water pressure variation at point P with slope inclination is illustrated in Figure 6.47. At slope angle 26.56°, the pore pressure is negative (-1.7 kPa) for the model with Soil-2 at the top which increases to -0.9 kPa pressure at 65°. Similarly, for the model with Soil-3 at the top, the pressure for 26.56° slope angle is -30 kPa, which increases to -21 kPa for 65°. At slope angle 26.56°, the pore pressure is negative (-0.5 kPa) for Soil-1 which decreases to (-1.7 kPa) pressure at 65°. The water level after 24 hours passes very close to point P, hence the suction is less. For the slope with Soil-1, the pressure remains constant with an increase in slope angle. For the two-layered slopes, the pressure stays constant until 35°, but then the pressure increases with an increase in slope angle until 65°. Due to rainfall infiltration, flat homogeneous slopes with Soil-1 have positive pressure at point P, which shows negative values with an increase in slope angle. For the two-layered slopes, point P falls on the interface of the two layers. The pore pressures increase with slope inclination 35° onwards. The reason is that with an increase



TH-2008_136104008

in slope angle, the water cannot infiltrate with ease and hence follows the interface. Thus, the pore pressures show increased values at point P with an increase in slope inclination.

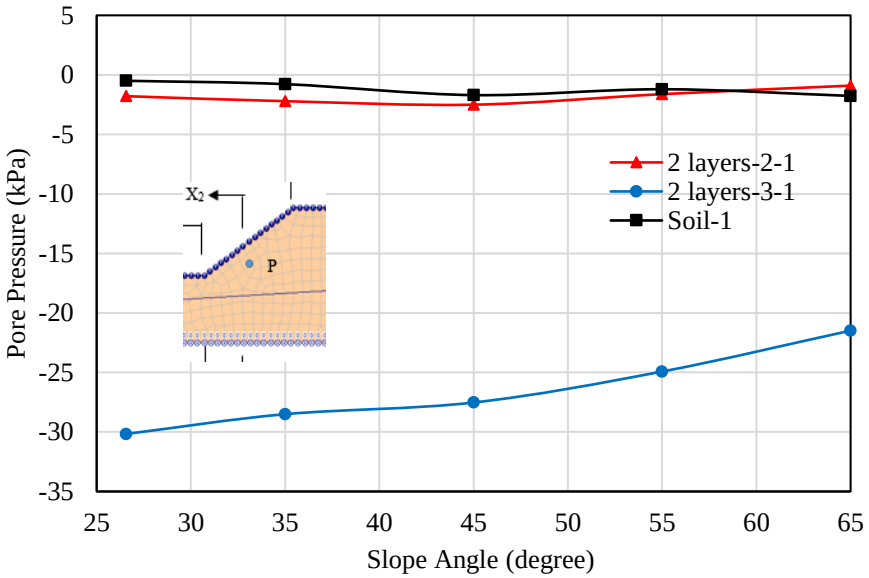


Figure 6.47 Variation of pore water pressure with slope angle at point P for the two-layered slopes after 24 hours

Figure 6.48 illustrates the pore pressure profiles at various inclinations for the homogeneous slope for non-homogeneous slope 2 layers-2-1at two sections of the slope. At the toe section (Figure 6.48a), the suction is zero at the surface after 24 hours of infiltration. The pressure profiles for different slope inclinations follow a similar path. The crest section (Figure 6.48b) of the slopes represent a different scenario with the 65° slope receiving the highest infiltration resulting in more reduction in suction. The slope inclined at 26.57° show the least reduction in suction indicating the least amount of infiltration. Steep slopes illustrate more reduction in suction at the crest section due to more infiltration occurring near the surface. The suction at the surface ranges from 16 kPa to 11 kPa for the slope inclinations varying from 26.57° to 65°.



TH-2008_136104008

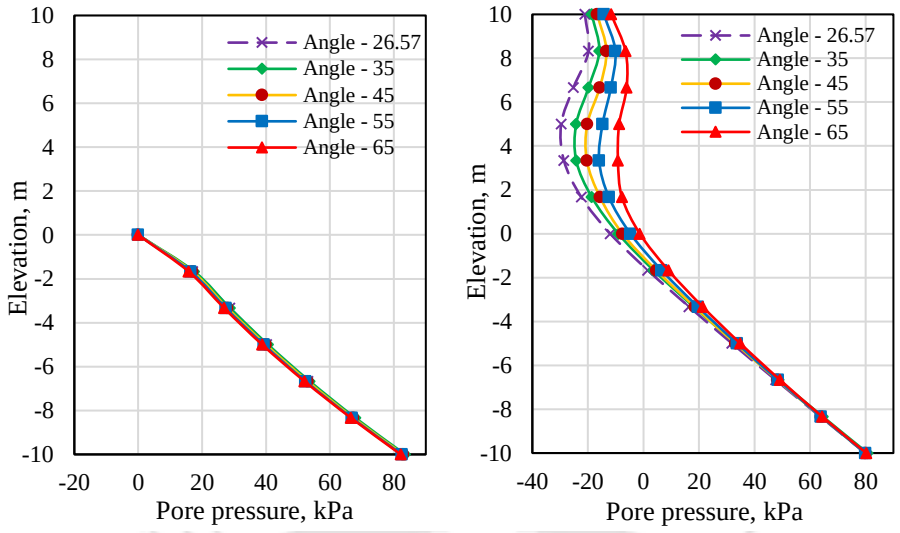


Figure 6.48 Pore water pressure profiles for different slope angles at (a) toe section (b) crest section after 24 hours for non-homogeneous slope 2 layers-2-1

Figure 6.49 illustrates the pore pressure profiles for various slope inclinations for non-homogeneous slope 2 layers-3-1 after 24 hours of rainfall infiltration. Figure 6.49a represent the pore water pressure profiles at the toe section of the slope. The profiles at different slope inclinations follow the same path where the soil is saturated throughout. At the interface, there is minimal suction noted for the two-layered slope.

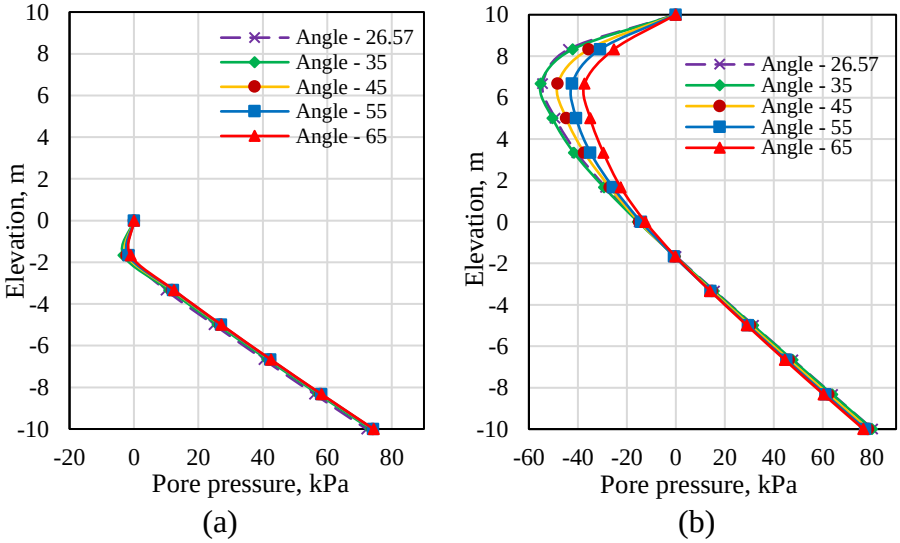


Figure 6.49 Pore water pressure profiles for different slope angles at (a) toe section (b) crest section after 24 hours for non-homogeneous slope 2 layers-3-1



TH-2008_136104008

The pressure profiles at the crest section (Figure 6.49b) show that the surface is saturated after 24 hours and hence most of the water flow as runoff. The decrease in suction due to infiltration is maximum for the 65° slope. Steep slopes show more reduction in suction due to more water infiltration at the crest section of the slope. Just below the surface, the suction increases due to the presence of low permeable soil (Soil-3) at the top layer.

Figure 6.50 depicts the change in the factor of safety of the slope with slope inclination for the non-homogeneous two-layered slopes after 24 hours of rainfall infiltration. The initial factor of safety (0 h) of the slopes before infiltration is also shown. The rise in water level due to rainfall infiltration saturates the soils and hence reduces the effective strength of soil thereby decreasing the stability of the slopes. The initial stability of the slope decreases as the slope inclination increases from 26.56° to 65°. For Soil-1, the safety factor decreases from 2.04 to 1.683 after 24 hours of infiltration. Similarly, for the two-layered slope with Soil-2 at the top, the safety factor decreases nonlinearly from 1.26 to 0.8 and for the slope with Soil-3 at the top, the factor of safety decreases from 2.5 to 1.5 after 24 hours of rainfall infiltration. The factor of safety of the homogeneous slope with Soil-1 does not reduce much after 55° slope inclination. The GWL levels for the 55° and 65° slopes are very similar in nature. The slope with Soil-2 at the top reaches failure (*FOS* - 0.8) at 65° slope inclination. Though, the initial *FOS* values vary similarly with slope angle for all the three slope models considered, after 24 h rainfall infiltration, the variations are significantly different. This indicates that the nature of soil stratifications influences the effects of slope angle inclination. Steep slopes with high permeable soil (Soil-2) as the top layer fails under the considered rainfall intensity. Flat slopes with low permeable soil (Soil-3) as the top layer represent a more stable combination.



TH-2008_136104008

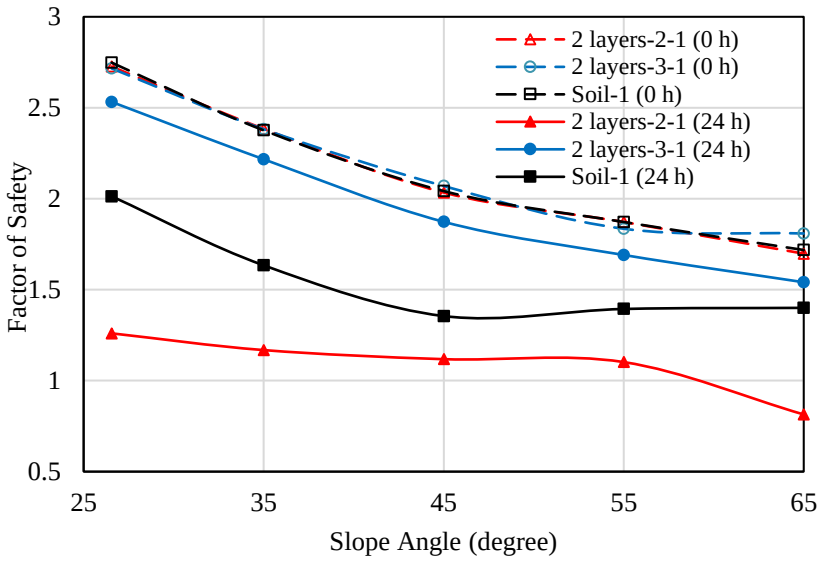


Figure 6.50 Variation of safety factor with slope angle for the two-layered slopes at the initial stage and after 24 h

The critical slip surfaces for the two-layered slopes at different slope inclinations are shown in Figure 6.51. For slope angle 26.56° (Figure 6.51a), a homogeneous slope with Soil-1 represents a toe failure mechanism. Two-layered slope with Soil-2 at the top depicts a shallow slope failure mode with the failure surface confined to the top layer only. The two-layered slope with Soil-3 at the top shows a base failure with a deep surface due to the higher cohesion of the soil material. Figure 6.51b represent the slip surfaces for slope inclination 35°. The failure mechanisms followed by the soils are the same as 26.56. Figure 6.51c, Figure 6.51d and Figure 6.51e represent slip surfaces for slope inclination 45°, 55° and 65° respectively. At slope inclination 55°, all the three slip surfaces represent base failure with the two-layered slope with Soil-3 at the top having the deepest surface. It was observed that with an increase in slope inclination, the area of the failure mass reduces and gradually shifts more towards (becomes shallow) the slope surface. At 65° slope angle, the non-homogeneous slope with Soil-2 at top exhibit shallow slope failure. Now the slip surfaces are very distinct from each other. At higher slope inclinations, less water infiltrates the surface and more run-off occurs leading to shallow failure surfaces.



TH-2008_136104008

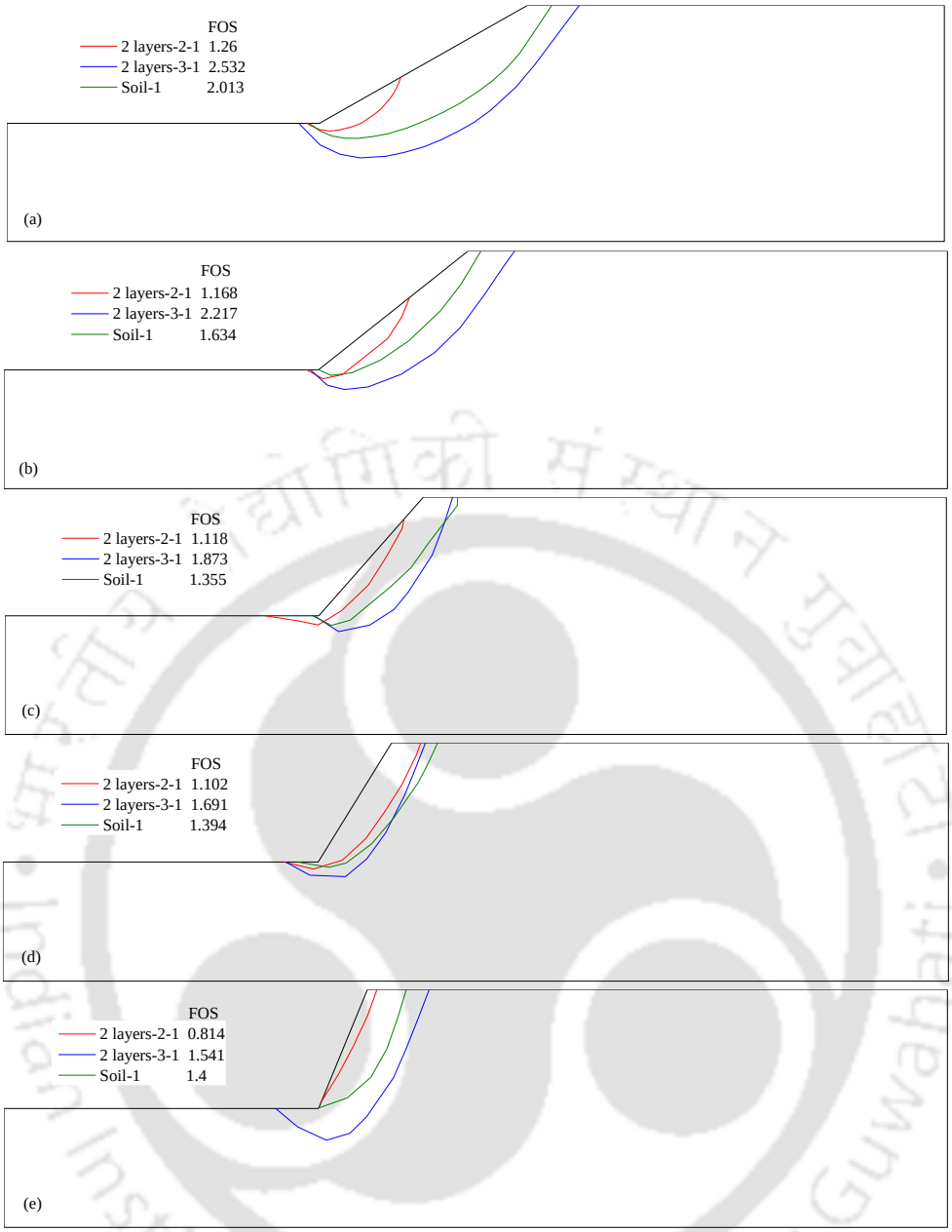


Figure 6.51 Critical Slip surfaces for the two-layered slopes after 24 h at different slope inclinations: (a) 26.56°, (b) 35°, (c) 45°, (d) 55° and (e) 65°

### 6.3.4 Effect of slope height

To investigate the effect of slope height on stability, four different slope heights (5 m, 10 m, 15 m and 20 m) were selected in the parametric study. Figure 6.52 depicts the two-layered non-homogeneous model used for the study of slope height variation. The slope inclination was kept constant at 35°. Pore water pressures at point P (2 m below at the midpoint of the inclined slope surface) for different slope heights at the initial stage and after 24h of rainfall are shown



TH-2008_136104008

in Figure 6.53. The external dimensions of the slope were kept same as Figure 5.53. In general, the pore water pressures decreases with increase with slope height.

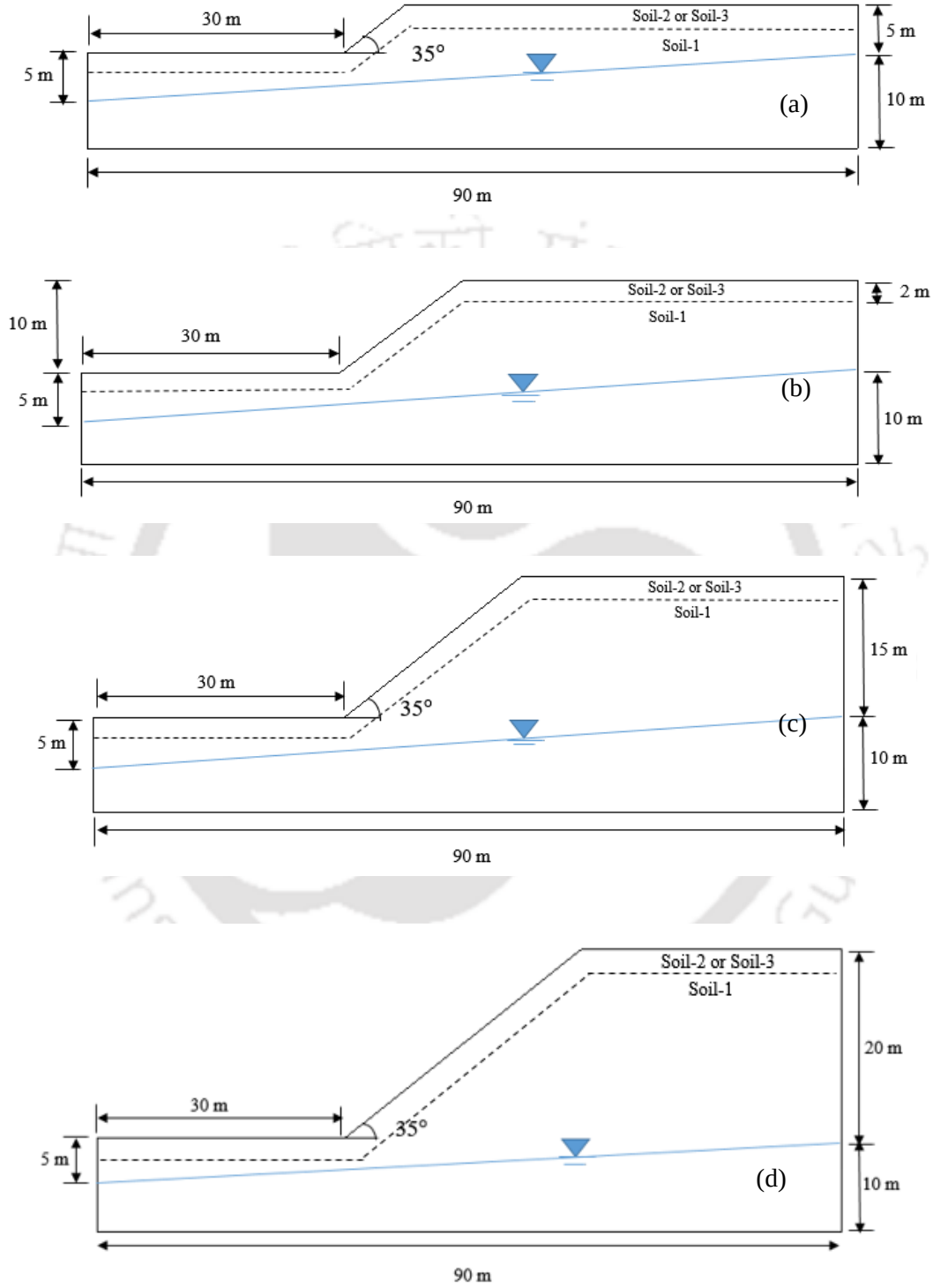


Figure 6.52 Model used to study the effect of slope height on stability under infiltration conditions



TH-2008_136104008

Pore water pressures at point P for different slope heights of the two-layered slopes at the initial stage and after 24 hours is depicted in Figure 6.53. The pore pressure is near to -15 kPa for all the slopes with 5 m slope height at the initial condition prior to rainfall infiltration. The negative pore pressure linearly increases with an increase in slope height because the distance of point P from the GWL increases with slope height increase. Negative pore pressures of around 118-120 kPa is observed for slope height 20 m for all the three slopes. With rainfall infiltration, the negative pore pressures reduce and therefore positive pressures in the range of 10 kPa are observed at point P for slope height 5 m. However, for the two-layered slope with Soil-3 at the top, the pore pressure for the 5 m slope is -4 kPa after 24 hours of infiltration. At 10 m slope height, the point P has negative pressure in the range of -1 kPa for both the homogeneous slope with Soil-1 and the two-layered slope with Soil-2 at the top. At even higher slopes (20 m), the negative pore pressures further reduce to 46 kPa.

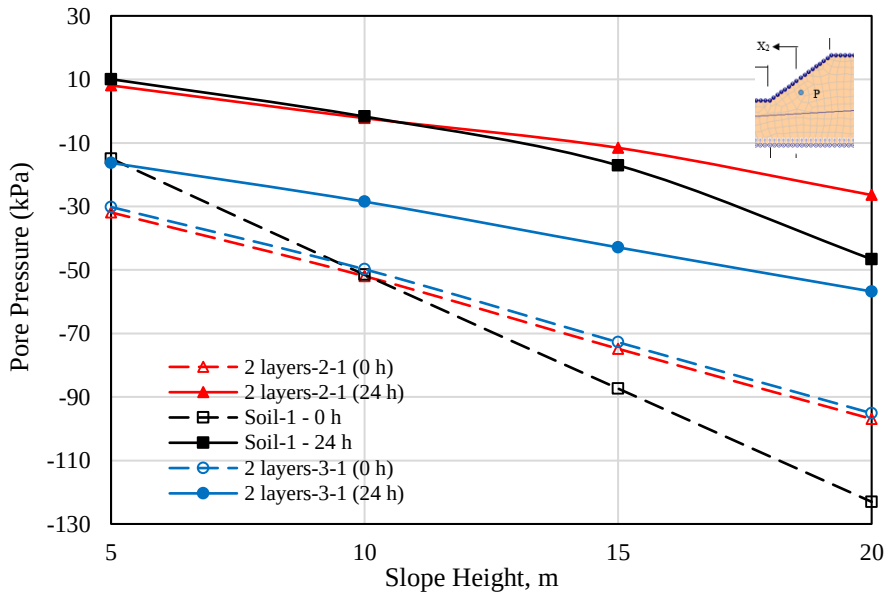


Figure 6.53 Variation of pore pressure at point P with slope height

Figure 6.54 shows the variation of a factor of safety with slope height for the two-layered slopes under infiltration conditions. The factors of safety prior to rainfall (0 h) is similar in nature for the two non-homogeneous slopes and the homogeneous slope with Soil-1. Before water



TH-2008_136104008

infiltrates the slope, the factor of safety for the homogeneous slope with Soil-1 and the two-layered slopes decrease nonlinearly with an increase in slope height. However, their behaviour after rainfall infiltration is very different for the three slope models.

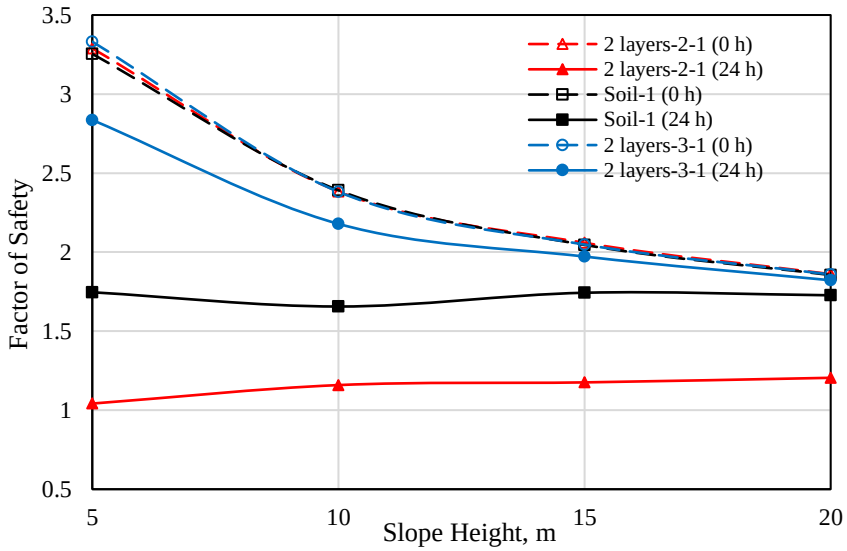


Figure 6.54 Variation of factor of safety with slope height for non-homogeneous slopes

After 24 hours of infiltration, it was observed that the factor of safety marginally increases with slope height for both the homogeneous slope with Soil-1 and two-layered slope with Soil-2 at the top. There is mounding of GWL for low slopes (5 m) for the model with Soil-2 as the top soil material. The factor of safety is observed to decrease with slope height after infiltration for the two-layered slope with Soil-3 at the top due to a decrease in matric suction caused by infiltration.

The critical slip surfaces for the two-layered slopes after 24 hours of rainfall infiltration for different slope heights are shown in Figure 6.55. For slope height, 5 m (Figure 6.55a), a homogeneous slope with Soil-1 depict toe failure mechanism. The two-layered slope with Soil-3 at the top and two-layered slope with Soil-2 at the top depicts base failure mechanism. The critical slip surface for the two-layered slope with Soil-2 at the top actually represent a stage approaching failure condition with a factor of safety of 1.039. Figure 6.55b depict the critical



TH-2008_136104008

surfaces for slope height 10 m. The two-layered slope with Soil-2 as the top material exhibit shallow slope failure with the slip surface confined to the top layer only. The homogeneous slope with Soil-1 shows a toe failure mode. The two-layered slope with Soil-3 at the top represents base failure mechanism.

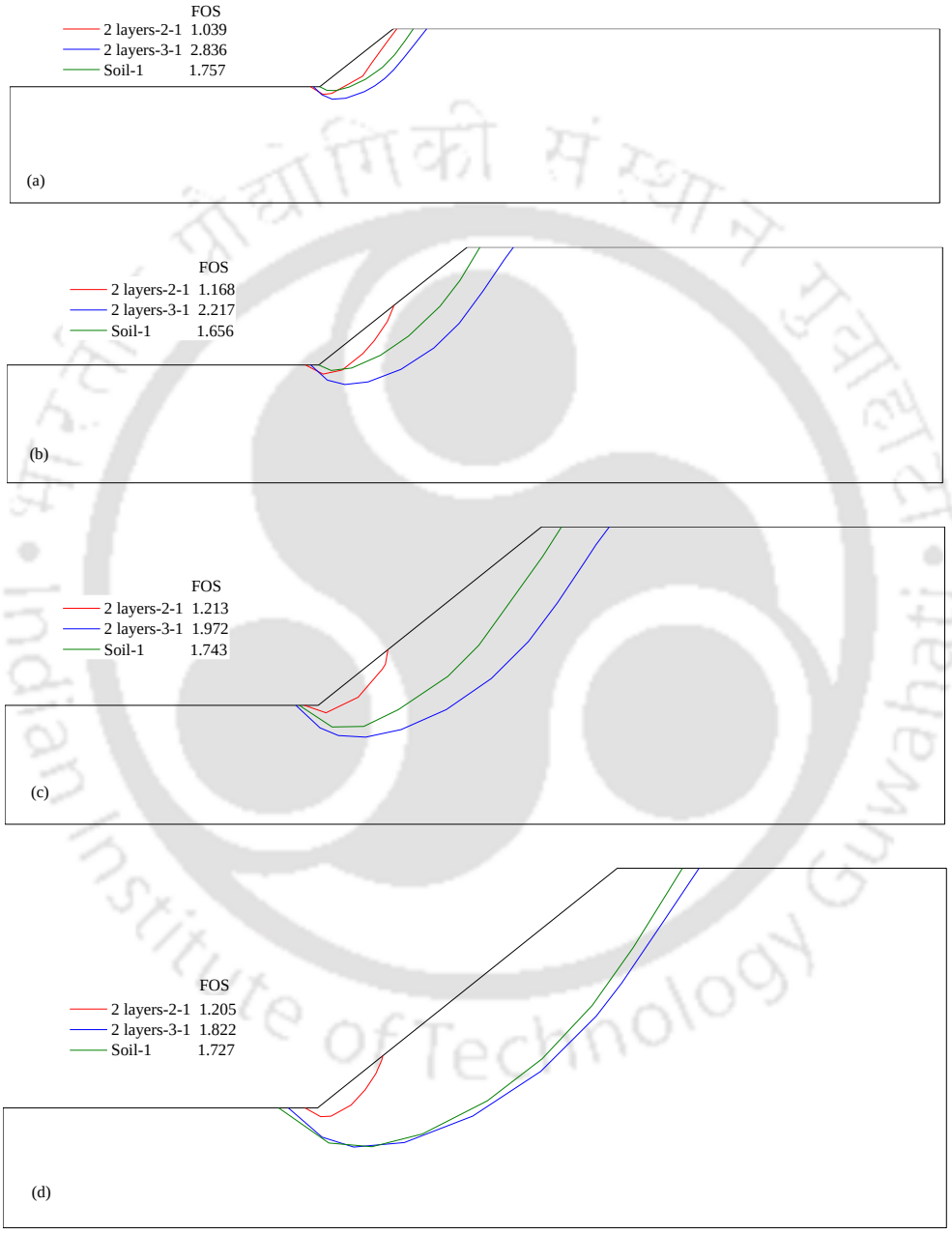


Figure 6.55 Critical slip surfaces for different slope heights: (a) 5 m, (b) 10 m, (c) 15 m, and (d) 20 m after 24 h of infiltration

The slip surfaces for slope height 15 m is illustrated in Figure 6.55c. Base failure is observed for Soil-1 and the two-layered slope with Soil-3 at the top. Shallow slope failure is seen for the



TH-2008_136104008

two-layered slope with Soil-2 as the top material. Figure 6.55d depict the slip surfaces for slope height 20 m. The base failure mode is observed for Soil-1 and the two-layered slope with Soil-3 at the top. The slope with Soil-2 at the top represents shallow slope failure within the top layer.

## 6.4 SUMMARY & DISCUSSION

Analysis of non-homogeneous slopes was performed under various conditions with three different type of soils creating various non-homogeneous configurations. The stability of the slopes was studied with and without seepage of water. The effect of moisture variation on non-homogeneous slopes were studied with degree of saturation of the soil varying from 20% to 80%. Under infiltration conditions, the effects of rainfall intensity, slope angle and slope height were studied for two-layered non-homogeneous slopes. The influence of long duration rainfall was also studied and compared with short duration rainfalls.

The study of the stability analysis of two-layered slopes with different foundation layer showed important outcomes. The slopes with Soil-1 as the foundation layer behaved differently as compared to slopes with Soil-1 as the top layer. With Soil-2 as the top layer, the slope had a very shallow critical slip surface while with Soil-3; the slope had a base failure mechanism with an increased factor of safety. The stability of the slope modelled with different moisture contents of the soil exhibited an increasing trend for the model with the saturation of the soil increasing with depth. Both two-layered and three-layered non-homogeneous slopes were stable (*FOS* – 2.4) with a GWL prior to the start of the infiltration process. The behaviour of the slopes under rainfall infiltration was different for the two-layered and three-layered slope models. The slope with Soil-2 at the top was more affected under infiltration than the other soil combination. Under rainfall infiltration, the slope with Soil-2 as the top layer (2 layers-2-1) showed more water infiltration than slope model 2 layers-3-1 due to the high-saturated permeability of Soil-2. The three-layered slope with Soil-2 as the top layer (3 layers-2-3-1)



TH-2008_136104008

reached failure conditions after 10 hours of infiltration. The slope with Soil-2 at the top reached failure conditions under 30 mm/h intensity after 34 hours of infiltration. With higher rainfall intensity, the slope reached failure stages much earlier. The effect of rainfall intensity on the stability of the slope with Soil-3 as the top material was very less due to the very low permeability of Soil-3, which did not allow the water to infiltrate freely. The parametric study with five different slope angles revealed that the stability of the slope naturally decreased with an increase in slope angle. Under rainfall infiltration, also the same behaviour was observed. The stability of the two-layered slope decreased nonlinearly with slope angle under infiltration conditions. The suction near the surface reduced more for steep slopes. Similarly, a parametric study was conducted with four slope heights to study the effect of slope height on the stability of two-layered non-homogeneous slope. The study showed that the initial stability of the slope decreased with an increase in slope height. However, under infiltration conditions, it was observed that the stability of the slope marginally increased with slope height for the slope with Soil-2 as the top layer. For high slopes, the decrease in stability was primarily due to the reduction of suction. A long duration rainfall (48 hours) was applied to the slope and its behaviour was compared with short duration rainfall. The behaviour of the slopes was similar up to 24 hours of infiltration for both the cases. As the infiltration stopped, the stability of the slopes increased due to an increase of suction. Under long duration rainfall (48 hours), the stability of the slope decreased 37% more than the short duration rainfall (24 hours).



TH-2008_136104008

# Chapter 7 CONCLUDING REMARKS

## 7.1 SUMMARY OF THE THESIS

Stability analysis of homogeneous and non-homogeneous slopes comprising of three different soils has been performed. Two soils were collected locally and the third was taken from literature. Different laboratory tests were performed to evaluate their properties. Numerical models were created to represent homogeneous and non-homogeneous slopes. Non-homogeneity in terms of variation in saturation level or variation in stratifications has been considered. Seepage analysis for different slope models was performed using the finite element method and slope stability analysis was performed using the limit equilibrium method. Analysis of homogeneous slopes was performed without GWL, with GWL, at different moisture contents and under rainfall conditions. Effect of rainfall intensity, slope angle and slope height under rainfall conditions were studied. The effect of long duration rainfall was also looked into. Analysis of non-homogeneous slopes was performed using two-layered and three-layered slopes without GWL, with GWL and under rainfall infiltration.

## 7.2 CONCLUSIONS

The numerical study on the non-homogeneous slopes suggest that their behaviour is different from homogeneous slopes. The effect of rainfall intensity, slope angle, slope height have different influence on the stability of layered slopes under infiltration conditions than slopes with a single material. The main conclusions from the research work are as follows:

- The three soils selected showed distinct failure modes. Fine-grained soil (Soil-1 and Soil-3) showed rotational failure while coarse-grained soil (Soil-2) showed the translational type of failure.



TH-2008_136104008

- Consideration of ground water level (GWL) and unsaturated soil characteristics is very essential in the analysis, as the slope behaviour totally depends on the suction levels and the associated shear strength values.
- Under rainfall conditions, different soils performed differently as per their SWCC and permeability functions. Change in the suction levels and GWL levels are significantly different for the three soils adopted for the study, under identical rainfall and geometric conditions.
- For the layered slope profiles, the type of failure is governed by the soil in the top layer for a two-layered slope.
- For the non-homogeneous slope model where the degree of saturation increased with depth, the stability of the slope decreased with an increase in its displacements as the layer thickness increased.
- For layered slopes, the pore water pressure increases at the surface if there is a high permeable soil (Soil-2) at the top and the pore water pressure decreases if there is a low permeable soil (Soil-3) at the top under infiltration conditions.
- The factor of safety for two-layered slopes is controlled by the soil in the top layer, i.e., if the top layer is of low permeability then the variation in the factor of safety with time under infiltration is less due to less water infiltration.
- Critical slip surface for two-layered slopes moved close to the surface of the slope when the top layer consisted of coarse-grained soil (Soil-2) under rainfall infiltration.
- At the first interface of a three-layered slope (3 layers-2-3-1) there is no suction which leads to failure after only 12 hours of infiltration while for the three-layered slope (3 layers-3-2-1) there is considerable suction maintained.
- The two-layered slope with Soil-2 at top reached failure conditions after 33 hours under the 30 mm/h rainfall intensity. The threshold intensity for this type of slope was found to



TH-2008_136104008

be 50 mm/h. The critical slip surfaces under different rainfall intensities were confined to the top layer only after the end of rainfall.

- Failure of slopes occurred due to the rise of GWL under higher rainfall intensities for the two-layered slopes with Soil-2 (high permeability) at the top.
- Under the long duration rainfall, the stability of the two-layered slope (2layers-2-1) decreased 37% more while the stability of the two-layered slope (2layers-3-1) decreased 6% more.
- The suction reduced more for steep slope inclinations (65°) for both the two-layered slopes under infiltration conditions.
- The factor of safety of the two-layered non-homogeneous slopes decreased nonlinearly with an increase in slope angle under infiltration situations.
- The critical slip surface moved closer to the surface with an increase in slope inclination under rainfall infiltration.
- The stability of the non-homogeneous slope decreased with the increase of slope height when the slope consisted Soil-3 (low $k_s$) at the top while the stability of the slope with Soil-2 (high $k_s$) at the top remained constant under rainfall infiltration.

The study highlights the behaviour of different types of soils under rainfall consideration with due importance to unsaturated soil behaviour. As the slope behaviour totally depends on the type of soil existing at the top layers, due consideration shall be given for the non-homogeneous nature including the variation of the moisture levels and the associated changes in suction and permeability characteristics.



TH-2008_136104008

## 7.3 LIMITATIONS OF THE STUDY

Stability of slopes is a statically indeterminate problem, so several things were assumed to make it determinate. With multiple materials considered, the problem became more complicated. Some of the limitations of the study are

- Only three types of soils were selected for the study.
- The ground water level was assumed at a single elevation.
- Only linear variation of shear strength due to matric suction was considered in the study.
- The SWCC of the soils were selected based on the basic properties of the soils.
- Constant rainfall intensity was used.

## 7.4 SCOPE OF FUTURE RESEARCH

Research pertaining to any topic is not complete; it has room for improvements so that the problem can be defined in the most realistic manner as possible. The future scope corresponding to the present study are as follows:

- Soils strength properties considering unsaturated behaviour need to be characterised.
- Use of nonlinear strength model (Vanapalli et al. 1996), the variation of apparent cohesion due to suction to realistically model unsaturated soil slopes.
- Multi-layered slopes need to be modelled with real rainfall data.
- Field data of GWL and pore pressure variations need to be obtained for better understanding the infiltration behaviour and comparing the field data with the results from the numerical analysis.



TH-2008_136104008

# REFERENCES


1. Abramson, L. W., Lee, T. S., Sharma, S., and Boyce, G. M. (1996). *Slope stability and stabilization methods*, Wiley, New York.

2. Ang, A. H. S., and Tang, W. H., (1984). *Probability Concepts in Engineering Planning and Design II: Decision, Risk and Reliability*, Wiley, New York.

3. Arai, K., and Tagyo, K. (1985). "Determination of noncircular slip surface giving the minimum factor of safety in slope stability analysis." *Soils Found.*, 25(1), 43-51.

4. ASTM D2487 (2011) Standard practice for classification of soils for engineering purposes (Unified Soil Classification System). Annual book of ASTM standards, West Conshohocken., PA, https://doi.org/10.1520/D2487-11.

5. ASTM D698 (2012). Standard test methods for laboratory compaction characteristics of soil using standard effort (12400 ft-lbf/ft$^3$ (600 kN-m/m$^3$)). *ASTM International*, West Conshohocken, PA, https://doi.org/10.1520/D0698-12E02

6. ASTM D7928 (2017). Standard test method for particle-size distribution (gradation) of fine-grained soils using the sedimentation (hydrometer) analysis, *ASTM International*, West Conshohocken, PA, https://doi.org/10.1520/D7928-17.

7. ASTM D854 (2014). Standard test methods for specific gravity of soil solids by water pycnometer. *ASTM International*, West Conshohocken, PA, https://doi.org/10.1520/D0854-14.

8. ASTM (2000) Standard Test Method for Unconfined Compressive Strength of cohesive Soil. D2166-0.

9. ASTM D2850 (2007) Standard test method for unconsolidated-undrained triaxial compression test on cohesive soils. ASTM International, West Conshohocken, PA.

10. Bai, T., Qiu, T., Huang, X., and Li, C. (2014). "Locating global critical slip surface using the Morgenstern-Price method and optimization technique." *Int. J. Geomech.*, 14(2), 319-325.

11. Bandini, P., and Salgado, R. (1999). *User guide for PCSTABL6*, Purdue Univ., West Lafayette, Ind.

12. Bishop, A. W. (1955). "The use of the slip circle in the stability analysis of slopes." *Geotechnique*, 5(1), 7-17.

13. Bordoloi, S., Yamsani, S. K., Garg, A., and Sreedeep, S. (2018). "Critical Assessment of infiltration measurements for soils with varying fine content using a mini disk infiltrometer." *J. ASTM Int.*, 47(2), 1–11.

14. Bouwer, H. (1969). "Infiltration of water into nonuniform soil." *Journal of Irrigation and Drainage Division*, ASCE, 95(4), 451–462.




TH-2008_136104008

15. Brooks, R. H., and Corey, A. T. (1964). "Hydraulic properties of porous medium." Colorado State University (Fort Collins), Hydrology Paper 3, Colorado State Univ., Fort Collins, Colorado. 27 pp.

16. Burdine, N. T. (1953). "Relative permeability calculations from pore-size distribution data." *Petr. Trans. Am. Inst.Mining Metall. Eng*., 198, 71-77.

17. Cai, F., and Ugai, K. (2004). **"**Numerical analysis of rainfall effect on slope stability.**"** *Int. J. Geomech.*, 10.1061/(ASCE)1532-3641(2004)4:2(69), 69–78.

18. Cai, J., Yan, E., Yeh, T. J., and Zha, Y. (2016) "Effects of heterogeneity distribution on hillslope stability during rainfalls." *Water Science and Engineering*, 9(2), 134-144.

19. Chang-yu, H., Jin-jian, C., Xiao-he, X., and Jian-hua, W. (2013). "Three-dimensional stability analysis of anisotropic and non-homogeneous slopes using limit analysis." *Journal of Central South University of Technology*, 21(3), 1142-1147.

20. Chen, W. F., Giger, M. W., and Fang, H. Y. (1969). "On the limit analysis of stability of slopes." *Soils Found.*, 9(4), 23-32.

21. Chen, W. F., Snitbhan, N. and Fang, H. Y. (1975). "Stability of slopes in anisotropic nonhomogeneous soils." *Can. Geotech. J.*, 12(1), 146-152.

22. Chen, W. F., and Sawada, T. (1982). "Seismic stability of slopes in anisotropic nonhomogeneous soils." Structural Engineering Report No. CE-STR-82-85, School of civil engineering, Purdue University, West Lafayette, Indiana, USA.

23. Chen, Z. Y., and Morgenstern, N. R. (1983). "Extensions to the generalized method of slices for stability analysis." *Can. Geotech. J.*, 20(1), 104-119.

24. Chen, W. F., and Liu, X. L. (1990). *Limit analysis in soil mechanics*, Elsevier Science Publishers B. V.

25. Cheng, Y. M., Lansivaara, T., and Wei, W. B. (2007). "Two-dimensional slope stability analysis by limit equilibrium and strength reduction methods." *Comput. Geotech.*, 34, 137-150.

26. Childs, E. C., and Collis-George, N. (1950). "The permeability of porous material." *Proceedings of the Royal Society of London*, A, 201, 392–405.

27. Childs, E. C., and Bybordi, M. (1969). "The vertical movement of water in stratified porous material." *Institution of Infiltration Water Resources Research*, 5(2), 446–459.

28. Cho, S. E., and Lee, S. R. (2001). "Instability of unsaturated soil slopes due to infiltration." *Computers and Geotechnics*, 28(3), 185–208.

29. Cho, S. E. (2009). "Infiltration analysis to evaluate the surficial stability of two-layered slopes considering rainfall characteristics." *Engineering Geology*, 105(3), 32–43.

30. Chowdhury, R., Flentje, P., and Bhattacharya, G. (2010). *Geotechnical Slope Analysis*, CRC Press, Taylor & Francis Group.



TH-2008_136104008

31. Chuang, P. H. (1992). ‘‘Stability analysis in geomechanics by linear programming. I: formulation.’’ *J. Geotech. Eng.*, 118(11), 1696–1715.

32. Dey, N. and Sengupta, A. (2018). “Effect of rainfall on the triggering of the devastating slope failure at Malin, India.” *Natural Hazards*, 94, 1391-1413.

33. Duncan, J. M. (1996). “State of the art: limit equilibrium and finite-element analysis of slopes.” *J. Geotech. Engng*, 122(7), 577-596.

34. Duncan, J. M., and Wright, S. G. (2005). *Soil strength and slope stability*, Wiley, New York.

35. Durner, W. (1994). “Hydraulic conductivity estimation for soils with heterogeneous pore structure.” *Water Resour. Res.*, 30(2), 211–233,https://doi.org/10.1029/93WR02676.

36. Eckersley, J. D. (1990) “Instrumented laboratory flowslides.” *Geotechnique*, 40(3), 489–502.

37. Elkamhawy, E., Wang, H., Zhou, B., and Yang, Z. (2018). “Failure mechanism of a slope with a thin soft band triggered by intensive rainfall.” *Environ Earth Sci*, 77(340), 1-15.

38. Elkateb, T., Chalaturnyk, R., and Robertson, K. P. (2003). “An overview of soil heterogeneity: quantification and implications on geotechnical field problems.” *Can. Geotech. J.*, 40(1), 1–15.

39. Fellenius, W. (1922) *Statens Jarnjvagars Geoteknniska Commission*, Stockholm, Sweden.

40. Fellenius, W. (1936). “Calculation of the stability of earth dams.” *Proc. 2nd congr. large dams*, Washington DC 4.

41. Filho, A. O. and Fernandes, A. M. (2018). “Landslide analysis of unsaturated soil slopes based on rainfall and matric suction data.” *Bull Eng Geol Environ.*, https://doi.org/10.1007/s10064-018-1392-5.

42. Fredlund, D. G. and Krahn, J. (1977). “Comparison of slope stability methods of analysis.” *Can. Geotech. J.*, 14(3), 429-439.

43. Fredlund, D. G., Morgenstern, N. R. and Widger, R. A. (1978). “The shear strength of unsaturated soils.” *Can. Geotech. J.*, 15(3), 313–321.

44. Fredlund, D. G., and Xing, A. (1994). “Equations for the soil–water characteristic curve.” *Can. Geotech. J.*, 31(4), 521–532.

45. Frolich, O. K. (1953). “The factor of safety with respect to sliding of a mass of soil along the arc of a logarithmic spiral,” *Proceedings of the 3rd International Conference on Soil Mechanics and Foundation Engineering*, Switzerland, 2, 230-233.

46. Gallipoli, D., Wheeler, S. J., and Karstunen, M. (2003). “Modelling the variation of degree of saturation in a deformable unsaturated soil.” *Geotechnique*, 53(1), 105–112.



TH-2008_136104008

47. Gasmo, J. M., Rahardjo, H., and Leong, E. C. (2000). "Infiltration effects on stability of a residual soil slope." *Comput. Geotech.*, 26, 145–165.

48. Gavin, K. and Xue, J. (2008). "A simple method to analyze infiltration into unsaturated soil slopes." *Comput. Geotech*., 35(2), 223–230.

49. Greco, V. R. (1996). "Efficient Monte Carlo technique for locating critical slip surface." *J. Geotech. Eng.*, 122(7), 517-525.

50. Griffiths, D. V. (1989). "Computation of collapse loads in geomechanics by finite elements." *Ing Arch, 59,* 237–244.

51. Griffiths, D. V. and Lane, P. A. (1999). "Slope stability analysis by finite elements." *Geotechnique*, 49(3), 387–403.

52. Hamdhan, I. N., and Schweiger, H. F. (2013). **"**Finite element method**–** based analysis of an unsaturated soil slope subjected to rainfall infiltration**."** *Int. J. Geomech*., 10.1061/(ASCE)GM.1943-5622.0000239, 653**–**658.

53. Hammond, C., Hall, D., Miller, S., and Swetik, P. (1992). "Level I Stability Analysis (LISA) documentation for version 2.0." General Technical Report INT- 285, US Department of Agriculture, Forest Service, Intermountain Research Station, Ogden, UT, 190.

54. Hammouri, A., Malkawi, A. I. H., and Yamin, M. M. A. (2008). "Stability analysis of slopes using the finite element method and limit equilibrium approach." *Bull Eng Geol Environ*, 67(4), 471-478.

55. Hicks, M. A., and Samy, K. (2015). "Influence of heterogeneity on undrained clay slope stability." *Quarterly Journal of Engineering Geology and Hydrogeology*, 35(1), 41-49.

56. Huang, Y. H. (1983). "Stability analysis of earth slopes." Van Nostrand Reinhold Co., Inc., New York.

57. Huang Y. H. (2014). "Slope Stability Analysis by the Limit Equilibrium Method." *ASCEPRESS.*

58. Janbu, N., Bjerrum, L., and Kjaernsli, B. (1956). *Veiledning ved Losning av Fundamenteringsoppgaver* (Soil Mechanics Applied to some Engineering Problems), Publication 16, Norwegian Geotechnical Institute.

59. Janbu, N. (1968). "Slope stability computations." *Soil Mech. Found. Engng Report*. Trondheim: Technical University of Norway.

60. Jiang, G. J., and Magnan, J. P. (1997). ''Stability analysis of embankments: comparison of limit analysis with methods of slices.'' *Geotechnique,* 47(4), 857–872.

61. Jimoh, A. Y. (2006). "Shear strength/Moisture content models for a laterite soil in Ilorin Kwara State Nigeria." *Proceedings of the 16th International Conference on Soil Mechanics and Geotechnical Engineering*, 521-525.



TH-2008_136104008

62. Kellezi, L., Allkja, S., and Hansen, P. B. (2005). "Landslide FE Stability Analysis." Proceedings International Association for Computer Methods and Advances in Geomechanics, Torino, Italy, 545–553.

63. Kim, J., Salgado, R., and Lee, J. (2002). "Stability analysis of complex soil slopes using limit analysis." *J. Geotech. Geoenviron. Eng.*, 128(7), 546-557.

64. Koppula, S. D. (1984). "Pseudo-static analysis of clay slopes subjected to earthquakes." *Geotechnique,* 34(1), 71-79.

65. Krabbenhoft, K., Lyamin, A. V., Hjiaj, M., and Sloan, S. W. (2005). **"**A new discontinuous upper bound limit analysis formulation.**"** *Int. J. Numer. Methods Eng.*, 63(7), 1069**–**1088.

66. Kumar, J. and Samui, P. (2006). "Stability determination for layered soil slopes using the upper bound limit analysis." *Geotechnical and Geological Engineering,* 24, 1803–1819

67. Lambe, T. W. and Whitman, R. V. (1969). Soil mechanics. New York: Wiley.

68. Leshchinsky, D., and Huang, C. (1993). ''Generalized slope stability analysis: interpretation, modification, and computation.'' *J. Geotech. Eng.*, 118(10), 1559–1576.

69. Li, X., Wen, H., Muhunthan, B., and Wang, J. (2015). "Modelling and prediction of the effects of moisture on the unconfined compressive and tensile strength of soils." *J. Geotech. Geoenviron. Eng*., ASCE, 141(7), 1-7.

70. Liang, R. Y., Nusier, O. K., and Malkawi, K. H. (1999). "A reliability based approach for evaluating the slope stability of embankment dams." *Engineering Geology,* 54(3-4), 271-285.

71. Lim, K., Li, A. J., and Lyamin, A. V. (2015). "Three-Dimensional Slope Stability Assessment of Two-Layered Undrained Clay." *Comput. Geotech.***,** 70, 1–17.

72. Lin, H., Zhong, W., Wang, H., and Xu, W. (2017). "Effect of soil–water characteristic parameters on saturation line and stability of slope." *Geotech. Geol Eng*, 35, 2715-2726.

73. Lin, H. and Zhong, W. (2018). "Influence of rainfall intensity and its pattern on the stability of unsaturated soil slope." *Geotech. Geol. Eng.*, https://doi.org/10.1007/s10706-018-0631-7.

74. Low, B. (1989). "Stability analysis of embankment on soft ground." *J. Geotech. Eng*., 115(2), 211–227.

75. Lowe, J., and Karafiath, L. (1959). "Stability of earth dams upon drawdown." *Proceedings of the 1st PanAmerican Conference on Soil Mechanics and Foundation Engineering*, Mexico City, 2, 537-552.

76. Lu, N., and Godt, J. (2008). "Infinite slope stability under steady unsaturated seepage conditions." *Water Resour. Res.*, 44, W11404.



TH-2008_136104008

77. Lu, N., and Godt, J. (2008). "Infinite slope stability under steady unsaturated seepage conditions." *Water Resources Research*, 44, 1-13.

78. Lu, N., and Godt, J. (2013). *Hillslope hydrology and stability*, Cambridge University Press.

79. Lu, N., and Likos, W. J. (2006). "Suction stress characteristic curve for unsaturated soil." *J. Geotech. Geoenviron. Eng.*, 132(2), 131– 142.

80. Lumb, P. (1962). "Effect of rain storms on slope stability." *In Symposium on Hong Kong Soils*, Hong Kong, 73–87.

81. Lyamin, A. V., and Sloan, S. W. (2002a). **"**Lower bound limit analysis using non-linear programming.**"** *Int. J. Numer. Methods Eng.*, 55(5), 573**–**611.

82. Lyamin, A. V., and Sloan, S. W. (2002b). **"**Upper bound limit analysis using linear *f*inite elements and non-linear programming.**"** *Int. J. Numer. Anal. Methods Geomech.*, 26(2), 181**–**216.

83. Malkawi, A. I. H., Hassan, W. F., and Sarma, S. K. (2001). "Global search method for locating general slip surface using Monte Carlo techniques." *J. Geotech. Geoenviron. Eng*., 127(8), 688-698.

84. Matsui, T., and San, K. C. (1992). "Finite element slope stability analysis by shear strength reduction technique." *Soils Found.*, 32(1), 59–70.

85. Moore, I. D. (1981). "Infiltration equations modified for surface effects." *Journal of Irrigation and Drainage Division*, ASCE, 107(1), 71–86.

86. Morgenstern, N. R., and Price, V. E. (1965). "The analysis of the stability of general slip surfaces." *Geotechnique*, 15(1), 79-93.

87. Mualem, Y. (1976). **"**A new model predicting the hydraulic conductivity of unsaturated porous media.**"** *Water Resour. Res.*, 12(3), 513**–**522.

88. Naylor, D. J. (1981). "Finite elements and slope stability." *Numer. Meth. In: Geomech*., Proceedings Of the NATO Advanced Study Institute, Lisbon, Portugal; p. 229–44.

89. Ng, C. W. W., and Shi, Q. (1998). "A numerical investigation of the stability of unsaturated soil slopes subjected to transient seepage." *Comput. Geotech.*, 22(1), 1**–**28.

90. Ni, P., Wang, S., Zhang, S., and Mei, L. (2016). "Response of Heterogeneous Slopes to Increased Surcharge Load." *Comput. Geotech.*, 78, 99–109.

91. Ni, P., Mei, G., and Zhao, Y. (2018). "Influence of raised groundwater level on the stability of unsaturated soil slopes." *Int. J Geomech*., 18(12), 1-13.

92. Potts, D. M., Dounias, G. T. and Vaughan, P. R. (1990). "Finite element analysis of progressive failure of Carsington embankment." *Geotechnique*, 40(1), 79-102.



TH-2008_136104008

93. Qian, Z. G., Li, A. J., Merifeld, R. S., and Lyamin, A. V. (2014). "Slope Stability Charts for Two-Layered Purely Cohesive Soils Based on Finite-Element Limit Analysis Methods." *Int. J Geomech.,* 15(3), 1–14.

94. Rahardjo, H., Li, X. W., Toll, D. G., and Leong, E. C. (2001). "The effect of antecedent rainfall on slope stability." *J. Geotech. Geological Eng.*, 19(3–4), 371–399.

95. Rahardjo, H., Ong, T. H., Rezaur, R. B., Leong, E. C. (2007). "Factors controlling instability of homogeneous soil slopes under rainfall." *Journal of Geotechnical and Geoenvironmental Engineering*, 133(12), 1532–1543.

96. Rahimi, A., Rahardjo, H., and Leong, E. C. (2010) "Effect of hydraulic properties of soil on rainfall-induced slope failure." *Comput. Geotech.*, 114(3-4), 135–143.

97. Rahimi, A., Rahardjo, H., and Leong, E. C. (2011) "Effect of antecedent rainfall patterns on rainfall-induced slope failure." *J. Geotech. Geoenviron. Eng*., 137(5), 483–491.

98. Rahardjo, H., Nio, A. S., Leong, E. C. and Song, N. Y. (2010). "Effects of groundwater table position and soil properties on stability of slope during rainfall." *J. Geotech. Geoenviron. Eng*., 136(11), 1555-1564.

99. Rahardjo, H., Satyanaga, A., Leong, E. C., and Ng, Y. S. (2012). "Variability of Residual Soil Properties." *J. Eng. Geol*. 141–142, 124–140.

100. Rahardjo, H., Satyanaga, A. and Leong, E. C. (2012). "Unsaturated soil mechanics for slope stabilization." *Geotechnical Engineering Journal of the SEAGS & AGSSEA*, March, 43(1), 48-58.

101. Ray, R. L., Jacobs, J. M., and Alba, P. (2010). "Impacts of unsaturated zone soil moisture and groundwater table on slope instability." *J. Geotech. Geoenviron. Eng*., ASCE, 136(10), 1448-1458.

102. Rocscience (2018a). SLIDE2 v8, Rocscience Inc., Toronto, Canada.

103. Rocscience (2018b). RS2 v9.0, Rocscience Inc., Toronto, Canada.

104. Sarma, S. K. (1973). "Stability analysis of embankments and slopes." *Geotechnique*, 23(3), 423-433.

105. Song, Y. S., Chae, B. G., and Lee, J. (2016). "A method for evaluating the stability of an unsaturated slope in natural terrain during rainfall." *Engineering Geology*, 210, 84–92.

106. Skempton, A. W. (1948). "The $\phi$ = 0 analysis of stability and its theoretical basis." *Proceedings of the 2n$^{d}$ International Conference on Soil Mechanics and Foundation Engineering*, Rotterdam, 1, 72-78.



TH-2008_136104008

107. Skempton, A.W. and Hutchinson, J.N. (1969) ″Stability of Natural Slopes and Embankment Foundations″ Proc. 7th Int. Conf. Soil Mechanics & Foundation Engineering, Mexico City, State-of-the Art Volume, 291–340.

108. Smith, I. M. and Hobbs, R. (1974). "Finite element analysis of centrifuged and built-up slopes." *Geotechnique*, 24(4), 531–559.

109. Spencer, E. (1967). "A method of analysis of the stability of embankments assuming parallel inter-slice forces." *Geotechnique*, 17(1), 11–26.

110. Taylor, D. W. (1948). *Fundamentals of soil mechanics*, Wiley, Hoboken, NJ.

111. Trauner, L., Dolinar, B., and Misic, M. (2005). "Relationship between the undrained shear strength, water content, and mineralogical properties of fine-grained soils." *Int. J. Geomech.*, ASCE 5(4), 350–355.

112. Tsaparas, I., Rahardjo, H., and Toll, D. G. (2002). "Controlling parameters for rainfall-induced landslides." *Comput. Geotech.*, 29(1), 1–27.

113. Ugai, K., and Leshchinsky, D. (1995). "Three-dimensional limit equilibrium and finite element analysis: a comparison of results." *Soils Found.*, 35(4):1–7.

114. Umrao, R. K., Singh, R., Sharma, L. K., and Singh, T. N. (2017). "Soil slope instability along a strategic road corridor in Meghalaya, north-eastern India." *Arab J Geosci.*, 10, 260.

115. U.S. Army Corps of Engineers (1970). *Engineering and Design: Stability of Earth and Rosckfill Dams*, Engineer Manual Em 1110-2-1902, Department of the Army, Corps of Engineers, Office of the Chief of Engineers, Washington, DC, April.

116. Vahedifard, F., Leshchinsky, D., Mortezaei, K., and Lu, N. (2016). **"**Effective stress-based limit-equilibrium analysis for homogeneous unsaturated slopes**."** *Int. J. Geomech.*, 0.1061/(ASCE)GM.1943-5622.0000554, D4016003.

117. Van Genuchten, M. T. (1980). "A closed-form equation for predicting the hydraulic conductivity of unsaturated soils." *Soil Science Society of America Journal*, 44(5), 892–898.

118. Van Genuchten, M. T., Leij, F. J., and Yates, S. R. (1991). "The RETC code for quantifying the hydraulic functions of unsaturated soils." U.S. Environmental Protection Agency, Ada, Oklahoma.

119. Whitman, R. V., and Bailey, W. A. (1967). "Use of computers for slope stability analysis." J. Soil Mech. Found. Div., ASCE, 93(4), 475-498.

120. Yubonchit, S., Chinkulkijniwat, A., Horpibulsuk, S., Jothityangkoon, C., Arulrajah, A., and Suddeepong, A. (2017). "Influence factors involving rainfall-induced shallow slope failure-numerical study." *Int. J. Geomech.*, 17(7), 1–13.



TH-2008_136104008

121. Zhang, L. L., Fredlund, D. G., Zhang, L. M., and Tang, W. H. (2004). "Numerical study of soil conditions under which matric suction can be maintained." *Can. Geotech. J.*, 41(4), 569–582.

122. Zhang, L. L., Zhang, L. M., and Tang, W. H. (2005). "Rainfall-induced slope failure considering variability of soil properties." *Geotechnique*, 55(2), 183–188.

123. Zhang, L. L., Zhang, J., Zhang, L. M., and Tang, W. H. (2011). "Stability Analysis of Rainfall-induced slope failure – A Review." *Geotechnical Engineering*, ICE proceedings, 164(5), 299–316.

124. Zhang, L. L., Zhang, L. M., and Tang, W. H. (2013). "Modelling the unsaturated soil zone in slope stability analysis." *Can. Geotech. J.*, 51(12), 1384-1398.

125. Zhang, L., Li, J., Li, X., Zhang, J. and Zhu, H. (2016). *Rainfall-induced soil slope failure: stability analysis and probabilistic assessment*, CRC Press, Taylor & Francis Group.

126. Zhang, F., Cui, Y., Zeng, L., Robinet, J. C., Conil, N., and Talandier, J. (2018). "Effect of degree of saturation on the unconfined compressive strength of natural stiff clays with consideration of air entry value." *Engineering Geology*, 237, 140-148.

127. Zhou, Y. D., Cheuk, C. Y., and Tham, L. G. (2009). "Numerical modelling of soil nails in loose fill slope under surcharge loading." *Comput. Geotech.*, 36(5), 837-850.

128. Zienkiewicz, O. C., Humpheson, C., and Lewis, R. W. (1975). "Associated and nonassociated visco-plasticity and plasticity in soil mechanics." *Geotechnique*, 25(4), 671–89.

129. Zheng, H., Sun, G., and Liu, D. (2009). "A practical procedure for searching critical slip surfaces of slopes based on the strength reduction technique." *Comput. Geotech.*, 36(1-2), 1-5.

130. Zhu, D. Y., Lee, C. F., Qian, Q. H., and Chen, G. R. (2005). **"**A concise algorithm for computing the factor of safety using the Morgenstern–Price method.**"** *Can. Geotech. J.*, 42(1), 272–278.



TH-2008_136104008

# PUBLICATIONS

**Journal Paper:**

1. Chatterjee, D., and Krishna, A. M. (2019) "Effect of slope angle on the stability of a slope under rainfall infiltration." *Indian Geotechnical Journal*, 49(2), 1-10.
2. Chatterjee, D., and Krishna, A. M. (2018) "Stability analysis of two-layered non-homogeneous slopes." *International Journal of Geotechnical Engineering*, 5(1), 1-7.
3. Chatterjee, D., and Krishna, A. M. (2019) "Stability analysis of non-homogeneous slopes under rainfall conditions." Submitted to *International Journal of Geomechanics, ASCE*. (Under review)
4. Chatterjee, D., Sarma, C.P. and Krishna, A. M. (2019) "Effect of moisture content variation on the stability of a slope." Submitted to *Geotechnical and Geological Engineering*. (Under review)

**Conference Papers:**

1. Chatterjee, D., and Krishna, A. M. (2019) "Stability of two-layered earth slopes under rainfall infiltration." *International Association for Computer Methods and Advances in Geomechanics, IACMAG-2019*. Paper No. 179.
2. Chatterjee, D., and Krishna, A. M. (2016) "Stability analysis of non-homogeneous soil slopes using numerical techniques." *Indian Geotechnical Conference-2016*, IIT Madras, Chennai, India. Paper No. 510
3. Chatterjee, D., and Krishna, A. M. (2015) "Seismic slope stability analysis for layered configurations." *Sixth International Geotechnical Symposium on Disaster Mitigation In Special Geoenvironmental Conditions*, IGS-Chennai-2015, IIT Madras, Chennai, India.
4. Chatterjee, D., and Krishna, A. M. (2014) "Seismic stability analysis of two-layered soil slopes." *North-East Students Geo-Congress on Advances in Geotechnical Engineering* (NESGC-2014**),** Guwahati, India, 18 Oct 2014.



TH-2008_136104008